N° d'ordre : 4717

# THÈSE

PRÉSENTÉE A

## L'UNIVERSITÉ BORDEAUX 1

ÉCOLE DOCTORALE DES SCIENCES CHIMIQUES

Par Maïté, MARGUET

POUR OBTENIR LE GRADE DE

DOCTEUR

SPÉCIALITÉ : POLYMERES

# Vésicules polymères biomimétiques: du virus à la cellule

**Polymer vesicles : from virus to cell biomimicry**

Directeur de thèse : Sébastien LECOMMANDOUX

Soutenue le : 19 décembre 2012

Devant la commission d'examen formée de :

| | | |
|---|---|---|
| Mme SYKES, Cécile | Directrice de Recherche CNRS, Institut Curie, Paris | Rapporteur |
| M. SCHERMAN, Oren | Directeur de Recherche, Université de Cambridge | Rapporteur |
| M. CRAMAIL, Henri | Professeur, Université de Bordeaux 1 | Président |
| M. LECOMMANDOUX, Sébastien | Professeur, Institut Polytechnique de Bordeaux | Examinateur |
| M. LUENGO Gustavo | Research Associate, L'Oréal Paris | Examinateur |
| M. MONDAIN-MONVAL, Olivier | Professeur, Université de Bordeaux 1 | Examinateur |
| M. VAN HEST, Jan | Professeur, Université de Radboud, Nijmegen | Examinateur |

**Résumé**

Les polymersomes, obtenus par auto-assemblage en solution aqueuse de copolymères à blocs amphiphiles en structure vésiculaire, sont présentés comme d'excellents mimes synthétiques des virus, dont les propriétés membranaires – principalement élasticité, perméabilité, fonctionnalité- peuvent être très proches. Il y a ainsi un fort engouement quant à leur utilisation en biotechnologie et surtout en vectorisation d'actifs pharmaceutiques ou cosmétiques. Afin d'aller encore plus loin dans le biomimétisme ou la bio-inspiration, une étape devait être franchie : encapsuler ces polymersomes les uns dans les autres. Ce cloisonnement ou multi-compartimentalisation permet de mimer cette fois la structure d'une cellule dite eukaryote, elle-même constituée de compartiments internes (organelles) et d'un cytoplasme (lui conférant entre autres une certaine stabilité mécanique) contenues dans le compartiment externe représenté par la membrane cellulaire. Toutefois, l'obtention d'un simple mime structural d'une structure si complexe représente déjà un challenge en soi, nécessitant maîtrise de la physico-chimie des systèmes, de la stabilisation des interfaces et des outils de formulation. Une méthode d'émulsion-centrifugation a été développée et a permis d'obtenir de telles structures compartimentalisées (mimes d'organelles) à cavité gélifiée (mime de cytoplasme). Finalement, différentes voies d'exploitation de ces systèmes sont présentées, allant de l'encapsulation multiple, la libération contrôlée jusqu'au développement de réactions enzymatiques en cascade confinées, mimant ainsi le métabolisme cellulaire.

**Mots-clés** : Vésicules, polymères, polymersomes, biomimétisme cellulaire, multicompartimentalisation, mimes d'organelles, vectorisation, auto-assemblage

**Summary**

Amphiphilic block copolymers self-assemble in water into vesicles, coined "polymersomes"; these vesicles are described as excellent synthetic mimics of viral capsids due to the resemblance of their respective membrane properties (in terms of elasticity, permeability, and functionality). As a result, they were massively investigated over the last years regarding applications in biotechnology and more particularly for the targeted delivery of pharmaceutical or cosmetic actives.
In order to go further towards bio-inspiration and cell biomimicry, the next step required the encapsulation of polymersomes in other polymersomes. This multicompartmentalization indeed enables to mimic the structure of an eukaryotic cell; an outer cellular membrane compartment encloses internal compartments (organelles) and a cytoplasm responsible amongst others for a certain mechanic stability. However, alone the controlled formation of a system mimicking such a complex structure represents a technological challenge in terms of control over the physical chemistry of these systems, the stabilization of their interfaces and their formulation. A formation method based upon an emulsion-centrifugation has been developed and enabled the formation of such multicompartmentalized structures (organelle mimics) with a gelified lumen (cytoplasm mimic). Finally, various potential applications of these systems are presented: from multiple encapsulation, controlled drug release, to the development of enzymatic and confined cascade reactions that mimick the cellular metabolism.

**Keywords**: Vesicles, Polymer, Polymersomes, Cell Biomimicry, Multicompartmentalization, Organelle mimics, Drug delivery, Self-assembly

*Je dédie ce manuscrit de thèse*

*A mes parents, Maryse et Alain*

*A Guillaume*

*A ma grand-mère Delphine*

*A mon petit frère Fabien*

**Remerciements**

*I feel very grateful and honoured that my jury accepted to judge this work. Thank you to my referees in particular, Dr. Cécile Sykes and Dr. Oren Scherman, to Prof. Henri Cramail, my president of jury and of course to Dr. Jan van Hest, Dr. Gustavo Luengo, and Prof. Olivier Mondain-Monval.*

*Je remercie le directeur du LCPO, le* ***professeur Henri Cramail*** *de m'avoir accueillie au sein de son laboratoire pendant ces 3 années.*

*Je remercie infiniment mon directeur de thèse le* ***professeur Sébastien Lecommandoux*** *: de m'avoir recrutée, et de m'avoir fait confiance en m'attribuant ce sujet précis, dont la nouveauté et l'originalité ont été des défis certains à relever initialement avant que nous ne surmontions les obstacles un par un. De m'avoir offert toute la liberté dont j'avais besoin pour travailler, tout en se rendant toujours disponible dès que j'en avais besoin, même lorsqu'il était en déplacement (souvent!). Comme il comprend tout très rapidement, il ne lui fallait jamais longtemps pour me rassurer et me remotiver jusqu'à la réussite d'un objectif ou pour trouver l'idée qui permettait enfin l'aboutissement, la valorisation de tout un projet. J'ai également beaucoup apprécié le fait qu'il ait toujours été à mon écoute; nous avons pris toutes les décisions ensemble et elles ont été nombreuses au regard de la complexité du sujet. Cela a parfois nécessité des argumentations de part et d'autre jusqu'à tomber d'accord. De plus, toutes nos discussions ont toujours été très enrichissantes pour moi et pour mon travail, je le remercie pour TOUT ce qu'il m'a appris, en sciences bien sûr, mais aussi en management, et en relations humaines. Cela me sera extrêmement profitable dans le futur, j'en suis sûre. Avoir pour encadrant et mentor, un chercheur et un manager aussi brillant m'a remplie de fierté et m'a toujours poussée à vouloir me surpasser pour être à la hauteur de mon modèle. Pour finir j'ai également apprécié les discussions philosophiques que nous avons parfois pu avoir, ainsi que les moments de « rigolade ».*

*I am also very grateful to* ***professor Jan van Hest*** *from Radboud University, Nijmegen, the Netherlands for accepting the collaborational project we submitted to him for my last year of PhD and last project, for giving me the great opportunity of working during 3 months in his group, and for treating me there, as one of his own students. Regardless of the result, I feel very honoured about this collaboration with such a famous professor. To finish I thank him for choosing his PhD candidate* ***Ruud Peters*** *to work together with me on this project.*

*Indeed, it was a real pleasure to finally work together with another PhD candidate on a project, and I do not think there would have been a better fit for me, at least on this project. Indeed in my opinion we proved out to work great together as a team, I had the chance to have a very talented colleague with me on this project. To finish, Ruud made also sure I felt*

*welcome and treated as everyone else in Nijmegen. I also thank him for the nice and fun moments we shared.*

*Sans financement, cette thèse n'existerait pas. Je remercie donc le Ministère de l'Enseignement Supérieur et de la Recherche pour les fonds alloués pendant ces 3 années, ainsi que la commission d'examen de Bordeaux 1, responsable du choix de ma candidature pour cette bourse. Je remercie aussi le European Science Foundation, et particulièrement le programme Precision Polymer Materials, pour leur bourse « Exchange Visit Grant » qui m'a permise d'aller aux Pays-Bas pour une campagne d'expériences de 3 mois.*

*J'aimerais aussi remercier ma stagiaire de Master 2,* ***Lise Edembe****, qui a réalisé les cinétiques de relargages de doxorubicine pendant ses 5 mois de stage au cours de ma 2e année. Ce fut un projet complexe à démontrer et un challenge de chaque instant, compressé en 5 mois de stage, en plus d'un ou deux mois de réflexion pré-projet de mon côté. Le travail expérimental en lui-même était souvent fastidieux et ingrat, mais nécessaire et je la remercie d'avoir si bien tenu le coup. Je l'ai vue progresser et évoluer au cours du stage, jusqu'à avoir des initiatives déterminantes à la fin, et j'espère y avoir contribué.*

***Sébastien Marais****, ingénieur au Bordeaux Imaging Center (mon 2*$^{e}$ *lieu de travai !), a aussi joué un rôle non négligeable quant au bon déroulement de cette thèse. Je le remercie de m'avoir si bien formée aux microscopes confocaux à balayage laser, spinning disk, et à ImageJ. A chaque problème, difficulté, et jusqu'à l'obtention de résultats publiables, j'ai toujours pu compter sur son soutien technique et sa connaissance aïgue de ces microscopes. Son soutien moral m'a aussi grandement aidé à travers ces longues heures et ces longs après-midis de microscopie. Surtout, par nos discussions, il m'a aidé à mettre au point la démonstration, la preuve de concept du dernier projet commencé dans le chapitre 4.*

*Je remercie le* ***Dr. Olivier Sandre****, chargé de recherche CNRS au sein de l'équipe pour sa collaboration sur le chapitre 2 (Langmuir), quant au travail sur le vidéo tracking, aux calculs de coefficient de diffusion, etc, ainsi que pour la production des nanoparticules magnétiques de la conclusion. J'aimerais aussi le remercier ainsi que* ***le Dr. Christophe Schatz*** *pour leurs conseils au début concernant la microscopie et particulièrement pour imager des vésicules géantes en solution C'était la base de tout, et cela m'était totalement inconnu.*

*J'aimerais remercier le* ***Dr. Colin Bonduelle*** *pour sa collaboration sur la revue Chemical Society Review (Chapitre 1), pour toutes les images qu'il a su si bien créer pour cette review (jusqu'à l'obtention de la couverture !) et ce manuscrit, et pour sa connaissance encyclopédique de la littérature parmi ses nombreuses autres compétences. Nos fréquentes discussions ont ainsi été très bénéfiques à ce travail, me permettant parfois de recentrer, recadrer, mieux comprendre certains aspects.*

*J'ai eu la grande chance que le* ***Dr. Julie Thévenot*** *travaille dans l'équipe et tienne notre labo en « patronne » d'une main de fer dans un gant de velours, de mon premier à mon dernier jour. Je la remercie pour le lot de PTMC-b-PGA qu'elle m'a généreusement offert mais aussi pour tous ses conseils et toutes ses suggestions qui m'ont souvent permis d'avancer. Je la remercie de m'avoir conduit au BIC lors des 2 derniers mois de « manipes » pour le bien de celles-ci. Elle a toujours été là pour moi, disponible pour m'aider et elle a contribué à ma maturation professionnelle et humaine.*

*Je voudrais aussi remercier une autre personne qui, comme Julie, a aussi été comme une « grande sœur » pour moi pendant cette thèse, le* ***Dr. Stéphanie Louguet****. Elle m'a également fait profiter de ses judicieux conseils et suggestions, notamment pour penser le projet sur les cinétiques de relargage de DOX.*

*Je remercie aussi notre biologiste maison, le* ***Dr. Hugo De Oliveira****, pour ses corrections quant à la biologie (et parfois l'anglais) dans mes écrits au cours du temps.*

*Je remercie le* ***Dr. Laurent Bui*** *pour les images de vésicules vert fluo, et sa bonne humeur jour après jour.*

*J'aimerais remercier tous les « étudiants » de l'équipe passée et présente dans leur ensemble : Adeline, Charles, Laurent, Autumn, Stéphanie, Julie, Elisabeth, Colin, Hugo, Silvia, Charlotte, Camille, Dan, Romain, Kévin.*
*J'ai en effet eu la chance de faire partie de cette équipe extrêmement riche tant d'un point de vue scientifique qu'humain. Je remercie les 5 post-docs de l'équipe actuelle, Julie, Colin, Hugo, Silvia et Kévin pour leurs corrections de finition sur le manuscrit et le powerpoint de soutenance, ils ont toujours répondu présent, même et souvent pour des demandes de dernière minute. Merci aussi à Silvia pour m'avoir conduite au BIC les derniers mois. Je remercie tous les anciens et actuels étudiants pour leur compréhension, notamment les 6 derniers mois de « manipes » lorsque les enzymes m'obligeaient à monopoliser beaucoup de matériel à la fois. Leur gentillesse, patience, enthousiasme et fous rires ont aussi été appréciés au cours du temps. Plus particulièrement, j'ai eu la chance de voir apparaître des « rayons de soleil » au cours de ma thèse, Charlotte, Camille et Dan pendant la 2$^{e}$ année, puis Silvia pendant la 3$^{e}$. Je suis vraiment heureuse qu'ils aient été présents car je n'aurais pas vécu ma thèse de la même façon sans eux, je les remercie tout simplement pour leur amitié.*
*Je remercie aussi Aurélien pour tout son soutien, sa présence m'a également été précieuse, et son départ fort regretté.*

*Je remercie le Dr. Christophe Schatz pour sa formation théorique et pratique à la diffusion de lumière et mesure de potentiel zéta (notamment au Malvern). Merci à Nicolas Guidolin pour les analyses GPC, Emmanuel Ibarboure pour la DSC et la TGA et le Dr. Jean-François Le Meins pour les mesures de rhéologie.*

*Je remercie également le pôle administratif et technique, Corinne Gonçalvès, Michèle Schappacher, Catherine Roulinat, Bernadette Guillabert et Nicole Gabriel pour leur aide au fil du temps, nous ne pourrions travailler sans elles.*

*I would also thank all the people that I met when working in Nijmegen particularly in the van Hest group (Ruud of course, but also Britta, Morten, Mark, Marlies, Sanne, Matthijs, David, Nanda, etc), and in the Huck group (Emilien whom I particularly thank for helping me settle in in the Netherlands at first, but also Maike, Aigars, who spent quite some time showing me how to use their spinning disk optimally, Julian whom I particularly thank for showing me his imaging chambers, Venkat, Sonia, Yujie, etc) and Henri from the Rutjes group. It was great to feel welcome and I thank them all for making my stay a great one, even though a busy one, and for sharing their experience and knowledge with me.*

*Je remercie également l'ensemble de mes collègues du LCPO, qui est un laboratoire où il fait bon vivre et travailler, c'est aussi grâce à eux. Donc merci à Bertrand, Antoine, Jean, Chantal, Stéphane, Célia, Maud, Lise, Paul, Thomas, Winnie, etc, etc.*

*Et pour finir j'aimerais remercier mes proches. Il me semble que c'est une tâche difficile et ingrate que d'accompagner un thésard et pourtant leur rôle, leur soutien et amour jour après jour, est loin d'avoir été négligeable quant au bon déroulement de ma thèse.*

*Je remercie mes formidables parents,* ***Maryse*** *et* ***Alain****, qui ont toujours TOUT fait pour moi, qui m'ont appris à ne jamais baisser les bras, le goût de la performance et de l'effort récompensé. Je les remercie de m'avoir soutenue au cours de mes études, et particulièrement durant ma thèse. Il n'y pas de mots assez forts pour les remercier de tout ce qu'ils font pour moi, de tout ce qu'ils ont été, depuis le jour de ma naissance. Ce manuscrit n'existerait pas sans eux non plus.*

*Enfin, je remercie* ***Guillaume,*** *pour son soutien et sa compréhension indéfectibles et inconditionnels durant ces 3 années. Je le remercie d'avoir été le premier lecteur de mes posters, de m'avoir écoutée répéter avant chaque présentation, et d'avoir accepté la place que ma thèse a occupé dans mon esprit et dans ma vie durant ces 3 années. Merci d'avoir toujours été là pour moi, grâce à toi je suis restée forte jour après jour, je ne l'oublierai jamais.*

*Merci à tous,*

*Le 2 janvier 2013,*
*Maïté*

Ce travail a été realisé au:

**L**aboratoire de **C**himie des **P**olymères **O**rganiques
Unité mixte de Recherche 5629 Université de Bordeaux/CNRS
Ecole Nationale Supérieure de Chimie, de Biologie et de Physique/
Institut Polytechnique de Bordeaux
16, avenue Pey-Berland
33607 Pessac Cedex
France

**Résumé étendu**

Le challenge de ce projet de thèse résidait en la formation contrôlée de mimes structuraux de cellules eukaryotes, grâce à des polymersomes et des matériaux polymères en général. Tout d'abord, une méthode de préparation adéquate devait être pensée et développée. Ensuite, cette méthode a permis l'élaboration des objets désirés ainsi que l'établissement des diverses preuves de concept, grâce aux outils de caractérisation appropriés. Enfin, la maîtrise des outils de formulation a permis d'étendre le projet au-delà du mimétisme structural, au mimétisme fonctionnel, avec l'incorporation de réactions enzymatiques en cascade, confinées *in situ* dans les mimes structuraux.

La stratégie repose sur une formation par lot (batch) en deux étapes (**Chapitre 2**) ; tout d'abord des polymersomes nanométriques de poly(triméthylène carbonate)-*b*-poly(L-acide glutamique) (PTMC-*b*-PGA) biodégradable, sont formées par nanoprécipitation, comme développé précédemment au laboratoire. Puis, ils sont encapsulés dans des vésicules micrométriques (géantes) de poly(butadiène)-*b*-poly(ethylène oxide) (PB-*b*-PEO) pendant l'assemblage de ceux-ci par la méthode d'émulsion-centrifugation. Cette méthode est basée sur une émulsion inverse (la suspension aqueuse des polymersomes internes nanométriques de PTMC-*b*-PGA constituant les gouttes d'eau), ce qui laisse supposer une efficacité d'encapsulation de 100%, ainsi que le groupe de Weitz, à Harvard l'a démontré. Le copolymère à bloc PB-*b*-PEO est dissous dans la phase organique et stabilise les gouttes d'émulsion à l'interface (constituant ainsi le feuillet interne de la bicouche polymère finale des vésicules). Une petite fraction de cette émulsion inverse est ensuite versée au-dessus d'une interface solution organique/eau. Dans une dernière étape, la force centrifuge force les gouttes à traverser l'interface et à être enveloppées par un second feuillet de copolymère à bloc amphiphile de PB-*b*-PEO, donnant ainsi lieu aux polymersomes géants attendus. Grâce à la maîtrise offerte par ce procédé, la structure des polymersomes multicompartimentalisés ou de «polymersomes dans des polymersomes» (PiPs) a pu être validée par des marquages fluorophores spécifiques et par microscopie confocale à disque rotatif (spinning disk) ; les tailles des diverses vésicules ont en effet été choisies pour être visible par cette technique. Nous avons ainsi pu obtenir un film où des polymersomes nanométriques rouge fluorescents sont en effet visiblement en mouvement dans la cavité du polymersome géant vert fluorescent[1]. Le mouvement 2D de ces mimes structuraux d'organelles a été suivie dans ce film, ce qui a permis de confirmer qu'il restait Brownien (étant donné que le mouvement reste isotrope et que les données respectent une distribution gaussienne, aléatoire) dans la cavité de

[1] Movie s1, http://onlinelibrary.wiley.com/doi/10.1002/anie.201106410/suppinfo

ce polymersome d'à peu près 20 µm. Par ailleurs, le rayon hydrodynamique et le coefficient de diffusion de ces vésicules internes nanométriques étaient les mêmes, avant encapsulation par diffusion dynamique de la lumière, et après, par cette méthode de suivi du mouvement particulaire. Ces résultats prouvent la validité de cette étude de suivi et confirme que le mouvement des vésicules n'a pas été perturbé par leur encapsulation. En ce qui concerne le biomimétisme cellulaire, le confinement dans le cytoplasme joue un rôle important pour l'activité et la régulation des cellules. Bien sûr, il y a certainement de nombreuses propriétés intéressantes découlant de la présence d'un mime cytoplasmique; la première réside dans une meilleure protection et donc stabilité mécanique et intégrité de forme, par absorption de stress mécanique. Le très complexe cytosquelette n'est pas simple à mimer, puisqu'il est composé de filaments protéiques d'actine, de microtubules et de filaments intermédiaires formés par nucléation-élongation. La croissance des filaments protéiques du cytosquelette est due à des interactions non covalentes, avec des procédés d'association/dissociation permanents et ce qui les rend dynamiques. En plus des propriétés mécaniques évidentes conférées par le cytosquelette à la cellule, les concentrations intracellulaires fort élevées en macromolécules sont la cause d'un effet nommé «encombrement (crowding) macromoléculaire». En 2001, R.J.Ellis a ainsi enjoint la communauté scientifique des biochimistes à arrêter de négliger cet effet pour leurs études, qui correspond à l'effet bien connu du volume exclu en science des polymères. Globalement les macromolécules du cytoplasme, cytosquelette et des compartiments internes représentent 20 à 30 vol.% d'une cellule, générant ainsi une forte répulsion stérique entre elles. Les conséquences sur la machinerie cellulaire avaient en effet rarement été prises en compte ; la plupart des réactions chimiques sont par exemple étudiées en solution diluée (idéale), alors que pour une cellule, il faudrait prendre en considération les coefficients d'activité pour les études cinétiques et thermodynamiques. Afin de répondre à ce problème, une suspension de polymersomes internes nanométriques de PTMC-*b*-PGA a cette fois été co-encapsulée avec des solutions d'alginate et de dextrane très concentrées, grâce au procédé d'émulsion-centrifugation. Là encore, les structures finales ont été filmées en microscopie confocale et le mouvement des vésicules internes a été suivi et analysé. Leur mouvement est ralenti de manière efficace comme le confirme un coefficient de diffusion 6.6 fois plus petit. De plus, la concentration de travail en polysaccharide dextrane de 300 mg/mL génère une viscosité au-delà de 0.01 Pa.s, dans la gamme de viscosité du cytoplasme des globules rouges, une fraction volumique proche de 30% et une pression osmotique au-delà de 1 MPa, conditions reproduisant l'effet d'encombrement macromoléculaire des protéines cellulaires. Etant donné l'importance de cet effet sur la machinerie cellulaire, nous pensons ainsi avoir créé un mime de cytoplasme approprié avec cette approche synthétique extrêmement simplifiée. Jusque là étaient parues des publications concernant séparément des

structures de liposomes dans des liposomes, des mimes cytoplasmiques dans des vésicules lipidiques ou polymères, ou dans des capsules LbL, et même des capsules dans une capsule en présence d'un mime cytoplasmique (voir **Chapitre 1**). Cependant, il nous semble que la combinaison des deux types de mimes, n'avait jamais été signalée jusqu'à maintenant dans des structures entièrement polymersomes.

Dans le **Chapitre 3**, nous étudions les avantages en termes d'applications, qui résultent de telles structures multicompartimentalisées pour la vectorisation d'actifs et la recherche biomédicale en général.

En principe, une telle structure devrait présenter un grand intérêt pour la délivrance de multiples actifs. Pour répondre à cette problématique, un mélange de deux suspensions différentes de vésicules PTMC-*b*-PGA (marquées respectivement avec des fluorophores rouges et verts) a été encapsulé dans une géante. Les deux types de polymersomes nanométriques sont clairement localisés dans la même vésicule micrométrique[2]. Tant que les suspensions de polymersomes internes sont assez concentrées, on peut potentiellement encapsuler bien plus que deux suspensions.

Pour finir, nous avons pu complexifier encore ce system en co-encapsulant un polymère de forte molaire et fluorescent, du FITC-dextrane, avec une suspension de vésicules internes marquées par des flurophores rouges. Comme le FITC-dextran fluoresce dans le vert, la membrane externe a cette fois été marquée par un fluorophore bleu, permettant d'imager séparément les vésicules géantes (bleues), les vésicules internes nanométriques (rouges) et le dextrane emplissant la cavité géante (vert). Une telle encapsulation dans trois compartiments différents, n'a jamais été signalée auparavant à notre connaissance, en particulier dans des vésicules polymères. Ces stratégies d'encapsulation multiple ouvrent la voie pour des applications futures en vectorisation multiple simultanée. Ceci est particulièrement important pour l'oncologie entre autres, avec l'encapsulation donc la délivrance potentielle de divers principes actifs, même incompatibles, dans un vecteur plus grand : cela rend ainsi possible une concentration délivrée assez élevée en principe actif pour avoir une réponse thérapeutique importante et synergétique (cf cocktails de principes actifs en oncologie).

Dans une approche de libération contrôlée et prolongée en vectorisation, nous avons pu mener à bien une étude *in vitro* de libération du principe actif anticancéreux doxorubicine encapsulé dans les vésicules nanométriques. Comme l'on pouvait s'y attendre, les cinétiques de libération étaient significativement ralenties lorsque les vésicules nanométriques étaient protégées par une couche supplémentaire de membrane polymère de PB-*b*-PEO, donc par une barrière de diffusion supplémentaire *in fine*. Dans le dernier cas, la perméation de la doxorubicine par les membranes polymères, induite par un gradient chimique dû au montage

[2] Movie s3, http://onlinelibrary.wiley.com/doi/10.1002/anie.201106410/suppinfo

de libération, ne pouvait que prendre plus de temps. En représentant les données avec une loi établie par Peppas et Ritger et en extrayant les constantes cinétiques k pour chaque système, nous avons même pu déterminer de façon quantitative que la vitesse de libération était à peu près deux fois (≈2.3) plus lente avec cette barrière de diffusion supplémentaire. Cette multicompartimentalisation, et en particulier cette membrane additionnelle nous a donc permis de démontrer les propriétés suivantes qui en découlent : un meilleur contrôle des cinétiques de libération grâce à une modulation de la perméabilité globale donc également théoriquement une meilleure protection des actifs encapsulés. De plus, de par leur nature polymère, ces deux membranes successives pourraient être pensées de telle sorte à avoir des stabilités spécifiques, différentes, et être désassemblées dans des milieux différents, de manière orthogonale. De telles conceptions sont vitales pour répondre à des moyens de délivrance nouveaux et stimulants, autre que l'injection intraveineuse classique en nanomédecine ; la délivrance transcutanée et l'administration orale pourraient en effet répondre à des grandes attentes en vectorisation et oncologie. Notre stratégie constitue donc une approche facile et présente de nouvelles opportunités pour l'utilisation de ces polymersomes dans le biomédical ou en cosmétique, où l'encapsulation d'ingrédients multiples, différents, et fragiles est parfois requise, avec des conditions de libération spécifiques à chaque membrane.

Une telle structure pourrait aussi impacter la façon dont une réaction chimique est pensée, ou induite dès le mélange de différents composés (confinés dans des compartiments internés) relargués sur commande. Dans un dernier chapitre **(Chapitre 4)**, nous avons donc cherché à remplacer dans nos mimes cellulaires, nos mimes structuraux d'organelles par des mimes fonctionnels, dans lesquels des réactions enzymatiques se produisent. Choisir des réactions enzymatiques complexes au lieu de réactions chimiques plus classiques, était pertinent dans une problématique de thèse portant sur le Biomimétisme cellulaire, et également par rapport au contexte de « Chimie verte » développé au laboratoire. En effet, dans les environnements confinés, et macromoléculairement encombrés d'une cellule, les réactions ne se passent pas comme en solution diluée (idéale). Nous avons voulu répondre à cela en produisant un modèle cellulaire adéquat, allant d'un Biomimétisme cellulaire structural à fonctionnel.

Une réaction en cascade à trois enzymes (encapsulées dans trois populations de polymersomes nanométriques différents) a donc été élaborée en collaboration le groupe du Professeur J. van Hest. L'objectif final consistait à encapsuler le mélange réactionnel (nanoréacteurs, substrat et cofacteurs enzymatiques) dans les vésicules de PB-*b*-PEO, en démarrant idéalement la réaction par «décageage» d'un substrat photocagé (illumination laser avec microscopie confocale), et en suivant l'augmentation attendue d'intensité de fluorescence du produit final fluorescent. Ce chapitre se concentre principalement sur

l'optimisation de la cascade complexe des nanoréacteurs ; en effet ces organelles artificielles, ces mimes fonctionnels constitués de polymersomes de poly(styrene)-*b*-poly(L-isocyanoalanine (2-thiophen-3-yl-ethyl) amide) PS-*b*-PIAT encapsulant des enzymes et dont la membrane possède une porosité intrinsèque, ont besoin de communiquer entre eux dans les bons rapports de concentration pour une réaction optimale. Cette étape s'est en effet révélée très complexe et problématique au regard de notre objectif final. Malgré cela, nous avons été en mesure de fournir une preuve de concept convaincante : en observant les mimes cellulaires fonctionnels par microscopie confocale, à partir d'une réaction démarrée avec un substrat non cagé, une fluorescence rouge était détectable après quelques heures seulement. Ce projet ambitieux n'en est cependant pour l'heure qu'à ses débuts et de plus amples études sont nécessaires. Maîtriser des réactions à partir de volumes de l'ordre de l'attolitre constitue certainement un challenge pouvant susciter un grand intérêt dans les développements industriels à long terme (notamment en terme de production biotechnologique, s'il s'agit de réactifs fragiles, chers, polluants, *etc*). De telles études ne peuvent donc qu'ouvrir des perspectives nouvelles en biotechnologie et dans la création de cellules artificielles thérapeutiques ou de thérapies complexes. De tels systèmes peuvent également contribuer à une meilleure compréhension par l'Homme de l'une des plus belles et des plus complexes créations de la Nature, la cellule biologique eukaryote.

**Abbreviations**

ABTS : 2,2′-azinobis(3-ethylbenzothiazoline- 6-sulfonic acid)
ADP : Adenine Diphoshpate
ATP : Adenonisine-5'-triphosphate
BR : bacteriorhodopsin
BVMO : Baeyer Villager monoxygenase
$CaCl_2$ : calcium chloride
$CaCO_3$ : calcium carbonate $CHCl_3$ : Chloroform
CALB : Candida Antartica lipase B
CL : caprolactone
CLSM : Confocal Laser Scanning Microscopy
Cy5-IgG : cyanine 5-Immunoglobuline G
Da : Dalton, g/mol
DDL : 12-dodecanolactone
DLS : dynamic light scattering
dex-HEMA : a dextran-hydroxylethylmethacrylate
DIC : differential interference contrast
DIPEA : N,N-Diisopropylethylamine
DMAEMA : dimethylaminoethyl methacrylate
DMF : Dimethylformamide
DMSO : Dimethyl sulfoxides
EDTA : Ethylenediaminetetraacetic acid
EE : encapsulation efficiency
FCS : Fluorescence Correlation Spectroscopy
FITC : Fluorescein isothiocyanate
FL : fluorescence lifetime
G6PDH : Glucose-6-phosphate dehydrogenase
GFP : Green fluorescent protein
GOX/GOD : glucose oxidase
GSH : glutathione
GSSG : glutathione disulfide
$H_2O_2$ : hydrogen peroxide
HRP : horseradish peroxidase
LbL : layer-by-layer
LCST : Lower critical solubility temperature
LPO : lactoperoxidase
Method A : Film rehydration, then extrusion
Method B : SD with redispersed lyophilized powder of a first nanoprecipitation
$M_n$ : Number average molecular weight
MWCO: Molecular weight cutoff
$Na_2CO_3$ : sodium carbonate
$NADP^+$ : β-Nicotinamide adenine dinucleotide phosphate hydrate

NADPH : nicotinamide adenine nucleotide (phosphate)
OL : 8-octanolactone
PAA : poly(acrylic acid)
PAMO : phenylacetone monoxygenase
PAs : Peptide Amphiphiles
PB-*b*-PEO : polybutadiene-*b*-poly(ethylene oxide)
PDMEAEM : poly(diethylamino ethyl methacrylate)
PEDOT : poly(ethylene dioxythiophene)
PEG : poly(ethylene glycol)
PEG-*b*-PDLLA : poly(ethylene glycol)-*b*- poly(*D,L*-lactide)
PEG-*b*-PLA : poly(ethylene glycol)-*b*-poly(lactic acid)
PMOXA-*b*-PDMS-*b*-PMOXA : poly(2-methyloxazoline)-*b*-poly(dimethylsiloxane)-*b*-poly(2-methyloxazoline)
PNIPAAm : poly(*N*-isopropylacrylamide)
POD : peroxidase
Poly(AAc-*co*- DSA) : poly(acrylic acid-*co*-distearin acrylate)
poly(propylene sulfide) blocks of PEG-*b*-PPS-*b*-PEG
PS-*b*-PIAT : poly(styrene)-*b*-poly(L-isocyanoalanine (2-thiophen-3-yl-ethyl) amide)
PSS : poly(sodium 4-styrene sulfonate)
PTMC-*b*-PBLG : poly(trimethylene carbonate)-*b*-(γ-benzyl-L-glutamate)
PTMC-*b*-PGA : poly(trimethylene carbonate)-*b*-poly($_{L}$-glutamic acid)
ROS : reactive oxygen species
$R_a$ : Radius of alginate chains
$R_v$ : Radius of PTMC-*b*-PGA nanosize vesicles
SD : Solvent displacement or nanoprecipitation
SDS-PAGE : sodium dodecyl sulfate-polyacrylamide gel electrophoresis
SOD : super oxide dismutase
TCDD : 4,7,10-tetraoxyacyclotetradecane-11,14-dione
TEM : Transmission electron micrography
THF : Tetrahydrofuran
TMB : 3,3',5,5'-tetramethylbenzidine
TRFA : time-resolved fluorescence anisotropy
Tris : tris(hydroxylmethyl)aminomethane
$T_t$ : relevant lipid-phase transition temperatures
TvNH *: Trypanosoma vivax*

# Table of Contents

# General introduction

Nanomedicine is the application of nanotechnology in medicine with the aim of developing especially drug delivery, diagnostic and therapeutic tools. To be more precise, according to a Forward Look Report on Nanomedicine[1] published by the European Science Foundation, nanomedicine aims at "ensuring the comprehensive monitoring, control, construction, repair, defense and improvement of all human biological systems, working from the molecular level using engineered devices and nanostructures, ultimately to achieve medical benefit."
Ultimately, estimated 130 nanotechnology-based drugs and delivery systems are currently being developed worldwide.[2] A number of crucial issues related to toxicity and environmental impact of nanoscale materials will however have to be solved before regulatory agencies can approve further products for sure. This field is only blooming yet; it was born in academia where it is currently in its golden age, before interesting industries not that long ago.[2] Indeed, liposomes that have been discovered by the scientist Bangham in the middle of the sixties,[3, 4] are only available today under five different commercial pharmaceutical formulations for cancer therapy (Myocet™, Doxil™/Caelyx™, LipoDox™, Lipoplatin™). However, if enough time and funding is devoted to this area, who knows how tremendous the results, success stories, and the size of resulting industrial markets may become.[1]

This PhD project was related more particularly to the subfield of **drug delivery polymeric nanomaterials**, a research specialty of the laboratory. Most of existing strategies are based upon organic or inorganic nanoparticles encapsulating contrast agents for detection, diagnosis and/or delivery of therapeutic actives for severe diseases. The group Polymer Nanotechnology and Life Sciences in which this work was conducted, is specialized in the design of amphiphilic block copolymers (i.e. with a hydrophilic and a hydrophobic block) able to self-assemble in polymer vesicles in water (non-solvent for the hydrophobic block). Such polymeric structures, discovered in the late 90's have been coined "polymersomes"[5] by structural analogy with liposomes. The membrane of these vesicles generally is a bilayer of assembled amphiphilic copolymers, enclosing a water pool, thus protected from the external aqueous solution. Ever since their discovery, many research groups over the world found interest in polymersomes because of their high mechanical and colloidal stability, and their potential ability to control the loading properties and release kinetics of different species. These delivery vectors may be of particular appeal for the Biomedical, Pharmaceutical and Cosmetic fields. Indeed, various formulation processes enable to get sizes ranging from 100

nm to 100 µm, whilst loading various (bio)molecules, like therapeutic drugs, both in the hydrophilic lumen and simultaneously in the hydrophobic membrane.[6-11] It is their macromolecular nature that confers them a thicker membrane, partly responsible for this high colloidal stability and high hydrophobic molecule loading capability (as hydrophobic components will go in the hydrophobic membrane). Furthermore, as for liposomes, between other delivery vectors, it is possible to functionalize their surface with ligands targeting a specific diseased organ or cell. This should enable a selective accumulation of polymersomes in targeted tissues (such as tumors or inflammatory sites), to locally increase drug payload thus treatment efficacy, while decreasing side effects due to intrinsic drug toxicity.[12] The main idea of drug delivery is indeed to improve bioavailability, which is a current challenge for pharmaceutical industries. The bioavailability represents the fraction of an active that will really be available *in vivo*, go where needed and used *in vivo* as intended. On top of the fact they can target specific locations, this is made possible by the typical sizes (in the range of hundred of nanometers) of drug delivery nanomaterials that allow them to be injected intravenously (the most efficient way, as 100% of active goes directly in blood circulation) on one hand. On the other hand, this drug delivery vectors or carriers can also be functionalized to be "invisible" to the immune system seeking to clear them from blood circulation (they are then called "stealth", which is traditionally reached by decorating them with hydrophilic polymer chains, mostly poly(ethylene oxide) chains). Going further, the concept of "smart", in other words, stimuli-responsive, materials has been launched a few years ago, enabling polymer-based materials to achieve their full potential. The goal is to reach a better control on the release properties of an active molecule by using polymers designed to respond to various stimuli (pH, temperature, ions,…) by a variation in behavior (mechanical, solubility, conformation, …).[7]

This PhD project was also strongly related to another research area, **Biomimicry**. The idea is to find inspiration in Nature (bio-inspiration), in biological existing systems that demonstrate attractive properties, to study the structure/property relationships enabling those attractive properties and with this new knowledge, to transfer them to technological reality. This should enable new methods, or synthesis pathways, or the design of new biomimetic materials, improved compared to already existing non biomimetic materials. The most ancient and known example, is the lotus leave, which presents a particular surface in terms of structure, conferring it a super hydrophobicity; water glides off of it. This concept has been applied to industrial applications, the first of them being Lotusan™, a self-cleaning paint. Related to the biomedical field, liposomes have been ascribed as biomimetic as their phospholipidic

membrane resembles that of the biological cell. The structure of polymersomes as for them, has been described as resembling that of viral capsids,[13, 14] highly efficient thus interesting biological systems.

For this PhD project, the main objective was to achieve the formation of materials mimicking the structure of a cell, one of Nature's most complex designs, able of a level of control and computing irreproducible with our current technologies. We wanted to push the borders from Biomimicry one step further, from the structural virus mimic (classic single polymersome) to a **structural eukaryotic cell-like system, eukaryotic cell mimic**. Briefly, a eukaryotic cell is made of an outer cellular membrane, in part constituting of phospholipids, enclosing and protecting a very complex system and machinery described as the "cytoplasm". Some of the components of the cytoplasm are various inner compartments also called organelles (the organelle is to the cell what the organs are to the body, examples being mitochondria, golgi apparatus, chloroplasts, *etc*). These organelles are hosting thousands of interactions and reactions essential to cells' every day life, protecting with their membrane their confined contents from the cytoplasm, or oppositely. Such a structure is hence described as **multicompartmentalized**. For clarity, in this manuscript the word cytoplasm refers to the intracellular compartment lacking organelles. Going further, these organelles are in their turn enclosed in the cytoplasm, that we will summarize by two components, the cytoskeleton and the cytosol. The ordered and dynamic one-dimensional supramolecular assembly defining the cytoskeleton, plays an important role in the way a cell functions. Long ordered filaments of protein monomers form and depolymerize (reversible phenomenon) dynamically for vital cell functions; allowing cell migration, attachment and division, and even serves as highway for internal transport of molecules to specific compartments. The cytosol plays also an important part in the cell's life; intracellular macromolecular crowding, confinement and adsorption between individual macromolecules and their immediate surroundings in the cellular interior, are inherent properties of biological systems, influencing of course everything occurring in them. More basically and globally, the cytoplasm confers the cell a certain mechanical robustness.

A structural mimic of such complex structure represents a scientific and technologic challenge, in terms of control over physical chemistry, stabilization of interfaces and formulation. Another fundamental justification of such a challenge lies in the generation of more accurate artificial cell models (more or less elaborate) that could provide a better understanding of the complex cell machinery. A cell is indeed a very peculiar system with a complex intracellular content, which is why it may be relevant to work on the closest possible

model in order to better study what happens in it (in terms of equilibria and rates of reactions for examples instead as opposed to studying them in dilute (ideal) solutions. On the other hand, a complete understanding of cell function was not yet accomplished, which is why synthetic models can help to get a better comprehension as they allow to dissociate parameters closely correlated in nature.[15] Furthermore, the sole building of such models is also relevant in that perspective, after all as Feynman used to say, "what I cannot create, I do not understand".[15, 16]

Finally, by mimicking Nature, and building biomimetic materials, we should get access to a whole new range of properties. Some of them will be illustrated throughout this manuscript. Such concrete industrial applications can only arise once proofs of concept have been established through controlled lab-scale production.

The choice of polymersomes and polymer-based materials in general, to achieve such structures is motivated by the fact that the state of the art in block copolymer synthesis allows a perfect control over molar masses, generating a better mechanical properties' tuning and self-assembly properties and formation. Moreover, their polymeric nature can or will eventually in further projects, enable specific design for specific targeting (*via* facile functionalization) or release upon trigger.

The design strategy to reach the desired cell-mimicking, multicompartmentalized structure, involved the ability to afterwards prove the structure. Hence, we decided to make both kinds of vesicles, inner and outer, large enough to be visible by confocal microscopy. The choice of confocal microscopy particularly, is motivated by the fact it represents a slice of the object, a thin confocal volume, which enables to prove the inner polymersomes actually are in the volume of the outer one. Another important risk to solve lied in quantitative encapsulation of hydrophilic solutions. Indeed, we needed at least one polymersome (organelle mimic) in another polymersome (outer cell membrane mimic), as well as introducing a massive viscosification or gelation in the lumen of the outer polymersome (cytoplasm mimic). To address this challenge, the safe, maybe the only option, lies in using emulsion-based processes. Initially, we planned to work with microfluidics. However, microfluidics involve several issues still needing to be solved before high throughput production of polymersomes can be achieved, the most important being the elimination of organic solvent from the vesicles. It is also rather time-consuming and needs quite a lot of inner hydrophilic solution to load (which may be problematic if containing rare components, like expensive enzymes, actives, etc). The method we finally chose for the second step, loading of inner polymersomes

into outer polymersomes *via* their formation by a process called emulsion-centrifugation, seemed us the safer and the better option.

After the success of this formation had been assessed with poly(butadiene)-*b*-poly(ethylene oxide) PB-*b*-PEO, we were planning to use the biodegradable synthesized poly(trimethylene carbonate)-*b*-poly(ethylene oxide). This proved however to be impossible which is why we decided to work throughout the project with the model PB-*b*-PEG, enough in itself for the proof of concepts we wanted to establish. Finally, in collaboration with the van Hest group in the Netherlands, we were able to investigate one of the possibilities arising from this multicompartmentalization, coming again closer to the eukaryotic cell; the conduction of enzymatic reactions (cellular function) in polymersomes in a polymersome, combination of structural and functional/metabolic cell mimicry.

This PhD manuscript is organized in four chapters. The first is a state of the art of polymeric structural and or functional cell mimics, with a special focus on polymersomes. The second chapter presents the method to reach our structural cell mimics, thoroughly assessed. The third chapter presents some applications of these cell mimics in drug delivery, particularly multiple simultaneous loading (hence future multiple delivery) and controlled, sustained drug release due to permeability tuning. Finally, the fourth chapter presents a tentative work about enzymatic reactions in the multicompartmentalized scaffold, with a special focus on the difficult development of the single inner polymersome reactors. In a last chapter, we will conclude on this PhD work and offer perspectives for future developments.

---

1. http://www.esf.org/publication/214/Nanomedicine.pdf.
2. *Nat Mater* **2006,** *5* (4), 243-243.
3. Bangham, A. D.; Horne, R. W., *Journal of Molecular Biology* **1964,** *8* (5), 660-IN10.
4. Bangham, A. D.; Standish, M. M.; Watkins, J. C., *Journal of Molecular Biology* **1965,** *13* (1), 238-IN27.
5. Discher, D. E.; Eisenberg, A., *Science* **2002,** *297* (5583), 967-973.
6. Upadhyay, K. K.; Agrawal, H. G.; Upadhyay, C.; Schatz, C.; Le Meins, J. F.; Misra, A.; Lecommandoux, S., *Critical Reviews in Therapeutic Drug Carrier Systems* **2009,** *26* (2), 157-205.
7. Peer, D.; Karp, J. M.; Hong, S.; Farokhzad, O. C.; Margalit, R.; Langer, R., *Nature Nanotechnology* **2007,** *2* (12), 751-760.
8. Rodríguez-Hernández, J.; Lecommandoux, S., *Journal of the American Chemical Society* **2005,** *127* (7), 2026-2027.
9. Sanson, C.; Schatz, C.; Le Meins, J. F.; Brûlet, A.; Soum, A.; Lecommandoux, S., *Langmuir* **2010,** *26* (4), 2751-2760.
10. Li, M. H.; Keller, P., *Soft Matter* **2009,** *5* (5), 927-937.

11. Du, J.; O'Reilly, R. K., *Soft Matter* **2009,** *5* (19), 3544-3561.
12. Kumar Upadhyay, K.; Le Meins, J. F.; Misra, A.; Voisin, P.; Bouchaud, V.; Ibarboure, E.; Schatz, C.; Lecommandoux, S., *Biomacromolecules* **2009,** *10* (10), 2802-2808.
13. Ahmed, F.; Photos, P. J.; Discher, D. E., *Drug Development Research* **2006,** *67* (1), 4-14.
14. Schatz, C.; Louguet, S.; Meins, J. F. L.; Lecommandoux, S., *Angewandte Chemie - International Edition* **2009,** *48* (14), 2572-2575.
15. Brizard, A. M.; Van Esch, J. H., *Soft Matter* **2009,** *5* (7), 1320-1327.
16. Hawking, S., *The Universe in a Nutshell*. Bantam Books: New York, 2001.

# CHAPTER 1

# From single to multi-compartmentalized polymeric systems : towards cellular structure and function biomimicry

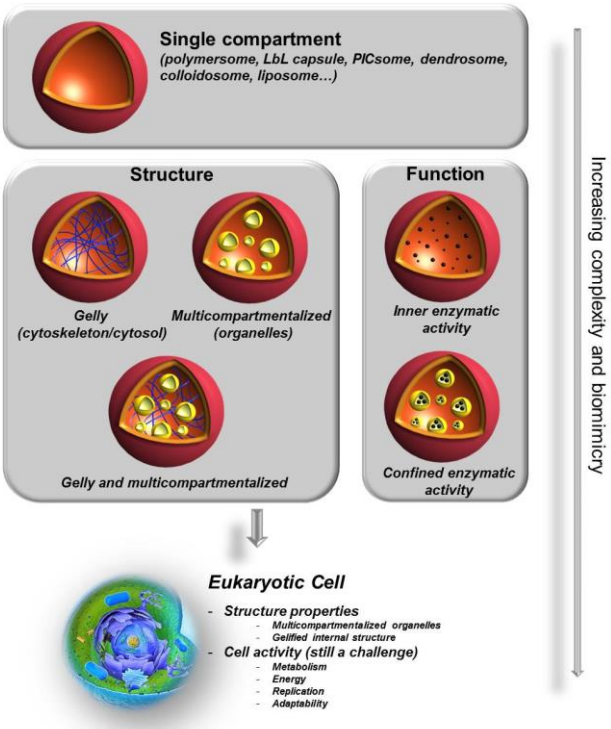

# 1. Introduction

How life arose from its prebiotic origins remains a deep mystery, possibly even one that Science will not be able to solve.[1, 2] In nature, the cell is the basic structural and functional unit of all known living organisms. The way we understand nowadays a living cell may be simplified as "a sack containing a number of reacting chemicals, studded with environmental sensors, allowing heat and certain chemicals to cross its walls".[3] The scientific community seems to agree upon a more precise definition of the cell as a "structure that is enclosed, self-replicating, energy dissipating and adaptive".[3] But which were the successive steps to get there? Synthetic biologists or protocell creationists[1] (proto from the ancient Greek "first") seek to build a minimally autonomous synthetic cell, coined minimal or artificial cell.[4] To reach this goal, the needed requirements to build minimal life have to be defined. Such a research should thus help to evaluate plausible scenarios of the origin of cellular life on the early Earth,[1, 5] which constitutes its first benefit or application. In a more concrete and industrial perspective, such engineered artificial minimal cells could open many prospects for therapy as biomedical devices[1, 5] (and even further, to test new artificial metabolisms[5]) and in biotechnology[1, 5], as bioreactors synthesizing pure proteins, only if at reasonable costs.

Materials scientists, and especially soft matter scientists, pursue other goals with other tools and disciplines and are highly excited by the relatively young field of biomimicry.[6] Biomimicry or biomimetics is "the study of the formation, structure, or function of biologically produced substances and materials (such as enzymes or silk) and biological mechanisms and processes (such as protein synthesis or photosynthesis) especially for the purpose of synthesizing similar products by artificial mechanisms which mimic natural ones".[7] Biomimetic materials science involves three steps:[8] 1) observing and studying mother Nature to understand structure-function relationships in natural systems that demonstrate attractive, inspirational properties, 2) extracting physical/chemical principles of these structure-function relationships by using theory and experiments to make them available as a concept useful in materials science and engineering, 3) developping new methods for the synthesis and the manufacturing of "biomimetic" materials based on these physical/chemical principles, which extend the scope of properties of existing non biomimetic materials,[9] taking into account the existing capabilities and constraints imposed by engineering and economy. To summarize, ***the idea is to borrow Nature's design strategies to achieve novel functional materials, with highly useful properties exceeding by far those available by current***

***methods***.[9] Finally, Antonietti *et al.*[10] quote another interesting definition: "Not to copy Biology: to learn in modesty from her principles and to transfer it to materials space and conditions previously not accessible to biology". To be more specific, butterfly wings, mollusk shells, bones, spider silk, gecko feet, plant cell walls, mussel byssi, Venus's Flower Basket, brittle star optics, and lotus leaves, are just some of the examples that have inspired materials scientists so far.[8] This field can naturally only exist at crossroads between materials science, chemistry, physics, biology, nanotechnology, and engineering. If we take a close look at the most complex machine there is, the cell, how could scientists not be challenged by it, not want to reproduce its perfection? How could researchers not be envious of what it is capable of and try to achieve the same formidable properties?

The present chapter focuses on cell biomimicry (Figure 1), i.e. the preparation of complex supramolecular assemblies from functional materials that mimic the structure and the function of a cell. As mentioned above, such high ordered structures are expected to bring new insights in biomedical applications as well as in biotechnology. As creation of such functional cell mimics can only be achieved step by step, we have to analyze which features are the most crucial. It is worth noting that cell mimics (i.e. biomimetic materials copying some of the features of a cell), as opposed to artificial minimally autonomous cells, do not require being living, highlighting the contrast of goals between biochemists (or synthetic biologists) and materials scientists. For materials scientists, the first and foremost challenge to address lies in the controlled formation of these cell mimics, which although non-living, will roughly approach the complexity and functionality of living cells.[11,2] Compartmentalization[12] is one of the key architectural principles of the cell.[11,13] The similarity found between prokaryote and single-compartment liposomes has already been extended to eukaryotes and synthetic multicompartment vesicular systems[11]. There is no life without compartmentalization and, as according to some of the leading theories, this process has even played a major role in the emergence of life.[14] In eukaryotic cells, organelles of various sizes, in a range of 10 nm to 500 nm (mitochondria, chloroplasts, golgi apparatus…), are visibly enclosed in the phospholidic cellular membrane.[12] Indeed, segregation of biomolecules in these compartments and their exchange through boundaries (thanks to selective transport processes) enable the exquisite control over metabolic reactions in space and time required for the proper functioning of cells. Inner compartmentalization also has some additional benefits for the eukaryotic cell: first, it allows each compartment to perform specific functions without interference from other cell functions due to confinement in various localizations; secondly, due to their confinement in various specific locations, it allows enzymes and substrates to reach higher concentrations

locally.[13] The second crucial aspect of life may lay in metabolism, "self-maintenance" or to be more accurate, self-maintaining chemical networks.[1,15] The metabolism is the set of chemical reactions that occur within the cell to sustain life. It is to note the boundary between "living" and "non-living" organisms (such as viruses) has long been defined by the possession of a metabolic system.[16] It is only thanks to multicompartmentalization and positional assembly that an eukaryotic cell is able to perform multiple, spatially separated, chemical processes simultaneously with high accuracy and specificity (every synthetic chemist's dream!).

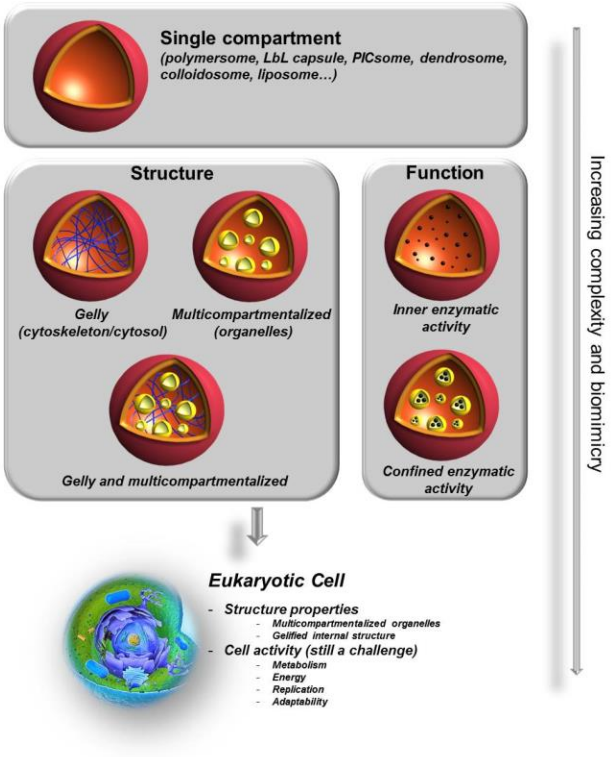


**Fig. 1** Eukaryotic cell biomimicry: towards cellular structure and function.

The choice of materials for building cell mimics is crucial. One safe option, often chosen for minimal cells, lies in liposomes, already considered as biomimetic due to their phospholipidic bilayer structure resembling that of biological cell membranes. More recently, many researchers started working with polymer-based materials. Indeed, the structural analogues of liposomes, coined "polymersomes"[17] have been proposed to better mimic the structural properties of viral capsids.[18, 19] Undeniably, their molar masses are much higher than those of phospholipids, which confers them an intrinsically thicker membrane, partly responsible for a much larger mechanical[16] and colloidal stability, and a lower permeability.[19] Therefore, polymer vesicles have been actively investigated in a perspective of drug delivery[20] (or as sensors, and nanoreactors[13, 21]) since their discovery in the late nineties', as they can load both hydrophilic (in their internal aqueous reservoir) and hydrophobic components (in their thick

membrane). In addition, the nature of each block can be carefully chosen to present a biodegradable behaviour[20, 22] or to respond to various stimuli,[20, 23] such as pH, temperature, ionic strength, *etc*. In the same way, they can be readily functionalized to target specific tissues or cells and provoke cellular internalization.[24] Finally, the latest techniques in block copolymer synthesis allow a perfect control over molar masses for a better mechanical properties' tuning, thus also an exquisite control on the self-assembly properties and formation of polymeric self-assembled supramolecular structures (as polymersomes for example)[20]. Once the generation of these cell mimics is controlled and optimized, material scientists should be able to take advantage of their structure to gain new properties and form completely innovative, with previously unmatched efficiency, soft materials.

Finally, from the most evident and fundamental point of view, mimics as model systems for molecular biologists and biochemists, enable to complement biological studies as they allow to study separately parameters closely correlated in Nature.[25,11] Quantitative measurements *in vivo* are currently still difficult to obtain. Freedom to change the parameters is so limited that one cannot investigate them completely for a given mechanism. Going further, a model which could enable the study of various cellular mechanisms coupled together, and help to understand how complexity is established step by step, would be of outmost relevance.

For all these reasons, this chapter aims at addressing specifically the field of eukaryotic cellular biomimicry, focusing on polymer-based materials, that can be considered as some of the most advanced and exciting systems designed over the last years. The first part focuses on recent developments to achieve in a controlled manner multicompartmentalized polymeric cell mimics, which is the first crucial hurdle from a physical-chemical point of view (***section 2* of this chapter**, see Figure 1). The second part presents enzymatic reactions confined in a single compartment to build organelle mimics, or even artificial organelles (***section 3* of this chapter**, see Figure 1). Finally, in order to reach the level of control presented by eukaryotic cells, the design of the first exciting systems presenting a multicompartmentalized enzymatic activity will be described (***section 4* of this chapter**, see Figure 1).

## 2. Structural eukaryotic cell mimicry

At some point, evolution led to multicompartmentalization by endosymbiosis (the emergence of the eukaryotic cells from prokaryotic cells). The mimicking of cellular structures using polymer-based building blocks is very recent but at the same time in strong development.[6] The mimicking of eukaryotic cellular structure will be presented in the following paragraphs.

It follows previous studies already published on surfactant-based vesicles and readers are encouraged to refer to reviews for an exhaustive description of these systems based on small molecules.[6, 11]

In addition, long ordered filaments of protein monomers forming the cytoskeleton, that polymerize and depolymerize in a reversible fashion, also dynamically control vital cell functions[26]; cell migration, attachment and division, and even internal transport of molecules to specific compartments.[27,28] Many experiments were designed to better understand how such motor proteins work together with the dynamic assembly and disassembly of actin filaments and microtubules to facilitate intracellular transport, organelle positioning, cell polarity, and motility. [16, 28 29] The cytosol plays also an important part: intracellular macromolecular crowding, confinement and adsorption are inherent properties of biological systems [30] The mimicking of these relevant cellular self-organized structural features mainly using polymer-based building blocks will be presented in the following paragraphs.

### 2.1 Multicompartmentalization: Mimicking organelles in cells.

Multicompartmentalization is a key principle of eukaryotic cells that distinguishes them from less evolved forms of life. Furthermore, once mimicked, the design of multicompartmentalized particles can bring unique properties and large benefits to the pharmaceutical field. At some point, evolution led to compartmentalization because a compartmentalized structure indeed offers multiple advantages that scientists should aim to seek for their synthetic materials. One of the most foreseeable lies of course in a better protection[31, 32] of the inner encapsulated actives that are often very fragile in the field of drug delivery. Furthemore, each compartment can be made of a different polymer material, enabling independent surface modification, control over extremely diverse functionalities, orthogonal disruption or degradation in specific environments for example.[12,33,41] As a result, the controlled formation of such highly ordered structures should also enable to design new vectors suitable for other methods of delivery than intravenous injection, such as transcutaneous[34] and oral administration systems [32, 33, 35], improving both the patient's compliance and the medical costs. Regarding intravenous injection, the traditional pathway for drug vectors, the challenge for multicompartmentalized systems would of course lie in respect of sub-micrometer range.

On another hand, each compartment can be independently loaded with a different drug, opening the door to development of novel anticancer cocktail-type drug delivery systems.[12,31]

Furthermore, Zasadzinski *and coll.*[36] first demonstrated a double membrane or barrier effect

in their liposomes in liposomes or "vesosomes". This proves drug delivery can be better controlled with compartmentalized systems because the permeability can be tuned more precisely; an active should in principle not be able to cross two or more successive barriers as fast as a single one.[33, 36] Compared to the developments of these lipid-based vesosomes, the field of multicompartmentalization is in its early stages regarding the use of polymeric materials. Multicompartmentalized systems based on polymers have been reported as early as 2000 by McPhail *et al.*[37] These authors designed a hybrid vesicle in vesicle system where the outer vesicle was made from a 2:1 weight ratio of polymer palmitoyl glycol chitosan and cholesterol. The inner vesicles were liposomes. Authors outline a potential application that we believe of outmost interest, namely one internal compartment bearing an enzyme, another one a prodrug, for site-specific activation. In a more recent approach, Nallani and coworkers[38] formed larger polymersomes of poly(styrene)-*b*-poly(L-isocyanoalanine (2-thiophen-3-yl-ethyl) amide) (PS-*b*-PIAT) by the solvent displacement method or nanoprecipitation using as an aqueous phase, a suspension of smaller polymersomes made of poly(2-methyloxazoline)-*b*-poly(dimethylsiloxane)-*b*-poly(2-methyloxazoline) (PMOXA-*b*-PDMS-*b*-PMOXA) already generated by film rehydration. However, the major drawback of this approach resides essentially in the poor encapsulation yield of nanoprecipitation. Indeed, transmission electron microscopy TEM of resulting suspensions enables to see single inner or outer polymersomes along with the desired multicompartmentalized inner in outer polymersomes. The presence of both kinds of single vesicles was established by time-resolved scanning confocal microscopy and encapsulation of green fluorescent GFP in the inner polymersome, and red fluorescent Cy5-IgG in the lumen of the outer ones (see Figure 2). Yellow spots should evidence co-localization or, in other words, the presence of multicompartmentalized vesicles.

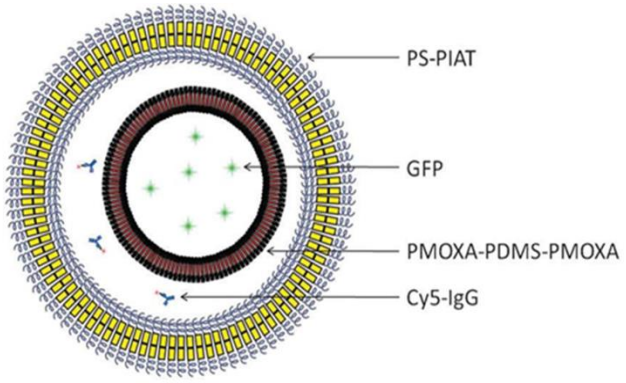


**Fig. 2** Schematic representation of a multicompartmentalized polymersome. The inner vesicle is made of PDMS-*b*-PMOXA-*b*-PDMS (ABA) block copolymers encapsulating green fluorescent proteins (GFPs), while the outer vesicle is made up of PS-*b*-PIAT block copolymers encapsulating the inner vesicle and cyanine-5 conjugated immunoglobulin G proteins (Cy5-IgG). Figure adapted from ref [38].

However, confocal acquisitions also showed numerous vesicles only green or red fluorescent, the fraction of multicompartmentalized vesicles being calculated as 45% by flow cytometry. To overcome this rather low efficiency, a powerful alternative lies in methods based on emulsions or double emulsions. Indeed, the concept of an emulsion is based on two immiscible fluids, thus a process based on emulsions involves in theory 100% encapsulation efficiency. Chiu *et al.*[39] therefore used two successive emulsions. Poly(AAc-*co*- DSA) poly(acrylic acid-*co*-distearin acrylate) polymersomes were formed by double emulsion using THF/$CHCl_3$ as organic phase, with varying volume ratios depending on desired target size (1- 15 µm).

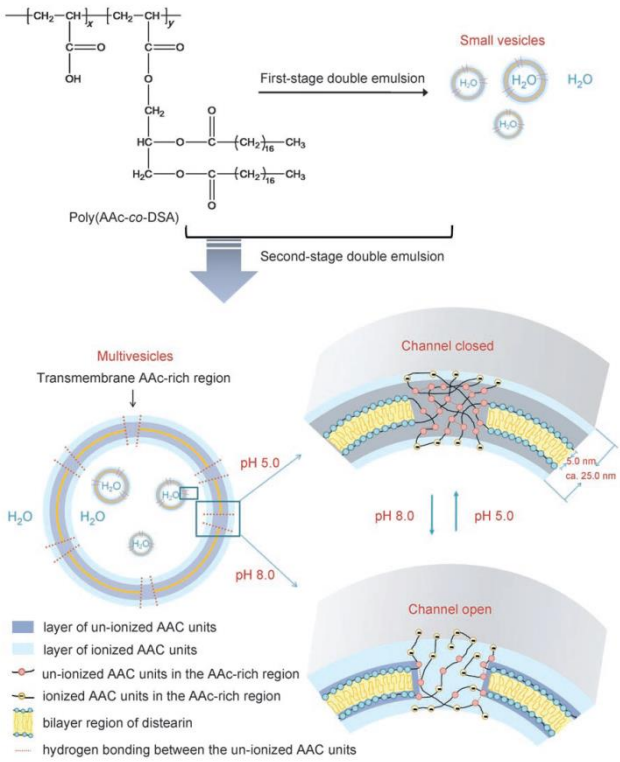


**Fig. 3** Illustration of multivesicle assemblies equipped with pH-responsive transmembrane channels from two-stage double emulsion of poly(AAc-*co*-DSA). The AAc-rich regions and the bilayer islets within the vesicle membrane are not drawn to scale. Scheme from ref [39].

The primary inverted emulsion ($w_1$/o) is first emulsified (with strong, thus potentially damaging, mechanical stirring input). It is then added to an excess of the same water phase ($w_2$=$w_1$ here) under stirring to get the final $w_1$/o/$w_2$ double emulsion. The vesicles can finally be formed after organic solvent evaporation. The water phase had to belong to a short pH range of 4 to 5.5 as a pH below 4 yielded large precipitates and above 5.5, micelles. To form multivesicular assemblies, the suspension of vesicles prepared as just described, was used as the first internal $w_1$ water phase of the primary inverted emulsion. Once the vesicles are formed, they can be further equipped with transmembrane channels depending on pH (Figure

3). Authors admit a lack of control in the number of encapsulated inner vesicles. Based on this process and the DIC (differential interference contrast) micrograph provided, one can expect a mixture of unilamellar and multilamellar membranes that may have different diffusion properties. Even though very original, such a method may not yield the most reproducible and homogeneous systems while being difficult to use on a daily basis.

That is why the recent developments by Weitz and coworkers of microfluidics to address this issue seems particularly promising. In a first step, they were able to control the formation of multicompartment polymersomes,[41] or aggregates of polymersomes, before yielding fully multicompartmentalized polymersomes (Figure 4).

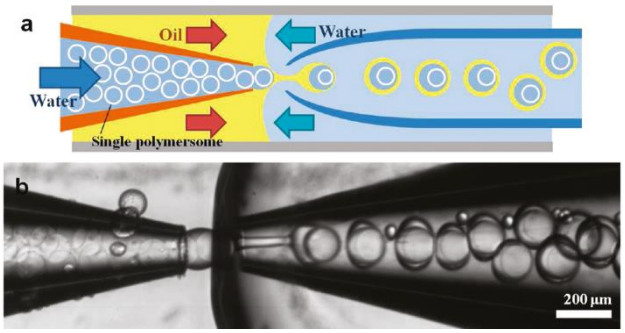


**Fig. 4** Schematic illustration of the microfluidic device for preparation of double polymersomes containing a single inner polymersome. (b) Optical microscope image showing injection of polymersomes into the innermost drops of double-emulsion drops, where the breakup of middle phase is triggered by the polymersomes. Figure from ref [40].

The principle is the same as just described, a sequential double emulsion formation leading to vesicles after elimination of organic solvent. The copolymer used was the biocompatible poly(ethylene glycol)-*b*-poly(lactic acid) (PEG-*b*-PLA). The number of inner polymersomes can be controlled by adjusting the size of the orifice of the collection capillary relative to the size of the polymersomes and the relative flow rates. Authors present "polymersomes-in-polymersome", also called "double polymersomes", with up to three different dye-loaded inner polymersomes. Weitz *and coll.* also proposed a programmed release of loaded species by using an external medium of water/ethanol 50/50 v.% and reinforcing depending on need, the polymersome bilayer with up to 50 wt.% hydrophobic homopolymer PLA. One could however make the hypothesis there is maybe just in total more mass of PLA to degrade before observing disassembly when comparing with classic polymersomes. Triple polymersomes or polymersome-in-polymersome-in-polymersome could also be prepared with this technique, resembling a set of three Russian dolls one in another. Finally, authors believe their systems to be promising for *in vivo* delivery of biomolecules such as growth factors. While they demonstrate a very nice *in vitro* proof of concept, *in vivo* circulation fluids cannot be reduced

or turned to water/ethanol (50/50 v.%). However size of particles is important for future biomedical development and will determine the mode of administration. While it is not problematic for the outer polymersomes to be micrometric for an oral administration, it would be preferable if the inner polymersomes (≈ 100 µm here) were in the nano-size range for such a scenario. For example, fully functional peptides and proteins, which are denatured by physiological conditions in the gastrointestinal tract,[42] have been reported to be taken up by Peyer's patches in the intestine when encapsulated in small liposomes, although only in very low concentrations.[43] To conclude, this approach presents the advantage of enabling a high level of control over the formed systems and is probably the most promising for the future large scale or industrial developments. Nevertheless, this method is rather tricky and several issues still need to be solved before achieving the high throughput production of polymersomes by microfluidics: possible coalescence of the internal and external aqueous phases, dewetting instability of the organic phase from the copolymer bilayer usually leading to excess polymer patched to the vesicles,[44] and unequal evaporation rate of solvents from the organic phase during the rather long drying step of the copolymer membranes with dramatic consequences on contact angles.[45,46]

Finally, Lecommandoux *and coll.* also demonstrated the generation of polymersomes in a polymersome,[33] with a facile, versatile, reproducible, and low-time and product-consuming technique based on the emulsion-centrifugation method. The inner polymersomes were formed by nanoprecipitation of poly(trimethylene carbonate)-*b*-poly($_L$-glutamic acid) (PTMC-*b*-PGA).[47] This suspension was then loaded in larger polymersomes of polybutadiene-*b*-poly(ethylene oxide) (PB-*b*-PEO) by emulsion–centrifugation,[48] a technique invented for the formation of giant liposomes with a quantitative loading efficiency[49]. Pautot et al. actually demonstrated this loading efficiency to be of 98% with such a technique.[49] Briefly, a small fraction of an inverted emulsion (droplets of water phase, i.e. the nanosize polymersome suspension of PTMC-*b*-PGA, in oil) was poured over an interface of oil phase and water phase. The PB-*b*-PEO diblock copolymer, dissolved in the oil phase, stabilized the emulsion droplets (forming the inner leaflet of the final bilayer) and this interface. In a final step, centrifugal force caused these droplets to cross the interface and to be enveloped by a second leaflet of amphiphilic PB-*b*-PEO block copolymer, resulting in an aqueous suspension of final giant polymersomes loaded with nanosize ones. It is worthwhile to note that this process can also potentially be scaled-up, and optimized to a non-sequential, but still batch-mode, process.[50] Confocal microscopy and specific fluorophore labelling could assess the multicompartmentalized polymersome structure. Such complex structures can primary be of interest for the simultaneous delivery of multiple active components.[31, 32] To address this

point, a solution of two different PTMC-*b*-PGA suspensions, labelled respectively with red and green fluorophores was encapsulated instead of a single nanosize vesicle suspension. The two nanosize polymersomes are clearly localized in the same giant polymersome.

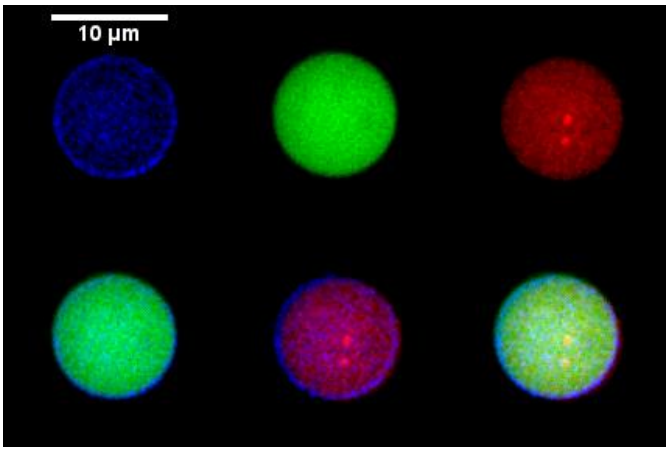


**Fig. 5** Spinning disk confocal microscopy acquisitions of red (Alexa Fluor 568) nanosize vesicles and green FITC-dextran in a blue (Alexa Fluor 405) giant polymersome. From top left to bottom right: blue channel, green channel, red channel, overlay blue and green, blue and red, and finally blue, green, and red channels. Scale bar: 10 µm. Figure from ref [33].

As long as the inner polymersome suspensions that are mixed, are concentrated enough, this encapsulation can be extended to far more than two different populations. Finally, Marguet *et al.*,[33] were able to further increase the complexity of this system by co-encapsulating a large polymer, FITC-dextran, with a red nanosize vesicle suspension. As the FITC-dextran was already green fluorescent, the membrane was labelled in blue, allowing separate imaging of the giant vesicles (blue), the inner nanosize vesicles (red) and the loaded dextran (green) in the giant lumen (Figure 5). Such a three-compartment encapsulation in vesicles was the first reported to date. As explained above, this multiple encapsulation opens avenues for future applications in combinatory drug delivery (multi-therapy). Furthermore, authors studied *in vitro* release kinetics of anticancer drug doxorubicin loaded in nanosize vesicles. As expected, the release was significantly faster than when the nanosize vesicles were protected by another polymer membrane, i.e. diffusion barrier. In the latter scenario, permeation of doxorubicin through the polymeric membranes, induced by the chemical gradient in the release setup, could only last longer. By representing the release data differently, with a law established by Peppas and Ritger[51] and extracting the kinetic constants k for each system, it could be quantitatively determined that the release rate was indeed about twice slower with an additional diffusion barrier. With this additional membrane, better control of release kinetics with a resulting controlled permeability tuning could thus be demonstrated. For further

information, Nallani and coworkers[52] exhaustively reviewed the design and structure of multicompartmentalized systems, which represent the section here described with a wider scope; we focus on systems with more than one layer of amphiphile (as emulsions for example).

### 2.2 Compartments with a gelly or gelified lumen: Mimicking the cytoskeleton in cells.

Regarding cell biomimicry, in addition to compartmentalized vesicles that can mimic the organelles, cytoplasm (here meaning everything in the cell, except for the organelles for sake of clarity) also plays an important role in cellular activity and regulation. In this respect, vesicles with a gelly or gelified cavity (to mimic more specifically the cytoskeleton), also named "hydrosomes" to acknowledge the hydrogel content, have been investigated for approximately a decade. Of course, there are again many interesting properties arising when mimicking a viscoelastic, highly complex, cytoskeleton like a potential slower diffusion of actives towards the outside environment and above all, a better protection and thus stability and shape integrity by absorption of mechanical stress. The most developed approach using polymers, especially by Viallat and coworkers, consists in encapsulating a poly(*N*-isopropylacrylamide) (PNIPAAm)-based solution in liposomes, which will *in situ* polymerize upon photoactivation into covalently cross-linked gels.[53-59] Jesorka, Orwar and coworkers reported other important contributions to the field using viscous solutions of non-crosslinked PNIPAAm that were microinjected in liposomes. Reversible sol-gel transitions were observed by heating above LCST,[60] and by doing so in presence of poly(acrylic acid) PAA, poly(sodium 4-styrene sulfonate) PSS and 2,000,000 g/mol dextran.[61] Very interestingly, heat-stimulated compression was successfully conducted on such PNIPAAm sol-containing liposomes.[62] In another work, a poly(ethylene dioxythiophene) (PEDOT) / PSS polyelectrolyte mixture previously microinjected in liposomes, was physically cross-linked by electrostatic complexation via $Ca^{2+}$ influx (through microinjection, vesicle fusion or electroporation).[63] Electrostatic complexation with calcium ions was also used to create alginate gels in liposomes. Smith *et al.*[42] for example designed 15-30 µm gel loaded liposomes specifically for oral delivery. The encapsulated enzyme seemed better protected by the presence of the gel, as demonstrated by enzymatic activity experiments following exposure to a simulated gastric pH. Tiwari *et al.*[64] used the pH-dependent solubility and thus gelling of PAA in liposomes. Viallat *et al.*[65] also used the thermoresponsive (gelling by decreasing temperature) agarose to rehydrate phospholipid films by electroformation. In addition, they also formed with the same technique what was called "viscous" vesicles by

using either a solution of 50,000 g/mol dextran or carboxymethylcellulose.[66] Long *et al.*[67] rehydrated their liposomes with a mixture of PEG and dextran, which undergo phase separation under specific conditions, inducing microcompartments in the liposomes and mimicking the crowded internal environment of living cells.[68] Finally Stupp's group[69] encapsulated their famous peptide amphiphiles in liposomes by film rehydration for protection of these peptides, which can possess bioactive epitopes. The peptides self-assembled in nanofibers (which give in specific conditions and concentrations, macroscopic gels) *in situ* thanks to a loaded photoacid generator.

In another perspective,[70] the same authors pushed further the concept of their "sac" like structures, assembled from a complex interaction between these PAs with a high molecular weight oppositely charged biopolymer.[71] By using alginate as the biopolymer (readily crosslinkable when introducing calcium ions) and a spray-based production of nebulized biopolymer microdroplets, they achieve 100 µm microcapsules. Regardless of any cytoskeleton aspect, these also mimic roughly cells in the sense that, they are permeable to large proteins which confers them the ability to deliver proteins as the cell does from its cytoplasm to the extracellular space. Their ability to encapsulate nanoscale compartments, cell components, and macromolecules make these microcapsules interesting candidates for the integration of cell-mimetic functions in therapeutic systems.

Such developments using polymersomes as compartments are more recent and have been initiated by Feijen and coworkers[69]. A PNIPAAm solution was encapsulated in polymersomes, and taking advantage from its LCST (32°C), a better permeability control[72] regarding release of actives was demonstrated for a hydrogel containing polymersome than for a bare polymersome (Figure 6). Nanosize polymersomes of poly(ethylene glycol)-*b*-poly(*D,L*-lactide) (PEG-*b*-PDLLA) were formed by nanoprecipitation, PNIPAAm being dissolved in the organic solvent, and purified by dialysis and ultrafiltration (100,000 g/mol cutoff to remove free PNIPAAm). Authors demonstrated colocalization of FITC-PNIPAAm and polymersomes at room temperature by Confocal Laser Scanning Microscopy (CLSM) and Fluorescence Correlation Spectroscopy (FCS). The sol-gel transition (a coil to mesoglobule aggregation[73]) of the FITC-PNIPAAm internalized in polymersomes was studied by fluorescence anisotropy and compared with free hydrogels and free FITC; the rotational freedom of labelled FITC was strongly hindered, particularly above LCST, proving the formation of internal hydrogel. Giant polymersomes for microscopy observations were also prepared using chloroform instead of THF for nanoprecipitation. The hydrogel seemed to localize preferentially near the membrane, rather than in center of the cavity, probably due to

the formation of hydrogen bonds between amide groups of PNIPAAm and ethylene oxide units of PEG.[74] An *in vitro* release of model compound FITC-dextran (4 kDa) was studied by FCS. By comparing results between empty polymersomes and PNIPAAm loaded ones, at 25°C and 37°C, the conclusion is however that while the release was slower in the presence of the hydrogel (1 month *versus* 6 days), the main parameter affecting the release kinetics was the membrane permeability that increases significantly with temperature. Overall release was indeed much faster at 37°C than at 25°C regardless of lumen gelation.

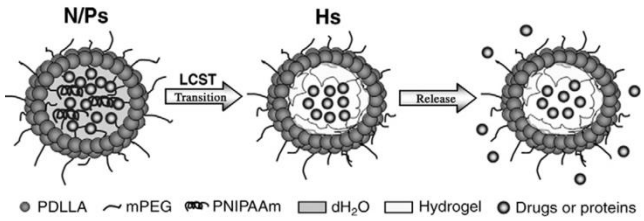


**Fig. 6** Schematic 2D-cross sectional illustration of Ps and Hs in which the PNIPAAm solution present in the core phase separates and partially turns into a gel at the LCST of the internal PNIPAAm aqueous solution, influencing the release rate of incorporated agents. Figure from ref [72].

Finally, Feijen and coworkers optimized their characterization techniques recently.[75] The phase behavior of internalized PNIPAAM was monitored by coupling fluorescence lifetime (FL) and time-resolved fluorescence anisotropy (TRFA) as a function of temperature, and compared to measurements on free hydrogel. They concluded that with increasing temperature, internalized PNIPAAm underwent a coil to globule transition, followed by intermolecular aggregation and possibly phase separation, before finally hydrogel formation, thus providing a deep understanding about gel formation mechanism.

Gaspard *et al.*[76] also reported "polymer hydrosomes" with the aim to extend the gap of polymersome dynamic-mechanical and surface properties and thereby the range of cell-like behavior. Gels with various crosslink densities were polymerized in situ from various ratios of acrylamide/methylenebisacrylamide after encapsulation in PB-*b*-PEO polymersomes by film rehydration with the appropriate pre-gel solutions. Cross-linking density of hydrogels was shown to affect only minimally overall polymersome permeability to molecules smaller than 430 Da. As for the Feijen group, authors observed that the acrylamide hydrogel interiors did not seem to affect particularly mass transport. The membrane represents again the primary diffusion barrier as evidenced by a noticeable change when increasing copolymer length ($PB_{33}$-*b*-$PEO_{20}$ to $PB_{120}$-*b*-$PEO_{89}$). Interestingly however, by increasing cross-linking density, the extent of vesicle deformation or surface contact length decreased, which was consistent with an observed increased resistance to compression strength.

To conclude about this part, and contrary to what could be instinctively expected, a cytoskeleton mimic does not seem to tune the diffusion behavior much, this parameter being mainly limited and controlled by membrane mass transport (depending from temperature).[72, 76] However, as expected and as for the cell, such a mimic improves the mechanical stability of the compartment in which it is enclosed.[76]

### 2.3 Perspectives: Combining organelle and cytoskeleton/cytosol mimics

An external microcapsule (150 µm) formed by the layer-by-layer LbL technique contained a gel bead enclosing 3 µm internal LbL microcapsules.[77] Both kinds of microcapsules were formed using core templates (calcium carbonate for the inner capsules, the microgels for the outer ones) and successive deposition of biopolyelectrolytes dextran sulfate and poly(L-arginine). The inner polymer-coated $CaCO_3$ microparticles were dispersed in a dextran-hydroxylethylmethacrylate (dex-HEMA) and dimethylaminoethyl methacrylate (DMAEMA) solution. Upon addition of a concentrated PEG solution, both polymers, which do not mix at such high concentrations, phase-separated and radical polymerization of methacrylate moieties in the final copolymer resulted in spherical gel beads loaded with internal microcapsules.

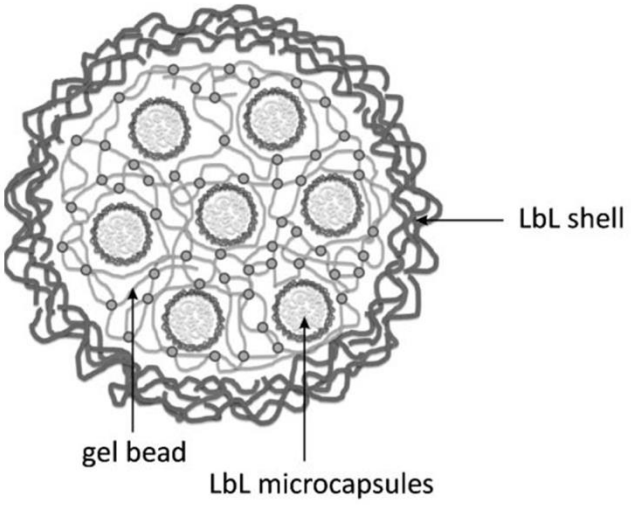


**Fig. 7** Schematic representation of a polyelectrolyte coated gel bead (>100mm) loaded with LbL microcapsules of a few micrometers in size. The o's represent the crosslinks of the gel bead. Figure from ref[77].

DMAEMA was copolymerized with dex-HEMA to get positively charged microgels. Then, authors only needed to coat the ensemble with the last LbL shell and dissolve the template core by EDTA addition. Once these biomimetic structures were formed in a controlled fashion, the self-exploding character of this structure could be established. Indeed, in

physiological conditions, the dex-HEMA gel beads are degraded in a few days or weeks depending on crosslinking density. As a result of this cross-link cleavage (through hydrolysis of the carbonate esters connecting the polymerized methacrylate groups with the dextran backbone), degradation products dextran and HEMA-co-DMAEMA oligomers increased inner osmotic pressure, causing internal swelling until the outer LbL shell cracked at localized spots, thereby releasing the inner LbL microcapsules. Authors outline two particularly promising applications for such systems: for time-controlled release of biological matter such as stem cells or insulin-producing cells, and as single shot vaccination delivering antigen-containing microparticles (thus avoiding the multiple injections currently needed to develop the immune response).

Finally, to the best of our knowledge, Marguet *et al.*[78] were the first to combine both of these structural cell mimics ("organelles" and a very rough "cytoplasm", mimicking more particularly the cytosol with intracellular macromolecular crowding conditions) in vesicles, particularly in polymersomes. The goal was to first achieve a completely original and innovative biomimetic structure before being able in later work to take advantage from the resulting properties. To address this challenge, a suspension of nanosize inner polymersomes of PTMC-*b*-PGA[47] was encapsulated in giant polymersomes of PB-*b*-POE together this time with highly viscous alginate

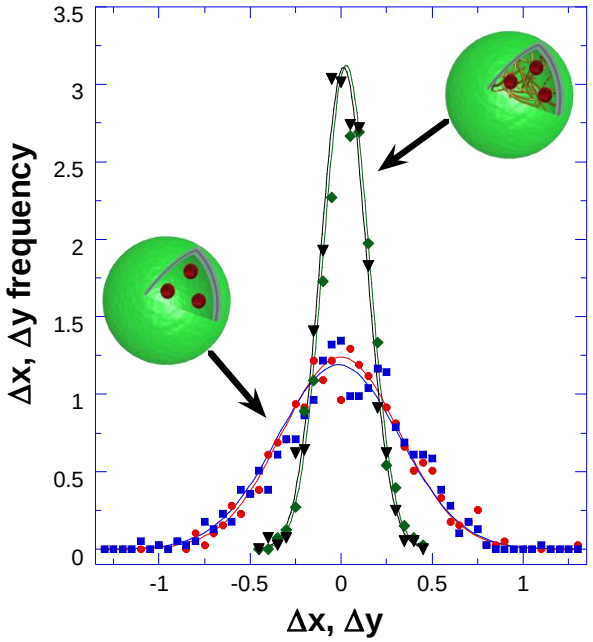


**Fig.8** Statistics of displacements (µm) in x and directions of nanosize inner polymersomes in a giant polymersome with (green and black) and without (red and blue) 300 mg/mL dextran. Figure from ref [78].

or dextran solutions, thanks to the emulsion-centrifugation process. Without cytoplasm mimic, the 2D motion of these organelle mimics tracked down in a movie, was confirmed to

still be Brownian (as motion stayed isotropic, and data respects a Gaussian, or random, distribution) inside the volume of an approximately 20 μm giant polymersome (Figure 8). Furthermore we found the same size and diffusion coefficient of inner nanosize vesicles after their encapsulation by this particle tracking analysis than by dynamic light scattering on the solution before its loading. This result assessed the validity of this tracking analysis and confirmed that the nanosize vesicles are not disturbed by their encapsulation. This analysis was then further repeated in the presence of "cytoplasm mimic dextran": this time, their motion was proved to be efficiently hindered (Figure 8) as confirmed by an approximately 6.6 times smaller diffusion coefficient. Furthermore, the concentration of 300 mg/mL of polysaccharide dextran brought a viscosity above 0.01 Pa·s, in the range of red blood cell cytoplasm viscosity,[54] a volume fraction near 30%[68], and an osmotic pressure above 1 MPa roughly resembling the intracellular conditions caused by global cellular proteins. By reproducing the intracellular "macromolecular crowding effect", which plays a crucial role in the cell machinery, [30] this synthetic and simplified approach constituted an appropriate cytoplasm, more specifically cytosol, mimic.

## 3. Polymersomes hosting enzymatic reactions: Mimicking functional organelles.

"Metabolism" is the set of chemical reactions that occurs within a cell. For eukaryotic cells, these reactions are catalyzed by enzymes in the cytoplasm or in specific cellular compartments. Inner compartmentalization allows fragile processes to remain protected against undesired influences and highly reactive, thus toxic, conditions (as can be found in peroxisomes and lyzosomes) to be prevented from harming the rest of the cell. In this context, this section focuses on the use of polymer-based materials to tackle the challenge of mimicking metabolism, the cell "function", with enzymes. Enzymes in organelles are indeed spatially confined, possibly in environments prone to macromolecular crowding, hence normal solution reaction kinetics are no longer valid.[79] This suggests entrapment of enzymes in artificial nanoreactors (i.e. compartments, herein polymersomes, hosting enzymatic reactions) may contribute to a better understanding of activity and interactions of these enzymes contained in confined spaces, before enabling scientists to come up with powerful innovations. For instance, Cornelissen and coworkers proposed that, in the case of enzymatic reactions occurring in viral capsids, the reaction velocity is inversely proportional to the number of enzymes encapsulated, which seems to outperform free enzymes.[79] It is important

to note that their enzyme, as other ones, is supposed to be more active when immobilized. Vancso and coll. reported that enzyme efficiency is increased with decreasing vesicles size. They observed a two-orders of magnitude increase of enzyme efficiencies compared to bulk reaction; this attributed to enhanced rate of enzyme to substrate and of molecule to wall collisions in such confined volumes.[80]

In any case, nanoreactors need to be able to perform enzymatic reactions *in situ*, while allowing membrane diffusion of substrates and products. The necessary permeability may for example be introduced by mixing in a very controlled fashion, two different kinds of polymers as vesicle building blocks, one of them designed to disappear, after solubilisation[81] in specific conditions or upon degradation. In addition, the enzymes' activity should not be too affected by encapsulation through block copolymers self-assembly, which is mainly performed in presence of organic solvents (nanoprecipitation).

Interestingly, the enzymatic activity in polymersomes is often maintained longer than in free solution, certainly due to a shielding of their degradation by microbes and enzymatic proteolysis[82, 83] that constitutes one of the major and most concrete advantages of nanoreactors. The field of nanoreactor hosting enzymatic reactions, particularly nanoreactors as artificial organelles, is a fast growing area that has already been reviewed in detail very recently.[13,21] In the following section, only the most relevant, recent and challenging systems will be discussed, focusing on systems that find potential long-term applications *in vivo*. The first and second parts of this section will distinguish between nanoreactors intended to become part of the metabolism, and nanoreactors designed to bring intracellular or at least *in vivo* therapeutic solutions for given amounts of time. In a third part, an overview of what nanoreactors are capable of in other applications will also be presented.

### 3.1 Functional artificial organelles designed to replace or substitute intracellularly for missing functions

To mimic nature more closely, a prerequisite step consists in controlling the positioning of encapsulated Intracellular use of nanoreactors for enzyme replacement therapy to compensate for lost, missing or decreased cellular function is of outmost importance. More globally, protein therapy aims at intracellularly replacing or complementing faulty ones (like growth hormone and insulin for example, or in a therapeutic perspective, use antibodies that will block blood supply to tumors) by *in vitro* produced proteins. This strategy against protein-deficiency disease is facing some difficulties regarding clinical trials as proteins do not present sufficient *in vivo* stability and are not easily taken up by cells, or *in vivo* intracellularly

trafficked.[84, 85] An alternative strategy has been envisaged to overcome these limitations where therapy involves the cell internalization and intracellular function of enzymatic nanoreactors, thus becoming artificial organelles. For the design of nanoreactors in general, a prerequisite step consists in controlling the positioning of encapsulated enzymes in the nanoreactor, in a sufficient concentration furthermore (see table 1). It is well known that high encapsulation efficiencies of hydrophilic components are complicated to master in polymersomes, which is why we believe it relevant to detail a little the different procedures in this chapter as well as in Table 1 (which is an experimental overview of section 3). Indeed, the amphiphilic character of enzymes and their often large molar mass render their loading even more challenging. In addition, an absolute requirement lies in the preservation of their bioactivity during the vesicle formation. This control was demonstrated in the van Hest group with encapsulation of glucose oxidase (GOX) in the lumen and horseradish peroxidase (HRP) in the membrane.[86] The strategy for encapsulation in the hydrophilic lumen was inspired from a previous work.[87] The effectiveness of enzyme encapsulation in hydrophobic membrane was demonstrated by visualizing incorporation of Alexa Fluor 488 (membrane) and 633 (lumen) labelled Candida Antartica lipase B (CALB) by epifluorescence microscopy. Interestingly enough, the enzymatic activity assay classically performed on the filtrate of polymersomes with membrane-bound Alexa Fluor 488 labelled CALB revealed that no free enzyme was present, apparently showing a quantitative membrane encapsulation. So, HRP was encapsulated in the membrane by nanoprecipitation (or solvent displacement); PS-PIAT in THF is injected in a small volume of HRP in buffer. A large amount of water is then added, before lyophilization of the sample. The resulting powder is then redissolved in THF and injected in a 5-fold bigger volume of GOX solution in buffer.

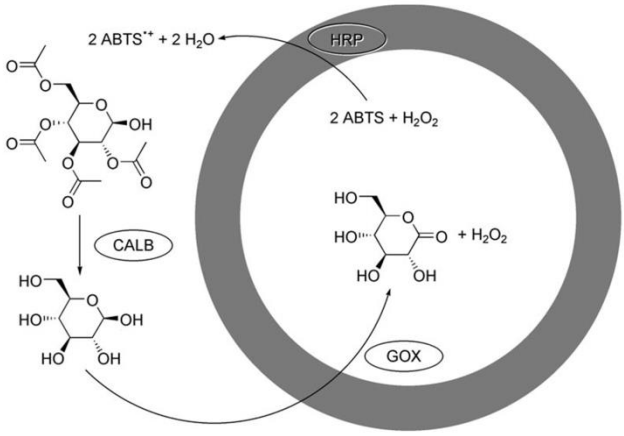


**Fig. 9** Schematic representation of the multistep reaction taking place in the three-enzyme–polymersome system. Scheme of ref [86].

Finally, the mixture is transferred to an Eppendorf with cutoff filter and centrifuged to dryness. Subsequently, polymersomes were redissolved in buffer and centrifuged again until no further enzymaticactivity was observed in the filtrate. It is to note that encapsulation of 3-fold times bigger GOX (160 kDa) in the membrane resulted only in disruption of polymersomes. Van Hest *and coll.* were then further able to perform a three-step cascade reaction (Figure 9): external CALB first hydrolyses a specific substrate into glucose, which then permeates through the polymersome membrane to be converted by the lumen GOX to its lactone and hydrogen peroxide. This peroxide is then converted together with permeating 2,2′-azinobis(3-ethylbenzothiazoline- 6-sulfonic acid) (ABTS) by HRP in membrane to water and a radical $ABTS^{\circ+}$ whose production can be monitored by UV-vis spectrophotometry. The obvious benefit of encapsulation was demonstrated by a prolonged lifetime: the enzyme was shown to still preserve 87±5% of its activity after one month whereas there was a complete loss in bulk within a few days. It was also evidenced that this cascade reaction could work with GOX encapsulated inside one population of polymersomes and HRP in another one, in the presence of proteases in the external environment furthermore.[82] More recently, the same group reported a similar multistep cascade reaction, this time with CalB in membrane, GOX in lumen and HRP attached to external surface by Huisgen cycloaddition.[88] Once all these techniques were mastered, van Hest and coworkers were ready for the final step of internalization in cells.[89] Indeed, their nanoreactors now functionalized with cell penetrating peptide tat were intracellularly routed and checked for activity in mammalian cells. The efficient uptake of tat-functionalized nanoreactors through macropinocytosis was demonstrated, highlighting a promising starting point for future *in vivo* use. Enzymatic activity of these "artificial organelle" in the cell was finally assayed with the cell-penetrating substrate TMB converted in presence of $H_2O_2$ and HRP in lumen to a blue precipitate. The rate of conversion seemed to be directly dependent in a linear manner from the administered dosage of polymersomes. Furthermore, the authors declared the catalytic activity observed in the cells was maintained at levels that were higher than those reported for soluble enzymes. Other highly interesting nanoreactors were reported by Montemagno and coworkers. As early as 2005, [90] the authors were able to recreate an ATP generation process in so-called "proteopolymersomes" in which they incorporated the proteins bacteriorhodopsin (BR, a light-driven transmembrane proton pump driving an influx of protons in the lumen) and motor protein F0F1-ATP synthase (able to hydrolyze ADP to ATP in presence of inorganic phosphate thanks to this proton influx). Their method presents the advantage of avoiding protein-damaging solvents: it is basically direct dissolution with precise additions of

components, followed by vortexing and sonication to favor mixing, dilution, filtration and dialysis to eliminate non-encapsulated proteins.

### 3.2 Targeted delivery in situ of fragile products generated by nanoreactors. "Therapeutic nanoreactors".

Better as a "simple" smart drug delivery vector, therapeutic nanoreactors aim at producing drugs *in vivo*, directly at the target site or helping the organism respond to pathological conditions such as oxidative stress and inflammation. The ultimate long-term concept of such a biologically-inspired nanofactory is schematically depicted in Figure 10 and represents an inspiration for material scientists.[91]

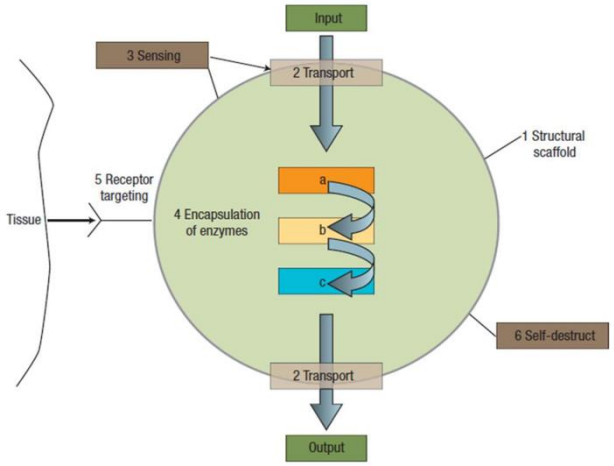


**Fig. 10** Schematic of six mechanisms in the biologically-inspired nanofactory: (1) a structural shell or scaffold, (2) transport to convey biomolecules to and from the environment, (3) sensing functionality, (4) encapsulation of biochemical machinery, (5) targeting of the factory within the body, and (6) externally triggered degradation to terminate a treatment in a controlled fashion. Figure from ref [91], perfectly illustrating the ultimate final application of this section.

While the field of drug delivery is currently in great development and seems as promising as ever, one cannot indeed ignore the challenges encountered: difficult control of release kinetics especially without any stimuli-sensitiveness, possible delivery of payload into undesired biological compartments, the problematic of controlling polymer degradation, etc.[92] Only the most recent contributions will be discussed in this sub-section. Importantly, Meier and coworkers pioneered the concept of nanoreactors, especially polymersomes ones, a decade ago[93,94] but their most recent advances could only be reported after succeeding in the control of several necessary steps like robust polymersome formation, successful incorporation of active transmembrane proteins or porins, loading of functional enzymes and cell-specific targeting. In that aspect, a very interesting work from Ranquin and Meier concerns the use of prodrug activating enzymes in nanoreactors (Figure 11).[95] This selective local enzymatic

activation of prodrugs is a means to increase local drug concentration in tumors while decreasing toxic side effects, the prodrug being inactive. With this strategy, immunogenicity of the enzyme is avoided *in vivo* while enzyme activity is protected. Diffusion of substrates was enabled with incorporation into the membrane of two porines: OmpF has a molecular weight cut-off of 600 Da while Tsx allows specific transport of nucleosides and nucleotides. The purine-specific nucleoside *Trypanosoma vivax* TvNH was encapsulated by film rehydration: first a dried film of polymer/ porine is generated which can then be rehydrated by a TvNH containing buffer. Three natural nucleosides, ionosine, adenosine, guanosine, and one prodrug fluoroadenosine (yielding the cytotoxic drug 2-fluoroadenine) were assayed for enzymatic activity in nanoreactors. TvNH catalyses hydrolysis of the N-glycosidic bond of the β-ribonucleoside separating the free nucleic base and deoxyribose. The reaction is stopped by addition of $CuSO_4$ where $Cu^{2+}$ is reduced to $Cu^{+}$ by the reaction product ribose. At low OmpF concentrations activity seems limited by substrate transport. With a 10-fold increase or use of more specific Tsx, authors observe this is no longer true (as shown by a 6-fold improvement of apparent $k_{cat}$ and $K_m$ values). Encapsulation efficiency of TvNH was determined to approach 15% by SDS-PAGE.

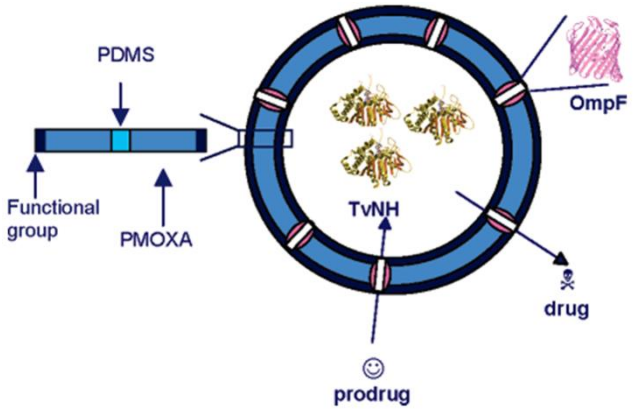


**Fig. 11** Schematic representation of a nanoreactor build up of poly(2-methyloxazoline)-*block*-poly(dimethylsiloxane)-*block*-(2 methyloxazoline) (PMOXA-*b*-PDMS-*b*-PMOXA), permeabilized by the bacterial outer membrane protein OmpF and encapsulated with *Trypanosoma* V*i*V*ax* nucleoside hydrolase (TvNH). Figure of ref [95].

There are also notable contributions resulting from Hunziker and Meier. The ultimate desired long-term application is the exhibition of a controlled and triggered diagnostic signal or therapeutic effect upon *in vivo* activation.[96] Encapsulated enzyme acid phosphatase is only active between pH 4 and 7, thus conferring the nanoreactors a pH-controlled bioswitchability. The enzyme and porines were encapsulated by nanoprecipitation and a hydrosoluble prodye was converted *in situ* into fluorescent precipitating ELF97. The fluorescence intensity was maximal after 3h, as evidenced by epifluorescence and confocal microscopy. It is to note that

kinetics seem 18 times slower than in bulk, certainly, as hypothesized by authors, because of diffusion limitation due to OmpF porines whose cutoff is less than twice the substrate molecular weight. Finally, this technology was enough mastered to pursue to the next level with cell integration.[97] Rapid *in vitro* cellular internalization was indeed demonstrated with specific cell type targeting, and cytoplasm localization before observation of polymersomes' trafficking to specific sites. The functionality of their nanoreactors intracellularly was demonstrated with an encapsulated protease (tripsin) converting a cell-penetrating derivative of Rhodamine 110 (BZiPAR) into green fluorescent Rhodamine 110.

In another very exciting therapeutic perspective, Meier and Palivan worked on enzymes inside nanoreactors in order to fight oxidative stress, logically coined "antioxidant nanoreactors" (see table 1). Cells reduce oxygen to produce energy, which is one of aerobic life's fundamentals. However as a result, oxygen radicals and derived radicals, i.e. "reactive oxygen species" ROS (like the superoxide anion radical, the hydroxyl radical or the assimilated ROS hydrogen peroxide) are constantly generated in almost all living tissues, being involved in various important physiological signaling processes. However, when ROS concentrations reach abnormal high levels, they can potentially damage vital tissue constituents, such as DNA, proteins, and lipids, inducing a so-called "oxidative stress" that may lead to a number of diseases, including cancer, AIDS, Parkinson's and arthritis, deregulation of physiological signals or chronic inflammation.[98] To ensure their function as signalling molecules, in healthy tissues ROS are balanced by cellular antioxidant defence mechanisms, i.e. they are rapidly scavenged by various types of antioxidants such as glutathione, vitamin C, and vitamin E. Antioxidant nanoreactors have been designed to *in situ* fight against oxidative stress, by detoxifying ROS species. Interestingly, PMOXA-*b*-PDMS-*b*-PMOXA polymersomes have the ability to let dioxygen and superoxide radical anions permeate through. In the first attempts, Cu,Zn-super oxide dismutase (SOD) was used as detoxifier.[83,99] Loaded SOD was confirmed to remain intact and active by circular dichroism, electron paramagnetic resonance spectroscopy and with the activity assay of course. SOD labeled with Alexa Fluor 488 was analyzed by FCS to confirm its presence in the polymersome lumen. Thanks to pulse radiolysis, the rate of dismutation of superoxide radical anions at 280 nm could be monitored instantly with high sensitivity. The reaction rate of dismutation of superoxide anion radicals inside the nanoreactor was estimated similar to the one of enzyme in bulk. Finally with a calibration curve of free SOD activity by pulse radiolysis, they were able to estimate a number of 10 enzymes per nanoreactor.

However, a major conceptual drawback of these systems lied in the fact that superoxide radical anions were dismutated into hydrogen peroxide, unfortunately yet another oxidative

molecule. Therefore the concept was further extended and improved with a dual enzyme cascade reaction resulting in the final products of oxygen and water, thereby a complete detoxification.[100] The system is schematically presented in Figure 12. OmpF porines enabled the diffusion of amplex red, the substrate for the second enzyme of the detoxifying cascade, namely lactoperoxidase LPO that produces resorufin, a fluorophore.

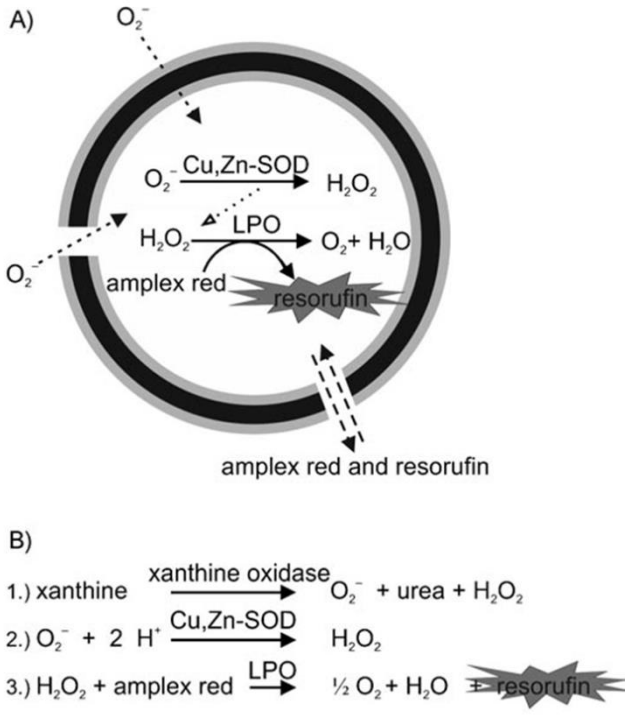


**Fig. 12** Design of the enzymatic cascade reaction inside polymeric nanocontainers for detection and superoxide radical detoxification. A) Schematic illustration of SOD–LPO cascade reaction inside a nanocontainer. B) Chemical reactions allowing the detection and detoxification of superoxide radicals: 1) generation of O2C_; 2) reactions involving SOD; 3) reactions involving LPO. Figure of ref [100].

Cu,Zn-SOD, LPO and OmpF were loaded through nanoprecipitation followed by extrusion and dialysis. The number of fluorophore labeled enzyme molecules per vesicle, i.e. enzyme encapsulation efficiency, was found by dividing the molecular brightness (count rates per molecule) of enzyme-containing vesicles by the molecular brightness of freely diffusing fluorophore thanks to FCS. The fraction of all combinations of vesicles (empty lumen, with only SOD, only LPO, LPO in excess to SOD, opposite, and finally LPO and SOD in stoichiometric amount) was established by combining FCS and FCCS fluorescence cross-correlation spectroscopy. The fraction of dual-containing enzyme nanoreactors was thus measured to be 10%. The polymersomes were finally incubated with THP-1 cells, internalized and the concept proven to be completely functional. Impressively, cells treated with intracellularly superoxide radical producing paraquat, revealed indeed a high resorufin forming signal, thereby proving not only detoxification but also demonstrating biosensor

ability. In their most recent optimization, Palivan and coworkers[101] loaded a dual- enzyme mimic of SOD and catalase, $Cu^{II}$ENZm, which gave the same final products than in the previous attempt, i.e. $O_2$ and $H_2O$. This molecule being smaller, the encapsulation efficiency goes in that case from32 to 46%. Cellular uptake by THP-1 monocytes was evidenced by flow cytometry, CLSM and TEM, and estimated to reach 11% after 24 hours even if notably only non-functionalized vesicles were involved. After 48 hours incubation, this fraction increased considerably, so that a protective antioxidant effect of 23% (cell death decrease) against paraquat induced oxidative stress could be demonstrated.

### 3.3 Nanoreactors for polymerization and catalysis purposes

In addition to the use of enzymatic polymer-based reactors as promising systems to mimic the cellular function for potential biomedical applications on the cutting edge of technology just described, these reactors have also been abundantly designed for other perspectives such as biocatalysis, biotechnology or classic Drug Delivery. Van Hest's group for example imagined purely catalytic applications for PS-*b*-PIAT nanoreactors.[102] Indeed "simple" *in vitro* enzymatic polymerizations have attracted much interest as non-favorable conditions by "classic routes" become possible, such as aqueous medium and room temperature.[102] The concept described on Figure 13, consists in polymerizing various monomers (caprolactone CL, 8-octanolactone OL, 12-dodecanolactone DDL and 4,7,10-tetraoxyacyclotetradecane-11,14-dione TCDD) with enzyme CalB encapsulated either in the water pool or in the membrane (see table 1).

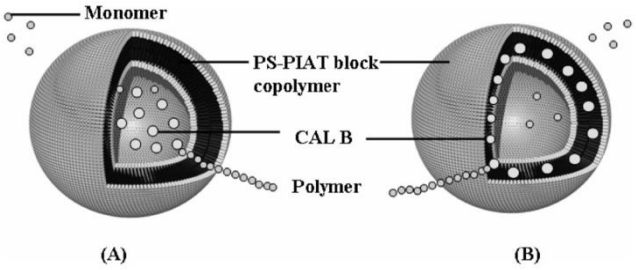


**Fig. 13** Schematic representation of enzymatic polymerization in polymersomes. (A) CALB in the aqueous compartment (B) CALB embedded in the bilayer. Figure of ref [102].

Starting from the same concentrations of CalB to encapsulate, CalB in the water pool seemingly generated a much higher activity than the one in the membrane bilayer. Authors hypothesized a restricted access of substrate molecules due to the thickness of hydrophobic PS layer. Interestingly, the oligomer polymerized from monomer DDL was quite the same (after 1, 3, and 6 days) for CalB in lumen, membrane or free, suggesting encapsulated enzyme

is freely accessible with no hindrance from the polymeric bilayer. While this polymer precipitates after reaching a certain molecular weight, this was not the case for oligomers of OL, where only CalB encapsulated in bilayer yielded far less high molecular masses. Polymersomes were completely disrupted after 3 days of polymerization of OL with CalB in bilayer, probably because the synthesized oligoesters plasticize this bilayer. For OL with CalB in water pool, morphological changes appeared after 3 days before complete disruption after 6 days.

The same group has again demonstrated a great level of technological control in confined enzymatic reactions by going further in the design of nanoreactors for biotechnological industrial applications.[103] Baeyer Villager monoxygenases (BVMO) belong to a class of oxidative enzymes, particularly interesting for the development of "green" biocatalytic processes, because they can perform oxidative processes with a high level of chemo-,regio-, and/or enantio-selectivity However, the flavin present in their active site needs to be reduced after each catalytic cycle, which can be performed through electron supply of NADPH nicotinamide adenine nucleotide (phosphate). A cofactor recycling system is here required as its stoichiometric use would severely affect reaction efficiency and be highly cost-expensive after scale-up. The system design is summarized in Figure 14. Glucose-6-phosphate dehydrogenase G6PDH is loaded in the water pool where it converts glucose-6-phosphate and $NADP^+$ into 6-phosphate- gluconolactone and recycled cofactor NADPH, which activates the BMVO phenylacetone monoxygenase PAMO (free in external medium or attached on external surface) for conversion of phenylacetone into phenylacetate. After 28 hours, 28% of substrate was converted which could be approximately doubled by doubling G6PDH concentration. In bulk however, 100% was converted in 30 min; authors attribute this difference to the membrane barrier between the two enzymes..

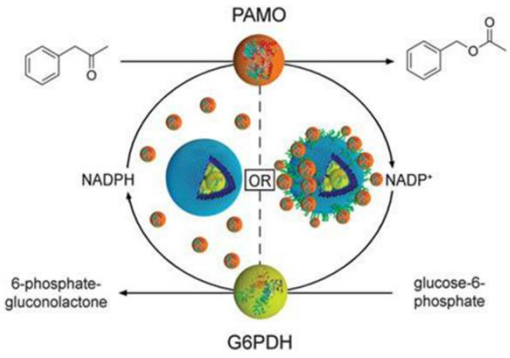


**Fig. 14** Diagram depicting the regeneration of cofactor NADP+ by G6PDH inside PS-b-PIAT polymersomes to sustain the conversion of phenylacetone catalyzed by PAMO. Two systems with encapsulated G6PDH were separately examined: PAMO in solution and PAMO covalently immobilized on the surface. (The CRE2-PAMO system is not shown here.) Figure 1 adapted from ref [103].

When PAMO was attached to the surface outside instead of added to external medium, conversion was only 5% after 24h Authors attributed this decrease of reactivity to inaccessibility of active sites, deformation of the enzyme following immobilization, or hindered diffusion of NADPH through polymersome membrane as a result of a PAMO covered surface. Following the same perspective, Cornelissen and coworkers[104] imagined a "continuous-flow polymersome reactor" where enzyme loaded vesicles are immobilized in a macroscopic hydrogel, substrate added to the top of the reactor and product collected at the bottom. Such a reactor is powerful as it enables recycling of enzyme retaining polymersomes. A recent and smart design of Battaglia and Voit[105] concerns a polymersome nanoreactor with pH dependent permeability. While the hydrophilic block is PEG, the hydrophobic one, is indeed the pH-sensitive poly(diethylamino ethyl methacrylate) PDMEAEM with a small percentage of a photo-cross-linking unit incorporated (needing only 30 s of photoactivation). When the polymersomes were cross-linked they showed swelling/deswelling cycles following pH switch (from 8 to 6), which could be repeated 5 times. In the swelled state, the permeability is sufficient for substrate diffusion and enzymatic conversion *in situ*

Enzymatic polymer based reactors have also been used for a quite different perspective that consists in using the enzymatic reaction to trigger a specific permeability[81] or membrane disruption in a controlled fashion. Napoli *et al.*[106] reported a nice example of such application. They incorporated thioethers in the hydrophobic poly(propylene sulfide) blocks of PEG-*b*-PPS-*b*-PEG vesicles that were converted into more hydrophilic sulfoxides and sulfones upon exposure to a hydrogen peroxide oxidative environment, changing the hydrophilic ratio and thus inducing its solubilization.GOX was encapsulated in the lumen by film rehydration, separated by SEC and glucose added to the external environment. With a classic HRP-ABTS assay based on $H_2O_2$ consumption, the enzymatic activity was assayed as well as a high enough membrane permeability to glucose demonstrated. This permeability may be explained by a low Tg of 230 K, implying a high mobility at room and body temperature. Indeed a really minimal delay of 0.5 s between addition of glucose and oxidation of ABTS was assessed. Finally the disruption due to hydrogen peroxide generation by GOX could be demonstrated. In the bloodstream there are mM concentrations of glucose that would be available to trigger compound release with such systems and the produced hydrogen peroxide would be diluted enough to be harmless for patients. Furthermore, whereas the free GOX lost activity after 5 to 6 days, the encapsulated one seemed to remain active at least 24 days.

Table 1 Nanoreactor polymersome characteristics

| Number of enzymes involved in cascade | Substrate (+ other reactive(s)) | Enzyme(s) | Enzyme(s)'s localization | Encapsulation&purifcation methods and encapsulation efficiency (EE) | Product(s) | Reference/ Main author(s) |
|---|---|---|---|---|---|---|
| **1** | TMB (+ $H_2O_2$) | HRP | Lumen | SD[a] (THF)/ Dialysis | Blue precipitate | [89] Brock/van Hest |
| | Prodye ELF97 phosphate | Acid phosphatase | Lumen | SEC[b] | Dye ELF97(solid) | [96] Hunziker/Meier |
| | BZiPAR | Trypsin | Lumen | | Dye Rhodamine 110 | [97] Hunziker/Meier |
| | $O_2^{\bullet-}$ (+ $H^+$) | Cu,Zn-SOD | lumen | SD [a] (ethanol)/ SEC 2-5 enzymes/vesicle. | $H_2O_2$ | [83] Palivan/Meier |
| | $O_2^{\bullet-}$(+ $H^+$) | Cu,Zn-SOD | Lumen | Method A[c]/SEC 2-5proteins/vesicle. EE[d] ≈ 43 -61 % depending on DP. | $H_2O_2$ | [99] Palivan/Meier |
| | Natural nucleosides (ionosine, adenosine, guanosine) | TvNH | Lumen | Method A[c]/chromatography EE[d] ≈15% | Free nucleotic bases and deoxyribose | [95] Ranquin/Meier |
| | Prodrug 2-fluoro-adenosine | TvNH | Lumen | Method A[c]/chromatography EE[d] ≈15% | 2-fluoroadenine | [95] Ranquin/Meier |
| | phenylacetone (+NADPH+ phosphite) | CRE2-PAMO | Lumen | SD[a] (dioxane)/ Method B[e] EE[d] ≈20% | Phenylacetate | [103] van Hest |
| | $O_2^{\bullet-}$ | $Cu^{II}$ENZm, | Lumen | Method A[c]/SEC 200 enzymes /nanoreactor (46% EE[d]) | $O_2$ + $H_2O$ | [101] Palivan |
| | DIFMU octanoate | CalB | Lumen | SD[a] (THF)/ SEC+ Method B[e] | Dye DIFMU | [81] van Hest |
| | Glucose | GOX | Lumen | Methods B[e]/ C[f] | Gluconolactone (+ $H_2O_2$) | [106] Sommerdijk |
| | Lactone monomers[g]: OL, DDL<br>CL,TCDD<br>DIFMU octanoate | CalB | Lumen + Membrane<br>*idem* | SD[a] (THF)+ Method C[f] (THF)/Method B[e]<br>*idem* | Polyesters<br>No polyesters<br>Dye DIFMU | [102] Cornelissen van hest, Nolte |
| | Guaiacol (+$H_2O_2$) | Myoglobin | Lumen | Using the tuned permeability of their designed reactor / KrosFlo™ | Oxidized guaiadacol | [105] Battaglia/Voit |
| **2** | phenylacetone (+NADPH)<br>glucose-6-phosphate (+$NADP^+$) | PAMO<br>G6PDH (regenerates NADPH for PAMO) | Outside and on external surface via click Lumen | SD[a] (dioxane)/ Method B[e]<br>SD[a] (THF)/ Method B[e] EE[d] ≈20% | Phenylacetate<br>6-phosphate--gluconolactone | [103] van Hest |
| | Glucose<br>ABTS (+$H_2O_2$) | GOX<br>HRP | Lumen<br>Lumen (2nd population) | SD[a] (THF)/ Method B[e]<br>*idem* | Gluconolactone (+$H_2O_2$)<br>Coloured $ABTS^{\circ+}$ (+ $H_2O$) | [82] Rowan/van Hest |
| | $O_2^{\bullet-}$ (+ $H^+$) | Cu,Zn-SOD | Lumen | SD[a] (THF) (ethanol) then extrusion/ Dialysis 4±3 SOD/vesicle | $H_2O_2$ | [100] Palivan/Meier |

| | | | | | | |
|---|---|---|---|---|---|---|
| | Amplex red ($+H_2O_2$) | Lacto-peroxidase | *idem* | *idem* 8±5 LPO | Dye Resorufin ($+O_2 + H_2O$) | |
| **3** | Glucose acetate | CalB | Membrane | SD[a] (THF)/ Method B[e] $EE^{d}$ = 17.2±2.96% | Glucose | [88] |
| | Glucose | GOX | Lumen | Method C[f]/ Method B[e] $EE^{d}$= 25±2.09% | gluconolactone ($+H_2O_2$) | van Hest |
| | ABTS ($+H_2O_2$) | HRP | Outside on external surface via click | Method B[e] $EE^{cd}$= 25.5±3.37% | Coloured $ABTS^{\circ+}$ ($+ H_2O$) | |
| | $GAc_4$[h] | CalB | Outside | | Glucose | [86] |
| | Glucose | GOX | Lumen | SD[a] (THF)/ Method B[e] | gluconolactone ($+H_2O_2$) | Rowan/van Hest |
| | ABTS ($+H_2O_2$) | HRP | Membrane | Method C[f]/ Method B[e] | Coloured $ABTS^{\circ+}$ ($+ H_2O$) | |

[a] Solvent displacement (SD) or nanoprecipitation. [b] SEC=Size exclusion chromatography [c] Method A=Film rehydration, then extrusion. [d] EE encapsulation efficiency. [e] Method B=Centrifugal filtration with Eppendorf cutoff filters to near dryness and redispersion, *etc*, until no more enzymatic activity detection [f] Method C=SD with redispersed lyophilized powder of a first nanoprecipitation. [g] 8-octonolactone (OL), Dodecalactone (DDL), ϵ-caprolactone (CL), 1,4,7,10-tetraoxacyclotetradecane-11,14-dione (TCDD). [h] 1,2,3,4-tetra-O-acetyl-b-glucopyranose

## 4. From cell structure mimic to controlled biofunctionality: the ultimate biomimetic materials with high-added value.

Once the structural cell mimicry is controlled, one can bring these structures to their full potential by tackling the challenge of functional cell biomimicry. The idea is to combine functional organelles as those described in the previous section in such multicompartmentalized cell mimics. Indeed, enzymatic reactions, spatially controlled and confined in (often crowded) compartments are some of the numerous functions performed by a cell. By combining architectural multicompartmentalization (organelles) and metabolism mimicry (enzymatic reactions in the above mentioned organelles), biomimetic cellular systems may become a powerful biomedical platform for the development of next-generation therapeutic carrier vehicles, to substitute for missing or lost cellular function,[12,18,107] or as small-scale bioreactors. [12,108, 109] One of the first researchers to adress this challenge were Vogel and coworkers, with small molecules based systems. They were able to trigger thermally the release and mixing of compounds from smaller lipsomes inside a larger liposome, one great property arising from multicompartmentalization.

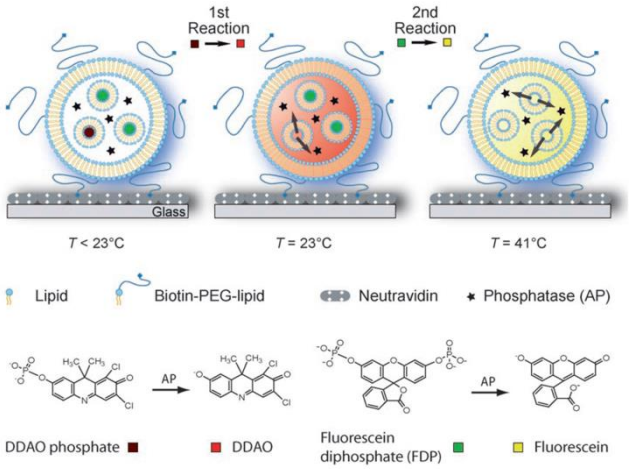


**Fig. 15** Consecutive enzymatic reactions in a single nanoreactor. The external nanoreactors surface comprises biotin for immobilization on a neutravidin-coated glass slide. Alkaline phosphatase (AP, star) is incorporated in the nanoreactor together with two kinds of SUVs,each loaded with a different nonfluorescent substrate for the enzyme. The first kind of SUV (Tt 23°C) is loaded with dichlorodimethylacridinone (DDAO) phosphate (dark red) and the second kind of SUV (Tt 41 °C) is loaded with fluorescein diphosphate (FDP, dark green). An increase of temperature triggers the release of the substrates in two distinct, consecutive steps at the two corresponding phase-transition temperatures, first DDAO phosphate at 23C° and then FDP at 41°C. After release from the SUVs, the substrates remain confined in the nanoreactor, where they are converted by the enzyme to their particular fluorescent products, DDAO (light red) and FDP (light green). Figure from ref [110]

By using relevant lipid-phase transition temperatures $T_t$, they were further able to perfect their system into a nanofluidic reactor controlling two consecutive enzymatic reactions with the same enzyme.[110] Indeed at these temperatures permeability increases as a result of the

transient defects that are generated by disturbances in lipid packing order. Two kinds of small unilamellar vesicles (SUV, 100 nm) (with two different fluorogenic substrates) were loaded in a micrometric large unilamellar vesicle (LUV, 1-10 µm). Phase transition temperatures from both SUVs were separated by 20°C, so that by reaching the first $T_t$, only one of the substrates could be released in the reaction vessel (LUV) due to enhanced permeability and be converted by the present enzyme into a green fluorescent product. The second substrate (yielding a red fluorescent product) was then released by reaching the second Tt (Figure 15). FCS enabled discriminating between freely diffusing model dyes in the LUV and those more hindered by their encapsulation in the SUVs, thereby giving information about the encapsulation efficiencies. By monitoring the kinetics for one reaction, authors declared no significant difference was observed between a reaction in bulk (with same conditions of pH, temperature, enzyme and substrate concentrations) and the one in the nanofluidic reactor. Finally, the authors stressed the need for miniaturized reactors to reduce sample consumption (which may be expensive or polluting) and throughput. As volumes as small as attolitric are mixed (from the inner nanometer-sized liposomes) in a femtoliter reactor vessel (the larger outer liposome), the control over the number of mixed reactants should thus approach this single-molecule precision!

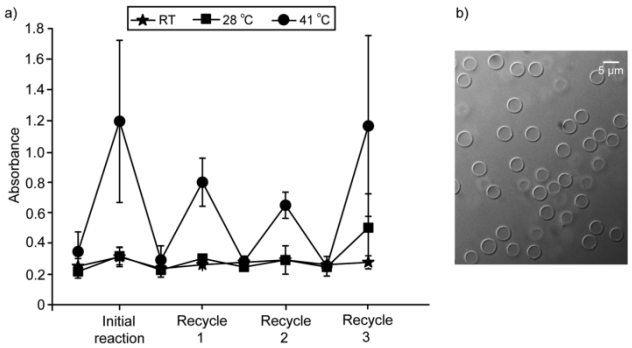


**Fig. 16** Consecutive Temperature-triggered enzymatic reaction in reusable capsosomes. (a) Absorbance readings of an enzymatic assay using capsosomes with β-lactamase-loaded DPPC liposomes ($C_{L(DPPC)-\beta}$) incubated at room temperature (23 °C) (Δ), 28 °C (▪), or 41 °C (●). The enzymatic conversion was only observed when the capsosomes were incubated at the phase transition temperature (*T*m) of the liposomal subunits. The retention of the functional enzymes inside of the liposomal subcompartments was confirmed by repetitively performing the temperature-induced assay.). Figure from ref [111].

As a source of inspiration for polymer chemistry, this early work on liposomes has highlighted the fruitful combination of multicompartmentalization and enzymatic activity. In that respect, exciting innovations in material sciences have been reported from Caruso's group. The concept of "capsosomes", or polymer layer-by-layer capsules deposited on liposomes was first thoroughly demonstrated and reported.[112] These capsosomes take advantage from both kinds of structures while their drawbacks are being counter-balanced:

indeed they inherit the very advantageous semi-permeable nature and mechanical stability of polymer capsules while the liposomes restrict access to solutes from the outside, therefore hindering their conversion by the encapsulated enzyme. The enzymatic reaction was triggered by addition of the surfactant Triton X, destroying the liposomes and allowing the reaction to take place in the resulting cross-linked polymer capsule. This system was then further optimized by maximizing the number of liposomes and cargo retention and above all allowing a temperature-triggered reaction.[111] As for Vogel's system, the phase transition temperature of phospholipids is taken advantage of to trigger remotely the initiation of the reaction by controlling the substrate release. The encapsulated enzymes can now furthermore be used for repeated conversions as the reaction can be reversibly triggered (see Figure 16). Finally, formation of capsosomes with free-floating internal liposome subcompartments was achieved, also going one step closer towards structural cell mimicry with "floating" enclosed organelles.[113] As before, these organelles can host an enzymatic reaction upon temperature activation (Figure 17).

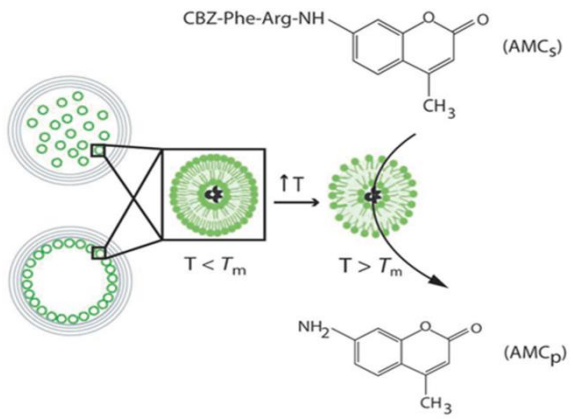


**Fig.17** Schematic illustration of the enzymatic conversion of AMC substrate into AMC product using capsosomes loaded with the protease subtilisin upon increasing the temperature above *T* m. At pH 4 the liposomes are bound to the membrane while at 7.4 they are free-floating. Figure from ref [113].

Finally, formation of capsosomes with free-floating internal liposome subcompartments was achieved, also going one step closer to structural cell mimicry with "floating" enclosed organelles.[113] As before, these organelles can host an enzymatic reaction upon temperature activation (Figure 18).

In the field of hollow polyelectrolyte microcapsules, the work of Kreft *et al.*[114] with shell-in-shell reactors also needs to be mentioned. Spherical calcium carbonate microparticles were here used as templates, which could be removed in a "biofriendly" way through EDTA complexation after polyelectrolyte multilayer build-up. The procedure to get a shell-in-shell structure was complex and well-thought, using successive co-precipitation of $CaCl_2$ and

$Na_2CO_3$, and enabled to retain one enzyme in the lumen of the inner shell (peroxidase POD), another one in the lumen of the more external one (GOX or GOD as they name it) (Figure 18). Glucose was added outside for hydrogen peroxide generation by GOX in the most external compartment. After addition of substrate Amplex Red for the second reaction of the cascade, fluorescent resorufin was obtained within a few seconds in the inner compartment before diffusing outside of the inner capsule. lumen of the inner shell (peroxidase POD), another one in the lumen of the more external one (GOX or GOD as they name it) (Figure 18). Glucose was added outside for hydrogen peroxide generation by GOX in the most external compartment. After addition of substrate Amplex Red for the second reaction of the cascade, fluorescent resorufin was obtained within a few seconds in the inner compartment before diffusing outside of the inner capsule. Kreft *et al.*[114] also evidenced a powerful property resulting from multicompartmentalization: the means to trigger remotely bioreactions. They incorporated gold nanoparticles in the inner shell of a similar shell-in-shell system that could be activated with a near-infrared laser illumination. This resulted in membrane disruption; the contents were released into the outer shell interior, providing a route for reactions in confined volumes and intermixing of contents of two or more compartments.

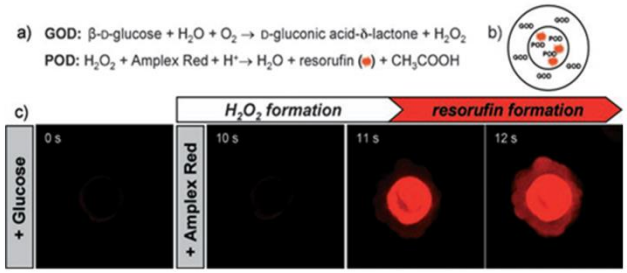


**Fig. 18** Coupled enzymatic test by using GOD and POD inside shell-in-shell capsules. a) Reaction schemes. b) Localization of GOD and POD within shell-in-shell capsules. c) CLSM imaging in situ of resorufin formation. Figure of ref. [114]

Kreft *et al.*[114] also evidenced a powerful property resulting from multicompartmentalization: the means to trigger remotely bioreactions. They incorporated gold nanoparticles in the inner shell of a similar shell-in-shell system that could be activated with a near-infrared laser illumination. This resulted in membrane disruption; the contents were released into the outer shell interior, providing a route for reactions in confined volumes and intermixing of contents of two or more compartments.

Bäumler and Georgieva[115] pushed Kreft's concept further. Indeed, co-precipitation between calcium chloride and sodium carbonate was also used to form concentric compartments after removal with EDTA. The shells were formed from biopolymer and enzymes cross-linked with glutaraldehyde or divinylsulfone, depending on the step. The three-enzyme cascade

performed can be seen in Figure 19. Enyzme β-glucosidase was in the most external compartment and converted a prodye into fluorescein and glucose. This glucose was then hydrolysed to glucuronic acid and hydrogen peroxide by GOX (in an intermediate concentric compartment) in presence of dioxygen. Finally, after addition of prodye amplex red, HRP produced fluorescent resorufin and dioxygen (necessary for the reaction of GOX) in the presence of the generated hydrogen peroxide, in a final inner compartment. As the first and the last product of the cascade were fluorescent, one can evaluate the time lag between the first and last enzyme starting to react. Interestingly, in one experiment, they also added enzyme-lacking "sandwich" concentric compartments, one between the β-glucosidase and GOX compartment, and one between GOX and HRP compartment. They could thus compare kinetics with and without these additional compartments (of roughly one micrometer) and evaluate the effect of component diffusion. Kinetics could be monitored by confocal microscopy on single particles, showing fluorescence increases much earlier and faster inside the particles

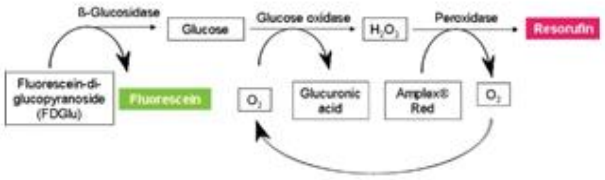


**Fig. 19** Chain reaction of the three-coupled enzymes with fluorogenic substrates for the first and third enzyme. Fig from ref [115].

as in the background. In both samples, the first product (fluorescein) appeared after about 30s. But where the third product resorufin became visible after 60s in the 3-compartment particles, it took 300 to 400 s in the case of 5-compartment particles (2 additional "empty" ones). This evidences the limiting parameter is clearly the diffusion of the intermediate products through the additional spacing compartments. Some experiments were also monitored in time by fluorimetry measurements. Authors stressed scattering and inhomogeneous distribution of absorbance may influence such measurements. Indeed reaction rate rate was significantly increased when followed by microscopy, as compared to a macroscopic scale by fluorimetry. Microscopy indeed represents the real concentration of products inside particles and is not influenced by its distribution in the surrounding solution. Another very interesting and "green" advantage arising is again the possible recycling of enzyme-bearing microparticles. After 5 runs, activity is divided by 5, but still present. Also, activity could be preserved over months.

Last but not least, a very smart design by Caruso and coworkers was constituted by the use of

an *in situ* bioreaction to trigger release of therapeutics. As we emphasize in all this chapter, mimicking a biological cell enables to construct new materials, with original and innovative properties. Here the conduction of an enzymatic reaction offers new perspective in terms of drug delivery. More precisely, the enzyme glutathione reductase in the liposomes of the capsosomes reacts in situ upon temperature triggering (i.e. near the lipid transition temperature). The enzyme can then reduce glutathione disulfide GSSG to glutathione GSH, a major cellular antioxidant. This GSH becomes available to cleave the disulfide bond between a loaded conjugate composed of a small therapeutic peptide and a large polymer, thereby enabling its subsequent release in the external medium. This can be monitored as the peptide is also labelled with a fluorophore. Authors aim to develop such systems further to get biomimetic platforms that will combine both enzyme therapy and controlled drug release in such a single structure.

Finally, it is worth mentioning the work of Caruso and coworkers[116] that have reviewed multicompartmentalized structures with a special focus on coupled enzymatic reactions in confined volumes.

In summary, the combination of multicompartmentalized structure and enzymatic activity is still at its earlier stage in materials science. Since soft matter scientists are now able to combine these two aspects, it is expected that the frontiers of cell biomimicry will be pushed further with polymer-based systems, from cell structure mimics towards a controlled and powerful biofunctionality.

## 5. Conclusions

The present chapter aims at demonstrating the relevance of polymer-based materials (with a special focus on polymersomes) when addressing the challenge of eukaryotic cell biomimicry. Mimicking the multicompartmentalized structure of the cell, i.e. the organelles enclosed in the cellular membrane, as well as the cytoskeleton, opens exciting avenues in many different research areas, particularly in biotechnology and nanomedicine. Regarding the latter, several successive membranes or layers encapsulating an active drug offer obviously a better protection as a single one, as well as a finer permeability tuning, hence a better control over release kinetics. The inner compartments (the organelle mimics) that loaded in the outer one (the cell membrane mimic) do not necessarily need to encapsulate the same content, where the various contents can even be incompatible or act synergistically. As a result, combinatory drug delivery becomes possible in one single vector. Also, the different kinds of membranes

or layers can be designed to present different polymeric natures, so that they disrupt or degrade in specific environments in an orthogonal fashion. All this should also enable to design new vectors suitable for other methods of delivery than intravenous injection, such as transcutaneous or oral absorption[32, 33, 35] which are much preferable for patient's compliance. Then, Mimicking the rest of cytoplasm (i.e. all but the organelles) should also impart drug delivery vehicles with new attractive properties. In particular regarding the cytoskeleton, one could expect it to render the overall structure more robust in terms of shape, mechanical stability, and to tune/decrease the release kinetics of loaded actives. Surprisingly, while this proves to be true for the mechanical reinforcement of the mimics, the membrane of polymersomes remains by far the most effective diffusion barrier. Furthermore, the cytosol is responsible for creating a very particular environment in the cell; macromolecular crowding, confinement and adsorption play an important part in the cell's life. Thus, materials scientists with biomimicry focuses should also provide biologists with appropriate cell models in order for the latter, to conduct their studies in more relevant environments, closer to that of the cell. Intracellular enzymatic reactions for example cannot be modeled with ideal (diluted) or normal solution kinetics, evidencing the relevance of mimicking the cytosol. Mimicking the other powerful property of cells, the metabolism represents the second step towards cell biomimicry. By using polymeric materials, this step can be achieved through the design of enzymatic reactions hosted in a compartment, as occurs in biological organelles, in a highly controlled, selective and efficient fashion. This field is of outmost interest for biocatalysis and biomedecine with the challenges of compensating for lost or missing cellular function (so-called artificial organelles), or for delivering the reaction product from their manufacturing site (the therapeutic nanoreactors) to the *in vivo* target. Compared to classic therapeutic strategies or normal synthetic processes, there are other advantages arising from such an advanced technology: protection of enzymes against proteolytic/microbial degradation, or harmful environments, and also, one could expect enhanced reaction probabilities and efficiencies due to spatial confinement or immobilization of enzymes. Furthermore, enzymatic reactions mainly take place in the cell's organelles, i.e. in a crowded, confined environment, thus studying them in such organelle mimics is fundamentally highly relevant.

One step further towards cellular structure and function biomimicry consists in using a multicompartmentalized structure as scaffold for multiple enzymatic reactions. Hence a completely new and powerful level of control arises, as in the eukaryotic cell. Indeed, even though a significant progress over cascade reactions in nanoreactors with enzymes placed in different locations has been demonstrated in the past years, the level of possibilities to immobilize or confine enzymes in a multicompartmentalized structure is more promising and

still needs to be fully explored. The manipulation of each individual enzyme involved in cascade steps or parallel reactions becomes facile. As a result, multistep reactions should not be influenced by toxic intermediates, formation of undesired byproducts and incompatible catalytic steps should be prevented.

. From a materials perspective, the exquisite control in polymer synthesis, self-assembly and advanced formulation that is available nowadays would certainly bring a real breakthrough in this cell biomimicry field. Therefore, one can expect the growing interest in such biomimetic approaches to soon offer many new opportunities in drug delivery, cell-like reactor systems, synthetic biology, biosensors and biomaterials, allowing better communication and interaction with living systems

---

This chapter has served as inspiration under a more synthetic form to:

Marguet Maïté, Colin Bonduelle, Sébastien Lecommandoux*, Multicompartmentalized polymeric systems : towards biomimetic cellular structure and function, *Chemical Society Reviews*, **2013**, 42, p.512-529.

## References


1. Mann, S., *Accounts of Chemical Research* **2012**.
2. Dzieciol, A. J.; Mann, S., *Chem. Soc. Rev.* **2012,** *41*, 79-85.
3. Whitesides, G. M.; Grzybowski, B., *Science* **2002,** *295* (5564), 2418-2421.
4. Noireaux, V.; Maeda, Y. T.; Libchaber, A., *Proceedings of the National Academy of Sciences of the United States of America* **2011,** *108* (9), 3473-3480.
5. Murtas, G., *Molecular BioSystems* **2009,** *5* (11), 1292-1297.
6. Pasparakis, G.; Krasnogor, N.; Cronin, L.; Davis, B. G.; Alexander, C., *Chemical Society Reviews* **2010,** *39* (1), 286-300.
7. http://www.merriam-webster.com/dictionary/biomimetics.
8. Aizenberg, J.; Fratzl, P., *Advanced Materials* **2009,** *21* (4), 387-388.
9. Kushner, A. M.; Guan, Z., *Angewandte Chemie International Edition* **2011,** *50* (39), 9026-9057.
10. Antonietti, M.; Fratzl, P., *Macromolecular Chemistry and Physics* **2010,** *211* (2), 166-170.
11. Paleos, C. M.; Tsiourvas, D.; Sideratou, Z., *Langmuir* **2011,** *28* (5), 2337-2346.
12. Mitragotri, S.; Lahann, J., *Nature Materials* **2009,** *8* (1), 15-23.
13. Peters, R. J. R. W.; Louzao, I.; van Hest, J. C. M., *Chemical Science* **2012,** *3* (2), 335-342.
14. Szostak, J. W.; Bartel, D. P.; Luisi, P. L., *Nature* **2001,** *409* (6818), 387-390.
15. Pohorille, A., *Early ancestors of living cells*. MIT Press: Cambridge, Massachusetts London, England, 2009.
16. Kamat, N. P.; Katz, J. S.; Hammer, D. A., *The Journal of Physical Chemistry Letters* **2011,** *2* (13), 1612-1623.
17. Discher, B. M.; Won, Y. Y.; Ege, D. S.; Lee, J. C. M.; Bates, F. S.; Discher, D. E.; Hammer, D. A., *Science* **1999,** *284* (5417), 1143-1146.
18. Schatz, C.; Louguet, S.; Meins, J. F. L.; Lecommandoux, S., *Angewandte Chemie - International Edition* **2009,** *48* (14), 2572-2575.
19. Ahmed, F.; Photos, P. J.; Discher, D. E., *Drug Development Research* **2006,** *67* (1), 4-14.
20. Brinkhuis, R. P.; Rutjes, F. P. J. T.; van Hest, J. C. M., *Polymer Chemistry* **2011,** *2* (7), 1449-1462.
21. Palivan, C. G.; Fischer-Onaca, O.; Delcea, M.; Itel, F.; Meier, W., *Chemical Society Reviews* **2012,** *41* (7), 2800-2823.
22. Meng, F.; Hiemstra, C.; Engbers, G. H. M.; Feijen, J., *Macromolecules* **2003,** *36* (9), 3004-3006.
23. Du, J.; O'Reilly, R. K., *Soft Matter* **2009,** *5* (19), 3544-3561.
24. De Oliveira, H.; Thevenot, J.; Lecommandoux, S., *Wiley Interdisciplinary Reviews: Nanomedicine and Nanobiotechnology* **2012,** *4* (5), 525-546.
25. Brizard, A. M.; Van Esch, J. H., *Soft Matter* **2009,** *5* (7), 1320-1327.
26. Aida, T.; Meijer, E. W.; Stupp, S. I., *Science* **2012,** *335* (6070), 813-817.
27. Fletcher, D. A.; Mullins, R. D., *Nature* **2010,** *463* (7280), 485-492.
28. Schwille, P.; Diez, S., *Critical Reviews in Biochemistry and Molecular Biology* **2009,** *44* (4), 223-242.
29. Pollard, T. D.; Borisy, G. G., *Cell* **2003,** *112* (4), 453-465.
30. Minton, A. P., *Journal of Cell Science* **2006,** *119* (14), 2863-2869.
31. Al-Jamal, W. T.; Kostarelos, K., *International Journal of Pharmaceutics* **2007,** *331* (2), 182-185.

32. Scholl, I.; Boltz-Nitulescu, G.; Jensen-Jarolim, E., *Journal of Controlled Release* **2005,** *104* (1), 1-27.
33. Marguet, M.; Edembe, L.; Lecommandoux, S., *Angewandte Chemie International Edition* **2012,** *51* (5), 1173-1176.
34. Mishra, V.; Mahor, S.; Rawat, A.; Dubey, P.; Gupta, P. N.; Singh, P.; Vyas, S. P., *Vaccine* **2006,** *24* (27-28), 5559-5570.
35. Ebato, Y.; Kato, Y.; Onishi, H.; Nagai, T.; Machida, Y., *Drug Development Research* **2003,** *58* (3), 253-257.
36. Wong, B.; Boyer, C.; Steinbeck, C.; Peters, D.; Schmidt, J.; van Zanten, R.; Chmelka, B.; Zasadzinski, J. A., *Advanced Materials* **2011,** *23* (20), 2320-2325.
37. McPhail, D.; Tetley, L.; Dufes, C.; Uchegbu, I. F., *International Journal of Pharmaceutics* **2000,** *200* (1), 73-86.
38. Fu, Z.; Ochsner, M. A.; De Hoog, H. P. M.; Tomczak, N.; Nallani, M., *Chemical Communications* **2011,** *47* (10), 2862-2864.
39. Chiu, H.-C.; Lin, Y.-W.; Huang, Y.-F.; Chuang, C.-K.; Chern, C.-S., *Angewandte Chemie International Edition* **2008,** *47* (10), 1875-1878.
40. Kim, S.-H.; Shum, H. C.; Kim, J. W.; Cho, J.-C.; Weitz, D. A., *Journal of the American Chemical Society* **2011,** *133* (38), 15165-15171.
41. Shum, H. C.; Zhao, Y. J.; Kim, S. H.; Weitz, D. A., *Angewandte Chemie - International Edition* **2011,** *50* (7), 1648-1651.
42. Smith, A. M.; Jaime-Fonseca, M. R.; Grover, L. M.; Bakalis, S., *Journal of Agricultural and Food Chemistry* **2010,** *58* (8), 4719-4724.
43. Maitani, Y.; Hazama, M.; Tojo, Y.; Shimoda, N.; Nagai, T., *Journal of Pharmaceutical Sciences* **1996,** *85* (4), 440-445.
44. Hayward, R. C.; Utada, A. S.; Dan, N.; Weitz, D. A., *Langmuir* **2006,** *22* (10), 4457-4461.
45. Shum, H. C.; Santanach-Carreras, E.; Kim, J. W.; Ehrlicher, A.; Bibette, J.; Weitz, D. A., *Journal of the American Chemical Society* **2011,** *133* (12), 4420-4426.
46. Perro, A.; Nicolet, C.; Angly, J.; Lecommandoux, S.; Le Meins, J. F.; Colin, A., *Langmuir* **2011,** *27* (14), 9034-9042.
47. Sanson, C.; Schatz, C.; Le Meins, J. F.; Brûlet, A.; Soum, A.; Lecommandoux, S., *Langmuir* **2010,** *26* (4), 2751-2760.
48. Mabrouk, E.; Cuvelier, D.; Pontani, L. L.; Xu, B.; Lévy, D.; Keller, P.; Brochard-Wyart, F.; Nassoy, P.; Li, M. H., *Soft Matter* **2009,** *5* (9), 1870-1878.
49. Pautot, S.; Frisken, B. J.; Weitz, D. A., *Langmuir* **2003,** *19* (7), 2870-2879.
50. Abkarian, M.; Loiseau, E.; Massiera, G., *Soft Matter* **2011,** *7* (10), 4610-4614.
51. Ritger, P. L.; Peppas, N. A., *J. Controlled Release* **1987,** *5* (1), 23-36.
52. De Hoog, H. P. M.; Nallani, M.; Tomczak, M., *Soft Matter* **2012,** *8* (17), 4552-4561.
53. Faivre, M.; Campillo, C.; Pepin-Donat, B.; Viallat, A., Responsive giant vesicles filled with poly(N-isopropylacrylamide) sols or gels. Science, P. i. C. a. P., Ed. 2006; Vol. 133, pp 41-44.
54. Campillo, C.; Pépin-Donat, B.; Viallat, A., *Soft Matter* **2007,** *3* (11), 1421-1427.
55. Kremer, S.; Campillo, C.; Pepin-Donat, B.; Viallat, A.; Brochard-Wyart, F., *EPL (Europhysics Letters)* **2008,** *82* (4), 48002.
56. Campillo, C. C.; Schroder, A. P.; Marques, C. M.; Pepin-Donat, B., *Soft Matter* **2008,** *4* (12), 2486-2491.
57. Campillo, C. C.; Schroder, A. P.; Marques, C. M.; Pépin-Donat, B., *Materials Science and Engineering C* **2009,** *29* (2), 393-397.
58. Kazakov, S.; Kaholek, M.; Teraoka, I.; Levon, K., *Macromolecules* **2002,** *35* (5), 1911-1920.

59. Hong, J. S.; Stavis, S. M.; Depaoli Lacerda, S. H.; Locascio, L. E.; Raghavan, S. R.; Gaitan, M., *Langmuir* **2010,** *26* (13), 11581-11588.
60. Jesorka, A.; Markström, M.; Orwar, O., *Langmuir* **2005,** *21* (4), 1230-1237.
61. Markström, M.; Gunnarsson, A.; Orwar, O.; Jesorka, A., *Soft Matter* **2007,** *3* (5), 587-595.
62. Osinkina, L.; Markström, M.; Orwar, O.; Jesorka, A., *Langmuir* **2010,** *26* (1), 1-4.
63. Jesorka, A.; Markström, M.; Karlsson, M.; Orwar, O., *Journal of Physical Chemistry B* **2005,** *109* (31), 14759-14763.
64. Tiwari, S.; Goyal, A. K.; Mishra, N.; Vaidya, B.; Mehta, A.; Dube, D.; Vyas, S. P., *Procedia in Vaccinology* **2009,** *1* (1), 148-163.
65. Viallat, A.; Dalous, J.; Abkarian, M., *Biophysical Journal* **2004,** *86* (4), 2179-2187.
66. Mader, M. A.; Vitkova, V.; Abkarian, M.; Viallat, A.; Podgorski, T., *European Physical Journal E* **2006,** *19* (4), 389-397.
67. Long, M. S.; Jones, C. D.; Helfrich, M. R.; Mangeney-Slavin, L. K.; Keating, C. D., *Proceedings of the National Academy of Sciences* **2005,** *102* (17), 5920-5925.
68. R.John, E., *Trends in Biochemical Sciences* **2001,** *26* (10), 597-604.
69. Lee, J. S.; Zhou, W.; Zhang, D.; Otto, C.; Feijen, J., *Journal of Controlled Release* **2008,** *132* (3), 28-29.
70. Rożkiewicz, D. I.; Myers, B. D.; Stupp, S. I., *Angewandte Chemie International Edition* **2011,** *50* (28), 6324-6327.
71. Capito, R. M.; Azevedo, H. S.; Velichko, Y. S.; Mata, A.; Stupp, S. I., *Science* **2008,** *319* (5871), 1812-1816.
72. Lee, J. S.; Zhou, W.; Meng, F.; Zhang, D.; Otto, C.; Feijen, J., *Journal of Controlled Release* **2010,** *146* (3), 400-408.
73. Binkert, T.; Oberreich, J.; Meewes, M.; Nyffenegger, R.; Ricka, J., *Macromolecules* **1991,** *24* (21), 5806-5810.
74. Polozova, A.; Winnik, F. M., *Langmuir* **1999,** *15* (12), 4222-4229.
75. Lee, J. S.; Koehorst, R. B. M.; Van Amerongen, H.; Feijen, J., *Journal of Physical Chemistry B* **2011,** *115* (45), 13162-13167.
76. Gaspard, J.; Hahn, M. S.; Siles, J. A., *Langmuir* **2009,** *25* (22), 12878-12884.
77. De Geest, B. G.; De Koker, S.; Immesoete, K.; Demeester, J.; De Smedt, S. C.; Hennink, W. E., *Advanced Materials* **2008,** *20* (19), 3687-3691.
78. Marguet, M.; Sandre, O.; Lecommandoux, S., *Langmuir* **2012,** *28* (4), 2035–2043.
79. Minten, I. J.; Claessen, V. I.; Blank, K.; Rowan, A. E.; Nolte, R. J. M.; Cornelissen, J. J. L. M., *Chemical Science* **2011,** *2* (2), 358-362.
80. Chen, Q.; Schonherr, H.; Julius Vancso, G., *Small* **2009,** *5* (12), 1436-1445.
81. Kim, K. T.; Cornelissen, J. J. L. M.; Nolte, R. J. M.; Van Hest, J. C. M., *Advanced Materials* **2009,** *21* (27), 2787-2791.
82. Kuiper, S. M.; Nallani, M.; Vriezema, D. M.; Cornelissen, J. J. L. M.; Van Hest, J. C. M.; Nolte, R. J. M.; Rowan, A. E., *Organic and Biomolecular Chemistry* **2008,** *6* (23), 4315-4318.
83. Axthelm, F.; Casse, O.; Koppenol, W. H.; Nauser, T.; Meier, W.; Palivan, C. G., *Journal of Physical Chemistry B* **2008,** *112* (28), 8211-8217.
84. C. De Duve, R. W., *Annu. Rev. Physiol.* **1966,** *28*, 435-492.
85. Christian, D. A.; Cai, S.; Bowen, D. M.; Kim, Y.; Pajerowski, J. D.; Discher, D. E., *European Journal of Pharmaceutics and Biopharmaceutics* **2009,** *71* (3), 463-474.
86. Vriezema, D. M.; Garcia, P. M. L.; Sancho Oltra, N.; Hatzakis, N. S.; Kuiper, S. M.; Nolte, R. J. M.; Rowan, A. E.; Van Hest, J. C. M., *Angewandte Chemie - International Edition* **2007,** *46* (39), 7378-7382.

87. Vriezema, D. M.; Hoogboom, J.; Velonia, K.; Takazawa, K.; Christianen, P. C. M.; Maan, J. C.; Rowan, A. E.; Nolte, R. J. M., *Angewandte Chemie - International Edition* **2003,** *42* (7), 772-776.
88. Van Dongen, S. F. M.; Nallani, M.; Cornelissen, J. J. L. M.; Nolte, R. J. M.; Van Hest, J. C. M., *Chemistry - A European Journal* **2009,** *15* (5), 1107-1114.
89. Van Dongen, S. F. M.; Verdurmen, W. P. R.; Peters, R. J. R. W.; Nolte, R. J. M.; Brock, R.; Van Hest, J. C. M., *Angewandte Chemie - International Edition* **2010,** *49* (40), 7213-7216.
90. Choi, H.-J.; Montemagno, C. D., *Nano Letters* **2005,** *5* (12), 2538-2542.
91. LeDuc, P. R.; Wong, M. S.; Ferreira, P. M.; Groff, R. E.; Haslinger, K.; Koonce, M. P.; Lee, W. Y.; Love, J. C.; McCammon, J. A.; Monteiro-Riviere, N. A.; Rotello, V. M.; Rubloff, G. W.; Westervelt, R.; Yoda, M., *Nat Nano* **2007,** *2* (1), 3-7.
92. Tanner, P.; Baumann, P.; Enea, R.; Onaca, O.; Palivan, C.; Meier, W., *Accounts of Chemical Research* **2011,** *44* (10), 1039-1049.
93. Nardin, C.; Thoeni, S.; Widmer, J.; Winterhalter, M.; Meier, W., *Chemical Communications* **2000,** (15), 1433-1434.
94. Nardin, C.; Widmer, J.; Winterhalter, M.; Meier, W., *European Physical Journal E* **2001,** *4* (4), 403-410.
95. Ranquin, A.; Versées, W.; Meier, W.; Steyaert, J.; Van Gelder, P., *Nano Letters* **2005,** *5* (11), 2220-2224.
96. Broz, P.; Driamov, S.; Ziegler, J.; Ben-Haim, N.; Marsch, S.; Meier, W.; Hunziker, P., *Nano Letters* **2006,** *6* (10), 2349-2353.
97. Ben-Haim, N.; Broz, P.; Marsch, S.; Meier, W.; Hunziker, P., *Nano Letters* **2008,** *8* (5), 1368-1373.
98. Dröge, W., In *Oxidative Stress, Disease and Cancer*, ; Singh, K. K., Eds. Imperial College Press: London, 2006; pp 885-895.
99. Onaca, O.; Hughes, D. W.; Balasubramanian, V.; Grzelakowski, M.; Meier, W.; Palivan, C. G., *Macromolecular Bioscience* **2010,** *10* (5), 531-538.
100. Tanner, P.; Onaca, O.; Balasubramanian, V.; Meier, W.; Palivan, C. G., *Chemistry - A European Journal* **2011,** *17* (16), 4552-4560.
101. Balasubramanian, V.; Onaca, O.; Ezhevskaya, M.; Van Doorslaer, S.; Sivasankaran, B.; Palivan, C. G., *Soft Matter* **2011,** *7* (12), 5595-5603.
102. Nallani, M.; de Hoog, H. P. M.; Cornelissen, J. J. L. M.; Palmans, A. R. A.; van Hest, J. C. M.; Nolte, R. J. M., *Biomacromolecules* **2007,** *8* (12), 3723-3728.
103. Meeuwissen, S. A.; Rioz-Martínez, A.; De Gonzalo, G.; Fraaije, M. W.; Gotor, V.; Van Hest, J. C. M., *Journal of Materials Chemistry* **2011,** *21* (47), 18923-18926.
104. De Hoog, H. P. M.; Arends, I. W. C. E.; Rowan, A. E.; Cornelissen, J. J. L. M.; Nolte, R. J. M., *Nanoscale* **2010,** *2* (5), 709-716.
105. Gaitzsch, J.; Appelhans, D.; Wang, L.; Battaglia, G.; Voit, B., *Angewandte Chemie International Edition* **2012,** *51* (18), 4448-4451.
106. Napoli, A.; Boerakker, M. J.; Tirelli, N.; Nolte, R. J. M.; Sommerdijk, N. A. J. M.; Hubbell, J. A., *Langmuir* **2004,** *20* (9), 3487-3491.
107. Städler, B.; Price, A. D.; Zelikin, A. N., *Advanced Functional Materials* **2011,** *21* (1), 14-28.
108. Pohorille, A.; Deamer, D., *Trends in Biotechnology* **2002,** *20* (3), 123-128.
109. Zhang, Y.; Ruder, W. C.; LeDuc, P. R., *Trends in Biotechnology* **2008,** *26* (1), 14-20.
110. Bolinger, P. Y.; Stamou, D.; Vogel, H., *Angewandte Chemie - International Edition* **2008,** *47* (30), 5544-5549.
111. Chandrawati, R.; Hosta-Rigau, L.; Vanderstraaten, D.; Lokuliyana, S. A.; Stadler, B.; Albericio, F.; Caruso, F., *ACS Nano* **2010,** *4* (3), 1351-1361.

112. Stadler, B.; Chandrawati, R.; Price, A. D.; Chong, S. F.; Breheney, K.; Postma, A.; Connal, L. A.; Zelikin, A. N.; Caruso, F., *Angewandte Chemie - International Edition* **2009,** *48* (24), 4359-4362.
113. Hosta-Rigau, L.; Chung, S. F.; Postma, A.; Chandrawati, R.; Städler, B.; Caruso, F., *Advanced Materials* **2011,** *23* (35), 4082-4087.
114. Kreft, O.; Skirtach, A. G.; Sukhorukov, G. B.; Möhwald, H., *Advanced Materials* **2007,** *19* (20), 3142-3145.
115. Bäumler, H.; Georgieva, R., *Biomacromolecules* **2010,** *11* (6), 1480-1487.
116. Chandrawati, R.; Van Koeverden, M. P.; Lomas, H.; Caruso, F., *J. Phys. Chem. Lett.* **2011,** *2* (20), 2639-2649.

# CHAPTER 2

# Polymersomes in “gelly” polymersomes: towards structural cell mimicry

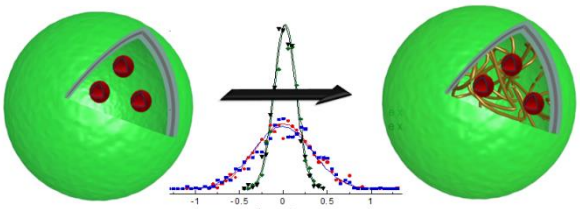


From compartmentalized to gelly compartmentalized polymersomes: one step further towards cell mimicry

*In the previous chapter* ***(Chapter 1),*** *a state of the art concerning self-assembly for Cell Biomimicry has been presented, with a special focus on polymers as building blocks. Thanks to their versatility, their robustness and the current state of polymer chemistry science, we believe polymer-based materials (especially polymersomes) to constitute ideal candidates to address the challenges of Biomimicry. The cell is certainly one of the most complex and exciting systems that scientists are still trying to fully understand; hence this field is fundamentally highly interesting. Several successive steps have been identified and investigated: 1) mimicking the cell's structure (its inner compartments), the organelles, through multicompartmentalization, and the intracellular milieu, i.e. cytoskeleton/cytosol using gels or particular solutions (highly concentrated for example) in one compartment, and finally the combination of both. Our contribution to this aspect is detailed in* ***Chapters 2*** *and* ***3****. Then 2), achieving enzymatic reactions in a compartment, as occurs in the organelles, in a highly controlled, selective and efficient fashion to mimic metabolic function (****Chapter 4****). And finally 3) combining these steps to push the frontiers of Biomimicry further: from cell structure mimics towards a controlled cell-like biofunctionality. Our tentative to address this challenge can also be found in* ***Chapter 4****. It is to note that in order to reach an truly autonomous minimal synthetic cell which is the goal pursued in the field of synthetic biology, other steps and challenges would need to be faced, such as self-replication, energy transfer, selective chemicals diffusion, etc.*

*In this chapter (****Chapter 2****), we demonstrate the formation of multicompartmentalized polymersomes (polymersomes in a polymersome) with an internal « gelly » cavity using an original and versatile process. Nanosize polymersomes of poly(trimethylene carbonate)-b-poly($_L$-glutamic acid) PTMC-b-PGA, formed by a solvent displacement method (or nanoprecipitation) are encapsulated with a rough "cytoplasm mimic" in giant/micrometric polymersomes of poly(butadiene)-b-poly(ethylene oxide) PB-b-PEO by emulsion-centrifugation. Such a system constitutes a first step towards the challenge of structural cell mimicry with both "organelles" and "cytoplasm mimics". The structure is demonstrated with fluorescence labeling and confocal microscopy imaging yielding movies that feature the motion of the inner nanosize polymersomes in larger vesicles. Without "cytoplasm mimic", the motion was confirmed to be Brownian by particle tracking analysis. The inner nanosize polymersomes motion was blocked in the presence of alginate, but only hindered in the presence of dextran. With the use of such high molecular weight and concentrated polysaccharides, the crowded internal cell milieu, responsible for the so-called "macromolecular crowding" effect that influences every intracellular macromolecular association, seems to be efficiently mimicked. This study constitutes a major progress in the field of structural biomimicry and will certainly enable the rise of new, highly interesting properties in the field of soft matter.*

## 1. Introduction

Polymer vesicles or polymersomes are resulting from the self-assembly of amphiphilic block copolymers in aqueous media, and are often presented as the structural analogues of liposomes.[1, 2] They can load both hydrophilic (in their internal aqueous reservoir) and hydrophobic components (in their membrane). Their similarity to liposomes is however limited to this closed bilayer structure. Indeed, due to their polymeric nature, polymersomes present an intrinsically thicker membrane, therefore with higher hydrophobic component loading capacity, which confers them a larger mechanical stability and lower permeability compared to liposomes.[3] These properties, in addition with the inherent chemical versatility of polymer building blocks, are responsible for their considerable interest and development[4] as drug delivery systems[5], more particularly stimuli-sensitive carriers,[6-8] as sensors and nanoreactors[9-13].

While liposomes mimic the semi-permeable living cell membrane with their intrinsic phospholipid nature, polymersomes' structure and properties are much closer to those of viral capsids.[14] However, neither liposomes nor polymersomes can be described as cell mimics as an essential key towards cell mimicry lies in compartmentalization. Yet, one could question the relevance of biomimicry and an elegant answer by Feynman was "what I cannot create, I do not understand".[15, 16] From the most evident and fundamental point of view, artificial mimics as model systems enable to complement biological studies as they allow to dissociate parameters closely correlated in nature.[15] Moreover, the first step that consists in mimicking the multicompartmentalized structure of a cell is already very challenging. It is only once their formation is controlled and optimized that it becomes possible to take advantage of these mimics to gain new properties with innovative soft materials. As a matter of fact, Nature evolved with compartmentalization because such a structure offers multiple advantages. For artificial compartmentalized cell mimics, one of the most foreseeable benefits obviously lies in a better protection[17, 18] of inner encapsulated actives, often very fragile in the field of drug delivery. Furthermore, several compartments that each contains a different active in the same structure open a path to combinatory drug delivery.[17-19] Such an approach is of particular interest in oncology as it enables to load and potentially deliver incompatible drug cocktails together.[20, 21] Going further, while a certain permeability is necessary for drug delivery systems, compartmentalization can also circumvent undesirable prematurely drug leakage especially in liposomes, as demonstrated by Zasadzinski and coworkers.[22] Indeed, compartmentalized systems can be used to finely tune permeability.[17, 18, 23] Such complex

structure can also impact the way we design a chemical reaction or induce a reaction only when different components are mixed.[24-26] Caruso and coworkers in particular pointed out the great level of possibilities arising from microencapsulated reactors, one example being their promising capsosomes.[27-29]

In a perspective of compartmentalization, some very interesting work has already been achieved with liposomes but this field is only in its early stages regarding polymersomes. In a recent approach, solvent displacement method was used, with the aqueous solution being a suspension of smaller polymersomes previously generated by a film rehydration of a lamellar forming amphiphilic block copolymer.[30] The main drawback of this method is essentially based on the poor encapsulation yield during the solvent displacement process. To overcome this limitation, the most promising alternative lies in methods based on emulsions or double emulsions. Chiu *et al.*[31] were the first to tackle this challenge with polymersomes; however, even though their method consisting of two successive double emulsions was very original, it may not yield the most reproducible and homogeneous systems while being difficult to use on a daily basis. In order to gain in reproducibility and homogeneity of the preparation, Weitz and coworkers developed highly sophisticated microfluidics devices. In a first step, they were able to control the formation of polymersome aggregates or multicompartment polymersomes[20] before yielding fully multicompartmentalized polymersomes.[21] The size of the internal polymersomes is however limited to quite larger dimensions (≈ 100 µm), depending on the capillary size. In addition, this method is rather tricky since several issues need to be solved before achieving the high throughput production of polymersomes by microfluidics: possible coalescence of the internal and external aqueous phases, dewetting instability of the organic phase from the copolymer bilayer usually leading to excess polymer patched to the vesicles,[32] and unequal evaporation rate of solvents from the organic phase during the rather long drying step of the copolymer membranes with dramatic consequences on contact angles.[33]

Regarding cell biomimicry, in addition to compartmentalized vesicles that can mimic the organelles, cytoplasm also plays an important role in cellular activity and regulation. In this respect, vesicles with gelly or gelified cavity, also names "hydrosomes", have been investigated for approximately a decade. Of course, there are again many interesting potential properties arising when mimicking a viscoelastic cytoplasm like a slower diffusion of actives towards the outside environment and above all a better protection and thus stability and shape integrity, by absorption of mechanical stress. An approach that is often used, in particular by A. Viallat and coworkers, consists in encapsulating a poly(N-isopropylacrylamide) PNIPAAm based solution, which will in situ photopolymerize into covalently cross-linked

gels upon UV irradiation.[34-41] However, in cells, the cytoskeleton is composed of the protein filaments actin, microtubules and intermediate filaments, formed by nucleation-elongation processes. The growth of the protein filaments of this cytoskeleton is driven by non-covalent interactions, making them very dynamic with constant association/dissociation processes.[15] For that reason, non-covalent or physical gels constitute in our opinion a better alternative. Limozin and Sackmann[42] were impressively able to form liposomes with dynamic actin networks cross-linked by the natural cross-linkers α-actinin and filamin. Other approaches were developed using the LCST character of non-crosslinked PNIPAAm,[43,44] electrostatic complexation,[45-47] pH-dependent solubility and thus gelling,[48] polysaccharide based systems,[49, 50, 46, 47, 51] or more recently peptide amphiphiles[52] to gelify the inside reservoir of liposomes . To the best of our knowledge Feijen and coworkers were the first to tackle this aim with polymersomes using PNIPAAm as a gelator.[53, 54]

The aim of this work is to go on step further towards structural cell mimicry and to combine both compartmentalized structures (to mimic organelles) and a "gelly" cavity (as cytoplasm mimic) in polymersomes. Such a realization requires an exquisite control of the physical parameters and interaction components, together with an efficient process. The achievement of this original and innovative biomimetic structure constitutes a first necessary step before taking advantage of it to address other challenges in controlled catalysis and chemical (bio)reactions.

## 2. Experimental Section

### 2.1. Materials and reagents

Poly(butadiene)$_{46}$-*b*-poly(ethylene oxide)$_{30}$ ($PB_{46}$-*b*-$PEO_{30}$) (P9095-BdEO, $M_{n\ PB}$=2,500 g/mol and $M_{n\ PEO}$=1,300 g/mol, I=1.04) and amino-terminated poly(butadiene)$_{20}$ ($PB_{31}$) (for polymersome membrane labeling) (P3977-Bd$NH_2$, $M_n$=1,700 g/mol, I=1.11, f>0.98%) were purchased from Polymer Source. Alexa Fluor 568-carboxylic acid, succinimidyl ester (A20003-1mg, mixed isomers, 791.8 g/mol) and Alexa Fluor 488 carboxylic acid, succinimidyl ester (A20000-1mg, mixed isomers, 643.41 g/mol) were purchased from Invitrogen. Alginic acid sodium salt from brown algae (Fluka 71238, 50g) and Dextran from leuconostoc ssp. (Fluka 31389, $M_r$=40,000 g/mol, 100g) were from Fluka Biochemika. Sucrose 99% was from Alfa Aesar (A15583 L 13300, 2.5g) and D-(+)-glucose from Sigma Aldrich (G5767-500g). Solvents from Sigma Aldrich for fluorophore labeling (DMSO and

DMF) were anhydrous. All products were used as received unless otherwise specified. Poly(trimethylene carbonate)$_{30}$-*b*-poly($_L$-glutamic acid)$_{19}$ PTMC$_{30}$-*b*-PGA$_{19}$ diblock copolymer was synthesized by ring-opening polymerization (ROP) of δ-benzyl-L-glutamate N-carboxyanhydride (NCA) initiated by a primary amine end-functionalized PTMC macroinitiator according to a previously described method.[55] All the experiments described were performed on PTMC$_{30}$-*b*-PGA$_{19}$ diblock copolymer ($M_n$=5,492 g/mol, I=2).

## 2.2. Methods

### 2.2.1. Synthesis and self-assembly

**Fluorescent dye labeling.**

- *Alexa Fluor 568 labeled PTMC$_{30}$-b-PGA$_{19}$:* After flame-drying of a round-bottom flask under vacuum, the following reagents were introduced under inert nitrogen atmosphere: primary end-functionalized amine PTMC$_{30}$-*b*-PGA$_{19}$ (99.9 mg, 18.2 µmol), anhydrous DMSO (2 mL), DIPEA (140 µL, 804 µmol) and reactive Alexa Fluor 568-carboxylic acid, succinimidyl ester (1 mg, 1.26 µmol) in DMSO (120 µL). The reaction was then allowed to proceed for one night under static nitrogen atmosphere. The conjugate PTMC$_{30}$-*b*-PGA$_{19}$-Alexa Fluor 568 was purified by dialysis (5 L, 3 h, MWCO : 3,500 g/mol) after dilution in the flask by DMSO for a better recovery. External medium was renewed six times in course of dialysis. After lyophilization, the conjugate was recovered in a 97 % yield (determined by gravimetry).
- *Alexa Fluor 488 labeled poly(butadiene):* After flame-drying under vacuum of a round-bottom flask, the following reagents were introduced under inert nitrogen atmosphere: primary end-functionalized amine PB$_{20}$ (84.1 mg, 49.5 µmol), anhydrous DMF (2 mL), DIPEA (8 µL, 45.9 µmol) and reactive Alexa Fluor 488-carboxylic acid, succinimidyl ester (1 mg, 1.55 µmol) in DMF (120 µL). The reaction was then allowed to proceed for overnight under static nitrogen atmosphere. After concentrating the mixture by evaporation of DMF under vacuum, the polymer was precipitated and washed with water. Finally, it was dissolved in THF and recovered after drying under dynamic vacuum.

**Nanoprecipitation yielding nanosize polymersomes of PTMC$_{30}$-*b*-PGA$_{19}$ for encapsulation inside giant polymersomes.** For the preparation of fluorescently labeled nanosize polymersomes to be tracked by confocal microscopy, we followed a nanoprecipitation method described previously. [55] Briefly, 4.5 mL Tris Buffer, 50 mM, pH 7.4 was added slowly at a controlled rate of 2.25 mL/h on a DMSO solution containing 5 mg

of PTMC-*b*-PGA-Alexa Fluor 568 (0.5 mL) under stirring at 500 rpm at 25 °C. The sample was then dialyzed with a 50,000 g/mol cut-off in 5 L Milli Q water with 3 renewals. Size and polydispersity were characterized by dynamic light scattering (DLS).

**Emulsion-centrifugation yielding giant PB-*b*-PEO encapsulating a PTMC-*b*-PGA nanosize vesicle suspension (Scheme 1).** In a typical procedure inspired from Li and col.,[56, 57] 5 µL of a nanosize vesicle suspension in 380 mOsm sucrose solution was first poured in 500 µL toluene containing 3 mg/mL PB-*b*-PEO (including, depending on the experiment, 0 or 10 wt% of Alexa Fluor 488 labeled PB) in a Eppendorf tube (step 1, Scheme 1). The PB-*b*-PEO solution in toluene was previously stirred for at least 2 hours to ensure a complete dissolution of the copolymer, as verified by DLS (no intensity scattered). In another tube (step 2, Scheme 1), 30 µL of the same organic solution was poured over 30 µL of a 380 mOsm aqueous glucose solution and allowed to stabilize for 30 min.

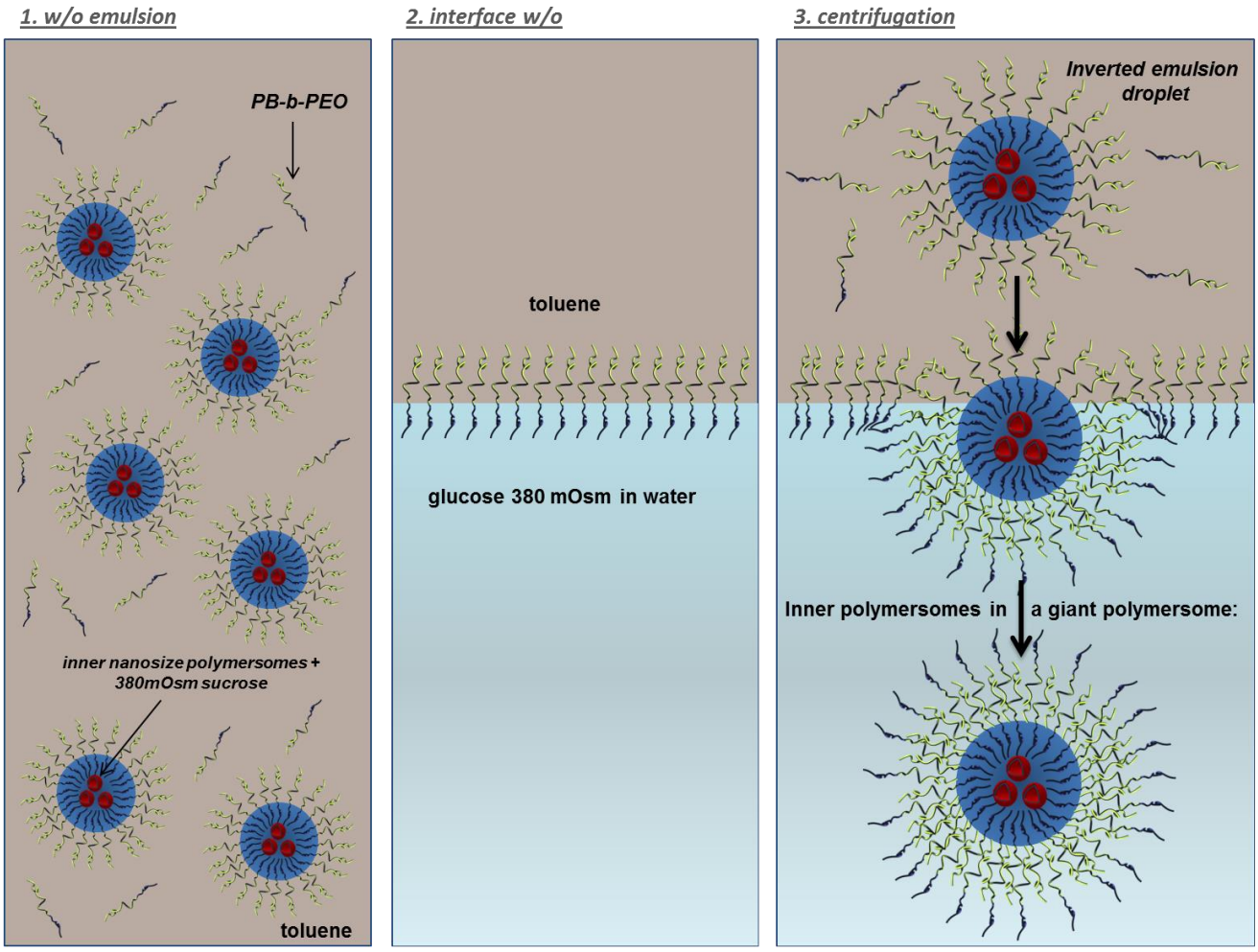


**Scheme 1.** Scheme of the emulsion-centrifugation process yielding either giant polymersomes (Figure 2) or polymersomes in polymersomes (when, like here a suspension of nanosize polymersomes (in red) is used as inner aqueous phase of the w/o emulsion).

Finally (step 3, Scheme 1), the first tube was emulsified with vigorous agitation by hand yielding quite homogeneous (see Figure 1) inverted emulsion droplets (alternatively, repeated pipetting works as well). Then 50 µL of this emulsion was poured slowly over the second interface tube. The sample was then immediately centrifuged at 20 °C at 500g for 4 min and the aqueous polymer vesosome suspension was recovered in the lower phase (Figure 2).

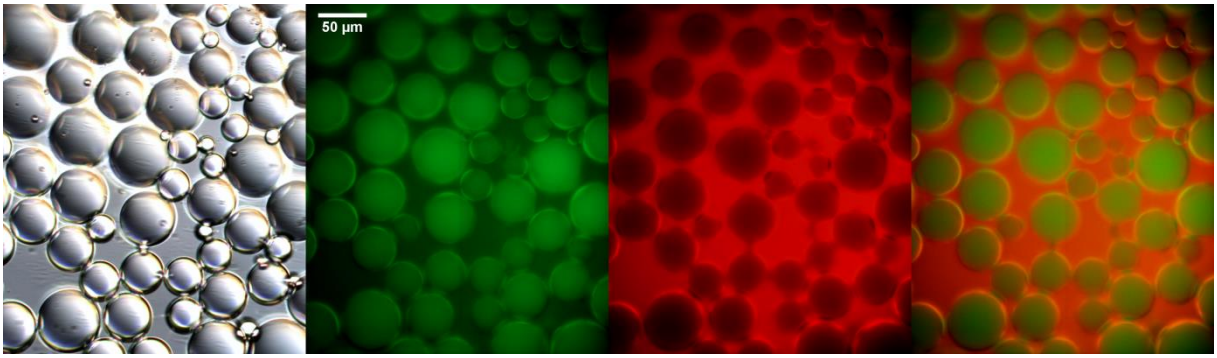


**Figure 1.** Optical microscopy acquisitions of the w/o emulsion stabilized by poly(butadiene)-*b*-poly(ethylene oxide). From left to right: bright field, epifluorescence (green channel), epifluorescence (red channel) and overlay of red and green channels. The green channel features the encapsulated FITC-dextran (1 mg/mL), the red channel features Nile Red (0.05 mg/mL) solubilized in toluene.

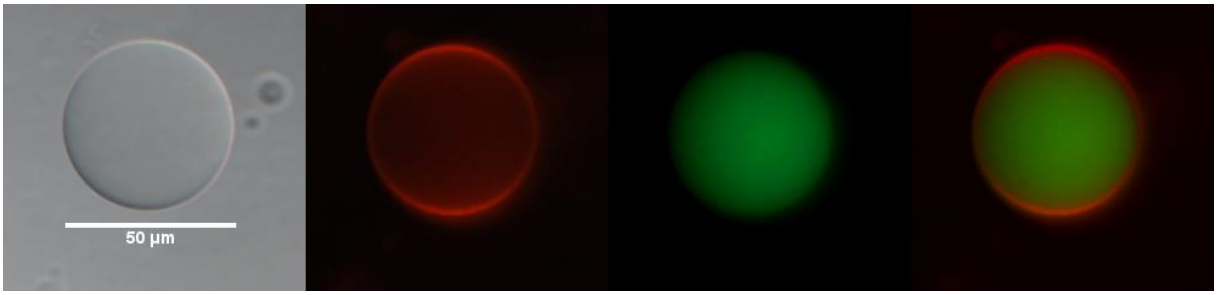


**Figure 2.** Microscopy acquisitions of a giant polymersome of poly(butadiene)-*b*-poly(ethylene oxide). From left to right, bright field microscopy, red channel epifluorescence with Nile Red membrane labeling (0.05 mg/mL), green channel with 10.000 g/mol FITC-dextran (1 mg/mL), and overlay of red and green.

The process has been described to quantitatively encapsulate hydrophilic solutions,[58] such as FITC-dextran as shown in Figure 2. Of course, any aqueous solution can be encapsulated using this method. For experiments regarding "cytoplasm mimic", the appropriate amount of respectively alginate/dextran was added to the nanosize polymersome suspension (at 380mOsm sucrose) to a final concentration of respectively 10/300 mg/mL. In both cases, the centrifugation time was reduced to 3 min.

### 2.2.2. Characterization methods

**Dynamic Light Scattering (DLS).** DLS measurements were conducted on a Malvern Zeta Sizer Nano ZS instrument with 90° angle analysis. The mean hydrodynamic diameter and its distribution were determined using Cumulant and CONTIN methods. For particle tracking,

viscosity and refractive index were determined for each solution using a rheometer (AR2000) and an Abbe refractometer.

**Spinning disk confocal microscopy.** The spinning disk microscope was a Leica DMI6000 (Leica Microsystems, Wetzlar, Germany) equipped with a confocal Scanner Unit CSU-X1 (Yokogawa) using for this experiment objective HCX PL Apo 100X oil NA 1.4 and an Evolve EMCCD camera (Roper Scientific, Evry, France). Z-stack analysis was performed with a galvanometric stage (Leica Microsystems, Wetzlar, Germany). The diode laser excitation wavelengths used were 491 nm and 561 nm and a Semrock emission filter with narrow bandpass windows in the blue (420 to 460 nm), green (506 to 536 nm) red (587 to 627 nm) and near infrared (670 to 730nm) spectral regions was used. Microscopy chambers were fabricated by sealing a slide against a coverslip with two layers of Parafilm™ featuring the three sides of the chamber. The sample was then injected by capillarity through the last open side. Finally, the last aperture was sealed with molten paraffin wax. Experiments were carried out in the *Bordeaux Imaging Center of the University of Bordeaux Segalen.* The help of Sébastien Marais is gratefully acknowledged, particularly for 3D reconstruction of z-stacks with the Imaris software.

**Epifluorescence and optical microscopy.** Bright field and fluorescence microscopy images of giant polymersomes (Figure 1 and 2) were taken on a Zeiss Axiovert 40 CFL inverted microscope with a EC Plan-NEOFLUAR 40x DIC Na 0.75 objective captured with a 2Mbytes digital Gigabit Ethernet CCD camera (Viewvorks VG-2M, South Korea). For epifluorescence microscopy, a mercury lamp was used as source with excitation and emission filters of narrow bandpass windows in the green (464.5 to 499.5 nm for excitation and 516 to 556 nm for emission) and red (532 to 544 nm for excitation and 573 to 637 nm for emission) spectral regions (provided by Semrock). The samples were placed between a glass slide and a coverslip separated by a Parafilm™ spacer as mentioned above for confocal microscopy imaging.

**Particle tracking.** The 2D Brownian motion of inner polymersomes labeled in red and encapsulated in a giant polymersome (Movie S1 in ESI) was tracked down. The 2D position ($x_M$,$y_M$) for each frame and each nanosize vesicle of the 50s movie (500 frames and $\tau$=100ms) was reported. By linking the trajectories (79 in total) for each nanosize vesicle frame by frame, we have access to displacements $\Delta x$, $\Delta y$ (788 in total) versus time. For the polymer

vesosome with the "cytoplasm mimick" Dextran, 187 frames of a longer movie (Movie S2 in ESI) were tracked yielding 810 displacements (56 trajectories).

**Instrumentation and Measurements for synthesis.** $^{1}$H (400 MHz) Nuclear Magnetic Resonance NMR spectra were recorded on a Bruker Avance DPX400 instrument at 23 °C and were referenced internally using the residual $^{1}$H solvent resonance relative to tetramethylsilane (δ=0). $M_{n\ SEC}$ and ($M_w/M_n$) values for copolymers PTMC-*b*-PBLG (3 mg/mL) were determined by Size Exclusion Chromatography SEC at 60 °C, using dimethylformamide (DMF) with LiBr (1 g/L) as eluent (0.8 mL/min), on a Jasco apparatus equipped with both Varian refractive index and UV detectors and two PL gel 5 µm mixed-C columns.

## 3. Results and Discussion

### 3.1. Formation of biomimetic compartmentalized polymersomes

Thanks to the emulsion-centrifugation process[56, 57] and its quantitative loading efficiency[58] (see Scheme 1, Experimental section), a suspension of red fluorescent Alexa 568 labeled polymersomes (or nanosize vesicles) was encapsulated in a green fluorescent Alexa 488 labeled giant polymersome, as shown in Figure 3 where inner red PTMC-*b*-PGA polymersomes can clearly be seen in a green giant PB-*b*-PEO polymersome. Movie S1[d] shows the Brownian motion of these inner nanosize polymersomes. The 3D reconstruction of the z-stack observation by spinning disk confocal microscopy of this polymer vesosome, evidences the localization of each nanosize polymersome inside the internal volume of the larger vesicle (Figure 3, 2[d]).

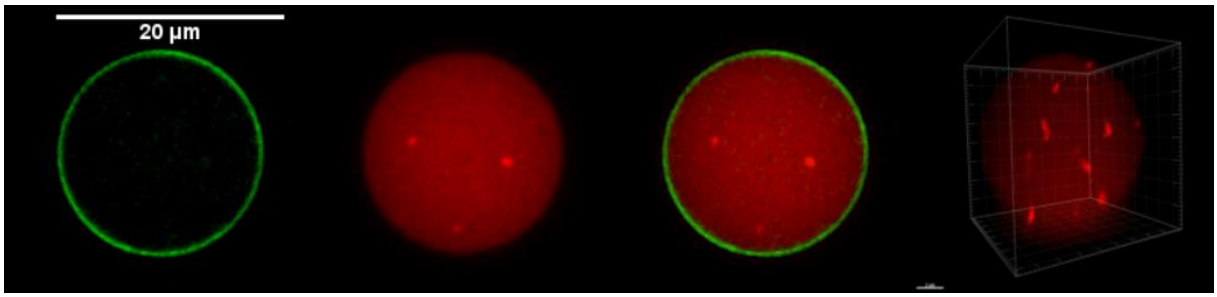


**Figure 3.** Spinning disk confocal microscopy acquisitions of a polymer vesosome. From left to right, green channel (membrane of the giant polymersome), red channel (nanosize inner polymersomes), overlay, and 3D reconstruction of z stack in red channel.

[d] Movie si_001 and [d] Movie si_002, http://pubs.acs.org/doi/suppl/10.1021/la204018w

By analogy with liposomes, such compartmentalized structures can be named polymer vesosomes[18, 19, 22, 59], polymersomes in polymersomes or double polymersomes[21, 60]. Only three groups[21, 30, 31] have tackled the challenge of compartmentalized polymersomes so far. We present here an original, facile, versatile, reproducible and low-product consuming technique. Solely the microfluidic method recently developed by Weitz and coworkers[21] presents in our opinion a better process control. However, the internal polymersome size is limited in that case to micrometric one by the process itself and the capillary diameters. The obtained morphology roughly resembles to organelles in a cell which are lipid bilayer compartments (endosomes, lysosomes, mitochondria...) encapsulated themselves in the plasmic membrane.

One step closer to the challenge of cellular biomimicry consists in adding another component with a relevant structure and function, the cytoplasm (here not including the organelles, whose mimicry has already been adresses). In addition to the obvious mechanical properties given by the cytoskeleton, the high macromolecular concentrations found intracellularly are also responsible for the so-called macromolecular crowding effect.[45, 51, 61] In 2001, R. John Ellis *and col.*[61] launched a call to biochemists to stop neglecting this "macromolecular crowding" in their studies, which is known in polymer science as the "excluded volume effect". All together, macromolecules in the cytoplasm, cytoskeleton and internal compartments occupy 20-30 vol.% of a cell, generating a strong steric repulsion between them. The consequences on the cell machinery have been rarely considered: for instance, most biochemical reactions are studies in dilute (ideal) solutions, while in real cells one should consider the activity coefficients for both thermodynamic and kinetic studies. He thus advises to use crowding agents under the following criterions: a molecular weight ranging from 50,000 to 200,000 g/mol, a high water solubility, not being prone to self-aggregation, and last but not least, no interaction with the tested system other than steric repulsion.

In a first attempt, the nanosize polymersome suspension was thus mixed with a highly water-soluble alginate at a final concentration of 10 mg/mL (Figure 4). For this strongly charged natural polymer, the molar mass distribution was reported in the literature: $M_n$=107,700 g.mol$^{-1}$ and $M_w$=231,500 gmol$^{-1}$,[62] so that the molar concentration of Alginate is 0.1 mM in our case. A 2 wt.% solution of this product has a viscosity of 1.07 Pa.s,[63] therefore the viscosity is around 0.5 Pa.s at 10 mg/mL. Thus we can predict a 350-fold reduction of the diffusion coefficient compared to the pure sucrose solution (0.00144 Pa.s). Actually, as observed in Movie S3[e] , the motion of inner nanosize polymersomes is not only hampered but

[e] Movie si_003, http://pubs.acs.org/doi/suppl/10.1021/la204018w

in fact completely blocked. One can assume that the high alginate concentration provokes a phase separation phenomenon induced by depletion layers around the PTMC-*b*-PGA vesicles excluding the alginate chains (Figure 4). The diffusion of spherical particles inside a concentrated macromolecular solution with a depletion layer of the chains around the spheres has been considered in theory, predicting anomalous diffusion with mean square displacements not linear *versus* time.[64] The case of our giant vesicles containing nanosize vesicles mixed with rather stiff alginate polyelectrolyte chains is even more dreadful since the diffusion is totally arrested. The fact that both alginate and the PGA chains (present on the outer shell of the nanosize polymersomes) are negatively charged must also play an important role in this segregation process, due to additional electrostatic repulsion forces. The 3D reconstruction of this vesosome (Figure 4 and Movie S4[f]) clearly evidences different clusters of inner PTMC-*b*-PGA polymersomes in the volume that always seem pushed against the "plasmic membrane" mimic; this is presumably due to the alginate chains exerting an osmotic pressure Π on them estimated around 260 Pa from the molar concentration of chains. The potential between two vesicles brought at contact by depletion attraction can be estimated by $2\pi \cdot \Pi \cdot R_v \cdot {R_a}^2 \approx 220\, k_B T$ ,[65] which explains why it overcomes thermal motion.

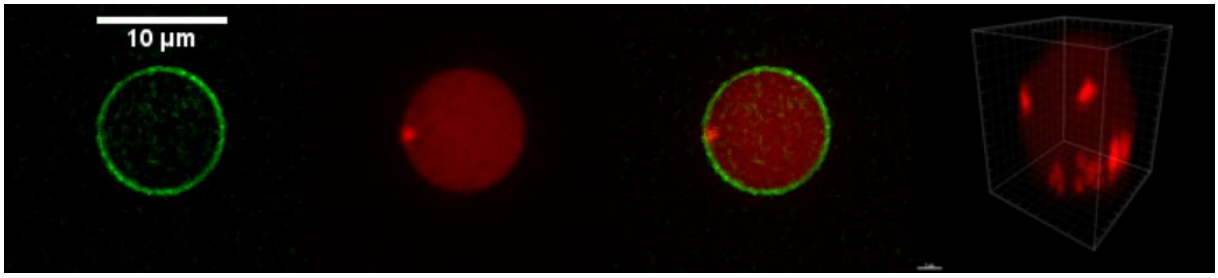


**Figure 4.** Spinning disk confocal microscopy acquisitions of a polymer vesosome with "cytoplasm mimic" alginate in the cavity of the giant polymersome. From left to right, green channel (membrane of the giant polymersome), red channel (nanosize inner polymersomes), overlay and 3D reconstruction in red channel.

In another set of experiments, a 4,000 g/mol neutral dextran was used as cytoplasm mimic at a concentration of 300 mg/mL. This concentration roughly corresponds to an intracellular macromolecular concentration of 20-30 vol.% and can be considered realistic to mimic the intracellular crowding.[61] For example, the total concentration of protein and RNA inside a cell of *Escherichia coli* lies between 300-400 mg/mL, in good correlation with our simplified synthetic model.[66] Finally, the choice of dextran is also motivated by the fact that its use is accepted in hard particle excluded volume models at high concentration for crowding effect.[61]

[f] Movie si_004, http://pubs.acs.org/doi/suppl/10.1021/la204018w

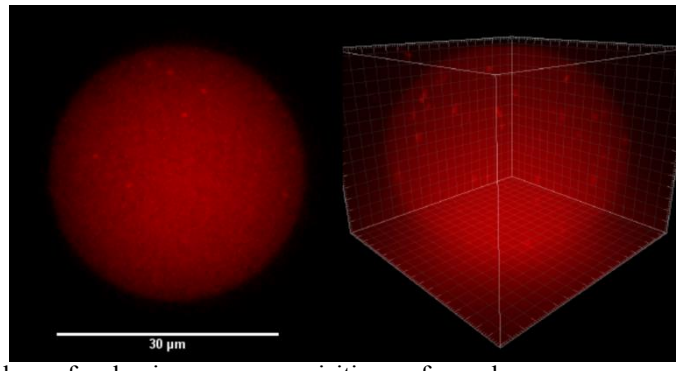


**Figure 5.** Spinning disk confocal microscopy acquisitions of a polymer vesosome with "cytoplasm mimic" dextran in the cavity of the giant polymersome. Red channel (nanosize inner polymersomes), and 3D reconstruction in red channel.

The resulting polymer vesosomes obtained in these conditions are reported in Figure 5. As observed on Movie S5[g], motion of the inner polymersomes is now considerably decreased and hindered, but not blocked, clearly illustrating this crowding effect at high volume fractions of macromolecules in a confined volume.

### 3.2. Quantitative analysis of the dynamics of internal vesicles

The observation of the stochastic motion of the nanosize polymersomes alone seems to be in agreement with a Brownian motion, showing that their loading into a giant polymersome does not affect their dynamic properties. In order to quantitatively analyze this parameter, the 2D positions of each distinct nanosize vesicle in Movie S1 were tracked ($\tau$=100 ms) and their displacement from frame to frame calculated. 788 $\Delta$x and $\Delta$y displacements or in other words 79 full trajectories could be obtained. The frequency of these displacements versus $\Delta$x and $\Delta$y is plotted in Figure 6.

In statistical physics, the normal (or Gaussian) distribution (Equation 1) is usually associated to random walks like particles in Brownian motion. In the case of pure diffusion (no translation), the mean position $\langle x \rangle = \mu$ is zero, while the mean square displacement $\langle x^2 \rangle$ is linear in time with a slope equal to $2\sigma^2$ (in one dimension).

$$f(x) = \frac{1}{\sqrt{2\pi\sigma^2}} \cdot e^{\frac{(x-\mu)^2}{2\sigma^2}} \qquad \text{Equation 1}$$

The presented data can be well fitted with a Gaussian distribution (Figure 6a), attesting that the motion of nanosize polymersomes is not affected by their encapsulation in a polymersome of approximately 20 µm diameter. However, the outer membrane could have restricted the diffusion of the small vesicles in some limiting volume (as a cage). This is not the case because the diameter of the giant vesicle is much larger (20 µm) than the mean square

[g] Movie si_005, http://pubs.acs.org/doi/suppl/10.1021/la204018w

displacement of the small internal ones and this giant vesicle is also prone to a slight translational diffusion itself. Another way to analyze the data consists in representing the mean square displacements of some of the longest lasting trajectories in a log-log representation (Figure 6b).

The trajectories represented here have the same slope in log-log representation than a model trajectory $r^2 = \Delta x^2 + \Delta y^2 = 4D_{diff} \times t$ estimated with the mean Diffusion coefficient (see Equation 2) calculated for these nanosize vesicles, again in agreement with purely diffusive (Brownian) motion. The scattering of the prefactor ( $4D_{diff}$ ) for the shown trajectories in blue is ascribed to the inherent size-dispersity of the internal vesicles (see Table 1).

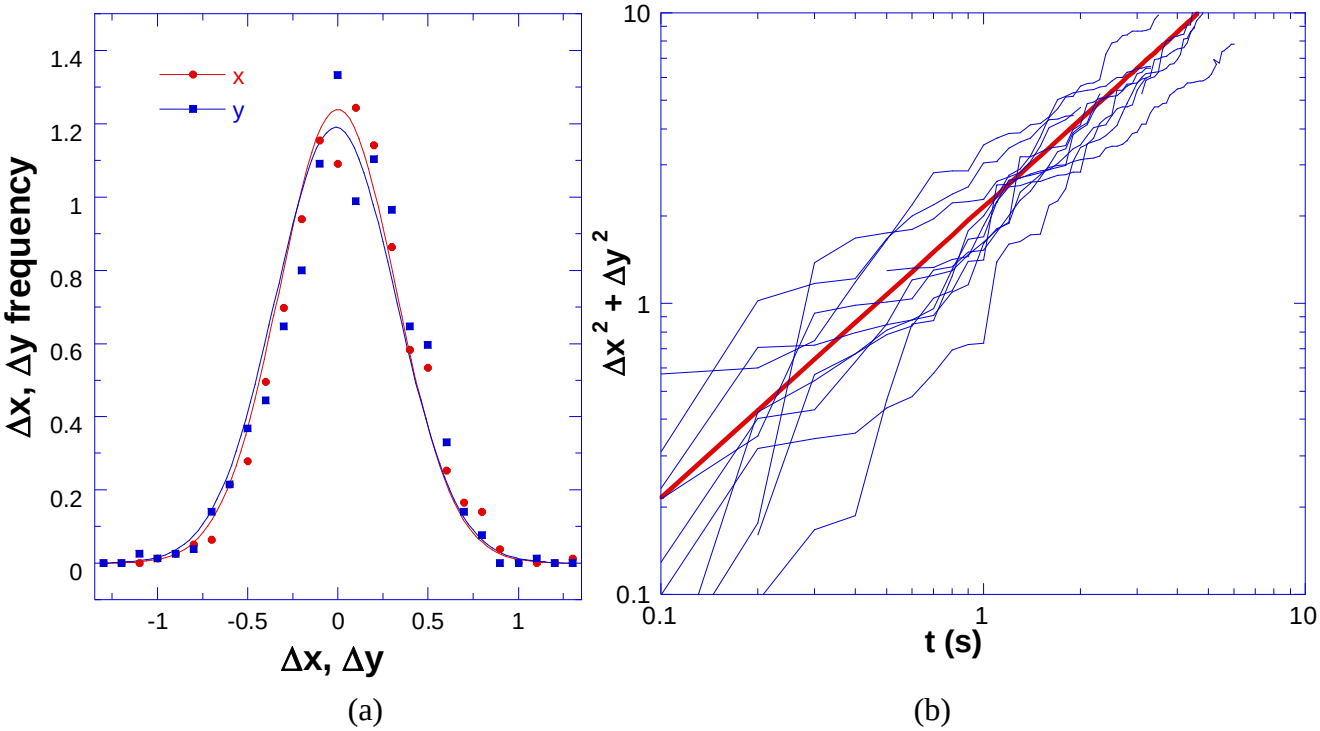


**Figure 6.** (a) Statistics of displacements (µm) in x (red circles) and y (blue squares) directions of nanosize inner polymersomes in vesosome corresponding to Figure 3 (Movie S1 ESI). (b) Mean square displacement $\Delta x^2$ and $\Delta y^2$ (µm$^2$) plotted *versus* time (s). Blue lines represent the experimental trajectories. The red line features the model trajectory with the mean calculated diffusion coefficient.

With the 788 $\Delta x$ and $\Delta y$ elementary steps, an average diffusion coefficient $D_{diff}$ can then be estimated following equation 2, and be converted into a hydrodynamic diameter $R_H$ using the well-known Stokes Einstein relation (Equation 3).

$$D_{diff}\left(\frac{\mu m^2}{s}\right) = \frac{\sigma^2(\mu m^2)}{2\tau(s)} \qquad \text{Equation 2}$$

$$R_H = \frac{k_B \cdot T}{6 \cdot \pi \cdot D_{diff} \cdot \eta} \qquad \text{Equation 3}$$

The obtained $D_{diff}$ and $R_H$ values can now be quantitatively compared to data resulting from the nanosize polymersomes initially prepared (Table 1). The values measured in solution by DLS are in excellent correlation with the ones determined inside giant polymersomes by video tracking, assessing the validity of the method and confirming quantitatively the randomness of the vesicles' motion.

***Table 1.*** Characteristics of nanosize polymersome suspension before and after encapsulation in a giant polymersome[a]

| Without cytoplasm mimic (380 mM sucrose, $\eta$ =0.00144 Pa.s [b,e]) | | | | | With cytoplasm mimic (dextran 300 mg/mL, 380 mM sucrose, $\eta$ =0.0367 Pa.s [b,f]) |
|---|---|---|---|---|---|
| Mean $R_H$ (nm)[c] | PDI[c] | Mean $D_{diff}$[c] ($\mu m^2/s$) | Mean $R_H$[d] (nm) | Mean $D_{diff}$[d] ($\mu m^2/s$) | $D_{diff}$[d] ($\mu m^2/s$) |
| 257±9 (Contin)[f] | 0.1±0.02 | 0.718±0.004[f] | 271±21[e] | 0.55±0.042[e] | 0.082±0.011[f] |

*[a] For each value, error represents the standard error $\sigma/\sqrt{n}$ where n represents the numbers of trajectories or measurements [b] Determined by rheometry [c] Determined by Dynamic Light Scattering in 380mM sucrose. PDI means Polydispersity Index. [d] Determined by particle tracking in 380mM sucrose with and without dextran 300 mg/mL. [e] determined at 21°C. [f] determined at 25°C.*

It seems visible in Movie S5, that the presence of 300 mg/mL dextran considerably and efficiently hinders the motion of the nanosize vesicles. Once again, their 2D positions was tracked from Movie S5, yielding to 810 Δx and Δy displacements or in other words 56 full trajectories. The frequency of the displacements versus Δx and Δy is plotted in Figure 7a and data properly fitted with a Gaussian distribution. The value of the diffusion coefficient of the nanosize polymersomes calculated in these "cytoplasm mimic" conditions is nearly 6.6 times slower than in low viscosity conditions (Table 1, Figure 7b). This significant decrease is however lower than the approximately 30-fold increase of viscosity for this solution of dextran compared to the initial aqueous solution. For this dextran T40 ($M_r$=40000 $gmol^{-1}$), M. Prouty and R. Podgornik derived a power law of osmotic pressure *versus* weight concentration,[67, 68] from which we calculate $5.3\times10^5$ Pa for a 300 mg/mL concentration. Prepared initially in pure water, the nanosize PTMC-*b*-PGA vesicles are submitted to hypertonic conditions inside the giant PB-*b*-PEO vesicle: the osmotic pressure exerted both by dextran and by 380 mM sucrose is estimated around $1.5\times10^6$ Pa. Therefore the hydrodynamic size of the PTMC-*b*-PGA vesicles might decrease by osmotic deflation through water permeability across their membrane.

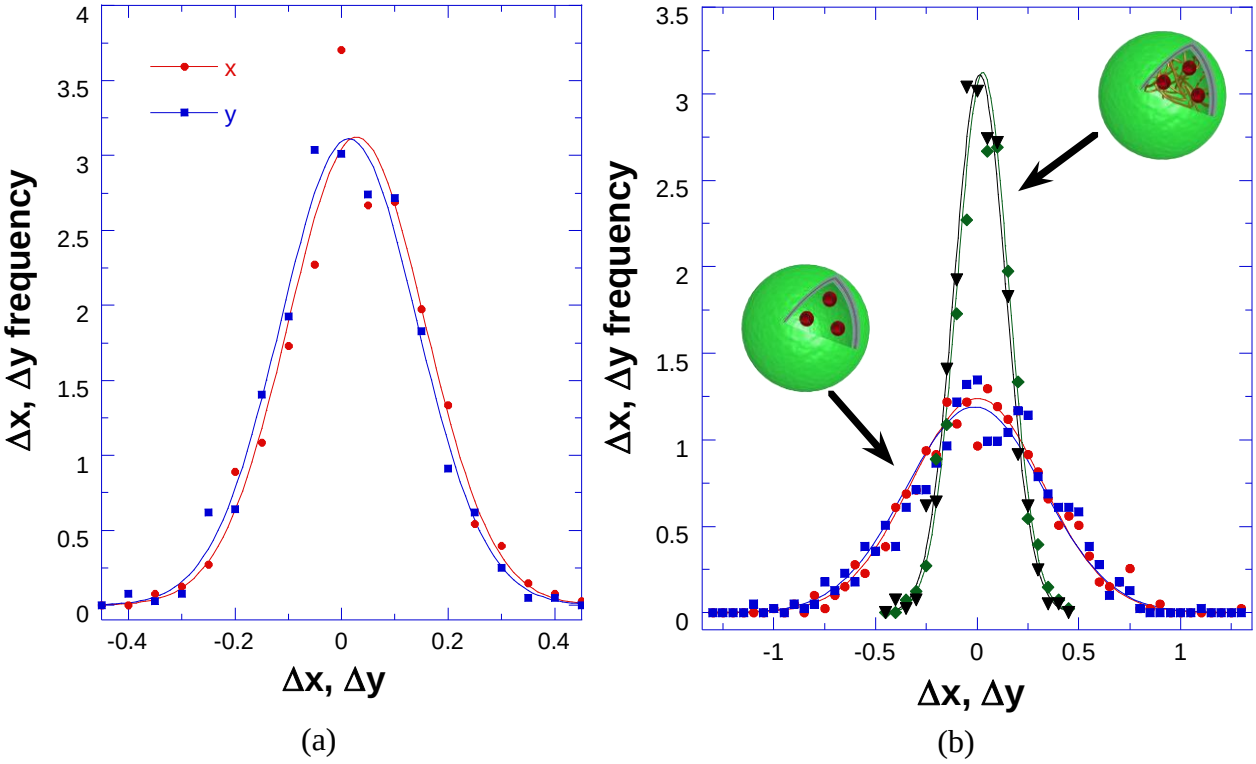


**Figure 7.** (a) Statistics of displacements in x (red circles) and y (blue squares) directions of nanosize inner polymersomes in 300 mg/mL dextran in giant polymersome, corresponding to Figure 5 and Movie S5 (ESI). (b) Comparison of displacement frequency without and with Dextran: overlay of Figures 6a and 7a.

Another explanation going in the same direction is the increase of the Brownian diffusion constant of vesicles due to the crowding effect (the volume taken by dextran chains being excluded to them). S. Longeville and coworkers have indeed evidenced by SANS a two-fold compaction of coil chains such as PEG in a 30 vol.% solution of a crowding agent such as the Ficoll 70 polysaccharide, exerting an osmotic pressure around $3\times10^5$ Pa.[69, 70] Therefore we can suspect a similar effect on the hydrophilic blocks of the polymersomes' membranes (PGA for the small vesicles, PEO for the giant vesicles). The two effects combined (osmotic deflation and hydrophilic chains compaction by the crowding agent) are explaining why particle tracking yielded a 6.6-fold decrease of the diffusion constant of the internal vesicles, while the ratio of viscosities with and without dextran is larger (about 30-fold). Finally, the viscosity of the dextran system (Table 1) is of the order of magnitude of the usual cytoplasm viscosity reported for red blood cells (0.01 Pa.s),[35] thereby confirming that is was a good choice for mimicking the interior of cells on a physical point of view.

## 4. Conclusion

In this work, we demonstrated the formation of artificial structural cell mimics with organelles and a "model cytoplasm" with a facile, versatile, reproducible and low product and time-consuming technique. To the best of our knowledge, this is the first report where both these aspects have been combined, especially with polymersomes. A suspension of nanosize inner polymersomes of PTMC-*b*-PGA (formed by nanoprecipitation) is encapsulated in giant polymersomes of PB-*b*-POE together with highly viscous alginate or dextran solutions, thanks to the emulsion-centrifugation process. The formation of this biomimetic structure was evidenced by fluorescence confocal microscopy. Moreover, the 2D motion of these artificial organelles was tracked down and confirmed as still being Brownian inside the volume of an approximately 20 µm giant polymersome. This analysis was repeated in presence of "cytoplasm mimic dextran", their motion being efficiency hindered as confirmed by a 6.6 times smaller diffusion coefficient. Furthermore, the concentration of 300 mg/mL of polysaccharide (dextran T40) brings a viscosity above 0.01 Pa.s, in the range of red blood cell cytoplasm viscosity, a volume fraction near 30% and an osmotic pressure above 1 MPa resembling the intra-cellular conditions caused by global cellular proteins. By reproducing the intracellular "macromolecular crowding effect" which plays a crucial role in the cell machinery, we believe that this synthetic and simplified approach constitutes an appropriate cytoplasm mimic. Even with such simplified cell mimics, soft materials with innovative properties can arise and extend the domain of possibilities in the fields of cosmetics, fragrance encapsulation, drug delivery and fine chemical additives.

## Annexes

**Supporting Information Available on http://pubs.acs.org/doi/suppl/10.1021/la204018w**

Movie S1 (http://pubs.acs.org/doi/suppl/10.1021/la204018w, si_001) acquired with a spinning disk confocal microscopy featuring the polymer vesosome in Figure 3, where the loaded red inner polymersomes can be clearly observed in Brownian motion as they are labeled with Alexa Fluor 568. Movie S2 (http://pubs.acs.org/doi/suppl/10.1021/la204018w, si_002) with the vesosome of Movie S1 reconstructed in three dimensions showing the localization of the inner polymersomes in the giant one. Movie S3 (http://pubs.acs.org/doi/suppl/10.1021/la204018w, si_003) featuring inner red-labeled polymersomes blocked in alginate loaded in the giant polymersome of Figure 5. Movie S4 (http://pubs.acs.org/doi/suppl/10.1021/la204018w, si_004) featuring the 3D reconstruction of the vesosome with alginate ("cytoplasm mimick") in Movie S3. Movie S5 (http://pubs.acs.org/doi/suppl/10.1021/la204018w, si_005) featuring inner red-labeled polymersomes in hindered motion in dextran ("cytoplasm mimick") loaded in a giant polymersome. Movie S6 (http://pubs.acs.org/doi/suppl/10.1021/la204018w, si_006) featuring the 3D reconstruction of the vesosome with Dextran in Movie S5.

---

This chapter has been published in *Langmuir*:

Marguet Maïté, Olivier Sandre, Sébastien Lecommandoux*, Polymersomes in "gelly" polymersomes: toward structural cell mimicry, *Langmuir*, **2012**, 28, p. 2035-2043

## References


1. Discher, B. M.; Won, Y. Y.; Ege, D. S.; Lee, J. C. M.; Bates, F. S.; Discher, D. E.; Hammer, D. A., *Science* **1999,** *284* (5417), 1143-1146.
2. Discher, D. E.; Eisenberg, A., *Science* **2002,** *297* (5583), 967-973.
3. Bermudez, H.; Brannan, A. K.; Hammer, D. A.; Bates, F. S.; Discher, D. E., *Macromolecules* **2002,** *35* (21), 8203-8208.
4. Brinkhuis, R. P.; Rutjes, F. P. J. T.; van Hest, J. C. M., *Polymer Chemistry* **2011**.
5. Christian, D. A.; Cai, S.; Bowen, D. M.; Kim, Y.; Pajerowski, J. D.; Discher, D. E., *European Journal of Pharmaceutics and Biopharmaceutics* **2009,** *71* (3), 463-474.
6. Meng, F.; Zhong, Z.; Feijen, J., *Biomacromolecules* **2009,** *10* (2), 197-209.
7. Cheng, R.; Feng, F.; Meng, F.; Deng, C.; Feijen, J.; Zhong, Z., *Journal of Controlled Release* **2011,** *152* (1), 2-12.
8. Li, M.-H.; Keller, P., *Soft Matter* **2009,** *5* (5), 927-937.
9. Van Dongen, S. F. M.; Verdurmen, W. P. R.; Peters, R. J. R. W.; Nolte, R. J. M.; Brock, R.; Van Hest, J. C. M., *Angewandte Chemie - International Edition* **2010,** *49* (40), 7213-7216.
10. Van Dongen, S. F. M.; Nallani, M.; Cornelissen, J. J. L. M.; Nolte, R. J. M.; Van Hest, J. C. M., *Chemistry - A European Journal* **2009,** *15* (5), 1107-1114.
11. Renggli, K.; Baumann, P.; Langowska, K.; Onaca, O.; Bruns, N.; Meier, W., *Advanced Functional Materials* **2011,** *21* (7), 1241-1259.
12. Onaca, O.; Hughes, D. W.; Balasubramanian, V.; Grzelakowski, M.; Meier, W.; Palivan, C. G., *Macromolecular Bioscience* **2010,** *10* (5), 531-538.
13. Tanner, P.; Baumann, P.; Enea, R.; Onaca, O.; Palivan, C.; Meier, W., *Accounts of Chemical Research* **2011**, null-null.
14. Schatz, C.; Louguet, S.; Meins, J. F. L.; Lecommandoux, S., *Angewandte Chemie - International Edition* **2009,** *48* (14), 2572-2575.
15. Brizard, A. M.; Van Esch, J. H., *Soft Matter* **2009,** *5* (7), 1320-1327.
16. Hawking, S., *The Universe in a Nutshell*. Bantam Books: New York, 2001.
17. Al-Jamal, W. T.; Kostarelos, K., *International Journal of Pharmaceutics* **2007,** *331* (2), 182-185.
18. Scholl, I.; Boltz-Nitulescu, G.; Jensen-Jarolim, E., *Journal of Controlled Release* **2005,** *104* (1), 1-27.
19. Walker, S. A.; Kennedy, M. T.; Zasadzinski, J. A., *Nature* **1997,** *387* (6628), 61-64.
20. Shum, H. C.; Zhao, Y. J.; Kim, S. H.; Weitz, D. A., *Angewandte Chemie - International Edition* **2011,** *50* (7), 1648-1651.
21. Kim, S.-H.; Shum, H. C.; Kim, J. W.; Cho, J.-C.; Weitz, D. A., *Journal of the American Chemical Society* **2011**, null-null.
22. Wong, B.; Boyer, C.; Steinbeck, C.; Peters, D.; Schmidt, J.; van Zanten, R.; Chmelka, B.; Zasadzinski, J. A., *Advanced Materials* **2011,** *23* (20), 2320-2325.
23. McPhail, D.; Tetley, L.; Dufes, C.; Uchegbu, I. F., *International Journal of Pharmaceutics* **2000,** *200* (1), 73-86.
24. Bolinger, P. Y.; Stamou, D.; Vogel, H., *Angewandte Chemie - International Edition* **2008,** *47* (30), 5544-5549.
25. Kreft, O.; Prevot, M.; Möhwald, H.; Sukhorukov, G. B., *Angewandte Chemie - International Edition* **2007,** *46* (29), 5605-5608.
26. Kreft, O.; Skirtach, A. G.; Sukhorukov, G. B.; Möhwald, H., *Advanced Materials* **2007,** *19* (20), 3142-3145.

27. Stadler, B.; Price, A. D.; Chandrawati, R.; Hosta-Rigau, L.; Zelikin, A. N.; Caruso, F., *Nanoscale* **2009,** *1* (1), 68-73.
28. Chandrawati, R.; Hosta-Rigau, L.; Vanderstraaten, D.; Lokuliyana, S. A.; Stadler, B.; Albericio, F.; Caruso, F., *ACS Nano* **2010,** *4* (3), 1351-1361.
29. Hosta-Rigau, L.; Chung, S. F.; Postma, A.; Chandrawati, R.; Städler, B.; Caruso, F., *Advanced Materials* **2011,** *23* (35), 4082-4087.
30. Fu, Z.; Ochsner, M. A.; De Hoog, H. P. M.; Tomczak, N.; Nallani, M., *Chemical Communications* **2011,** *47* (10), 2862-2864.
31. Chiu, H.-C.; Lin, Y.-W.; Huang, Y.-F.; Chuang, C.-K.; Chern, C.-S., *Angewandte Chemie International Edition* **2008,** *47* (10), 1875-1878.
32. Hayward, R. C.; Utada, A. S.; Dan, N.; Weitz, D. A., *Langmuir* **2006,** *22* (10), 4457-4461.
33. Shum, H. C.; Santanach-Carreras, E.; Kim, J. W.; Ehrlicher, A.; Bibette, J.; Weitz, D. A., *Journal of the American Chemical Society* **2011,** *133* (12), 4420-4426.
34. Faivre, M.; Campillo, C.; Pepin-Donat, B.; Viallat, A., *Progress.in Colloid and Polymer Science.*, **2006**; 133, pp 41-44.
35. Campillo, C.; Pépin-Donat, B.; Viallat, A., *Soft Matter* **2007,** *3* (11), 1421-1427.
36. Kremer, S.; Campillo, C.; Pepin-Donat, B.; Viallat, A.; Brochard-Wyart, F., *Europhysics Letters* **2008,** *82* (4).
37. Campillo, C. C.; Schroder, A. P.; Marques, C. M.; Pepin-Donat, B., *Soft Matter* **2008,** *4* (12), 2486-2491.
38. Campillo, C. C.; Schroder, A. P.; Marques, C. M.; Pépin-Donat, B., *Materials Science and Engineering C* **2009,** *29* (2), 393-397.
39. Kazakov, S.; Kaholek, M.; Teraoka, I.; Levon, K., *Macromolecules* **2002,** *35* (5), 1911-1920.
40. Saleem, Q.; Liu, B.; Gradinaru, C. C.; MacDonald, P. M., *Biomacromolecules* **2011,** *12* (6), 2364-2374.
41. Hong, J. S.; Stavis, S. M.; Depaoli Lacerda, S. H.; Locascio, L. E.; Raghavan, S. R.; Gaitan, M., *Langmuir* **2010,** *26* (13), 11581-11588.
42. Limozin, L.; Sackmann, E., *Physical Review Letters* **2002,** *89* (16).
43. Jesorka, A.; Markström, M.; Orwar, O., *Langmuir* **2005,** *21* (4), 1230-1237.
44. Osinkina, L.; Markström, M.; Orwar, O.; Jesorka, A., *Langmuir* **2010,** *26* (1), 1-4.
45. Jesorka, A.; Markström, M.; Karlsson, M.; Orwar, O., *Journal of Physical Chemistry B* **2005,** *109* (31), 14759-14763.
46. Smith, A. M.; Jaime-Fonseca, M. R.; Grover, L. M.; Bakalis, S., *Journal of Agricultural and Food Chemistry* **2010,** *58* (8), 4719-4724.
47. Hong, J. S.; Vreeland, W. N.; Lacerda, S. H. D.; Locascio, L. E.; Gaitan, M.; Raghavan, S. R., *Langmuir* **2008,** *24* (8), 4092-4096.
48. Tiwari, S.; Goyal, A. K.; Mishra, N.; Vaidya, B.; Mehta, A.; Dube, D.; Vyas, S. P., *Procedia in Vaccinology* **2009,** *1* (1), 148-163.
49. Viallat, A.; Dalous, J.; Abkarian, M., *Biophysical Journal* **2004,** *86* (4), 2179-2187.
50. Mader, M. A.; Vitkova, V.; Abkarian, M.; Viallat, A.; Podgorski, T., *European Physical Journal E* **2006,** *19* (4), 389-397.
51. Long, M. S.; Jones, C. D.; Helfrich, M. R.; Mangeney-Slavin, L. K.; Keating, C. D., *Proceedings of the National Academy of Sciences* **2005,** *102* (17), 5920-5925.
52. Lee, H. K.; Soukasene, S.; Jiang, H.; Zhang, S.; Feng, W.; Stupp, S. I., *Soft Matter* **2008,** *4* (5), 962-964.
53. Lee, J. S.; Zhou, W.; Meng, F.; Zhang, D.; Otto, C.; Feijen, J., *Journal of Controlled Release* **2010,** *146* (3), 400-408.
54. Lee, J. S.; Zhou, W.; Zhang, D.; Otto, C.; Feijen, J., *Journal of Controlled Release* **2008,** *132* (3), e28-e29.

55. Sanson, C.; Schatz, C.; Le Meins, J. F.; Brûlet, A.; Soum, A.; Lecommandoux, S., *Langmuir* **2010,** *26* (4), 2751-2760.
56. Mabrouk, E.; Cuvelier, D.; Pontani, L. L.; Xu, B.; Lévy, D.; Keller, P.; Brochard-Wyart, F.; Nassoy, P.; Li, M. H., *Soft Matter* **2009,** *5* (9), 1870-1878.
57. Mabrouk, E.; Cuvelier, D.; Brochard-Wyart, F.; Nassoy, P.; Li, M. H., *Proceedings of the National Academy of Sciences of the United States of America* **2009,** *106* (18), 7294-7298.
58. Pautot, S.; Frisken, B. J.; Weitz, D. A., *Langmuir* **2003,** *19* (7), 2870-2879.
59. Mishra, V.; Mahor, S.; Rawat, A.; Dubey, P.; Gupta, P. N.; Singh, P.; Vyas, S. P., *Vaccine* **2006,** *24* (27-28), 5559-5570.
60. Ebato, Y.; Kato, Y.; Onishi, H.; Nagai, T.; Machida, Y., *Drug Development Research* **2003,** *58* (3), 253-257.
61. R.John, E., *Trends in Biochemical Sciences* **2001,** *26* (10), 597-604.
62. Gomez, C. G.; Rinaudo, M.; Villar, M. A., *Carbohydrate Polymers* **2007,** *67* (3), 296-304.
63. Gomez, C. G.; Pérez Lambrecht, M. V.; Lozano, J. E.; Rinaudo, M.; Villar, M. A., *International Journal of Biological Macromolecules* **2009,** *44* (4), 365-371.
64. Ochab-Marcinek, A.; Holyst, R., *Soft Matter* **2011,** *7* (16), 7366-7374.
65. Lekkerkerker, H. N. W.; Tuinier, R.; Lekkerkerker, H., *Stability of Colloid–Polymer Mixtures Colloids and the Depletion Interaction*. Springer: Berlin / Heidelberg. 2011; Vol. 833, pp 131-175.
66. Zimmerman, S. B.; Trach, S. O., *Journal of Molecular Biology* **1991,** *222* (3), 599-620.
67. Prouty, M. S.; Schechter, A. N.; Parsegian, V. A., *Journal of Molecular Biology* **1985,** *184* (3), 517-528.
68. Chik, J. K.; Lindberg, U.; Schutt, C. E., *Journal of Molecular Biology* **1996,** *263* (4), 607-623.
69. Le Coeur, C.; Demé, B.; Longeville, S., *Physical Review E* **2009,** *79* (3), 031910.
70. Le Coeur, C.; Teixeira, J.; Busch, P.; Longeville, S., *Physical Review E* **2010,** *81* (6), 061914.

# CHAPTER 3

## Polymersomes in Polymersomes: multiple loading and permeability control

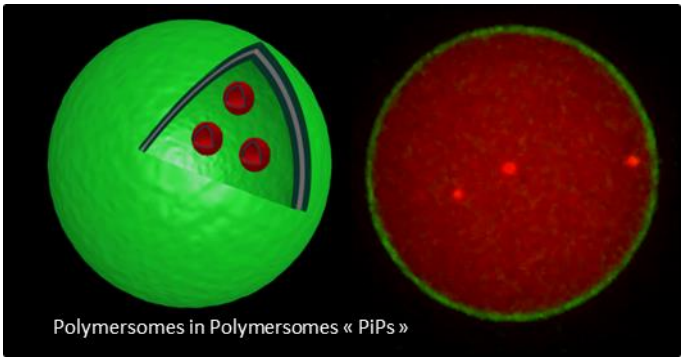

*In the previous chapter (**Chapter 2**), we have demonstrated the formation of structural cell mimics, with organelle mimics enclosed in a cytoplasm mimic, enclosed in a larger polymer vesicle.*
*Cell biomimicry is fundamentally important as it may help to better understand the eukaryotic cell. Studying any machine and its components is indeed not always sufficient to completely understand its full complexity; it may sometimes be necessary to put it together from its parts. This is particularly valid for Life. Feynman with his famous sentence "what I cannot create, I do not understand" would certainly have not disagreed. From the most evident and fundamental point of view, mimics as model systems enable molecular biologists and biochemists to acquire new tools to complement biological studies as they allow to study separately parameters closely correlated in nature. Quantitative measurements in vivo are currently still difficult to obtain and the freedom to change parameters is so limited that one cannot investigate them completely for a given mechanism. Then, the establishment of a model which could enable the study of various cellular mechanisms coupled together, and to understand how complexity is established, step by step, would be of outmost relevance. In a more concrete and applied perspective, such engineered cell mimics could open many prospects for therapy as biomedical devices and in biotechnology as bioreactors to synthesize pure proteins. In any case, the first and foremost challenge to address lies in the controlled formation of these cell mimics, which although non-living, will roughly approach the complexity and functionality of living cells. This vision is represented in **Chapter 2**.*

*Once the generation of these cell mimics is controlled and optimized, material scientists can take advantage of their structure to gain new properties and form innovative, with previously unmatched efficiency, soft materials. More particularly, for the biomedical/pharmaceutical field, we have identified several potential long-term benefits arising from multicompartmentalized polymersomes (or polymer vesosomes). The work presented in this Chapter (**Chapter 3**) highlights two of these properties, that we were able to evidence. Indeed, our approach enables multiple encapsulation in these multiple available compartments, providing a first path towards multi-therapy, together with an exquisite control over permeation properties, tuned for a better control of the system release kinetics.*

## 1. Introduction

Polymersomes are vesicles obtained from the self-assembly of amphiphilic block copolymers in aqueous solution as a result of free energy minimization.[1] Their potential use as drug delivery systems[2-6], sensors, and/or nanoreactors[7-9] has recently attracted a great deal of interest.[10] Polymersomes exhibit larger mechanical stability and lower permeability than liposomes, their structural analogues that often suffer from prematurely induced drug leakage.[11] To circumvent this limitation, J.A. Zasadzinski and coworkers developed liposomes in liposomes structures, also referred as "vesosomes".[12] With such a compartmentalized structure, a molecule encapsulated in the inner liposomes, would have to permeate through two successive membranes, instead of a single one before leaking into the outside environment. This double membrane effect was demonstrated by observing the serum half-life of ciprofloxacin drug increasing from 10 minutes in single liposomes to 6 hours in vesosomes.[13] Other reports evidenced the biomedical impact of such vesosomes for transcutaneous[14], and oral administration[15, 16]; an important future challenge in drug delivery and cancer therapy. More complex or compartmentalized structures in general, have started to appear because they enable an unprecedented level of control, in particular in the fields of drug delivery[17, 18] and confined reactors.[19-21] However, it is still very challenging[22, 23] to encapsulate multiple distinct components in a single compartment[24] and control their stability and release properties.

Such vesosome structures based on polymers that can be named "polymersomes in polymersomes", have been recently reported. The most recent approach consisted in forming the larger polymersomes by film rehydration with a suspension of smaller polymersomes previously formed by the solvent displacement method (or nanoprecipitation).[25] The drawback of this technique lies essentially in the poor encapsulation yield during film rehydration. In order to overcome this limitation, other options such as emulsions or double emulsions techniques have been investigated. The first team taking up this challenge used two successive emulsions.[26] Even if very original, such a process is not the most easy to use and may suffer from a lack of reproducibility and homogeneity. Weitz and coworkers formed another type of complex polymersomes, aggregates of polymersomes, or multicompartment vesicles using microfluidics, such approach allowing a high level of control and reproducibility.[24]

Herein, we demonstrate the generation of polymer vesosomes, i.e. polymersomes in polymersomes, with an original, facile, versatile, reproducible and low product-consuming

technique. Our method allows multiple compartment encapsulation and the formation of systems of controlled permeability, as they present a significant decrease in the release rate of an anticancer drug doxorubicin (DOX) encapsulated in the inner polymersomes.

## 2. Experimental Section

### 2.1. Materials and reagents

Poly(butadiene)$_{30}$-*b*-poly(ethylene oxide)$_{46}$ ($PB_{30}$-*b*-$PEO_{46}$) (P9095-BdEO, $M_{n\ PB}$=2500 g/mol and $M_{n\ PEO}$=1300 g/mol, I=1.04) and amino-terminated poly(butadiene)$_{20}$ ($PB_{20}$) (for polymersome membrane labeling) ($M_n$=1700 g/mol, I=1.11, f>0,98%, P3977-BdNH2) were purchased from Polymer Source. Alexa Fluor 405-carboxylic acid, succinimidyl ester (1 mg, A 30000, 1028.26 g/mol), Alexa Fluor 568-carboxylic acid, succinimidyl ester (*mixed isomers*, 1mg A20003, 791.8 g/mol) and Alexa Fluor 488 carboxylic acid, succinimidyl ester (*mixed isomers*, 1mg A20000, 643.41 g/mol) were purchased from Invitrogen. Fluorescein isothiocyanate isomer 1 (F7250, 250 mg, 389.4 g/mol) and Fluorescein isothiocyanate dextran (FD20S-100mg, 20,000g/mol) were received from Sigma Aldrich. Sucrose 99% was from Alfa Aesar (A15583 L 13300, 2.5g) and D-(+)-glucose from Sigma Aldrich (G5767-500g). Doxorubicin hydrochloride was purchased from Discovery fine chemicals. Solvents from Sigma Aldrich for fluorophore labeling (DMSO and DMF) were anhydrous. All products were used as received unless otherwise specified.

Poly(trimethylene carbonate)$_{30}$-*b*-poly($_L$-glutamic acid)$_{19}$ $PTMC_{30}$-*b*-$PGA_{19}$ diblock copolymer was synthesized by ring-opening polymerization (ROP) of δ-benzyl-L-glutamate N-carboxyanhydride (NCA) initiated by a primary amine end-functionalized PTMC macroinitiator according to a previously described method.[27] All the experiments described were performed on $PTMC_{30}$-*b*-$PGA_{19}$ diblock copolymer ($M_n$=5492 g/mol, I=2).

### 2.2. Methods

#### 2.2.1. Fluorophore labeling and self-assembly

**Fluorophore labeling**.

- *Alexa Fluor 568 labeled $PTMC_{30}$-b-$PGA_{19}$*: After flame-drying of a round-bottom flask under vacuum, the following reagents were introduced under inert nitrogen atmosphere:

primary end-functionalized amine $PTMC_{30}$-*b*-$PGA_{19}$ (99.9 mg, 18.2 µmol), anhydrous DMSO (2 mL), DIPEA (140 µL, 804 µmol) and reactive Alexa Fluor 568-carboxylic acid, succinimidyl ester (1 mg, 1.26 µmol) in DMSO (120 µL). The reaction was then allowed to proceed for one night under static nitrogen atmosphere. The conjugate $PTMC_{30}$-*b*-$PGA_{19}$-Alexa Fluor 568 was purified by dialysis (5 L, 3 h, MWCO : 3500 g/mol) after dilution in the flask by DMSO for a better recovery. External medium was renewed six times in course of dialysis. After lyophilization, the conjugate was recovered in a 97 % yield (determined by gravimetry).

- *Fluorescein labeled $PTMC_{30}$-b-$PGA_{19}$:* After flame-drying of a round-bottom flask under vacuum, the following reagents were introduced under inert nitrogen atmosphere: primary end-functionalized amine $PTMC_{30}$-*b*-$PGA_{19}$ (200.1 mg, 36.4 µmol), anhydrous DMSO (1.9 mL), DIPEA (140 µL, 804 µmol) and reactive Fluorescein isothiocyanate (18 mg, 46.2 µmol) in DMSO (3.6 mL). The reaction was then allowed to proceed for one night under static nitrogen atmosphere. The conjugate $PTMC_{30}$-*b*-$PGA_{19}$-Fluorescein was purified by dialysis (5 L, 3 h, MWCO : 3500 g/mol). External medium was renewed four times in course of dialysis. After lyophilization, the conjugate was recovered in an 81 % yield (determined by gravimetry).

- *Alexa Fluor 488 labeled poly(butadiene):* After flame-drying under vacuum of a round-bottom flask, the following reagents were introduced under inert nitrogen atmosphere: primary end-functionalized amine $PB_{20}$ (84.1 mg, 49.5 µmol), anhydrous DMF (2 mL), DIPEA (8 µL, 45.9 µmol) and reactive Alexa Fluor 488-carboxylic acid, succinimidyl ester (1 mg, 1.55 µmol) in DMF (120 µL). The reaction was then allowed to proceed for overnight under static nitrogen atmosphere. After concentrating the mixture by evaporation of DMF under vacuum, the polymer was precipitated and washed with water. Finally, it was dissolved in THF and recovered after drying under dynamic vacuum.

- *Alexa Fluor 405 labeled poly(butadiene):* After flame-drying under vacuum of a round-bottom flask, the following reagents were introduced under inert nitrogen atmosphere: primary end-functionalized amine $PB_{20}$ (81.5 mg, 48 µmol), anhydrous DMF (2 mL), DIPEA (20 µL, 115 µmol) and reactive Alexa Fluor 405-carboxylic acid, succinimidyl ester (1 mg, 0.97 µmol) in DMF (120 µL). The reaction was then allowed to proceed for overnight under static nitrogen atmosphere. After concentrating the mixture by evaporation of DMF under vacuum, the polymer was precipitated and washed with water. Finally, it was dissolved in THF and recovered after drying under dynamic vacuum.

**Nanoprecipitation yielding nanosize polymersomes of $PTMC_{30}$-*b*-$PGA_{19}$ for confocal microscopy.**

*Red fluorescent nanosize vesicles.* For confocal microscopy acquisitions, 4.5 mL Tris Buffer, 50 mM, pH 7.4, were added slowly with a push syringe at a rate of 2.25 mL/h over 5 mg of PTMC-*b*-PGA-Alexa Fluor 568 in DMSO (0.5 mL) stirred at 500 rpm at 25 °C. The sample was then dialyzed with a 50,000 g/mol cut-off in 5 L Milli Q water with 3 renewals. Size and polydispersity (Table S1) were characterized by dynamic light scattering (DLS).

*Green fluorescent nanosize vesicles for double loading.* Same procedure as above was used, but with 0.5 mL copolymer in DMSO taken from a DMSO solution (1.4 mL) of 7 mg $PTMC_{30}$-*b*-$PGA_{19}$ and 7 mg $PTMC_{30}$-*b*-$PGA_{19}$-fluorescein. Size and polydispersity (Table 1) were characterized by dynamic light scattering (DLS).

**Table 1.** Dynamic Light Scattering size measurement of nanopolymersomes at 25°C

| | Red polymersomes | Green polymersomes |
|---|---|---|
| $D_H$/nm | 500 | 655 |
| PDI[a] | 0.06 | 0.09 |

[a] Polydispersity index

**Double nanosize polymersome loading.** Red (PTMC-*b*-PGA-Alexa Fluor 568) and green ($PTMC_{30}$-*b*-$PGA_{19}$-fluorescein) labeled nanosize vesicle suspensions were mixed at 50% v/v (with 380mM sucrose). Prior to mixing and encapsulation by emulsion-centrifugation, both suspensions were concentrated by ultrafiltration (MWCO: 1,000 g/mol, 400 rpm) from 4 to approximately 1 mL, yielding a final concentration of approximately 4 mg/mL.

**Triple fluorophore loading.** A 0.5 mL solution of PB-*b*-PEO in toluene at 3 mg/mL (mixed with 10 wt.% PB-Alexa Fluor 405 included) as the organic phase, was used to encapsulate by emulsion-centrifugation a 50% v/v mixture of FITC-dextran and red fluorescent nanosize vesicles (PTMC-*b*-PGA-Alexa Fluor 568). FITC-dextran was at 2 mg/mL and the red nanosize vesicle suspension was the one obtained by ultrafiltration for the double nanosize polymersome loading experiment and diluted first by ¾ (≈ 3 mg/mL).

**Emulsion-centrifugation yielding giant PB-*b*-PEO encapsulating a PTMC-*b*-PGA nanosize vesicle suspension.** In a typical procedure inspired from Min-Hui Li's team[28, 29], 5

µL of a nanosize vesicle suspension formed by nanoprecipitation with 380 mOsm sucrose were poured in 500 µL toluene at 3 mg/mL PB-*b*-PEO (including, depending on each experiment, 0 or 10 wt% of Alexa Fluor 488 or 405 labeled PB) in a classic Eppendorf tube. The solution was stirred for at least 2 hours. The complete dissolution was confirmed by DLS (no intensity scattered). In another tube, 30 µL of the same organic solution was poured over 30 µL of a 380 mOsm aqueous glucose solution and allowed to stabilize for 30 min (Mabrouk et al.[28] verified that 10 min were enough for complete coverage of the interface with polymer). Finally, the first tube was emulsified with vigorous agitation by hand yielding quite homogeneous emulsion droplets (alternatively, repeated pipetting works as well) and 50 µL of it was taken and poured slowly and immediately over the second interface tube. Immediately following this step, the sample was centrifuged at 20 °C at 500g for 4 min and the aqueous polymer vesosome suspension was recovered. Of course, any aqueous solution can be encapsulated instead of the PTMC-*b*-PGA nanosuspension.

### 2.2.2. Loading and *in vitro* release of Doxorubicin

To conduct the present study rigorously, for this section we did not only rely on volumes as indicated by Eppendorf micropipettes to calculate the various concentrations, but we always weighed samples to calculate as accurately as possible the actual volume added, thus the most precise possible concentration.

**Nanosize polymersomes' Doxorubicin loading.**[30] Doxorubicin (DOX) loading was performed at a feed weight ratio of 15 % (fwr (%) = $m_{Dox}/m_{polymer\ in\ initial\ solution} \times 100$) by nanoprecipitation. 15.4 mg of Dox was dissolved in DMSO (10.1 mL) with block copolymer PTMC-*b*-PGA (102 mg). Tris buffer at pH 7.4 (60 mL; 50 mM) was then quickly added (5 s) to the organic phase under magnetic stirring (1000 rpm, 25 °C). Excess drug and DMSO were removed by dialysis (4 L, 3 h, 25 °C; MWCO: 3500 g/mol) against Tris buffer (10 mM Tris, pH 7.4, ionic strength 150 mM). External medium was renewed two times in the course of dialysis. It was verified in a previous work[30] that all the DMSO was removed during this time by elemental analysis. The nanosuspension was then retrieved and concentrated by ultrafiltration to a final volume of 4.6 mL. Vesicle concentration after dialysis was 22.2 mg/mL. For every quantification of doxorubicin from these nanosize polymersomes, the suspension was diluted to a final concentration of 0.4 mg/mL (final dilution of 50) to avoid saturation of UV-vis spectrophotometer.

Doxorubicin loading content was determined by absorbance spectroscopy. Loaded vesicles were first broken by adding a large excess of DMSO (80 vol% of the final mixture) and by vortexing the solution for 5 s. The sample was then subjected to UV analysis at $\lambda_{max}$=485 nm.

Quantification was performed from the calibration curve of doxorubicin in a DMSO/Tris buffer 10 mM, pH 7.4, 150 mM NaCl (80/20 v/v) mixture (Figure S4, undirect method). To cross-check this value, absorbance at $\lambda_{max}$=485 nm was also directly measured on loaded vesicles in Tris buffer. The vesicles alone did not significantly absorb at this wavelength and their absorbance spectra (at same copolymer concentrations) could be subtracted from the loaded vesicle spectra to extrapolate the absolute absorbance of doxorubicin (see Figure S5). Quantification was performed from the calibration curve of doxorubicin in Tris buffer 10 mM (Figure S6, direct method). Each experiment was carried out in triplicate, and average values established from measurement of four different samples (Table 2). Quantification of the DOX loading will be given through the loading efficiency (%) (mass of Dox in vesicles /mass of DOX in the initial solution) and loading content (%) (mass of Dox in vesicles / mass of polymer).

**Table 2.** Characteristics of doxorubicin (Nano-DOX) loaded nanosize polymersomes

| FWR /wt.% [a] | $D_H$/ nm | PDI [b] | Loading content/wt.% | Loading efficiency/wt.% |
|---|---|---|---|---|
| 15 | 218 | 0.06 | 9 ± 0.33[c]<br>9 ± 0.32[d] | 57 ± 2.2[c]<br>59 ± 2.14[d] |

*[a] Feed weight ratio [b] Polydispersity index [c] Determined by absorbance of loaded vesicles in Tris Buffer [d] Determined by absorbance of vesicles in Tris Buffer broken with DMSO (80%)*

**Vesosome Doxorubicin loading.** After one experiment, the volume of a typical vesosome suspension is about 50 µL at 50 µg/mL of doxorubicin, volume that is not sufficient for an *in vitro* release experiment. Thus five suspensions were mixed together for each experiment. The doxorubicin loading content was determined by fluorescence measurements. Loaded vesosomes were broken by adding 87 v % of a 25/75 v% MeOH/THF mixture and vortexing this sample for 5 s. This solvent mixture was chosen because it is the only solvent able to break both the PB-*b*-PEO and PTMC-*b*-PGA vesicles, as confirmed by DLS. This sample was then subjected to fluorescence measurement at $\lambda_{max}$=590 nm ($\lambda_{exc}$=485 nm). Quantification was performed from the calibration curve of doxorubicin in a 87 v% [25/75 v.%MeOH/THF] / 13 v.% [Tris buffer 10 mM 380 mM glucose] solution (Figure S7). We further checked that different vesosome suspension samples were reproducible (Figure 1) in terms of DOX loading content and above all, that after mixing several samples, three successively taken fractions of 25 µL and the remaining volume of 125 µL yielded the same fluorescence, and thus DOX concentration.

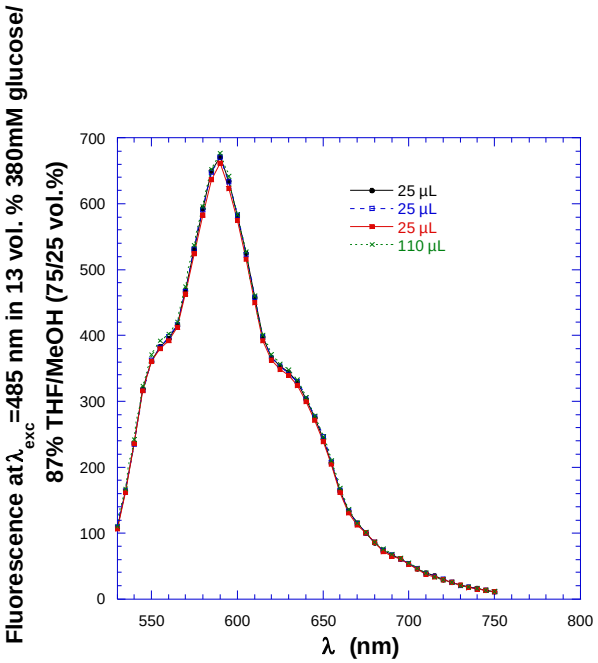


**Figure 1.** Fluorescence of Dox in multiple samples of broken veso-DOX with multiple pipetting withdrawals to assess reproducibility.

For a typical in vitro release experiment 5 vesosome suspensions were mixed, a fraction of 25 µL was taken to assess its loading content by addition of MeOH/THF and the rest of the sample was used for the experiment. This way, each release experiment was normalized with its own precise loading content (measured right before each experiment) in order to compare release experiments of veso-DOX, nano-DOX and free DOX.

**In vitro doxorubicin release.** The required quantity of drug-loaded vesicles or vesosomes was put in the donor chamber of a tailor-made drug release device (Figure S1) inspired by Franz cells. The whole device was kept in a water bath at 37 or 20°C. A membrane separates the donor chamber from the receptor chamber (1.8 mL external medium) (Spectra/Por MWCO: 50,000 g/mol). The donor chamber, containing (225 µL) of Dox-loaded polymersomes or vesosomes) solution, was this way dialysed against a release medium containing 1.8 mL Tris buffer (10 mM Tris, pH 7.4, ionic strength 380 mM glucose) in the receptor chamber. The doxorubicin concentration was measured in the receptor chamber during release by withdrawing an aliquot (200 µL) from the sampling port. Samples removed for analysis every hour were replaced by fresh release medium in order to maintain sink conditions. The amount of drug released was estimated from fluorescence measurements at $\lambda_{max}$=590 nm ($\lambda_{exc}$=485 nm) and calibration curves of doxorubicin in 10 mM Tris, pH 7.4, 380mM glucose (Figures S8 and S9). The drug concentration could be directly calculated from the measured fluorescence. All experiments were conducted with approximately the same initial LC (concentrated DOX and nano-DOX were diluted to the veso-DOX's LC) but

in order to better compare, all the data was still normalized with its respective LC measured on the sample prior to the release, by fluorescence (disruption with MeOH/THF for veso-DOX,) or absorbance (disruption with DMSO for nano-Dox). Each experiment at 37 °C was carried out in duplicate, and average values plotted. Error bars represent standard deviation.

### 2.2.3. Characterization methods

**Dynamic Light Scattering (DLS).** DLS measurements were conducted on a Malvern Zeta Sizer Nano ZS instrument with 90° measurements at 25°C. The mean hydrodynamic diameter and its distribution were determined using Cumulant and CONTIN analysis methods.

**Spinning disk confocal microscopy.** The spinning disk microscope was a Leica DMI6000 (Leica Microsystems, Wetzlar, Germany) equipped with a confocal Scanner Unit CSU-X1 (Yokogawa) using for this experiment objective HCX PL Apo 100X oil NA 1.4 and an Evolve EMCCD camera (Roper Scientific, Evry, France). Z-stack analysis was performed with a galvanometric stage (Leica Microsystems, Wetzlar, Germany). To prove the vesosome structure, the diode laser used were at 491 nm and 561 nm and a Semrock emission filter with narrow bandpass windows in the blue (420 to 460 nm), green (506 to 536 nm) red (587 to 627 nm) and near infrared (670 to 730nm) spectral regions was used. For double nanosize polymersome loading, the same diode lasers were used but with Semrock emission filters with narrow bandpass windows in the green (506 to 544 nm) and in the red (573 to 637 nm). For triple fluorophore labeling, the same latter filters were used but also in addition, the 405 nm diode laser was needed as well as the quad bandpass filter described for the proof of vesosome structure, for the blue fluorescence acquisition.
Microscopy chambers were fabricated by sealing a slide against a coverslip with two layers of parafilm featuring the three sides of the chamber. The sample could then be injected by capillarity through the last open side. Finally, the last aperture would be sealed with melted paraffine wax.
The experiments were realized in the *Bordeaux Imaging Center of the University of Bordeaux Segalen.* The help of Sébastien Marais is gratefully acknowledged.

**Instrumentation and Measurements.** 1H (400 MHz) Nuclear Magnetic Resonance NMR spectra were recorded on a Bruker Avance DPX400 instrument at 23 °C and were referenced internally using the residual 1H solvent resonance relative to tetramethylsilane (δ=0). $M_{n\ SEC}$ and ($M_w/M_n$) values for copolymers PTMC-*b*-PBLG (3 mg/mL) were determined by Size Exclusion chromatography SEC at 60 °C, using dimethylformamide (DMF) with LiBr (1 g/L)

as eluent (0.8 mL/min), on a Jasco apparatus equipped with both Varian refractive index and UV detectors and two PL gel 5 µm mixed-C columns.

For doxorubicin quantification with absorbance and fluorescence measurements, a SpectraMax M2 Ɛt SpectraMax M2$^{e}$ Multimode Plate Readers, equipped with a high powered Xenon flashlamp, was used. All measurements were performed at 22°C.

## 3. Results and Discussion

The inner polymersomes are formed by nanoprecipitation of poly(trimethylene carbonate)-*b*-poly(L-glutamic acid) PTMC-*b*-PGA synthesized following a previously reported method.[27] This suspension is then loaded in larger polymersomes of poly(butadiene)-*b*-poly(ethylene oxide) PB-*b*-PEO by emulsion-centrifugation[31] with a quantitative loading efficiency. The procedure for forming giant PB-*b*-PEO polymersomes was inspired from Li and coworkers[28]. Briefly (Figure 2), a small fraction of an inverted emulsion of aqueous solution (here a nanosize polymersome suspension of PTMC-*b*-PGA with 380 mOsm sucrose) in toluene is poured over an interface of toluene and an aqueous solution of 380 mOsm glucose. The PB-*b*-PEO diblock copolymer is dissolved in toluene at 3 mg/mL and stabilizes the emulsion droplet (forming the inner leaflet of the final bilayer) of this interface.

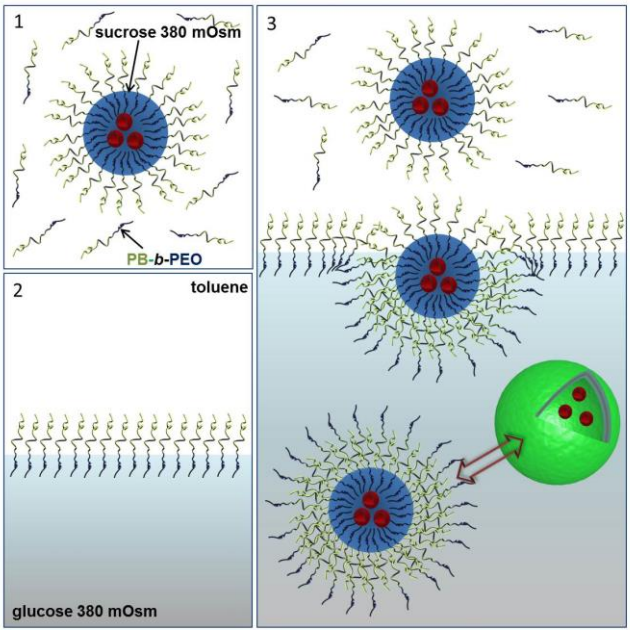


**Figure 2.** Schematic representation of the emulsion-centrifugation process generating giant polymersomes or polymer vesosomes (the smaller red vesicles representing the inner nanosize polymersomes).

In a final step, both centrifugal force and denser sucrose (as compared to glucose) inside the droplets, force them to cross the interface and to be enveloped by a second leaflet of amphiphilic PB-*b*-PEO block copolymer, yielding the final giant polymersomes or polymer vesosomes (if a nanosize polymersome suspension is used as aqueous inner solution).
The control provided by this process enabled imaging the compartmentalized polymersome structure by spinning disk confocal microscopy. In Figure 3 the Alexa Fluor 568 (red) labeled inner polymersomes are visibly encapsulated in a green giant polymersome (with 10 wt.% of a Alexa Fluor 488 conjugated polybutadiene).

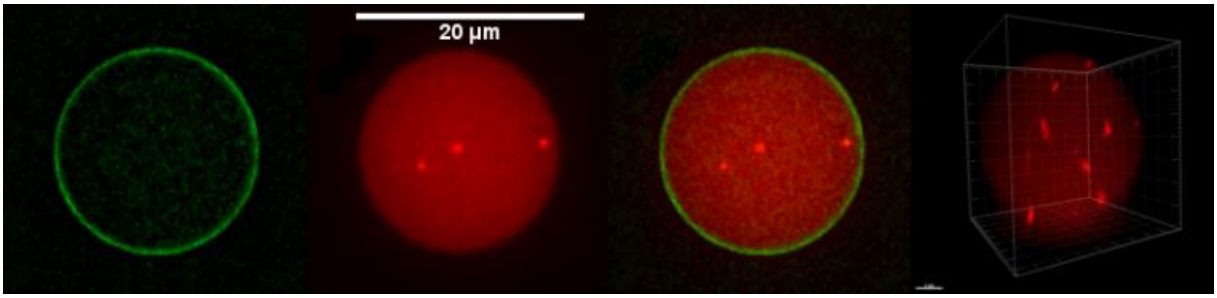


**Figure 3**. Spinning disk confocal microscopy images of red nanosize vesicles (Alexa fluor 568) in a green giant polymersome (Alexa Fluor 488). From left to right: green channel, red channel, overlay and 3D reconstruction (red channel).

The red inner polymersomes in Brownian motion can clearly be observed (see Movie S1[g] ). The giant vesicle has also been reconstructed in 3D for better visualization (see Movie S2[b]). Such compartmentalized structures are of particular interest for the delivery of multiple actives[32]. To address this point, a 50/50 vol.% solution of two different PTMC-*b*-PGA suspensions, labeled with red (Alexa Fluor 568) and green (fluorescein isothiocyanate FITC) fluorophores was encapsulated instead of a single nanosize vesicle suspension (Figure 4).

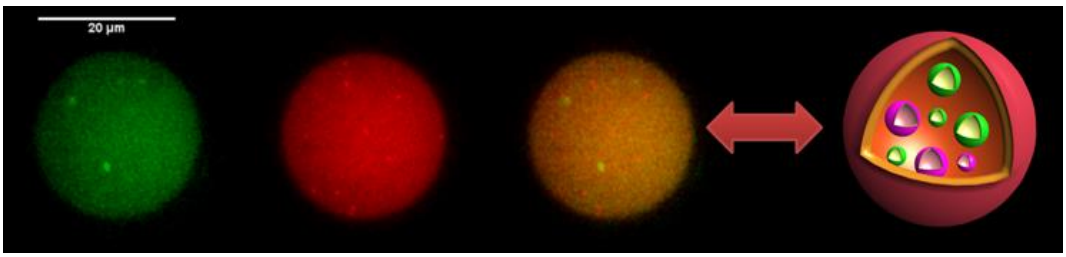


**Figure 4**. Spinning disk confocal microscopy images of red (Alexa fluor 568) and green (FITC) nanosize vesicles in a giant polymersome. From left to right: green channel, red channel, and overlay.

[g] Movie s1, [b] Movie s2 and [c] Movie s3 http://onlinelibrary.wiley.com/doi/10.1002/anie.201106410/suppinfo

The two nanosize polymersomes are clearly localized in the same giant polymersome; the Movie S3[c] shows the distinct motion of each kind of fluorescent nanosize polymersome. Finally, we were able to further increase the complexity of this system by co-encapsulating a large polymer, FITC-dextran (20,000 $g.mol^{-1}$), with a red nanosize vesicle suspension (Figure 5).

As the FITC-dextran was already green fluorescent, the membrane was this time labeled in blue (with 10wt.% Alexa Fluor 405 conjugated polybutadiene), allowing separate imaging of the giant vesicles (blue), the inner nanosize vesicles (red) and the loaded dextran (green). Such a three-compartment encapsulation in vesicles is, to the best of our knowledge, the first reported to date.

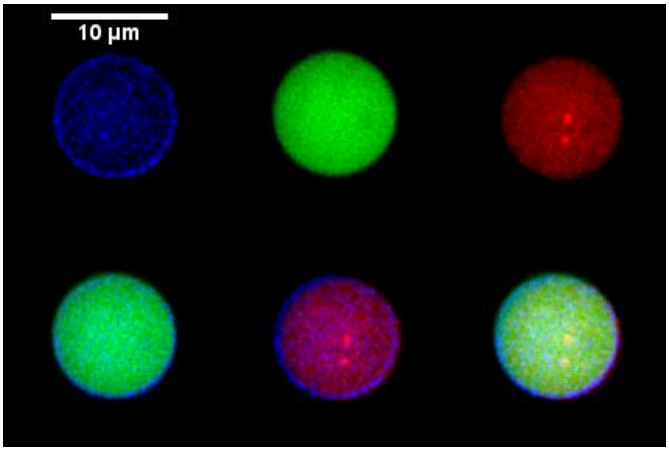


**Figure 5.** Spinning disk confocal microscopy acquisitions of red (Alexa fluor 568) nanosize vesicles and green FITC-dextran in a blue (Alexa Fluor 405) giant polymersome. From top left to bottom right: blue channel, green channel, red channel, overlay blue and green, blue and red, and finally blue, green and red channels.

The double membrane barrier effect of these polymer vesosomes was then studied by measuring the release profile of doxorubicin (DOX) as a model drug. DOX was encapsulated in the inner PTMC-*b*-PGA polymersomes.[30] The resulting suspension was concentrated as much as possible in order to have the highest possible drug concentration (loading content of 9 wt%). *In vitro* drug release experiments were then conducted on solutions of free DOX, of PTMC-*b*-PGA nanosize polymersomes loaded with doxorubicin (nano-DOX) and polymer vesosomes loaded with nano-DOX as inner polymersomes (veso-DOX). These solutions were placed in the donor chamber of a tailor-made drug release device inspired by Franz cells (Figure S1). The release of DOX was followed by monitoring the absorption and fluorescence of the drug (Figure S2).

A significant decrease of the DOX release rate from nano-DOX to veso-DOX can be observed at 37°C (Figure 6). Indeed, in veso-DOX, the drug has not only a PTMC-*b*-PGA polymeric membrane but also a PB-*b*-POE one to cross. At 20°C the release is negligible in

the time frame of the measurement, this temperature being efficient for storage. The data can also be represented (Figure S3) by an experimental law established by Peppas,[33] where $m_t$ and $m_f$ represent the DOX release at time $t$ and infinite time (initial amount in µg) respectively, $k$ is a kinetic constant dependent of the matrix and the drug, and $n$ is the release exponent:

$$\frac{m_t}{m_f} = k \times t^n \qquad \text{Equation (1)}$$

The release data consequently analysed can be fitted by a linear regression, thus suggesting a fickian, purely diffusive release regime. Moreover, by extracting the kinetic constants $k$ for each system, one determines that the release rate of nano-DOX is about twice the one of veso-DOX, for which there is an additional diffusion barrier.

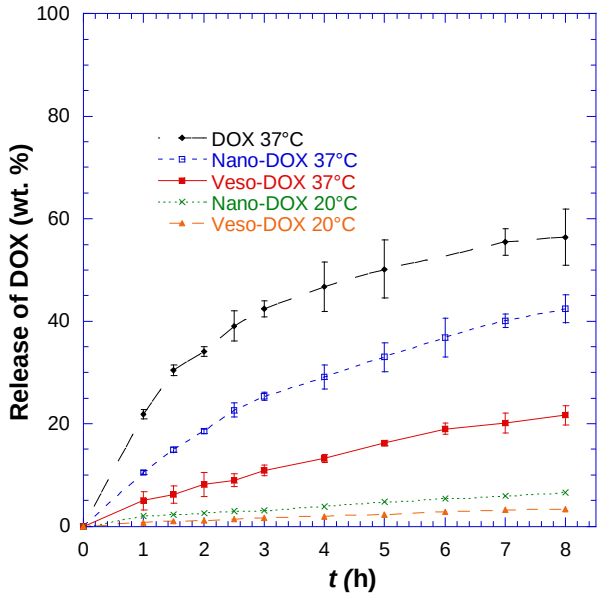


**Figure 6.** *In vitro* drug DOX release (wt.%) from top to bottom: free DOX(▼,10.34 µg), Nano-DOX(●, 9.25 µg), Veso-DOX (■, 9.95 µg) at 37°C, Nano-DOX(x, 9.33 µg) at 20°C and Veso-DOX(▲,11.35 µg) at 20°C (experiments performed in duplicate, error bars represent standard deviation).

## 4. Conclusion

In summary, polymersomes in polymersomes (or polymer vesosomes) were obtained with an original, versatile and efficient method. Using such an emulsion centrifugation process, nanosize vesicles and any other material (nanoparticles, proteins, …) can be quantitatively loaded in larger polymersomes. Moreover, this highly controlled technique enabled encapsulating different nanosize polymersomes inside larger ones (constituting the first path towards the delivery of multiple and/or incompatible actives), and also encapsulating

molecules and (bio)macromolecules in at least three different compartments (in the membrane/lumen of the inner nanosize polymersomes, in the cavity and in the membrane of the giant vesicles). Finally, the encapsulation of highly concentrated doxorubicin-loaded nanosize vesicles was performed. A double membrane barrier effect has been demonstrated, allowing a specific stability and disruption in different environments. This strategy presents a straightforward approach and new opportunities for the use of these polymersomes in polymersomes in biomedical or cosmetic applications, where the encapsulation of multiple, distinct and fragile ingredients are required, together with specific release conditions.

## Annexes

**Description of the videos presented as supporting information on http://onlinelibrary.wiley.com/doi/10.1002/anie.201106410/suppinfo**

Movie S1 (http://onlinelibrary.wiley.com/doi/10.1002/anie.201106410/suppinfo, movie_s1) features the polymer vesosome in Figure 1, where the loaded red inner polymersomes can clearly be observed in Brownian motion. The acquisition was done with a spinning disk confocal microscope, the red nanosize polymersomes are labeled with Alexa Fluor 568, the green giant polymersome with Alexa Fluor 488.

The vesosome of movie 1 is reconstructed in three dimensions (red channel only) in Movie S2 (http://onlinelibrary.wiley.com/doi/10.1002/anie.201106410/suppinfo, movie_s2), showing the localization of the inner polymersomes in the giant one.

Movie S3 (http://onlinelibrary.wiley.com/doi/10.1002/anie.201106410/suppinfo, movie_s3) features the polymer vesosome with two populations of inner nanosize polymersomes in Figure 2. The acquisition was done with a spinning disk confocal microscope, the red nanosize polymersomes are labeled with Alexa Fluor 568, the green ones with FITC. The distinct motion of each kind of vesicle is clearly visible.

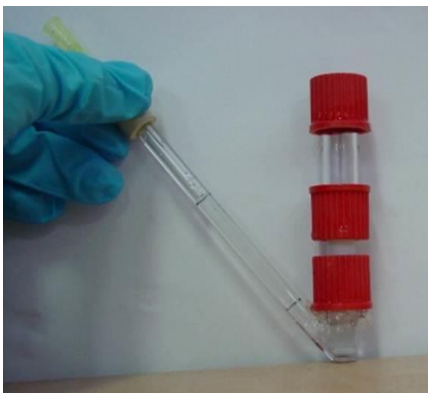

**Figure S1**. Tailor-made drug release device inspired from Franz cells

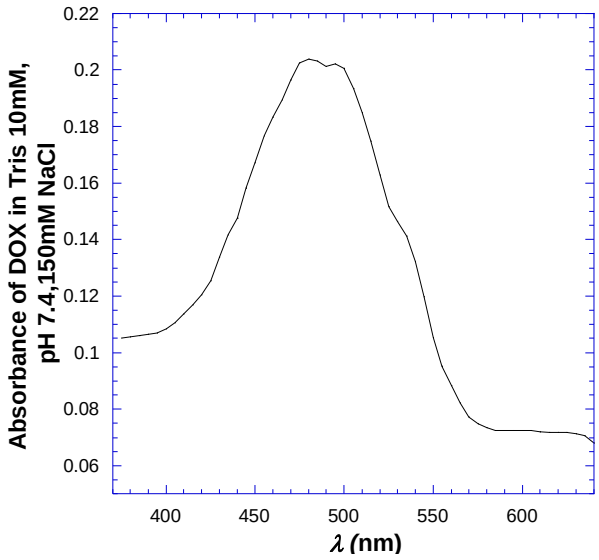


**Figure S2a.** Absorbance of drug Doxorubicin in Tris buffer 10mM, pH 7.4, 150mM NaCl**.**

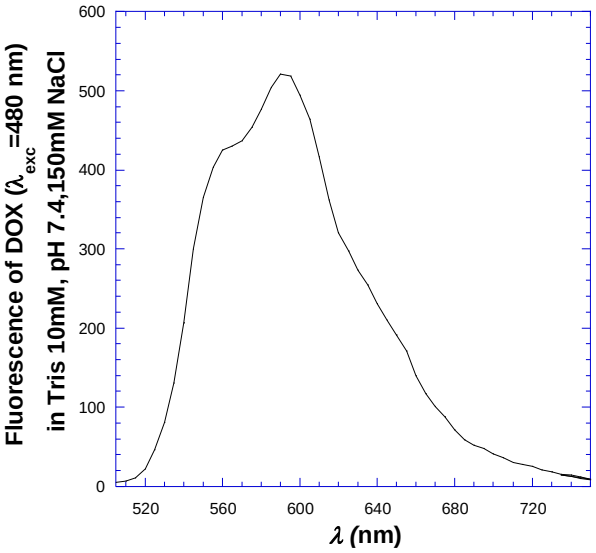


**Figure S2b.** Fluorescence of drug Doxorubicin in.Tris buffer 10mM, pH 7.4, 150mM NaCl.

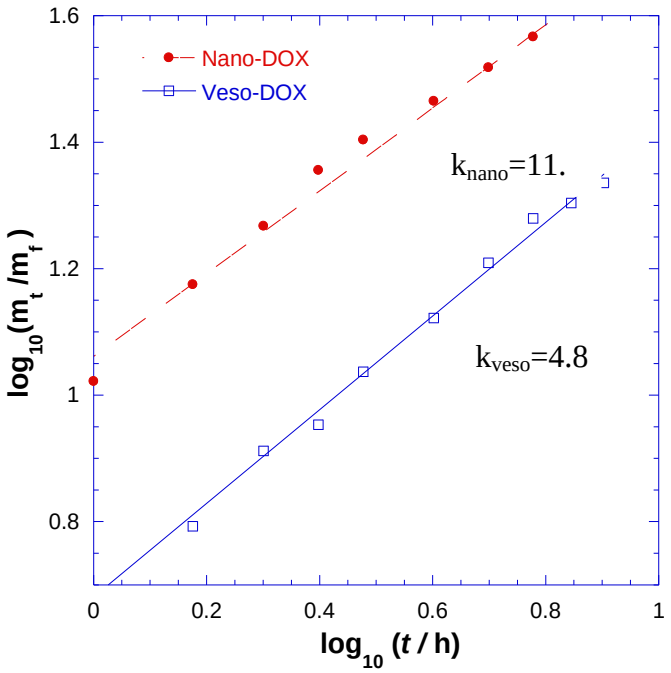


**Figure S3.** *In vitro* drug DOX release (wt.%): Peppas fit of DOX release from Nano- (●) and Veso-DOX(□) at 37°C.

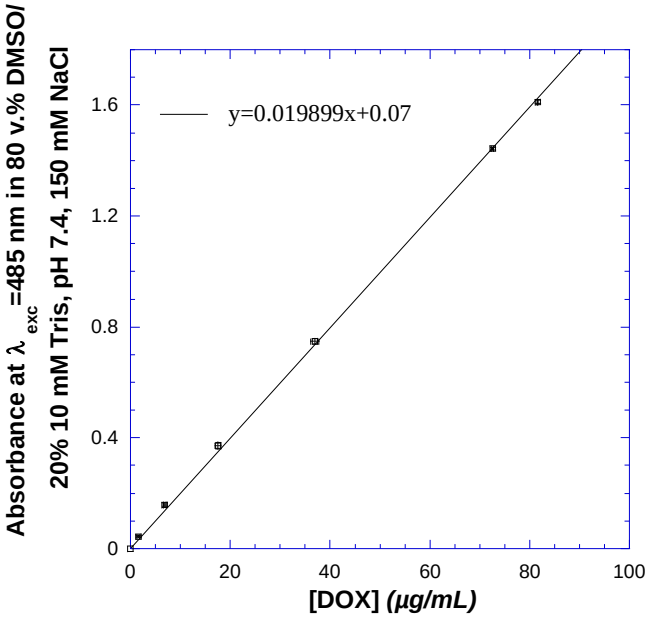


**Figure S4.** Calibration curve of Doxorobucin absorbance at 485 nm in 80/20 v.% DMSO/10mM Tris pH 7.4,150 mM NaCl (indirect method).

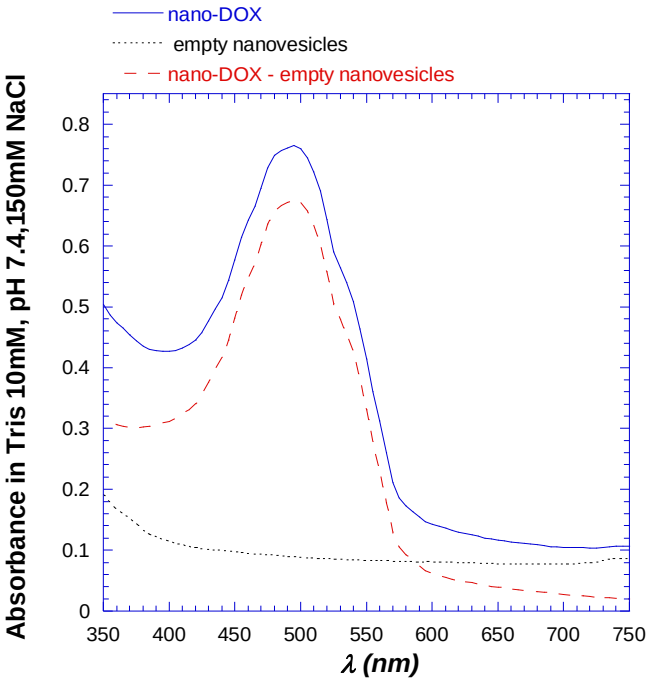


**Figure S5.** Absorbance in 10mM Tris pH 7.4,150 mM NaCl: of doxorubicin loaded in nanosize PTMC-*b*-PGA polymersomes (nano-DOX, straight line), of empty polymersomes (dotted line), and substraction of both to get the absolute Doxorubicin absorbance in nanosize vesicles(dotted line with longer dots). Final polymer concentration of 0.4 mg/mL. Such a spectra (last plot) can then be used to extrapolate a doxorubicin concentration from calibration curve in Figure S6 (what we call the direct method).

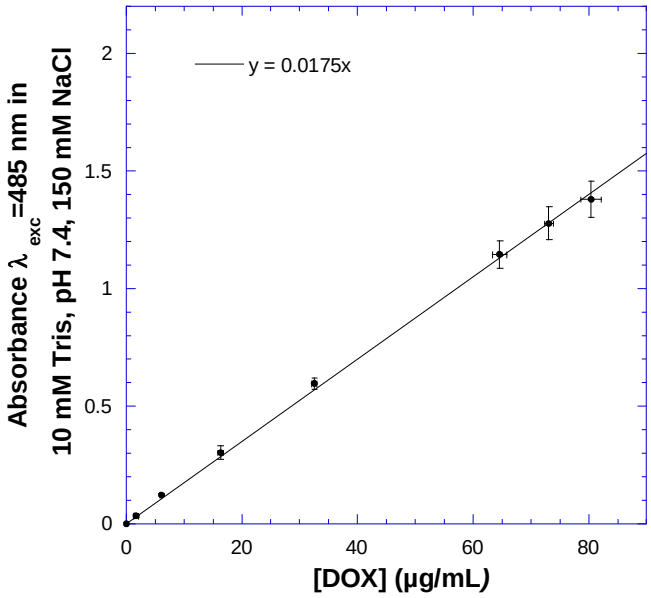


**Figure S6.** Calibration curve of Doxorobucin absorbance at 485 nm in 10mM Tris pH 7.4,150 mM NaCl.

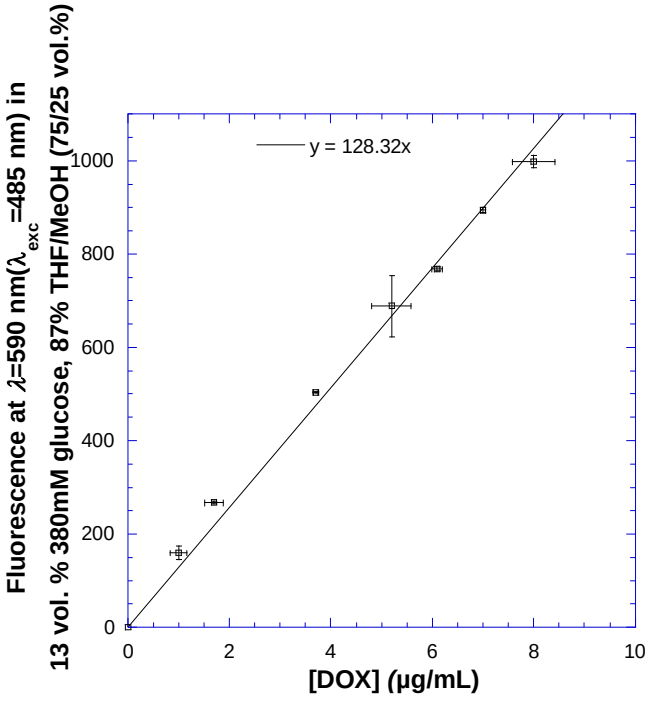


**Figure S7.** Calibration curve of Doxorobucin fluorescence at 485 nm excitation, 590 nm emission in 13/87 v.% 380 mM glucose/[THF/MeOH (75/25 v.%)].

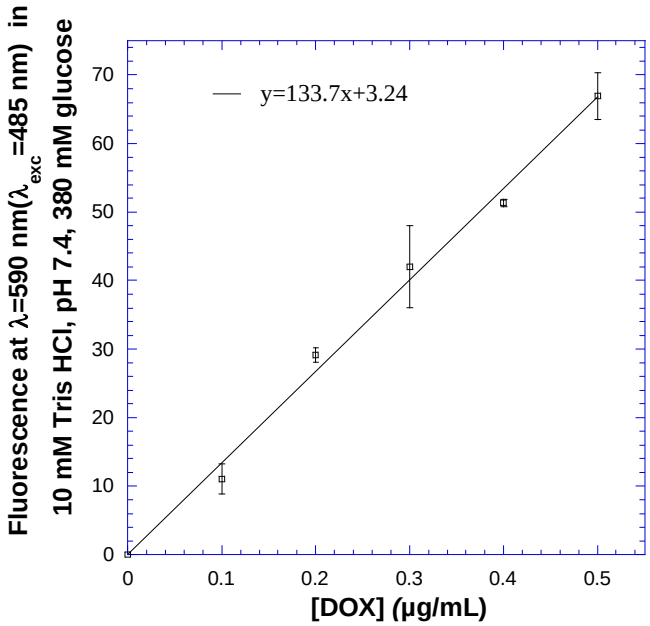


**Figure S8**. Calibration curve of Doxorobucin fluorescence (from 0-0.5µg/mL) at 485 nm excitation, 590 nm emission in 10 mM Tris/HCl, pH 7.4, 380 mM glucose.

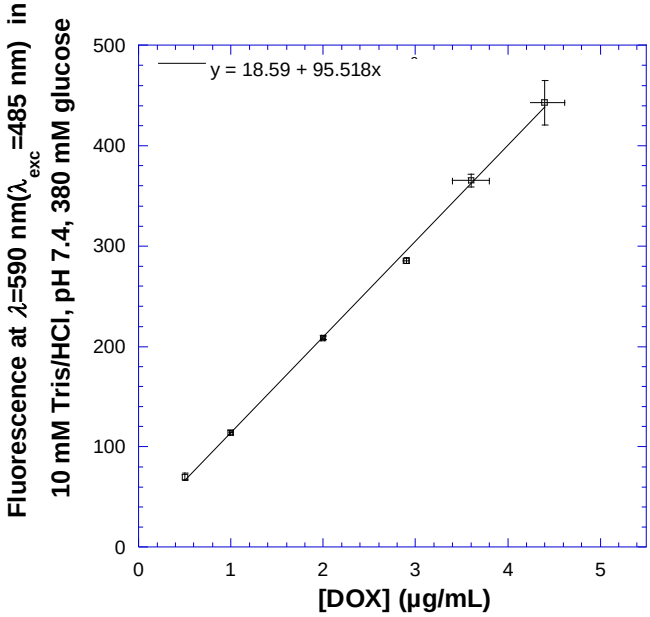


**Figure S9.** Calibration curve of Doxorobucin fluorescence (from 0.5-4.4µg/mL) at 485 nm excitation, 590 nm emission in 10 mM Tris/HCl, pH 7.4, 380 mM glucose.

---

This chapter has been published in *Angewandte Chemie International Edition*:

Marguet Maïté, Edembe Lise, and Lecommandoux Sébastien*, Polymersomes in Polymersomes: multiple loading and permeability control, *Angewandte Chemie International Edition*, **2012**. 51,p. 1173-1176.

## References


1. Discher, D. E.; Eisenberg, A., *Science* **2002,** *297* (5583), 967-973.
2. Christian, D. A.; Cai, S.; Bowen, D. M.; Kim, Y.; Pajerowski, J. D.; Discher, D. E., *European Journal of Pharmaceutics and Biopharmaceutics* **2009,** *71* (3), 463-474.
3. Meng, F.; Zhong, Z.; Feijen, J., *Biomacromolecules* **2009,** *10* (2), 197-209.
4. Cheng, R.; Feng, F.; Meng, F.; Deng, C.; Feijen, J.; Zhong, Z., *Journal of Controlled Release* **2011,** *152* (1), 2-12.
5. Li, M.-H.; Keller, P., *Soft Matter* **2009,** *5* (5), 927-937.
6. Kim, M. S.; Lee, D. S., *Chemical Communications* **2010,** *46* (25), 4481-4483.
7. Van Dongen, S. F. M.; Verdurmen, W. P. R.; Peters, R. J. R. W.; Nolte, R. J. M.; Brock, R.; Van Hest, J. C. M., *Angewandte Chemie International Edition* **2010,** *49* (40), 7213-7216.
8. Renggli, K.; Baumann, P.; Langowska, K.; Onaca, O.; Bruns, N.; Meier, W., *Advanced Functional Materials* **2011,** *21* (7), 1241-1259.
9. Onaca, O.; Hughes, D. W.; Balasubramanian, V.; Grzelakowski, M.; Meier, W.; Palivan, C. G., *Macromol. Biosci.* **2010,** *10* (5), 531-538.
10. Brinkhuis, R. P.; Rutjes, F. P. J. T.; van Hest, J. C. M., *Polymer Chemistry* **2011**.
11. Bermudez, H.; Brannan, A. K.; Hammer, D. A.; Bates, F. S.; Discher, D. E., *Macromolecules* **2002,** *35* (21), 8203-8208.
12. Walker, S. A.; Kennedy, M. T.; Zasadzinski, J. A., *Nature* **1997,** *387* (6628), 61-64.
13. Wong, B.; Boyer, C.; Steinbeck, C.; Peters, D.; Schmidt, J.; van Zanten, R.; Chmelka, B.; Zasadzinski, J. A., *Advanced Materials* **2011,** *23* (20), 2320-2325.
14. Mishra, V.; Mahor, S.; Rawat, A.; Dubey, P.; Gupta, P. N.; Singh, P.; Vyas, S. P., *Vaccine* **2006,** *24* (27-28), 5559-5570.
15. Ebato, Y.; Kato, Y.; Onishi, H.; Nagai, T.; Machida, Y., *Drug Development Research* **2003,** *58* (3), 253-257.
16. Scholl, I.; Boltz-Nitulescu, G.; Jensen-Jarolim, E., *Journal of Controlled Release* **2005,** *104* (1), 1-27.
17. De Geest, B. G.; De Koker, S.; Immesoete, K.; Demeester, J.; De Smedt, S. C.; Hennink, W. E., *Advanced Materials* **2008,** *20* (19), 3687-3691.
18. McPhail, D.; Tetley, L.; Dufes, C.; Uchegbu, I. F., *International Journal of Pharmaceutics* **2000,** *200* (1), 73-86.
19. Bolinger, P. Y.; Stamou, D.; Vogel, H., *Angewandte Chemie International Edition* **2008,** *47* (30), 5544-5549.
20. Kreft, O.; Prevot, M.; Möhwald, H.; Sukhorukov, G. B., *Angewandte Chemie International Edition* **2007,** *46* (29), 5605-5608.
21. Chandrawati, R.; Hosta-Rigau, L.; Vanderstraaten, D.; Lokuliyana, S. A.; Stadler, B.; Albericio, F.; Caruso, F., *ACS Nano* **2010,** *4* (3), 1351-1361.
22. Perro, A.; Nicolet, C.; Angly, J.; Lecommandoux, S.; Le Meins, J. F.; Colin, A., *Langmuir* **2011,** *27* (14), 9034-9042.
23. Hanson, J. A.; Chang, C. B.; Graves, S. M.; Li, Z.; Mason, T. G.; Deming, T. J., *Nature* **2008,** *455* (7209), 85-88.
24. Shum, H. C.; Zhao, Y. J.; Kim, S. H.; Weitz, D. A., *Angewandte Chemie International Edition* **2011,** *50* (7), 1648-1651.
25. Fu, Z.; Ochsner, M. A.; De Hoog, H. P. M.; Tomczak, N.; Nallani, M., *Chemical Communications* **2011,** *47* (10), 2862-2864.

26. Chiu, H.-C.; Lin, Y.-W.; Huang, Y.-F.; Chuang, C.-K.; Chern, C.-S., *Angewandte Chemie International Edition* **2008,** *47* (10), 1875-1878.
27. Sanson, C.; Schatz, C.; Le Meins, J. F.; Brûlet, A.; Soum, A.; Lecommandoux, S., *Langmuir* **2010,** *26* (4), 2751-2760.
28. Mabrouk, E.; Cuvelier, D.; Pontani, L. L.; Xu, B.; Lévy, D.; Keller, P.; Brochard-Wyart, F.; Nassoy, P.; Li, M. H., *Soft Matter* **2009,** *5* (9), 1870-1878.
29. Mabrouk, E.; Cuvelier, D.; Brochard-Wyart, F.; Nassoy, P.; Li, M. H., *Proceedings of the National Academy of Sciences of the United States of America* **2009,** *106* (18), 7294-7298.
30. Sanson, C.; Schatz, C.; Le Meins, J. F.; Soum, A.; Thévenot, J.; Garanger, E.; Lecommandoux, S., *Journal of Controlled Release* **2010,** *147* (3), 428-435.
31. Pautot, S.; Frisken, B. J.; Weitz, D. A., *Langmuir* **2003,** *19* (7), 2870-2879.
32. Al-Jamal, W. T.; Kostarelos, K., *International Journal of Pharmaceutics* **2007,** *331* (2), 182-185.
33. Ritger, P. L.; Peppas, N. A., *Journal of Controlled Release* **1987,** *5* (1), 23-36.

# CHAPTER 4

## Enzymatic cascade reactions confined in Polymersomes in a Polymersome.

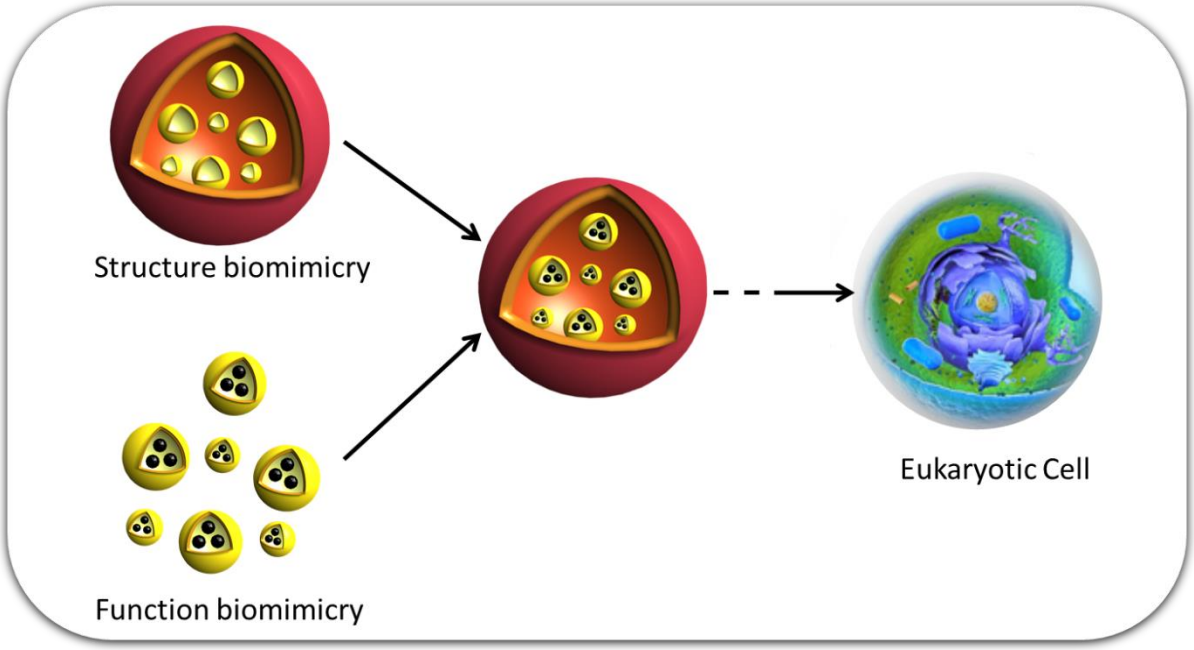

*In the previous chapter (**Chapter 3**), we have demonstrated the achievement of two of the properties arising in the biomedical field with the controlled formation of structural cell mimics (polymersomes in a polymersome),i.e. multiple loading and permeability tuning for exquisite control over release kinetics.*

*After addressing the first step or barrier of structural cell mimicry, we then faced another challenge, metabolic function. In this search for increased complexity towards functional cell mimicry (the second step) it is then paramount to first achieve the conduction of enzymatic reactions inside single compartments, as occurs in a highly controlled, selective and efficient fashion in the organelles. Such so-called nanoreactors are also coined artificial organelles. Polymersomes are powerful compartments to use for such purposes. Finally, after achieving control over these two prerequisites (eukaryotic cell structure and metabolic function in organelle mimics), it becomes possible to combine them and push the frontiers of Biomimicry further: from cell structure mimicry towards a controlled cell-like biofunctionality. This was the last but not least challenge that we faced during this PhD project. We believe that such a Research will enrich considerably the fields of drug delivery, (bio)sensors, (bio)catalysis and (bio)technology. The first part of this project consisted in the design, study and optimization of a nanoreactor biomimetic cascade based on PS-b-PIAT polymersomes, and was performed in Nijmegen in collaboration with Prof. Van Hest and his PhD candidate Ruud Peters; in this first part of **Chapter 4** we present work regarding metabolic function within artificial organelles, constituting a major part of the chapter as it revealed rather complex to set up. The second part consists in the loading of these nanoreactors in a giant PB-b-PEO polymersome and in the study of the final reaction system by confocal microscopy. Although this project requests further investigations, we were able to prove the concept of enzymatic cascade reactions confined in polymersomes.*

## 1. Introduction

It is only thanks to multicompartmentalization and positional assembly that eukaryotic cells are able to perform multiple, spatially separated chemical processes simultaneously with high accuracy and specificity. Such a control in confinement of reactive species and (bio)chemical reactivity is a source of inspiration to scientists, and a dream for chemists.

Once ***structural cell mimicry*** is controlled (Chapters 2 and 3)[1,2], one can bring these structures to their full potential by tackling the challenge of ***functional cell biomimicry***. The idea is to combine functional synthetic organelles (metabolism/functional mimicry) in such structural cell mimics. These synthetic organelles, also called nanoreactors, indeed often host enzymatic cascade reactions. This field, using polymersomes as single compartments has been extensively studied for a decade.[3-6] However by using a multicompartmentalized structure as scaffold for multiple enzymatic reactions, a completely new and powerful level of control arises, as for the eukaryotic cell. Indeed, even though significant progress has been demonstrated in the past years in cascade reactions using nanoreactors with enzymes placed in different locations, the level of possibilities to immobilize or confine enzymes in a multicompartmentalized system is in theory improved but still needs to be fully explored.

Vogel and coworkers were pioneers in this field and developed a system able to release and mix reactive compounds from small liposomes inside large ones upon a thermal trigger,[783] one great property arising from multicompartmentalization. By using relevant lipid-phase transition temperatures (Tt of lipids), they were further able to perfect their system into a nanofluidic reactor controlling two enzymatic consecutive reactions.[7] Indeed above the Tt, the liposome's permeability increases as a result of the transient defects that are generated by disturbances in lipid packing order. First prodye dichlorodimethylacridinone (DDAO) phosphate is released in the outer vesicle and converted by alkaline phospatase into DDAO, then prodye fluorescein diphosphate can be converted after triggered release into fluorescein. In this early development, only one enzyme is used to react with the two substrates consecutively. By monitoring the kinetics for one reaction by fluorescence correlation spectroscopy (FCS), the authors observed no significant difference between a reaction in bulk and in the nanofluidic reactor, applying the same conditions of pH, temperature, enzyme and substrate concentrations. These observations are particularly important, as the miniaturization of reactors allows a reduction of sample consumption, which may be expensive or polluting. As volumes as small as attolitric are mixed (from the inner nanometer-sized liposomes) in a femtoliter reactor vessel (the larger outer liposome), the control over the number of mixed reactants should approach single-molecule precision!

Other exciting innovations in this field are from Caruso's group. The concept of "capsosomes", or polymer layer by layer capsules (semi-permeable) deposited on liposomes (relatively access-restricting under Tt) was first thoroughly demonstrated and reported.[8] This system was then further optimized by maximizing the number of liposomes and cargo retention and above all allowing a temperature-triggered reaction.[9] As for Vogel's system, the phase transition temperature of phospholipids is taken advantage of, to trigger remotely the initiation of the reaction by controlling the substrate release. Interestingly, the encapsulated enzymes can thus be used for repeated conversions as the reaction can be reversibly triggered.

Kreft *et al.*[10] also bring a significant contribution in the field of hollow polyelectrolyte microcapsules, with shell-in-shell reactors. Spherical calcium carbonate microparticles are here used as templates, which can be removed in a "biofriendly" way through EDTA complexation, after polyelectrolyte multilayer build-up. The procedure to get a shell-in-shell structure is complex and well-thought, using successive coprecipitation of $CaCl_2$ and $Na_2CO_3$, and enables to retain one enzyme in the lumen of the inner shell (HRP), another one in the lumen of the more external one (GOX). Glucose is added outside for hydrogen peroxide generation by GOX in the most external compartment. After addition of substrate Amplex Red for the second reaction of the cascade, fluorescent resorufin is obtained within a few seconds in the inner compartment, before diffusing outside of the inner capsule. The Authors emphasize that this test remains however qualitative. Kreft *et al.* also evidenced a powerful property resulting from multicompartmentalization: the means to trigger remotely bioreactions.[11] They incorporated gold nanoparticles in the inner shell of a similar shell-in-shell system that could be activated with a near-infrared laser illumination. As a result of the local heating thus created, this results in membrane disruption: the contents are released into the outer shell interior, providing a route for reactions in confined volumes and intermixing of contents of two or more compartments. Bäumler and Georgieva[12] pushed Kreft's concept further. Indeed, coprecipitation between calcium chloride and sodium carbonate was also used to form concentric compartments after removal with EDTA. The shells were formed from biopolymer and enzymes cross-linked with glutaraldehyde or divinylsulfone. They designed a three-enzyme cascade reaction that consisted of enyzme β-glucosidase in the most external compartment which converted first a prodye intro fluorescein and glucose. This glucose was then hydrolysed to glucuronic acid and hydrogen peroxide by GOX (in an intermediate concentric compartment) in presence of dioxygen. Finally, after addition of prodye amplex red, HRP produced fluorescent resorufin and dioxygen (necessary for the reaction of GOX) in the presence of the generated hydrogen peroxide. Authors stressed scattering and inhomogeneous distribution of absorbance may influence fluorimetry measurements

(performed at a "macroscopic" scale) as reaction rate was significantly increased when followed by microscopy. Microscopy indeed represents the real concentration of products inside particles and is not influenced by its distribution in the surrounding solution. Another very interesting and "green" advantage arising is again the possible recycling of enzyme-bearing microparticles. Indeed, after 5 runs, activity is decreased fivefold, but still present, and could be preserved over a few months.

Last but not least, a very smart design by Caruso and coworkers constituted in using an *in situ* bioreaction to trigger the release of therapeutics.[13] The conduction of an enzymatic reaction is actually offering new perspectives in terms of drug delivery. More precisely, the enzyme glutathione reductase in the liposomes of the capsosomes reacts *in situ* upon temperature activation (above Tt). The enzyme can then reduce glutathione disulfide GSSG to glutathione GSH, a major cellular antioxidant. This GSH becomes available to cleave the disulfide bond between a loaded conjugate composed of a small therapeutic peptide and a large polymer, thereby enabling its subsequent release in the external medium. This can be monitored as the peptide is also labelled with a fluorophore. Authors aim to develop such systems further to get biomimetic platforms that will combine both enzyme therapy and controlled drug release in such a single structure.

The purpose of the present work is to take advantage of the multicompartmentalization in polymers that we have been able to design to conduct cascade enzymatic reactions with an unprecedented level of spatial and temporal control over reactivity. As evidenced in literature (see section 3, chapter 1), we need however a diffusion of reactive species through the membranes of the inner compartments in a controlled manner. In the fields of materials, possibilities to achieve such a property are limited. Either people work with liposomes, inducing a controlled permeability at the transition temperature,[7, 14] or in the polymer field, they work with intrinsically semi-permeable walls as in the case of Lbl capsules.[8-10, 12, 13] More specifically with polymer vesicles, there are two main kinds of reports. Either people are more or less related to the group of Wolfgang Meier who initiated polymersomes of PDMS-PMOXA-PDMS poly[-2-methyloxazoline)-*b*-poly-(dimethylsiloxane)-*b*-poly-(2 methyloxazoline)], [15-20] able to incorporate transmembrane channels or porins in their membranes to allow specific or non-specific diffusion. Or the polymersomes present an intrinsic permeability, which is the case of PS-*b*-PIAT poly[styrene-*b*-poly(L-isocyanoalanine(2-thiophen-3-yl-ethyl) amide)] polymersomes developed by Jan van Hest's group. That is why we developed a collaboration with Professor Jan van Hest, who has as a result a long experience in the use of PS-*b*-PIAT polymersomes hosting enzymatic cascade

reactions. Indeed, these polymersomes bear the interesting intrinsic property to be permeable to molecules below a critical molecular weight threshold (substrates which are small molecules, are able to diffuse through the polymer shell, while enzymes that are large macromolecules remain confined in the vesicles), as extensively demonstrated by the van Hest group.[21-26] We first present the general design of the enzymatic cascade reaction in multicompartmentalized polymersomes investigated (section 3.1). Then, loading and study of the enzymatic cascade in PS-*b*-PIAT polymersomes in solution will be investigated (section 3.2, functional organelle mimics). Finally, in a last step, we had to exclude one of the enzymes from the polymersomes and to keep it free in solution for better efficacy (section 3.3), which enabled us to have some first results regarding the ultimate goal of this project (functional cell mimics, section 4).

## 2. Experimental Section

### 2.1.Materials and reagents

Poly(butadiene)$_{46}$-*b*-poly(ethylene oxide)$_{30}$ ($PB_{46}$-*b*-$PEO_{30}$) (P9095-BdEO, $M_{n\ PB}$=2,500 g/mol and $M_{n\ PEG}$=1,300 g/mol, I=1.04) was purchased from Polymer Source.

$PS_{40}$-*b*-$PIAT_{50}$ was purchased from Encapson. Synthesis of non-caged and caged substrate was performed by Ruud Peters, PhD candidate from Radboud University, Nijmegen, the Netherlands. Cyclohexanone monooxygenase (CHMO), recombinant from *Acinetobacter* sp., expressed in E. coli, (≥12 U/mL, C1622-1ML, suspension in 80% saturated ammonium sulfate, 20 mM K-Na-phosphate buffer pH 7, 3.5 mM 1,4-Dithioerythritol) was from Sigma Aldrich. The suspension was estimated to have a concentration of 32 mg/mL by Nanodrop 1000 (Thermo Scientific). Lipase B *Candida antarctica*, recombinant from *Aspergillus oryzae* (CalB) (9 U/mg, 66228-250 mg) was from Sigma Aldrich. Recombinant histidine-tagged PAMO[27] and its self-sufficient analogue CRE2-PAMO[28, 29] were overexpressed and purified as described previously, and kindly donated by the group of Marco Fraaije, in Groningen, the Netherlands. $NADP^+$ dependent Alcohol Dehydrogenase ADH from *Thermoanaerobium brockii* was bought from Sigma Aldrich (A8435).

β-Nicotinamide adenine dinucleotide 2′-phosphate reduced tetrasodium salt hydrate (NADPH) (N1630) and β-Nicotinamide adenine dinucleotide phosphate hydrate ($NADP^+$, N5755) were from Sigma Aldrich. Sucrose, ≥99.5% (84097) and D-(+)-glucose (G5767) were from Sigma Aldrich. THF was distilled under Ar from sodium/ benzophenone. The water

utilized throughout this work for preparation of buffers, for the self-assembly, dialysis of polymersomes and enzymatic assays was double deionized with a *Labconco Water Pro PS* purification system (18.2 MΩ). All other reagents and solvents were of the highest quality grade available and acquired from commercial sources. Unless stated otherwise, chemicals were used without further purification.

### 2.2 Instrumentation and measurements

*Typical preparation of enzyme loaded polymersomes*

As a typical experiment, the enzyme solution (merely enzyme dissolved in the buffer or commercial suspension) was mixed with buffer (either 50mM Tris/HCl or 20mM phosphate at various pH) to a final volume of 2.5 mL (final enzyme concentration 0.2 mg/mL) with conditions described in Table 1 depending on the enzyme. To this solution, PS-*b*-PIAT (0.5 mg) dissolved in 500 µL of the corresponding solvent was gently added in a drop wise fashion under 600 rpm stirring. Depending on the enzyme, we tested THF (the reference), dioxane, DMF and dioxane/DMSO 90/10 v.% until the finding THF was optimal for every enzyme, and was used from then on. The vesicles were immediately transferred to dialysis bags after preparation. Indeed solvents and non-encapsulated enzymes were removed by dialyzing with a 1,000 kDa cut-off in 1 L buffer with 5 renewals for at least 36 hours, maximum 48 h following a previously published procedure.[17] Such membranes tend to concentrate the thereby purified solutions, which is why after recovery, solutions were adjusted to 2 mL.

**Table 1.** Conditions for loading of various enzymes during nanoprecipitation

| Enzyme | Initial enzyme concentration | Volume of enzyme solution |
|---|---|---|
| *Cyclohexanone monooxygenase (CHMO)* | 32 mg/mL | 16 µL |
| *Phenylacetone monooxygenase (wild-type PAMO)* | 125 µM | 60 µL |
| *Phenylacetone monooxygenase (fusion protein CRE2-PAMO)* | 145 µM | 39 µL |
| *Lipase B Candida Antarctica (CalB)* | 2.5 mg/mL | 200 µL |
| *Alcohol Dehydrogenase (ADH)* | 25 mg/mL | 20 µL |

The polymersomes were stored at 4 °C before use and consumed within 5 days after dialysis recovery.

Emulsion-centrifugation yielding giant PB-*b*-PEO encapsulating a PS-*b*-PIAT nanoreactor solution.

Following a procedure published elsewhere,[2] 5 µL of the nanoreactors suspension with substrate and NADPH, in 380 mOsm sucrose solution was first poured in 500 µL toluene containing 3 mg/mL PB-*b*-PEO in an Eppendorf tube (step 1). The PB-*b*-PEO solution in toluene was previously stirred for at least 2 hours to ensure a complete dissolution of the copolymer, as verified by DLS (no intensity scattered). In another tube (step 2), 30 µL of the same organic solution was poured over 30 µL of a 380 mOsm aqueous glucose solution and allowed to stabilize for 30 min. Finally (step 3), the first tube was emulsified with vigorous agitation by hand yielding inverted emulsion droplets (alternatively, repeated pipetting works as well). Then 50 µL of this emulsion was poured slowly over the second interface tube. The sample was then immediately centrifuged at 20 °C at 500 g for 4 min and the aqueous polymersomes in polymersomes (PiPs or polymer vesosomes) suspension was recovered in the lower phase.

***Enzymatic assays by fluorescence in microplate reader.*** Measurements were conducted on a TECAN Infinite Pro 2000. Each experiment presented a total volume of 200 µL. 3 times 60 µL of each experiment were divided in 3 wells of a black 384 well microplate (Greiner) to have triplicates per sample. Temperature was set to 25°C. Excitation was set at 561 nm (with a bandwidth of 9 nm), emission at 590 nm (with a bandwidth of 20 nm). Integration time was 20 µs with 25 flashes. Gain was set either at 100 (part 3.3) or 150 (part 3.2). Generally, measurements were performed during 14 hours with a measurement every 10 min. It is to note that micropipettes calibrated for water (at a viscosity of about 1 g/mL at ambient temperature) were used to pipet DMSO (with a viscosity of about 1.1 g/mL at ambient temperature). By weighing the added DSMO volume during stock solution preparation, we can correct a theoretical 3 mM stock solution to an actual 2.9 mM concentration (so 3 µM is really 2.9, 50=> 48.3, 102=> 98.6, 30 => 29 and 45 => 43.5 µM) and a 10 mM stock solution to 9.9 mM (so 150 µM is really 148.5 and 300 => 297 µM).

***Dynamic Light Scattering (DLS).*** DLS measurements of nanosize PS-*b*-PIAT polymersomes were conducted on a Malvern ZetaSizer Nano ZS instrument with 173° backscattering measurements at 20°C. The mean hydrodynamic diameter and its distribution were determined using Cumulant and CONTIN analysis methods.

***Spinning disk confocal microscopy.*** The spinning disk microscope was a Leica DMI6000 (Leica Microsystems, Wetzlar, Germany) equipped with a confocal Scanner Unit CSU-X1

(Yokogawa) using for this experiment objective HCX PL Apo 63X oil NA 1.4 and an EMCCD camera Photometrics Quantem (Roper Scientific, Evry, France). The diode laser used was at 561 nm and a Semrock emission filter with narrow bandpass windows in the red (593 to 627 nm) spectral region was used. The experiments were performed in the *Bordeaux Imaging Center of the University of Bordeaux Segalen* with the gratefully acknowledged help of Sébastien Marais.

Transmission electron microscopy (TEM) was performed on a *JEOL JEM 1010* microscope with an acceleration voltage of 60 kV equipped with a charge-coupled device (CCD) camera. Sample specimens were prepared by placing a drop (6 μL) of aqueous vesicle solution on an *EM science* carbon-coated copper grid (200 mesh) for 15 min. The grid was purified from salts and other impurities by placing 3 times a drop of MilliQ water on it, which was immediately removed by blotting. The grid was finally air dried overnight and analyzed without further treatment.

Inductively coupled plasma – mass spectrometry (ICP-MS) measurements were performed on a *Thermo Fisher Scientific Xseries I* quadrupole machine using 5.0 mL samples containing 0.49 mg/L InCl3 solutions as internal standard.

## 3. Results and Discussion

### 3.1 Design of enzymatic cascade, concept and general results

The aim of this project was to conduct a biomimetic enzymatic cascade in our multicompartmentalized structures, our cell mimics, in collaboration with Professor van Hest's Group, Radboud University, Nijmegen, The Netherlands. In order to prove such a concept, reaction kinetics needed to be monitored, moreover by confocal microscopy to demonstrate that the cascade really takes place inside the multicompartmentalized structure. As a result, the final product of the cascade needed to be fluorescent. PhD candidate of Radboud University, Ruud Peters, hence designed a complex enzymatic cascade yielding the red fluorescent dye Resorufin (maximas: excitation 561 nm, emission 591 nm)(see Figure 1).

The enzymatic cascade, schematized in Figure 2, is following previous work performed in the van Hest group using Baeyer Villager MonoOxygenase Enzyme (BVMO).[30] The proposed cascade pathway was inspired by earlier work on the development of fluorescent assays for detecting BVMO activity in bacterial cells.[31]

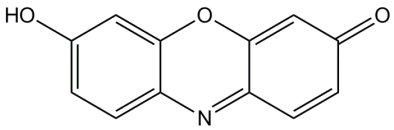


**Figure 1.** Resorufin dye

The initial Baeyer Villager reaction is followed by ester hydrolysis using Candida Antarctica Lipase B (CalB), and lastly by oxidation of an alcohol by alcohol dehydrogenase (ADH) followed by spontaneous β-elimination. It also relies on the cofactors NADPH and $NADP^+$ that are naturally present in animal and plant cells where they play various roles. Cofactors are organic or inorganic components (but not proteins) that bind to enzymes so that these can play their catalytic function. NADPH (Nicotinamide adenine dinucleotide phosphate) is the reduced form of $NADP^+$, thus the reducing agent of the redox couple. The BVMO enzyme needs the cofactor NADPH to perform its catalytic function, thereby inducing the oxidation of NADPH into $NADP^+$. In the last enzymatic step, ADH needs the cofactor $NADP^+$, which is thereby reduced to NADPH. This resembles oxidation-reduction cycles of NADPH/$NADP^+$ occurring in cells, which is why we describe this cascade as biomimetic. We have identified three BVMO enzymes able to work in that cascade, Cyclohexanone monooxygenase CHMO, the one originally planned for this cascade, Phenylacetone monooxygenase PAMO, and a fusion enzyme CRE2-PAMO that itself can regenerate $NADP^+$ to NADPH *via* the attached phosphate dehydrogenase CRE2. Furthermore, this cascade meets the needed requirement of producing a dye as final product, and was never conducted so far in polymersome nanoreactors.

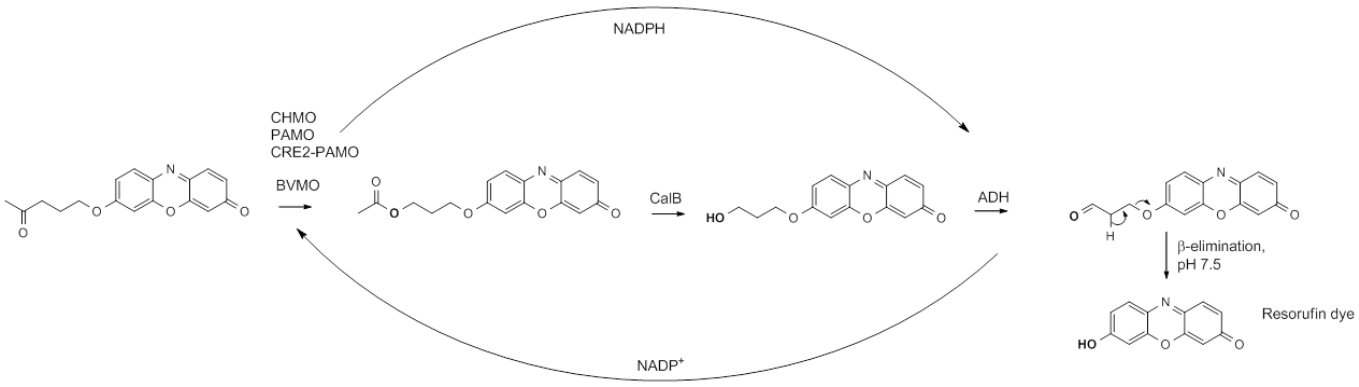


**Figure 2.** Scheme of enzymatic cascade

The final aim of this work was to make this cascade react inside multicompartmentalized polymersomes. If the eukaryotic cell exhibits such multicompartmentalized reactions, it is because such a structure offers much more powerful possibilities than a prokaryotic, single

compartmentalized structure. In chapters 2 and 3[1,2], we emphasize about one of the great properties arising from the multicompartmentalization of actives, i.e. a better protection than if they are loaded into a single compartment only. This should remain true for the powerful and sensitive catalysts that enzymes are. Furthemore, one can, as we planned to in this project, segregate various enzymes into various populations of internal compartments, to conduct cascade or incompatible reactions in them. Such work may bring a better comprehension of the eukaryotic cell; indeed the enzymes are here also confined in inner compartments, the structure mimics the eukaryotic multicompartmentalized structure, and a crowded environment or cytoplasm mimic can also be added for even more accurate biomimicry. From a concrete point of view, we foresee two major long-term applications. The first consists in miniaturized reactors for biotechnology. The advantage lies in reduction of sample consumption, which may be expensive or polluting, at the same time, the multicompartmentalized cascade reaction should be more efficient than if the various internal compartments were not enclosed as well in another compartment as they are thus close to one another, encapsulated side by side. We also see interesting properties arising in the field of drug delivery as some of the few reports published so far on such work, and that have been described in the introduction, highlight.

In this work, each enzyme is loaded into PS-*b*-PIAT polymersomes, yielding 3 different PS-*b*-PIAT populations. As previously mentioned, PS-*b*-PIAT nanoreactors present an intrinsically porous nature, enabling substrate and products but not enzymes, to diffuse through them. The idea is then to mix these populations together in optimized volume ratios, add everything else needed for the reaction, substrate, cofactor, *etc*, and load this solution into PB-*b*-PEO micrometric polymersomes with the emulsion-centrifugation method as previously described (Chapters 2 and 3).[2] The substrate can be photocaged so that the enzymatic cascade can be initiated on demand once the sample is under a confocal microscope, by decaging with a 405 nm laser (FRAPPA mode). Then, the reaction kinetic should be followed by measuring the increase of fluorescence appearing either homogenously in the micrometric PB-*b*-PEO vesicle or first localized in the nanosize PS-*b*-PIAT polymersomes loaded with ADH, before diffusion in the lumen of the outer vesicle (see Figure 3). As a preliminary experiment, the free cascade reaction was tested in order to check if we could detect red fluorescence kinetics with a microplate reader.

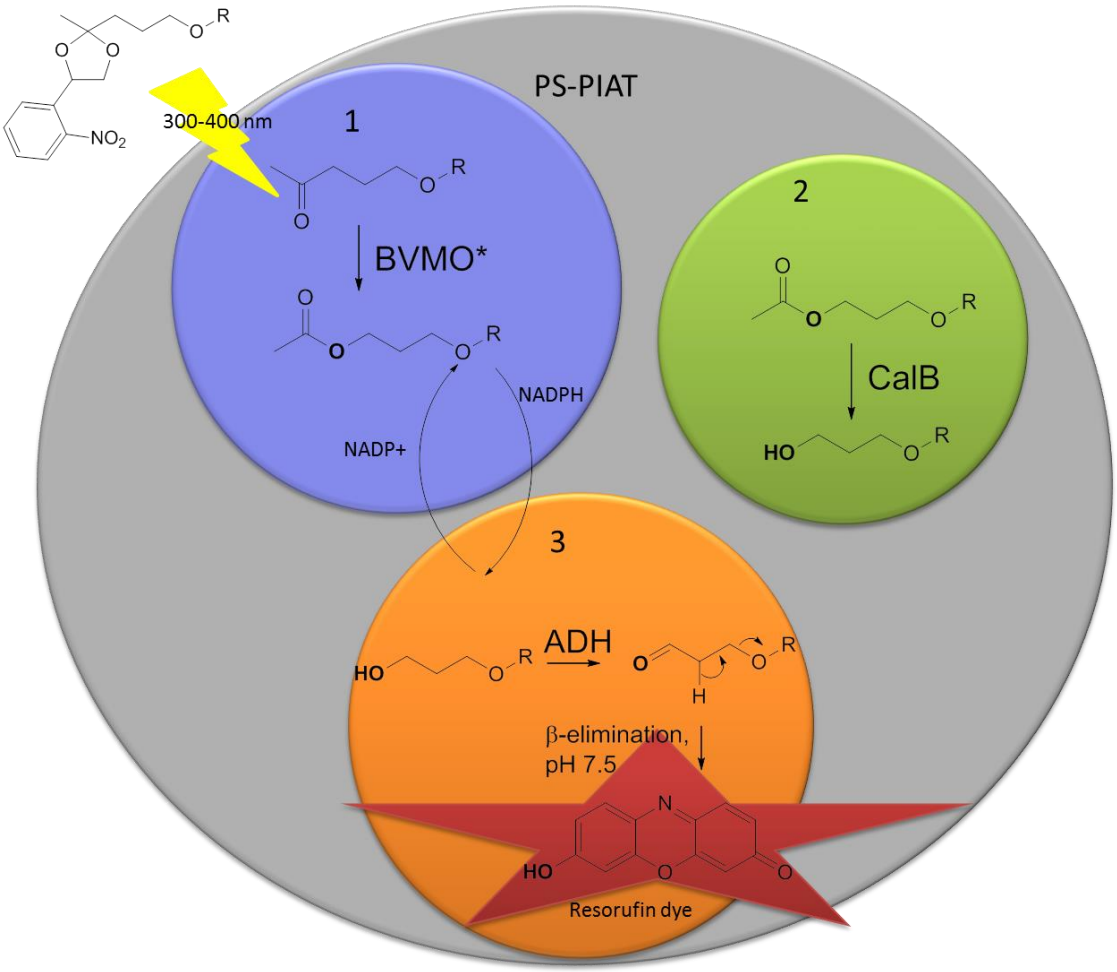


**Figure 3.** Scheme of multicompartmentalized enzymatic cascade

When we speak of kinetics throughout this chapter, it is as chemists, thus we mean the formation of product (dye), meaning the conversion versus time. However in biology or enzymology more particularly, a kinetic plot of an enzymatic reaction is in fact the rate of reaction versus the substrate concentration, allowing the extrapolation of various important kinetic parameters depending on the model of plot (Km and Kcat in the Michaelis-Menten representation for example). Thus we ask readers for clemency as we talk about enzymatic reactions throughout this chapter, yet discuss them as classic chemical reactions.

Here, one can visualize what we call an "optimal kinetics plot", as well as the two parameters that we needed to improve to prove our final concept:

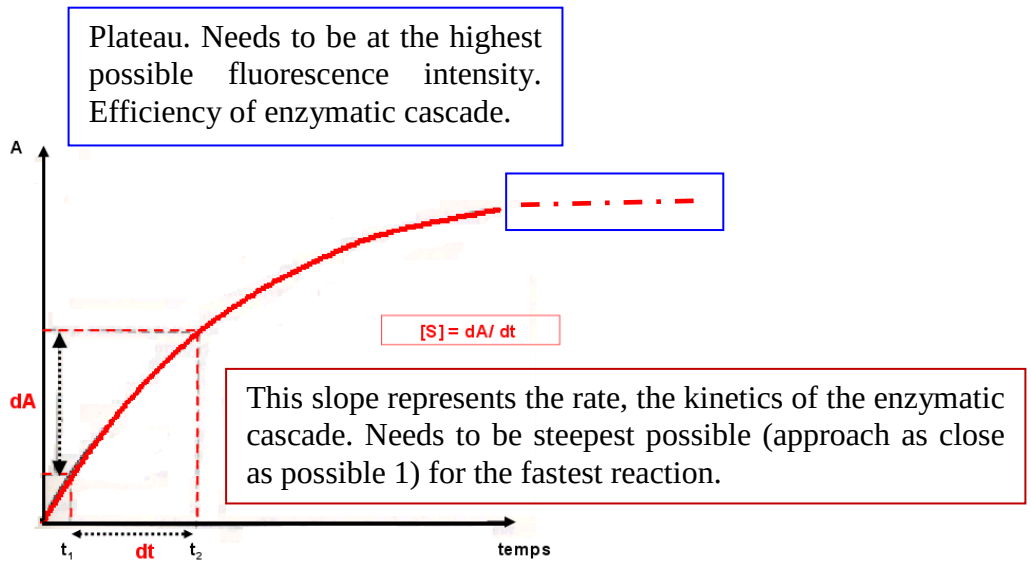


**Figure 4** : Example of our goal, of what we call an optimized plot. Here absorbance, and not fluorescence, with time. From the following web page: http://frontal.univ-angers.fr/unspf/2010_Nancy_Galteau_Enzymes/res/Sans%252520nom%25252071.png&w=574&h=419&ei=UYNyUOyKKIyDhQfNsYGYDw&zoom=1&iact=hc&vpx=1134&vpy=306&dur=275&hovh=192&hovw=263&tx=175&ty=113&sig=104352963191211969135&page=1&tbnh=142&tbnw=185&start=0&ndsp=24&ved=1t:429,r:11,s:0,i:102

Considering the final goal of our physical-chemical project (monitor the kinetics of an enzymatic cascade reaction in polymersomes in a polymersome), we needed indeed the fastest possible reaction (to detect fluorescence early, as soon as possible), the fastest rate, which is represented by the slope parameter. The steeper the slope (the closer to one), the better. This is a truly kinetic parameter. The faster the reaction, the sooner the "plateau" is reached; the plateau is the timepoint after which conversion is maximal, nothing happens any more, thus intensity remains constant. We needed also this plateau to reach the highest possible, most intense fluorescence (for optimal and early detection, and/or detection at all). This is a thermodynamic parameter, representing the efficiency of the various enzymes involved.

Interestingly, in the free cascade CHMO the BVMO enzyme originally planned gave a very steep slope but leveled off very early (i.e. reached its "plateau" at a very low intensity), with disappointingly low fluorescence intensity, while wild-type PAMO (stored in the freezer as a solution for over a year) gave a less steep curve but with much higher final intensity.
After one night, the fluorescence intensity induced by the PAMO cascade did not reach a plateau yet, indicating good potential as the kinetics did not present optimized behavior. After this qualitative proof of concept attesting that the enzymatic cascade was feasible, we decided

to pursue directly to the nanoreactors as the behavior of enzymes strongly depends from the nanoprecipitation process used to load them. In addition, there are some diffusion limitations of substrates and products when polymersome membranes are involved, even though they are intrinsically porous.

However as a first step, and before testing a fully loaded cascade, we performed two experiments where the "new" enzymes (never loaded and studied for application in nanoreactors in the van Hest group so far) were checked for loading in PS-*b*-PIAT polymersomes:

- ADH was loaded with the other two kept free in solution,
- CHMO or PAMO were loaded with the other two in solution.

It was encouraging to see we could still detect a kinetic, so it seemed possible to load these never tested enzymes in PS-*b*-PIAT nanoreactors. Interestingly however, results were intense and steep for the ADH-loaded cascade (others kept free) whereas they were much lower for the BVMO's, indicating already that nanoprecipitation process was possibly damaging them and the first BVMO step would probably be problematic, for sure the limiting step. Table 2 summarizes the various conditions used for the loading of these "new" enzymes in PS-*b*-PIAT, the enzymatic activity tests as well as the preservation of vesicular structure, as determined by TEM and DLS analysis. Interestingly, THF was the best solvent for all the enzymes tested and chosen as optimal solvent for the following experiments.

**Table 2.** Various enzymes tested for use in PS-PIAT nanoreactors

| **Enzyme** / **Solvent** | **CHMO** | **PAMO** | **CRE2-PAMO** | **ADH** |
|---|---|---|---|---|
| **THF** | S E | S E | S E | S E |
| **DMF** | | S E | | |
| **Dioxane** | E | E | E | |
| **90/10 vol.% Dioxane/ DMSO** | E | E | | E |

*S means structure acceptable by DLS and TEM*
*E means enzymatic activity acceptable by fluorimetry measurements*
*Highlighted cell means best system*

Some of these enzymes were also tested for encapsulation efficiencies inside PS-PIAT vesicles by ICP-MS measurements and Ru-labelling of enzymes (table 3). Results for ADH and the already often loaded CalB in the van Hest group are consistent with the approximately 20% efficiency always reported by this group. Interestingly, CRE2-PAMO however, presents a much lower efficiency of 7 %, which also helps understand the deceiving results observed with CRE2-PAMO in the following chapter, especially if on top of that, this enzyme is more sensitive to organic solvents than ADH and CalB.

**Table 3.** Encapsulation efficiencies

| **Enzyme** | **CRE2-PAMO** | **ADH** | **CalB** |
|---|---|---|---|
| **Encapsulation efficiency** | 7±0.35% | 24±0.6% | 21±0.14% |

*Error represents the standard error σ/√n, where n represents the number of estimations, 4.*

The repeatability of the nanoprecipitation process was then tested by DLS measurements, especially for the optimal THF conditions (Table 4).

**Table 4.** DLS of all enzymes tested for use in PS-PIAT nanoreactors

| **Enzyme**<br>**Solvent** | **CHMO** | **PAMO** | **CRE2-PAMO** | **ADH** | **CalB** |
|---|---|---|---|---|---|
| **THF** | 200±12.6<br>208±12.3<br>0.09±0.01<br>n=3 | 172±5.4<br>192±18<br>0.13±0.03<br>n=2 | 176±7.9<br>211±17.2<br>0.15±0.01<br>n=6 | 217±9.5<br>248±12<br>0.17±0.01<br>n=8 | 196±7<br>205±9.4<br>0.12±0.01<br>n=8 |
| **DMF** | | 140±3.3<br>146±4.3<br>0.09±0.01<br>n=3 | | | |
| **Dioxane** | 187<br>214<br>0.16 | 124<br>538<br>0.16 | 131±0.08<br>155±1.3<br>0.17±0.01<br>n=2 | | |
| **90vol.% Dioxane/ DMSO** | 219<br>223<br>0.21 | 149<br>148<br>0.13 | | 877<br>1093<br>0.27 | |

*1st line is size by Cumulants algorithm, 2nd by Contin,, 3rd is PDI, 4th is the number of samples measured. Each value, error represents the standard error σ/√n, where n represents the numbers of measured samples.*

From both the average size measurement and polydispersity index (PDI), we can see that this reproducibility (for THF) is relatively acceptable as it is below 0.2. The best results are obtained for CHMO, the worst for ADH, which is also by very far the largest enzyme with a molecular weight of approximately 150,000 g/mol (CalB is at 60,000, CRE2-PAMO at 100,000, PAMO at 65,000, and CHMO at 60,000 g/mol). Sizes are also acceptable for nanosize polymersomes, especially loaded with such large components.

Regarding the optimization of the nanoreactor cascade, the primary step lies in the determination of the optimal ratios of the different polymersomes that together will give the best kinetic parameters. This was performed first with the BVMO's CHMO and wild-type PAMO, as we had initially no CRE2-PAMO. The set of experimental conditions tested first is summarized in table 5. Tables 5, 6, 7 are merely here to explain the rationale when addressing such Research, thus not detailed; indeed the BVMO enzymes used here are different from the CRE2-PAMO of the final system, and furthermore the substrate was not completely purified for these preliminary experiments. In sections 3.2 and 3.3, all experimental conditions and results will however be thoroughly presented.

Moreover, we chose to experimental conditions in terms of volume ratios of PS-*b*-PIAT suspensions, as we prepare these suspensions always in the same reproducible way. The parameter that is clearly varied throughout the experiment and is palpable, is the volume of respective polymersome suspensions. Of course, there are only mathematic operations separating those volumes from the final enzyme concentrations in the solution. We indicate respective enzyme concentrations for the final concentration ratios in Tables 9 section 3.2 and 24 section 3.3.

**Table 5.** First set of optimization of volume ratios for the three enzyme loaded PS-*b*-PIAT polymersomes

| **BVMO** | **CalB** | **ADH** |
|---|---|---|
| 10 | 10 | 10 |
| 10 | 10 | 1 |
| 1 | 10 | 10 |
| 10 | 1 | 10 |

The experiment that led to the most drastic decrease in reaction kinetics gives the indication about the rate-limiting enzyme. Then it is possible to tune more finely the other ones. In our

case, BVMO's were limiting so the next step was to perform experiments with increased loading of BVMO as described in Table 5.

**Table 6.** Second set of optimization of volume ratios

| BVMO | CalB | ADH |
|---|---|---|
| 10 | 1 | 1 |
| 20 | 1 | 1 |
| 10 | 5 | 1 |
| 10 | 1 | 5 |
| 20 | 5 | 1 |
| 20 | 1 | 5 |

Here, we saw that the volume of ADH could not be higher than the one of CalB, certainly because ADH also converts the starting substrate into an alcohol by using NADPH. As a result, in order to prevent this side-reaction and because ADH did not look rate limiting, we decided to limit the amount of ADH.

Finally, a third set of optimizations was performed as depicted in Table 7.

**Table 7.** Third set of optimization of volume ratios

| BVMO | CalB | ADH |
|---|---|---|
| 20 | 1 | 1 |
| 50 | 1 | 1 |
| 50 | 1 | 0.5 |

The best result was reached with 50:1:0.5 but we stopped the optimization of these ratios there because we could not add more BVMO polymersome volume without exceeding the final volume of 200 µL decided for our experiment. We did not want to increase that final volume as we did not want to consume every polymersome sample (2 mL) just with one or two assays. Indeed, even at such ratios, BVMO was still the limiting enzyme apparently, perhaps because it gets too degraded during polymersome formation, in presence of organic solvent. Also, and for sure, because its encapsulation efficiency is three-times lower than for

CalB and ADH (7% for CRE2-PAMO). Results were also disappointing in terms of final fluorescence intensity, which was not detectable by confocal microscopy.

These three tables are given to explain the ratios used in the following section with the final BVMO, CRE2-PAMO, they explain the rationale when addressing such a work. However they are only preliminary experiments and we will detail every experiment and parameter in the two following sections.

CRE2-PAMO, an engineered PAMO was shown to be more resistant to solvents, more robust, and already tested in PS-PIAT nanoreactors[30]. As a result, we used the conclusions drawn so far with the other BVMO's with the hope to get much better results with CRE2-PAMO and finally be able to continue with the last step of the project.

## 3.2 Optimization of cascade in PS-PIAT nanoreactors with CRE2-PAMO as BVMO

However, CRE2-PAMO turned out to not generate much better results than the other two BVMO's, which is why we cannot really present the optimized protocol or some assays grouped together. We expected the optimization of the cascade to be much faster; it should have represented basically the discovery of optimal respective volume ratios. But in our case, BVMO's really seemed problematic, and above all our enzymatic cascade relies upon two cofactors which appeared to complicate everything; thus this involved a lot of experiments to reach an optimized system. Above all, the ultimate goal of this project was not to get a kinetics plot of the nanoreactor cascade by fluorimetry measurements. We needed a high enough concentration for detection of the multicompartmentalized cascade by confocal microscopy, the microplate reader apparently and surprisingly being much more sensitive. Considering our ultimate project, we decided to follow a pragmatic approach, by optimizing the nanoreactor cascade empirically, using each overnight experiment as input for the following set of assays. This work will be detailed in this section.

### 3.2.1.First set of enzymatic assays

This experiment had two main goals:

- determine whether THF or dioxane was a better nanoprecipitation solvent to load CRE2-PAMO.
- for each solvent condition, test which buffer (Tris/HCl pH 7.5 or Phosphate buffer pH 7.6 or 8.5) was optimal. Enzymes are indeed very sensitive to such kind of

experimental conditions (buffer, pH of buffer, solvent). Resorufin also needs a slightly basic pH (7.5-7.6) for maximal fluorescence .

After each recovery of polymersomes after dialysis, we always checked the actual pH which can drift sometimes when diluting concentrated stock solutions of buffers for examples. So here, we actually had Tris pH 7.6 vs Phosphate pH 7.7 vs Phosphate pH 8.7.
Constant parameters of experiments can be found in Table 8.

**Table 8.** Experimental conditions for section 3.2.1

| **Conditions** | **CRE2-PAMO** | **CalB Vol. ratio** | **ADH** | **[NADPH]** | **Estimated [BVMO]** | **[NADPH] /[BVMO]** | **[substrate]** | **[NADPH] /[sub]** | **Total volume** |
|---|---|---|---|---|---|---|---|---|---|
| 1 | 20 | 1 | 0.5 | 64 µM | 0.06 µM* | 1,067 | 3 µM | 21 | 200 µL |

*assuming a 7% encapsulation efficiency and 100 kDa Molecular weight for CRE2-PAMO

Regardless of the nanoprecipitation solvent (THF or dioxane), at pH 8.7 phosphate buffer, no enzymatic activity could be detected. By comparing assays performed under exact same conditions, activity seems better for polymersomes formed with THF than dioxane. In addition, the polymersome morphology is less well-defined when they are formed in dioxane (see Table 2). Thus, from then on, we again kept THF as nanoprecipitation solvent. However, we could not clearly conclude yet whether Tris pH 7.6 or Phosphate pH 7.7 was best in terms of enzymatic activity. We also only used a volume ratio of 20 for CRE2-PAMO to confirm already the previous conclusions with the other BVMO's were transferable to this one, without wasting too much enzyme.

### 3.2.2. Second set of enzymatic assays

The aim of this second set of experiments was to definitely determine which buffer between Tris/HCl and Phosphate was the best to preserve the highest possible activity. Based on previous results, only high volume ratios of CRE2-PAMO of 50 were tested. Estimated enzyme concentrations for conditions 50:1:0.5 CRE2-PAMO:CalB:ADH can be found in table 9.

**Table 9.** Concentrations of CRE2-PAMO, CalB and ADH in enzymatic cascade for most common 50:1:0.5volume ratios of PS-*b*-PIAT polymersomes in section 3.2.

| | Mass used in nano-precipitation | Mass actually loaded | [ ] if final polymersome volume=2mL | Molecular weight g/mol | Volume of polymersomes in 200µL assay | [ ] in µM in enzymatic assay | [CRE2-PAMO]/ [enzyme] |
|---|---|---|---|---|---|---|---|
| CRE2-PAMO 7% | 0.5 mg | 0.035 mg | 0.0175 | 100,000 | 150 | 0.13 | |
| Cal B 21% | 0.5 mg | 0.105 mg | 0.0525 g/L | 60,000 | 3 µL | 0.013 | 10 |
| ADH 24%* | 0.5 mg | 0.12 mg | 0.06 mg/mL | 150,000 | 1.5 µL | 0.003 | 44 |

We also increased the NADPH concentration compared to previous experiments.
Constant experimental parameters can be found in Table 10.

**Table 10.** Experimental conditions for section 3.2.2.

| **Conditions** | **CRE2-PAMO** | **CalB Vol. ratio** | **ADH** | **[NADPH] mM** | **Estimated [BVMO]** | **[NADPH] /[BVMO]** | **[substrate]** | **[NADPH] /[sub]** | **Total volume** |
|---|---|---|---|---|---|---|---|---|---|
| 2 | 50 | 1 | 0.5 | 0.53 | 0.15 µM* | 3,533 | 3 µM | 177 | 200 µL |

*assuming a 7% encapsulation efficiency and 100 kDa Molecular weight for CRE2-PAMO

Experimental curves presenting the fluorescence intensity measured by the microplate reader as function of time can be seen in Figure 5. Each enzymatic assay of 200 µL is always divided in three wells (60 µL) to have triplicates as errors induced by pipetting variations easily happen. Presence of CRE2-PAMO also tends to produce foam, thus inducing errors by inducing height of total volume variations in wells. We decided to trust the result only when at least two kinetics are identical. Results are then plotted as an average of two or three identical kinetics with error bars representing standard error (i.e. standard deviation divided by the square root of the number of measurements, 2 or 3). For each set, we also monitor a blank, i.e. autohydrolysis of the substrate in buffer. To judge results, intensity of plateau is compared to intensity of the blank, to know the signal to noise ratio. Although each kind of intensity is relative to conditions, the difference between both is indeed absolute.
From these data, one can conclude that with same parameters (table 9), we have better results with Tris/HCl pH 7.6 than with Phosphate pH 7.7.

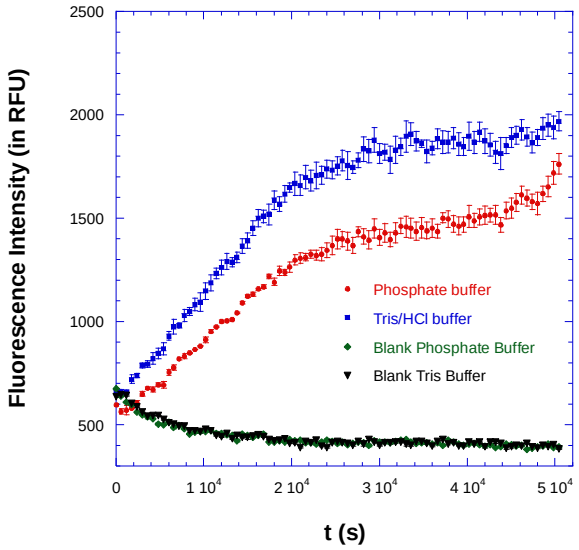


**Figure 5.** Fluorescence intensity with time, corresponding to conditions in table 10.
Experiments performed in triplicate, sometimes only in duplicate if one is not coherent. Error bars represent standard error, $\sigma/\sqrt{n}$ standard deviation divided by the square root of measurements, 2 or 3.

### 3.2.3. Third set of enzymatic assays

This set of experiments had four main goals:

- Increase substrate concentration to get an increase in fluorescence intensity.
- Optimize further CalB concentration by fine-tuning its optimal volume ratio.
- Find out whether concentrating CRE2-PAMO polymersomes helps.
- Investigate more the influence of NADPH concentration.

3.2.3.a. Until now we were indeed careful not to waste substrate, using a very small substrate concentration of 3 µM which was enough to detect a kinetic with the microplate reader. However, to make sure that adding substrate helps and having previously assessed with the other BVMO's the NADPH concentration needs to increase accordingly with substrate to improve the kinetic, we performed the experiments summarized in Table 11.

**Table 11.** Experimental conditions section 3.2.3.

| **Conditions** | **CRE2-PAMO** | **CalB Vol. ratio** | **ADH** | **[NADPH] mM** | **Estimated [BVMO] µM** | **[NADPH] /[BVMO]** | **[substrate] µM** | **[NADPH] /[sub]** | **Total volume µL** |
|---|---|---|---|---|---|---|---|---|---|
| 4 | 50 | 1 | 0.5 | 8.950 | 0.15* | 59,667 | **50** | **172** | 200 |
| 5 | 50 | 1 | 0.5 | 0.53 | 0.15* | 3,533 | **3** | **177** | 200 |

*assuming a 7% encapsulation efficiency and 100 kDa Molecular weight for CRE2-PAMO

In figure 6, we can indeed observe an increase in plateau intensity which was nearly 3-fold (always compared to its own blank, otherwise the global intensity is 4 times higher), and of course the slope much steeper as a result.

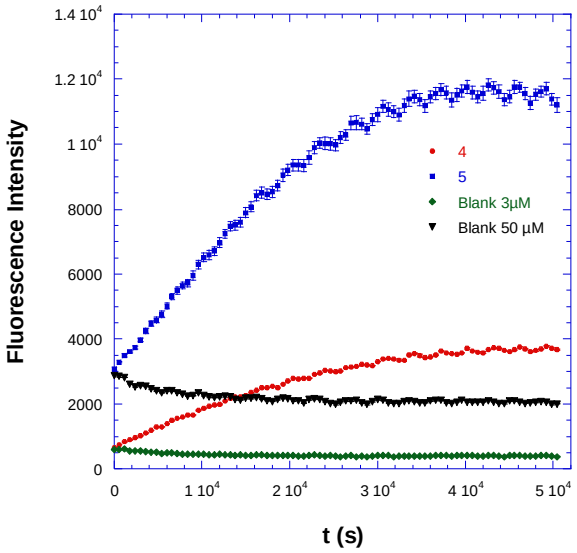


**Figure 6.** Fluorescence intensity with time, corresponding to conditions in table 11.

3.2.3.b. Using still the usual 3 µM concentration for substrate, we optimized further the CalB and CRE2-PAMO volume ratios (see Table 12).

**Table 12.** Experimental conditions section 3.2.3

| **Conditions** | **CRE2-PAMO** | **CalB Vol. ratio** | **ADH** | **[NADPH] mM** | **Estimated [BVMO] µM** | **[NADPH] /[BVMO]** | **[substrate] µM** | **[NADPH] /[sub]** | **Total volume µL** |
|---|---|---|---|---|---|---|---|---|---|
| 5 | **50** | **1** | 0.5 | 0.53 | 0.15* | 3,533 | 3 | 177 | 200 |
| 6 | 50 | **5** | 0.5 | 0.53 | 0.15* | 3,533 | 3 | 177 | 200 |
| 7 | 50 | **10** | 0.5 | 0.53 | 0.15* | 3,533 | 3 | 177 | 200 |

*assuming a 7% encapsulation efficiency and 100 kDa Molecular weight for CRE2-PAMO

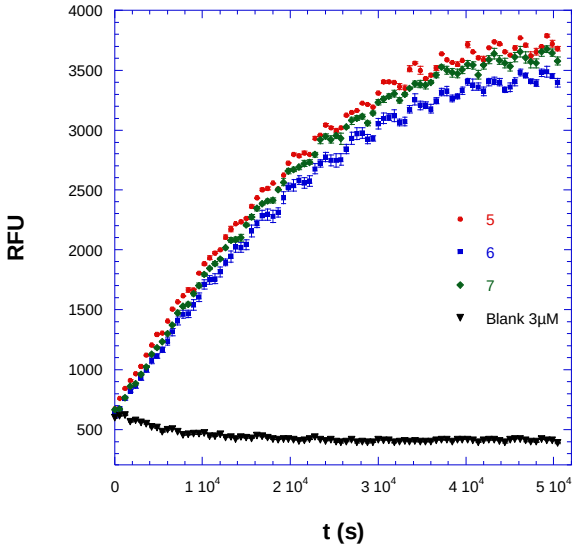


**Figure 7.** Fluorescence intensity with time, corresponding to conditions in table 12.

By using 5 (Serie 6) or 10 (Serie 7) instead of 1 (Serie 5) as CalB volume ratio, not only was there no improvement/increase in plateau intensity (Figure 7), but it actually decreased very slightly. As a result, on can definitely conclude that the ratio 1 CalB : 0.5 ADH is optimal, at least in this cascade.

For practical reasons we also tried a scenario where instead of filling up to 200 µL with buffer as usual, we used CRE2-PAMO loaded polymersomes instead (Series 5 and 8). Result (64 CRE2-PAMO volume ratio) is the same or maybe very slightly above for the one for 50, but again as NADPH concentration changes as well, it is more difficult to draw conclusions.

**Table 13.** Experimental conditions section 3.2.3

| **Conditions** | **CRE2-PAMO** | **CalB Vol. ratio** | **ADH** | **[NADPH] mM** | **Estimated [BVMO] µM** | **[NADPH] /[BVMO]** | **[substrate] µM** | **[NADPH] /[sub]** | **Total volume µL** |
|---|---|---|---|---|---|---|---|---|---|
| 5 | **50** | **1** | 0.5 | 0.53 | 0.15* | 3,533 | 3 | 177 | 200 |
| 8 | **64** | **1** | 0.5 | 0.68 | 0.19 * | 3,579 | 3 | 226 | 200 |

* assuming a 7% encapsulation efficiency and 100 kDa molecular weight for CRE2-PAMO

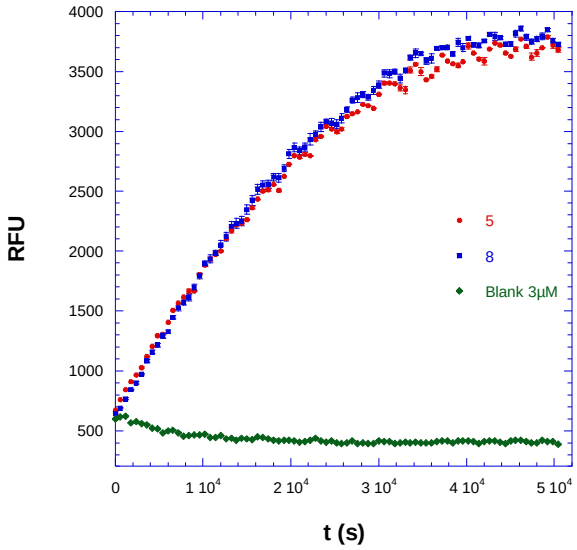


**Figure 8.** Fluorescence intensity with time, corresponding to conditions in table 13.

By using a CRE2-PAMO polymersome suspension that is twice as concentrated as usual because the final volume after dialysis is 1 and not 2 mL, the results are slightly improved in terms of plateau intensity and slope steepness (Series 5 vs. 9, 6 vs. 10 Figure 9) as NADPH is increased accordingly. Results are however not drastically increased, not twice for example, as would be expected for a double amount of polymersomes.

**Table 14.** Experimental conditions section 3.2.3

| **Conditions** | **CRE2-PAMO** | **CalB Vol. ratio** | **ADH** | **[NADPH] mM** | **Estimated [BVMO] µM** | **[NADPH] /[BVMO]** | **[substrate] µM** | **[NADPH] /[sub]** | **Total volume µL** |
|---|---|---|---|---|---|---|---|---|---|
| 5 | 50 | 1 | 0.5 | 0.53 | 0.15* | 3,533 | 3 | 177 | 200 |
| 9 | 50 | 1 | 0.5 | 1.06 | **0.3 *** | 3,533 | 3 | 353 | 200 |
| 6 | 50 | 5 | 0.5 | 0.53 | 0.15* | 3,533 | 3 | 177 | 200 |
| 10 | 50 | 5 | 0.5 | 1.06 | **0.3 *** | 3,533 | 3 | 353 | 200 |

*assuming a 7% encapsulation efficiency and 100 kDa Molecular weight for CRE2-PAMO

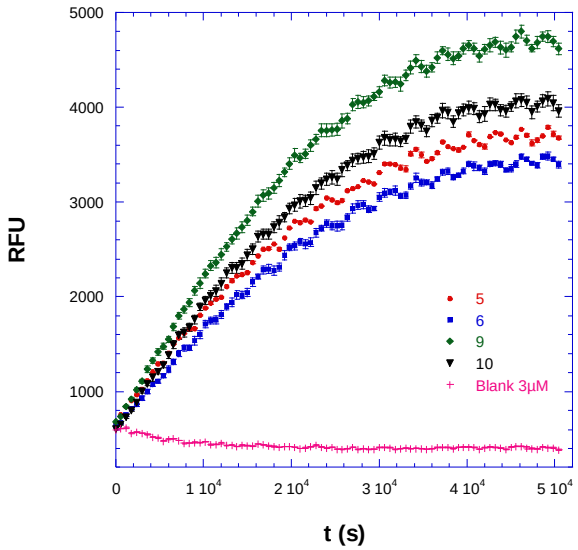


**Figure 9.** Fluorescence intensity with time, corresponding to conditions in table 14.

Finally the most important parameter definitely seems to be NADPH as by increasing 5 times its concentration (see Table 15), the plateau is nearly twice (1.6) more intense (see Figure 14, serie 11 vs.6).

**Table 15.** Experimental conditions section 3.2.3

| **Conditions** | **CRE2-PAMO** | **CalB Vol. ratio** | **ADH** | **[NADPH] mM** | **Estimated [BVMO] µM** | **[NADPH] /[BVMO]** | **[substrate] µM** | **[NADPH] /[sub]** | **Total volum µL** |
|---|---|---|---|---|---|---|---|---|---|
| 6 | 50 | 5 | 0.5 | **0.53** | 0.15* | 3,533 | 3 | **177** | 200 |
| 11 | 50 | 5 | 0.5 | **2.65** | 0.3* | **8,833** | 3 | **883** | 200 |

*assuming a 7% encapsulation efficiency and 100 kDa Molecular weight for CRE2-PAMO

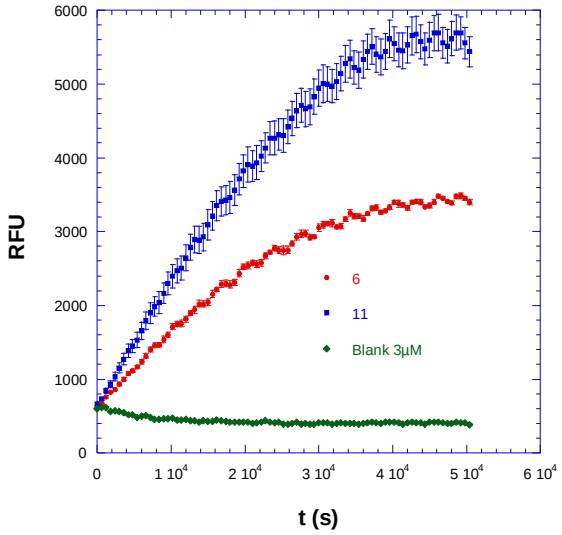


**Figure 10.** Fluorescence intensity with time, corresponding to conditions in table 15.

### 3.2.4. Fourth set of enzymatic assays

This experiment had one main goal:

- Investigate further influence of NADPH concentration.

To keep again the experiment more practical, we chose not to add any buffer, and use about 62 CRE2-PAMO instead of 50. At the same BVMO concentration (≈ 0.185 mM), adding only 3.350 mM NADPH instead of 8.888 mM provokes a decrease of 25% in plateau intensity (Table 16). Such a concentration of 8.888 mM presents however the problem to involve a lot of expensive NADPH, which is far from ideal.

**Table 16.** Experimental conditions section 3.2.4

| **Conditions** | **CRE2-PAMO** | **CalB Vol. ratio** | **ADH** | **[NADPH] mM** | **Estimated [BVMO] µM** | **[NADPH] /[BVMO]** | **[substrate] µM** | **[NADPH] /[sub]** | **Total volume µL** |
|---|---|---|---|---|---|---|---|---|---|
| 12 | 62 | 1 | 0.5 | **3.350** | 0.185 * | **18,108** | 3 | **1,117** | 200 |
| 13 | 62 | 1 | 0.5 | **8.888** | 0.185 * | **48,043** | 3 | **2,963** | 200 |

*assuming a 7% encapsulation efficiency and 100 kDa Molecular weight for CRE2-PAMO

Finally we investigated a two-fold increase of the concentration of a CRE2-PAMO loaded polymersome suspension, this time by keeping the same NADPH concentrations and NADPH to substrate ratio. The only varying parameter is the NADPH to CRE2-PAMO ratio that is twice smaller for the twice more concentrated suspension (table 17). Interestingly, the plot of

the less concentrated one was approximately the same as the more concentrated, maybe highlighting the NADPH to substrate ratio is far more important than the one to BVMO contrary to what was expected from previous experiments. It shows that for these conditions, it makes no point to increase beyond the value of 24,022 as NADPH to CRE2-PAMO ratio.
It is however to note that both suspensions came from different polymersome batches; for a better comparison, both suspensions should have been obtained from the same polymersome batch although the various polymersomes batches seemed reproducible so far (see Tables 3&4).

**Table 17.** Experimental conditions section 3.2.4

| **Conditions** | **CRE2-PAMO** | **CalB Vol. ratio** | **ADH** | **[NADPH] mM** | **Estimated [BVMO] µM** | **[NADPH] /[BVMO]** | **[substrate] µM** | **[NADPH] /[sub]** | **Total volume µL** |
|---|---|---|---|---|---|---|---|---|---|
| 13 | 62 | 1 | 0.5 | 8.888 | **0. 185 *** | **48,043** | 50 | 177 | 200 |
| 14 | 62 | 1 | 0.5 | 8.888 | **0.37 *** | **24,022** | 50 | 177 | 200 |

*assuming a 7% encapsulation efficiency and 100 kDa Molecular weight for CRE2-PAMO

To conclude NADPH seems key again, which is surprising as it is only a cofactor, that should be regenerated by the ADH reaction, and thus should not play such an important part once the cascade functions.

### 3.2.5. Fifth set of enzymatic assays

This experiment had two main goals:

- Increase substrate concentration to get an increase in fluorescence intensity.
- Investigate in more detail the influence of NADPH concentration with higher substrate concentration.

As a last chance to finally get a drastic and needed increase in intensity, we increased the substrate to the highest volume which seemed acceptable to us as a DSMO/water percentage, 6.8 µL/193.2 µL. By comparing with the same conditions at the usual 3 µM substrate (see table 18), plateau intensity is 4.5-times higher (in terms of fluorescence intensity, 3.5 when substracting the intensity of respective blanks to each of them to get the absolute intensity increase), and much steeper (series 15 vs. 5 Figure 11). By trying to keep the same molar NADPH to substrate ratio of 177, the concentration of NADPH is however much increased, from 0.53 mM to 17.474 mM NADPH, which seems barely acceptable.

**Table 18.** Experimental conditions section 3.2.5

| Conditions | CRE2-PAMO | CalB Vol. ratio | ADH | [NADPH] mM | Estimated [BVMO] µM | [NADPH] /[BVMO] | [substrate] µM | [NADPH] /[sub] | Total volume µL |
|---|---|---|---|---|---|---|---|---|---|
| 5 | 50 | 1 | 0.5 | 0.53 | 0.15 * | 3,533 | **3** | 177 | 200 |
| 15 | 50 | 1 | 0.5 | 17.475 | 0.15 * | 116,500 | **102** | 172 | 200 |

*assuming a 7% encapsulation efficiency and 100 kDa Molecular weight for CRE2-PAMO

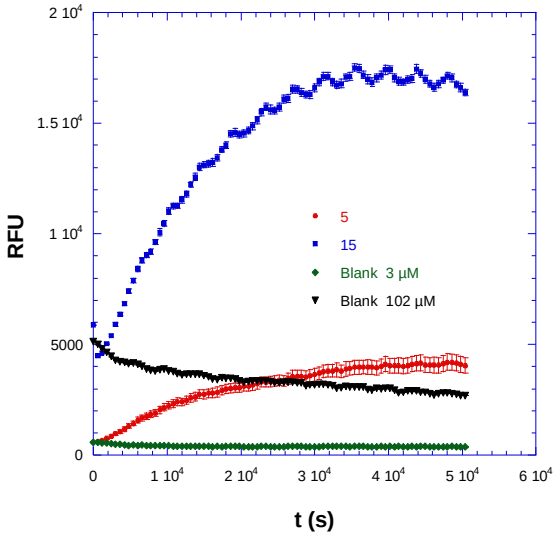


**Figure 11.** Fluorescence intensity with time, corresponding to conditions in table 18.

We also tried to investigate a little more the NADPH influence with a higher substrate concentration of 30 µM substrate, 10 times the usual amount, as it had become obvious we would have to work with a high substrate concentration for the microscopy monitoring (Table 19). Of course, results are better for 30 µM (Series 16 and 17) than for 3 µM substrate (Serie 5), but not 10 times higher. By keeping NADPH/substrate to 177, we get an approximately 2.5-fold increase in plateau intensity (after respective blank substraction, 3-fold in absolute terms) (Figure 12). With 30 µM, final intensity was actually at 13000 RFU for the 5.25 mM NADPH and only at 9000 for 26.25 mM NADPH, showing with these conditions, we overcame the limit where adding more NADPH becomes inhibitory instead of beneficial.

**Table 19.** Experimental conditions section 3.2.5

| Conditions | CRE2-PAMO | CalB Vol. ratio | ADH | [NADPH] µM | Estimated [BVMO] µM | [NADPH] /[BVMO] | [substrate] µM | [NADPH] /[sub] | Total volume µL |
|---|---|---|---|---|---|---|---|---|---|
| 5 | 50 | 1 | 0.5 | **0.53** | 0.15 * | 3,533 | **3** | **177** | 200 |
| 16 | 50 | 1 | 0.5 | **5.25** | 0.15 * | 35,000 | **30** | **175** | 200 |
| 17 | 50 | 1 | 0.5 | **26.25** | 0.15 * | 175,000 | 30 | **875** | 200 |

*assuming a 7% encapsulation efficiency and 100 kDa Molecular weight for CRE2-PAMO

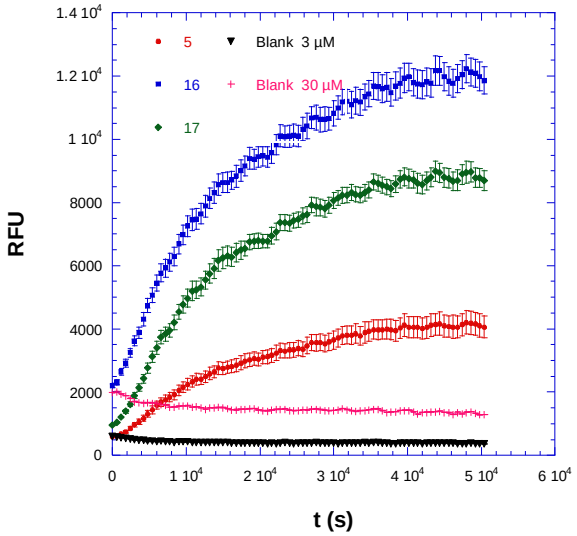


**Figure 12.** Fluorescence intensity with time, corresponding to conditions in table 19.

Still, even such a high signal was not high enough to be detected by spinning disk confocal microscopy once loaded in giant PB-*b*-PEO. In order to determine which signal could be expected first, two reference experiments were performed. A solution of 24 µM Resorufin in Milli Q water loaded in giant PB-*b*-PEO vesicles enabled to see those vesicles with a red fluorescent cavity. Such a 24 µM solution was saturating (i.e. above 60,000 units of fluorescence) in the microplate reader at a gain of 100. We had also loaded an assay based upon CalB and the substrate carboxyfluorescein diacetate (CFDA). After letting the cascade react one night (i.e. at maximal conversion), then loading it in PB-*b*-PEO polymersomes, the vesicles were perfectly visible with green fluorescence this time, by epifluorescence, spinning disk confocal, and laser scanning confocal microscopy in Bordeaux. We performed this assay in the microplate reader and it went up to 50,000 RFU with a 100 microplate reader PMT gain. However in all section 3.2, we were forced to set a gain of 150 as intensities were too

low to visualize efficiently the kinetic with the lower gain of 100. We were clearly not reaching such fluorescence intensities even with this much higher gain.
It is indeed crucial to check if the cascade at maximal conversion (which is the case for the assay solution, after one night reaction in the microplate reader) can be detected in giant PB-*b*-PEO under a confocal microscope. If even then it cannot be detected, there is no hope of monitoring a kinetics plot, with points underneath this maximum, and it means we have to optimize further.

### 3.3. Optimization of cascade in PS-PIAT nanoreactors with free CRE2-PAMO

Obviously, the problem came from the BVMO enzymes, which were apparently not loaded with a sufficient bioactivity remaining. A solution to overcome this hurdle was to keep the CRE2-PAMO free in solution while the other ones, CalB, and ADH, were still encapsulated.
From then on, we were able to use a microplate reader gain of 100 again, instead of the 150 for section 3.2, which demonstrates the drastic improvement between these two sections.
In the present section, the global volume per assay is as always 200 µL which is why we will not show it anymore.

#### 3.3.1. First set of enzymatic assays

This experiment had several main goals:

- Start afresh with a cascade where CRE2-PAMO was free, and optimize it, in terms of enzyme ratios, NADPH and substrate concentration.
- Determine whether in that case wild-type PAMO or fusion PAMO (CRE2-PAMO) was more efficient.

Experimental conditions can be found in Table 20:

**Table 20.** Experimental conditions section 3.3.1

| Conditions | BVMO | BVMO µL | CalB µL | ADH µL | [NADPH] mM | [BVMO] µM | [NADPH] /[BVMO] | [substrate] µM | [NADPH] /[sub] |
|---|---|---|---|---|---|---|---|---|---|
| 19 | **CRE2-PAMO** | 55.17 | 70 | 35 | 0.2 | 4 | **50** | 3 | 67 |
| 20 | **PAMO** | 62.02 | 70 | 35 | 0.2 | 4 | 50 | 3 | 67 |
| 21 | CRE2-PAMO | 55.17 | 70 | 35 | 1.5 | 4 | **375** | 3 | 500 |
| 22 | PAMO | 62.02 | 70 | 35 | 1.5 | 4 | 375 | **3** | 500 |
| 23 | CRE2-PAMO | 55.17 | 70 | 35 | 2 | 40 | 50 | 3 | 667 |
| 24 | CRE2-PAMO | 55.17 | 70 | 35 | 15 | **40** | 375 | 3 | 5000 |
| 25 | CRE2-PAMO | 55.17 | 70 | 35 | 0.2 | **4** | 50 | 45 | 4 |
| 26 | CRE2-PAMO | 55.17 | 70 | **35** | 1.5 | 4 | 375 | **45** | 33 |
| 27 | CRE2-PAMO | 55.17 | 70 | **70** | 0.2 | 4 | 50 | 3 | 67 |
| 28 | CRE2-PAMO | 55.17 | 70 | 70 | 1.5 | 4 | 375 | 3 | 500 |

*with 100 kDa Molecular weight for CRE2-PAMO

We kept the same volume ratios of CalB and ADH 1:0.5 and started with a reference concentration of BVMO, 4 µM[30]. First, we checked by comparing identical conditions, that CRE2-PAMO gave better results than wild-type PAMO (experiments 19 vs 20, 21 vs 22, see Figure 13). By multiplying the reference of 4 µM by ten, we finally obtained a 30-fold drastic increase in intensity. Interestingly, after a whole night Plateau was not reached yet for any assay, contrary to before (23 vs 25, 24 vs 26, see Figure 14). By comparing experiments 23 and 24, an increase in lag time duration becomes obvious with an increase in NADPH concentration. However, these concentrations of 40 µM CRE2-PAMO were tested on our very low and usual concentration of 3 µM substrate, where the enzyme cannot be considered as a catalyst any more…Nevertheless, we can see with the 4 µM assays that CRE2-PAMO is still the limiting step (no plateau's). This and the results of the 40 µM BVMO experiments indicate we need to test 40 µM (or more) with appropriate higher substrate concentrations and we should be able to extrapolate the conclusions of the 4 µM assays for that. 50 NADPH to BVMO was the ratio employed by Silvie Meuwissen[30] and when we based calculations on a

20% encapsulation efficiency of CRE2-PAMO (instead of the real, measured at 7%), our classic ratio was 375.

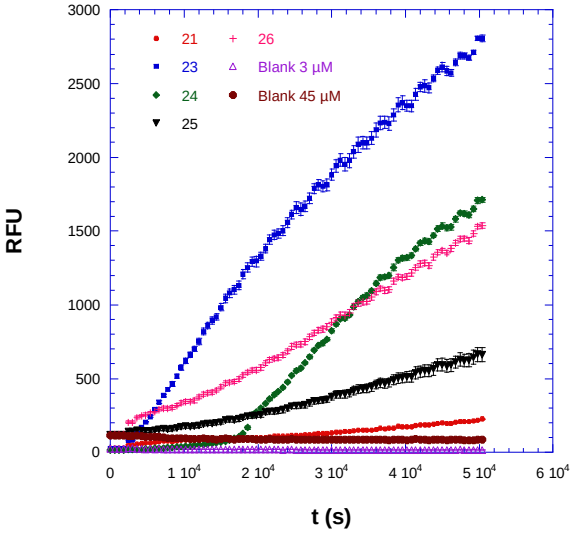


**Figure 12.** Fluorescence intensity with time corresponding to conditions in table 20.

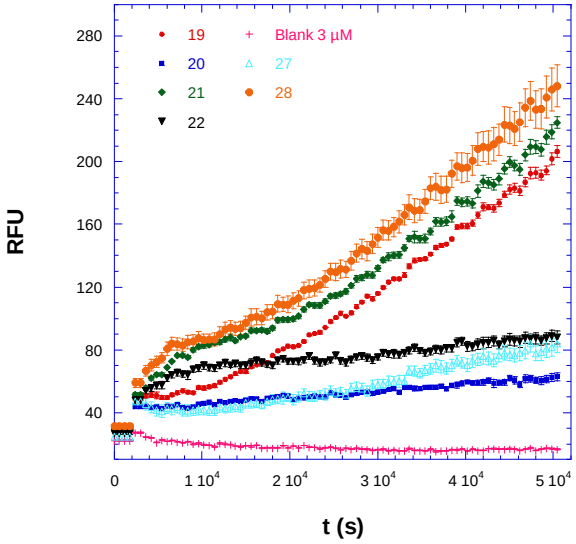


**Figure 13.** Zoom in Fluorescence intensity corresponding to conditions ion table 20.

For every 4 µM assay, a ratio of 375 NADPH to BVMO instead of 50 (ratio to substrate of 500 vs. 67 for 3 µM) is beneficial (28 vs 27, 22 vs. 20, 21 vs. 19). Of course, again we also believe the ratio of NADPH to substrate to have a certain relevance; unfortunately it cannot be kept constant in the same time as the NADPH to CRE2-PAMO, especially when we increase the substrate to 45 µM instead of the usual 3 µM. Then, the NADPH to substrate ratio is indeed only 33 vs. 4 for 45 µM when going from NADPH/BVMO=375 to 50. Experiments 26 vs 25 make us conclude as before that a higher NADPH/BVMO of 375 is much preferable, at least at low CRE2-PAMO concentrations of 4, with the plot of 26 actually looking nearly as good in terms of final intensity as experiment 24 with 40 µM CRE2-PAMO. Finally, we checked that by using twice more ADH (1:1 instead of 1:0.5), there was no change in results, meaning ADH is definitely not limiting and we can continue with these CalB:ADH volume ratios (experiments 27 vs. 19 with a decrease, 28 vs. 21 with no improvement)

As a general conclusion from this set of experiment (especially, experiments 25 vs. 19, 26 vs. 21), we conclude that in the next step we have to increase the CRE2-PAMO final concentration to at least 40 µM, highly increase substrate as well (even if it seems

problematic), and prefer a 375 NADPH ratio or above. We also need to keep using CRE2-PAMO instead of wild-type PAMO and continue with CalB:ADH 1:0.5.

### 3.3.2. Second set of enzymatic assays

With this obvious need to increase substrate concentration, we tried to force a higher stock solution in DMSO than the one we had and which seemed the maximum possible (3, maximum 4 mM) by heating the solution at 50°C, and from then on, heating the stock solution before the assays every time up to 50°C until the moment of adding it.

This experiment had several main goals:

- Optimize the current cascade with higher substrate concentrations.
- Optimize NADPH for these substrate concentrations.
- Optimize volume ratios of CalB:ADH for this final system.

Experimental conditions can be found in Table 21:

**Table 21.** Experimental conditions section 3.3.2

| **Conditions** | **CRE2-PAMO µL** | **CalB µL** | **ADH µL** | **[NADPH] mM** | **[BVMO] µM** | **[NADPH] /[BVMO]** | **[substrate] µM** | **[NADPH] /[sub]** |
|---|---|---|---|---|---|---|---|---|
| 29 | 55.17 | 70 | 35 | 0.2 | 4 | 50 | 150 | 11/3≈3.67 |
| 30 | 55.17 | **70** | **17.5** | 0.2 | 4 | 50 | 150 | 11/3≈3.67 |
| 31 | 55.17 | **105** | **35** | 0.2 | 4 | 50 | 150 | 11/3≈3.67 |
| 32 | 55.17 | 105 | 17.5 | 0.2 | 4 | **50** | 150 | 11/3≈3.67 |
| 33 | 55.17 | 70 | 35 | 0.4 | 4 | **100** | 150 | 22/3≈7.34 |
| 34 | 55.17 | 70 | 35 | 1.5 | 4 | 375 | 150 | 10 |
| 35 | 55.17 | 70 | 35 | 0.2 | 4 | 50 | **300** | 2/3 |
| 36 | 55.17 | 70 | 35 | 1.5 | 4 | 375 | **300** | **5** |

*with 100 kDa Molecular weight for CRE2-PAMO

With this now acceptable substrate concentration of 150 µM and a NADPH to BVMO ratio of 50 to limit NADPH consumption (200 µM NADPH), we checked once more with this system that our 1:0.5 CalB :ADH ratio was optimal, as 1:0.25, 1.5:0.5 and 1.5:0.25 did not change anything (see Figures 14 and 15, experiments 29, 30, 31, 32). Then with this definite1y optimal 1:0.5 ratio and 150 µM substrate, we went from 50 (experiment 29) to 100 NADPH/BVMO (experiment 33, 400 µM NADPH, 2 times faster than experiment 29) to 375 (experiment 34, 1500 µM NADPH, 6.4 times faster than experiment 29). There is a huge

improvement in terms of slope steepness, thus final intensity. We did not correct for the blank by substracting its value to the assays, but NADPH 50 gives indeed about 25 RFU/h, 100 about 50 RFU/min and 375 about 173 RFU/min.

By increasing the substrate concentration even more, from 150 (experiment 34) to 300 µM (experiment 36), and keeping the same NADPH to BVMO of 375 (1500 µM), it is to note the plot is exactly the same. It may be because in these conditions, the enzyme is saturated and will not convert any more substrate molecules, or because while the NADPH/BVMO stays the same, when we have only 150 µM substrate we have twice more NADPH to substrate (ratio 10) than when we have at 300 µM (ratio 5).

The most important conclusion from that set of experiments is that we were able to work with high enough, concentrations of substrate, even for 40 µM enzyme.

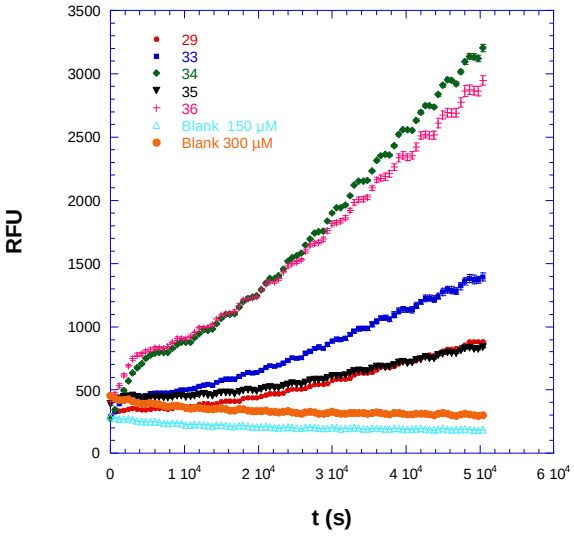


**Figure 14.** Fluorescence intensity with time, corresponding to conditions in table 21.

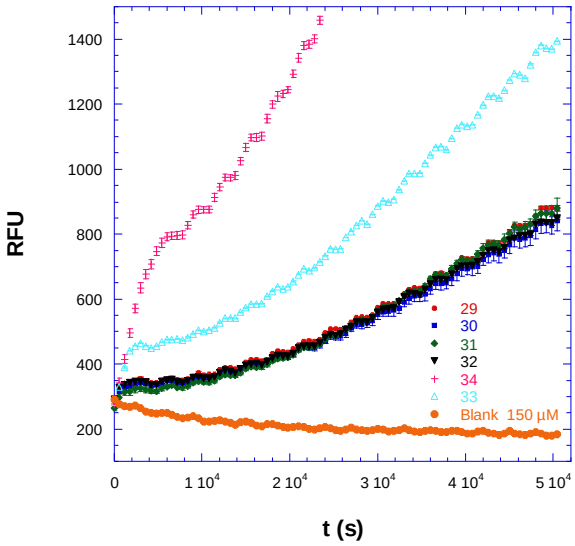


**Figure 15.** Zoom in Fluorescence intensity with time, corresponding to conditions in table 21**.**

### 3.3.3.Third set of enzymatic assays

This experiment had several main goals:

- Optimize NADPH ratio for 40 µM CRE2-PAMO, for a given substrate concentration of 300 µM.
- Investigate the optimal NAPH concentration (important for BVMO and substrate) with a lower and safer concentration of 4 µM CRE2-PAMO.

Experimental conditions can be found in Table 22:

**Table 22.** Experimental conditions section 3.3.3

| Conditions | CRE2-PAMO µL | CalB µL | ADH µL | [NADPH] mM | [BVMO] µM | [NADPH] /[BVMO] | [substrate] µM | [NADPH] /[sub] |
|---|---|---|---|---|---|---|---|---|
| 37 | 55.17 | 70 | 35 | 0.04 | 4 | **10** | 150 | 0.25 |
| 34 | 55.17 | 70 | 35 | 1.5 | 4 | 375 | 150 | 10 |
| 38 | 55.17 | 70 | 35 | 2 | 4 | **500** | 150 | 13.3 |
| 39 | 55.17 | 70 | 35 | 0.4 | 40 | 10 | 300 | 1.3 |
| 40 | 55.17 | 70 | 35 | 2 | 40 | 50 | 300 | 6.7 |
| 41 | 55.17 | 70 | 35 | 4 | 40 | 100 | 300 | 13.3 |

*with 100 kDa Molecular weight for CRE2-PAMO

The shape of the plot looks already much more optimized (steeper slope, not too long lag phases, *etc*) (experiments 40 and 41 Figure 16) even if we do not reach a plateau yet. We are indeed finally reaching the fluorescence intensities we know will be detected by confocal microscopy given our references, as we approach 50,000 RFU with a microplater reader gain of 100.

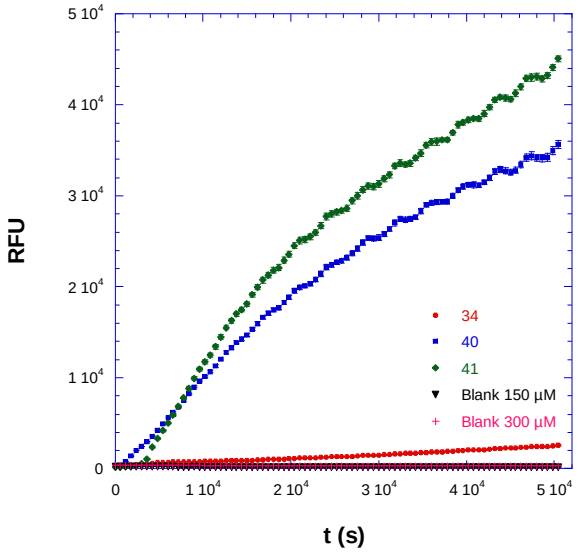


**Figure 16.** Fluorescence intensity with time, corresponding to conditions in table 22.

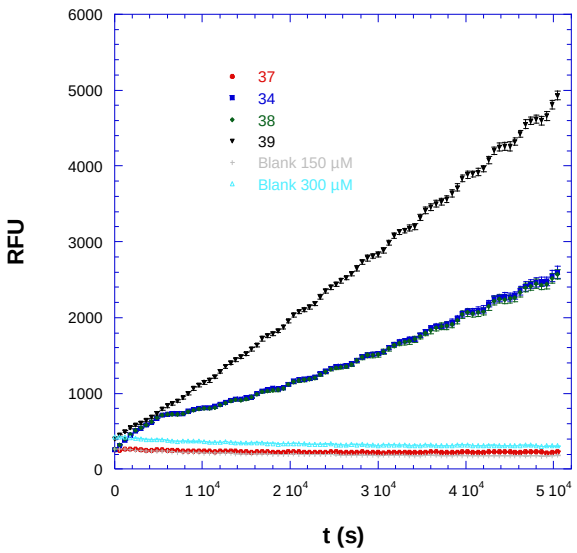


**Figure 17.** Zoom in Fluorescence intensity with time, corresponding to conditions in table 22.

For 40µM CRE2-PAMO, we use 300 µM substrate (corresponding to 6 µL DMSO in 194 µL aqueous solution, i.e. 3 v. %) with as usual 1:0.5 CalB to ADH. Going from NADPH/BVMO= 10 (400µM NADPH, experiment 39) to 50 (2000 µM, experiment 40) to 100 (4000 µM, experiment 41), the results are improved, impressively first with a 6.8-fold

increase in final intensity, then slightly (meaning that [NADPH] apparently becomes optimal for these conditions) with 1.2-fold increase from 50 to 100 (Figure 16). NADPH/substrate accordingly goes from 1.3 to 6.7 to 13.3. In order to optimize a bit further without consuming too much enzyme and NADPH, we also investigated NADPH ratios again with 4 µM CRE2-PAMO and 150 µM substrate (Figure 17). With a ratio of 10 (40 µM, experiment 37), no activity is detected, for 375 (1500 µM, experiment 34), it is exactly the same as for 500 (2000 µM, experiment 38) at least for these conditions (NADPH/substrate=0.25, 10 and 13.3). This means in these conditions, going above 375 NADPH ratio is unnecessary and between 10 and 375, 375 is optimal.

As CRE2-PAMO still seemed the limiting step, the cascade was optimized a little further by Ruud Peters.

One easy perspective to try out, was to increase CRE2-PAMO's volume ratio until it is not limiting any more. Until now, for the best assay conditions, 20 µL of buffer were used to fill up to 200 µL. Instead of adding 55 µL of fusion-PAMO to reach 40 µM, adding 80 µL to reach 60 µM would mean it is not necessary to use some buffer any more to reach the 200 µL final volume of the assay. Furthermore pH 8.5 and 9 vs. pH 7.5 were previously checked, but they were too high for the enzymes. pH 8 however proved to be beneficial. Finally adding right away some $NADP^+$ necessary for the last reaction of ADH, also seemed beneficial.

It was assessed clearly that for 100 NADPH to CRE2-PAMO ratio, there was practically no lag phase whereas for 200, there was one but once the resorufin production started, it was twice faster and more intense than for the 100. So in theory for microscopy experiments, 100 should be the ratio used when decaging and 200 when working with the non-caged substrate.

The final conditions are visible in Table 23:

**Table 23.** Experimental conditions section 3.3.3

| **Conditions** | **CRE2-PAMO µM** | **CalB µL** | **ADH µL** | **[NADPH] mM** | **[$NADP^+$] mM** | **[BVMO] µM** | **[NADPH] /[BVMO]** | **[substrate] µM** | **[NADPH] /[sub]** |
|---|---|---|---|---|---|---|---|---|---|
| 42 | 60 | 70 | 35 | 12 | 1.2 | 60 | **200** | 300 | 40 |
| 43 | 60 | 70 | 35 | 6 | 0.6 | 60 | **100** | 300 | 40 |

*with 100 kDa Molecular weight for CRE2-PAMO

Instead of Tris/HCl buffer at pH 7.5, the PS-PIAT suspensions were hence dialysed against pH 8 in the final protocol.

For the current best conditions in the final system, with 60 µM CRE2-PAMO, 35 µL CalB polymersomes and 17.5 µL ADH, the estimated concentrations of CalB and ADH can be found in table 24, based on their respectively measured encapsulation efficiencies (EE). Ratios of CRE2-PAMO to these enzymes are also given.

**Table 24.** Concentrations of CalB and ADH in enzymatic cascade

| | Mass used in nano-precipitation | Mass actually loaded | [ ] if final polymersome volume=2mL | Molecular weight g/mol | Volume of polymersomes in 200µL assay | [ ] in µM in enzymatic assay | [60] µM CRE2-PAMO/ [enzyme] µM |
|---|---|---|---|---|---|---|---|
| Cal B 21% | 0.5 mg | 0.105 mg | 0.0525 g/L | 60,000 | 70 µL | 0.30625 | ≈196 |
| ADH 24%* | 0.75 mg | 0.18 mg | 0.09 mg/mL | 150,000 | 35 µL | 0.105 | ≈571 |

*24% was assessed for nanoprecipitation of 0.5 mg of ADH.

## 4. Microscopy of multicompartmentalized cascade. Proof of concept of cellular function in cellular structure mimic.

The next step consists in assessing if our multicompartmentalized cascade can be detected by means of fluorescence *via* confocal microscopy.

The final system is depicted by Figure 18:

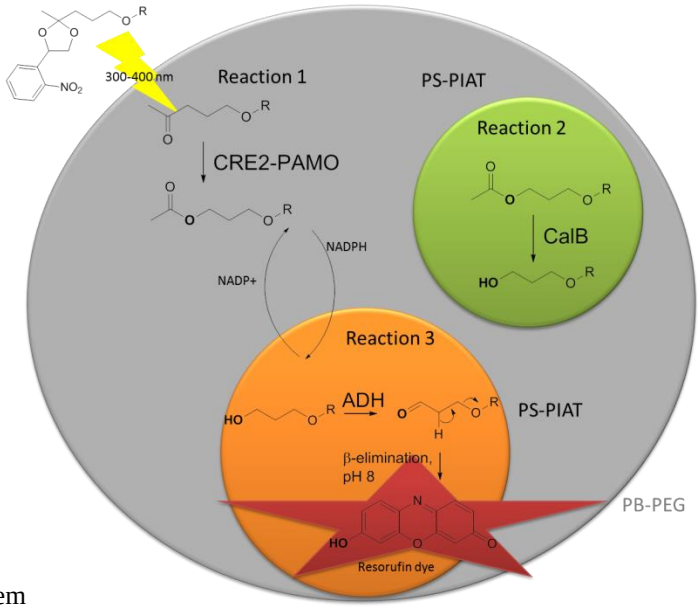


**Figure 18**. Final system

With the conditions as used for experiment 41, we had indeed been able to prove at least full, or advanced conversion by confocal microscopy on the multi-compartmentalized cascade in Nijmegen, which now made it interesting to try to acquire confocal kinetics.
After this necessary optimization step of nanoreactors, our ultimate goal was to monitor a kinetic plot with a caged substrate, decaged under the microscope with a 405 nm laser, in order to control the initiation time of the reaction. However, if this shows to be tricky/impossible of if we want to get a feeling about how long it takes before the reaction can be detected, we can use what we call "the stopwatch method". This method consists in (i) mixing all components of the cascade and start the stopwatch upon addition of the final component, i.e. the non-caged substrate, (ii) let the reaction proceed in a thermomixer™ at 25°C, (iii) load this nanoreactor mixture at a controlled time point in PB-*b*-PEO and (iv) start monitoring by microscopy eventually which will not be time 0 but adjusted to the correct time point thanks to the running stopwatch. We chose to first work with the non-caged substrate, get a feeling of the experiment, the kinetics, and the set-up, and address the difficulty of decaging later with this knowledge acquired.

In any case, regarding the chambers, and the imaging, one problem lies in the fact that the micrometric vesicles, suspended in water, are moving. The chambers we finally decided to use after multiple tests on various commercial or tailor-made chambers, were top chambers of hydrophobic plastic specially designed by Ibidi® for fluorescence microscopy. However, over a prolonged period of time, the vesicles move. This renders impossible imaging overnight for example (convenient for the monitoring of slow reactions!), and forced us to be able to constantly monitor the samples by transmission and replace them in the center of the frame, before each acquisition, during hours. Analysis treatments of movies then also have to be manual of course, making the experiment and the analysis time-consuming!

**Figure 19.** Ibidi µslides VI$^{0.4}$.

The height of the "tunnels", which is the section observed with the microscope, is 400 µm, so

far much than the PiPs, below 100 µm. We also tested chambers coated with polylysine (interacting with PEO), collagen and even their own mixture called IbiTreat™, but no improvement was noted, perhaps due to the fact that we have a compact outer layer of PEO. Vogel and coworkers[7] immobilized their liposomes with anchors on coated slides via biotin-neutravidin bonds. Bäumler et. al.[12] used the IbiTreat coated µslides (another reference) but their systems are Lbl capsules with charged layers, different from our neutral vesicles, and able to interact electrostatistically with charged surfaces.

With these chambers and constant replacing of giant vesicles in the middle of observation frame, we have been able to conduct some preliminary experiments with the following set-up (Figure 25):

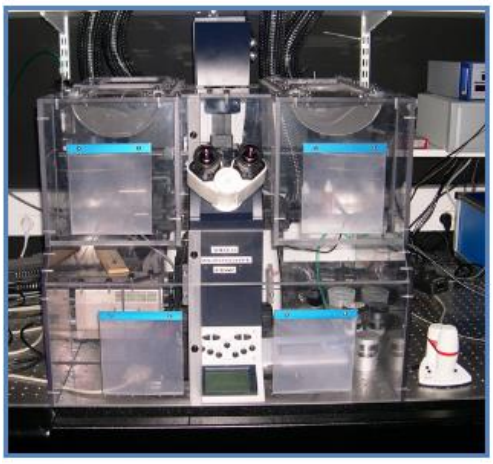

**Figure 20.** Spinning-disk confocal microscopy set-up.

Finally, One problem arising when working with microscopes in Nijmegen or Bordeaux, and enzymes, is that either the room is air-conditioned to 20°C or 21°C or/and the microscope is enveloped by an isotherm "box" controlled by a device heating at 37°C for biology experiments (see Figure 20). 37°C leads to an increase of the sample motion and some water evaporation during the timescale of the experiments. Moreover PB-*b*-PEO is rather permeable at such a temperature (see chapter 3). However these devices are unfortunately not able to cool and control another temperature than 37°C, which makes it difficult to adjust and control the "box" to the desired 25°C. As temperature and its slightest variations is a very important parameter for enzymatic reactions, we monitored for each experiment the temperature in the isotherm "box" *via* a probe, with the 37°C heating switched off; it was fortunately always about 25°C.

First the cell mimic cascade was monitored by confocal microscopy, with the stopwatch method. After 7 hours and 26 minutes of reaction at approximately 25°C, we indeed already

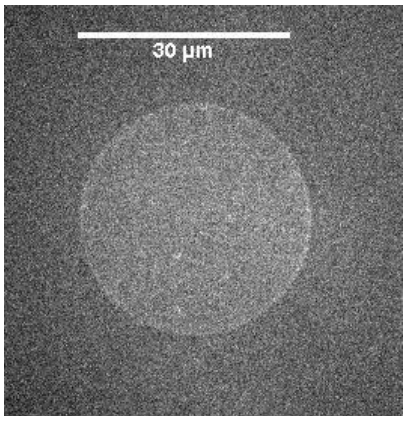


**Figure 21.** Spinning-disk confocal snapshot

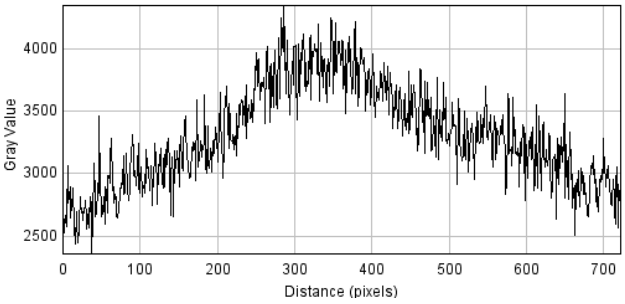


**Figure 22.** Intensity plot profile of line diagonally cutting Figure 26.

observed a cascade activity (Figure 21 and 23) created with the experimental conditions 43 in Table 23 (NADPH/BVMO=100)! This was a very important result as it proved the concept, the fact that we have enzymatic cascade reactions occurring in PS-*b*-PIAT polymersomes in a PB-*b*-PEO polymersome. It also shows we can already detect fluorescence after 7h26 of reaction even though we could not see a change in fluorescence intensity during the course of the day for that set of experiments

The intensity plot profiles (Figures 22 and 24, profiles of diagonals across the frame) are presented to show the background to signal ratio, which gives an idea about the quality of fluorescence. A good fluorophore is usually described as being at least 2.5 times more intense than the background. This is not yet the case here, which also not that surprising as this experiment is much more complex than just the loading of a fluorescent molecule.

Another sample is shown in another chamber (polylysine coated) in Figure 23, after 7 hours 28 minutes. We indeed tried to use chambers with an interaction with PEO (here polylysine) in order to have them immobilized for practical reasons. An increase of the background nose can clearly be observed under these conditions. The interaction between the surface and the PiPs is possibly too strong and destabilizes the PB-*b*-PEO polymersome membrane, leading

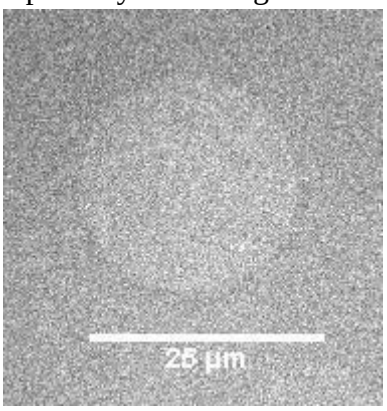


**Figure 23.** Spinning-disk confocal snapshot of functional cell mimic (conditions 43, 7h28, polylysine coated chamber).

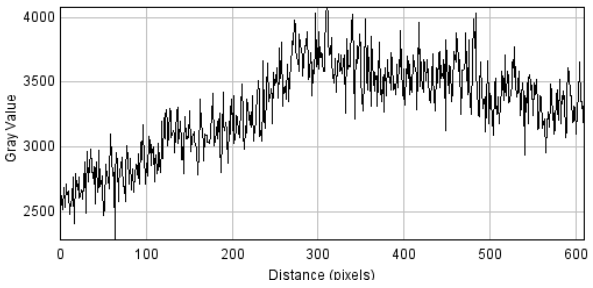


**Figure 24.** Intensity plot profile of line diagonally cutting Figure 28. Both mimics were captured with 500 ms, 600 electronical gain, and 25% laser power.

to leakage of the enzymatic content, thus the generated fluorescent dyes, in the solution.
In order to improve the experiment, we increased the NADPH to BVMO ratio from 100 to 200. With 100, there is no lag time, whereas for 200, there is a lag time around one hour. In addition, the reaction is about twice faster and twice more intense than with 100. Indeed, the results looked promising, also in terms of better signal to background ratio. The figures all correspond to a set of experiments performed on one day with conditions 42 of Table 23 (and 250 ms exposure time, 25% laser, 600 gain). Interestingly, Figure 25 is highly promising as a strong fluorescence signal can be observed after only 3h42 of reaction!

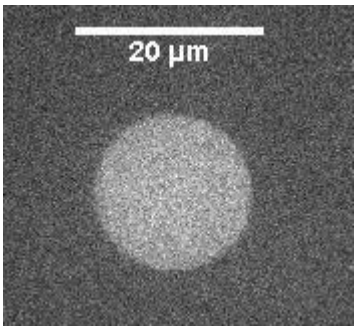


**Figure 25.** Spinning-disk confocal snapshot of functional cell mimic (conditions 42, 3h42).

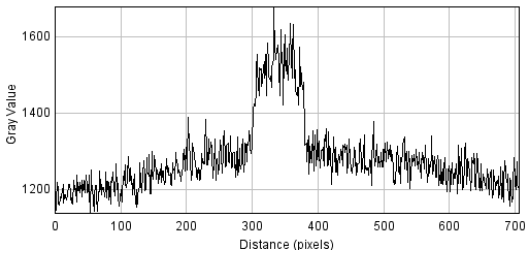


**Figure 26.** Intensity plot profile of line diagonally cutting Figure 30

We also present Figures 27 and 28 (another sample than the one in Figure 25), with multiple PiPs to evidence the fact that the phenomenon is not isolated, there are many fluorescent cell mimics per sample injected in a chamber. The level of fluorescence looks seemingly homogeneous in all the vesicles that are in the same focal plane.

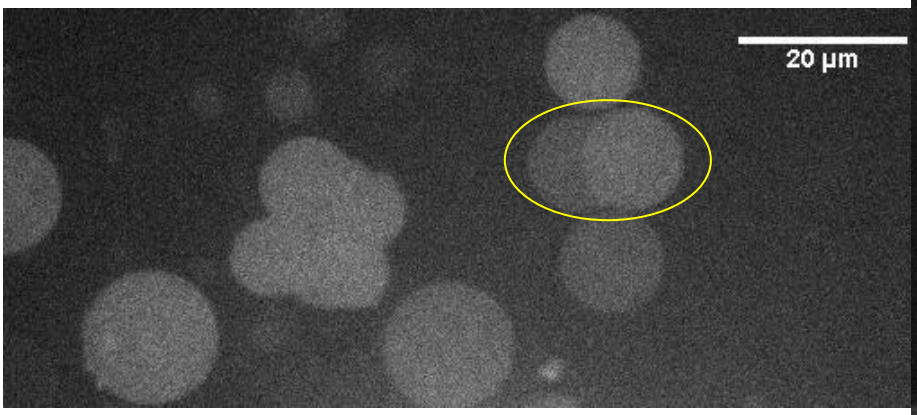


**Figure 27.** Spinning-disk confocal snapshot of functional cell mimic (conditions 42, 6h42,).

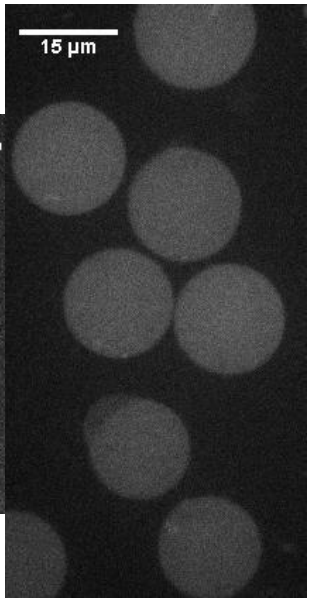


**Figure 28.** Spinning-disk confocal snapshot of functional cell mimic (conditions 42, 6h59).

In another sample corresponding to the same preparation conditions, the monitored intensity after about 9h30 of reaction is the highest ever observed so far (see Figure 29-34).

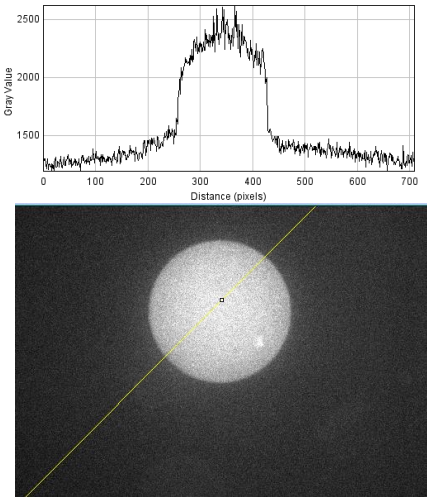


**Figure 29.**Vizualisation of method for extracting Intensity plot profile of line diagonally crossing a Spinning-disk confocal snapshot of functional cell mimic (conditions 42,timepoint 10h34).

We monitored this multicompartmentalized reactor during one hour and it seemed promising in terms of intensity increase, as at least to the eyes, an increased intensity was observed (Figures 30-34).

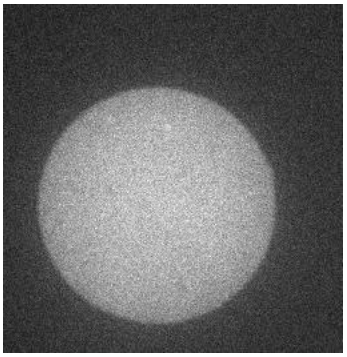

**Figure 30.** 9h34.

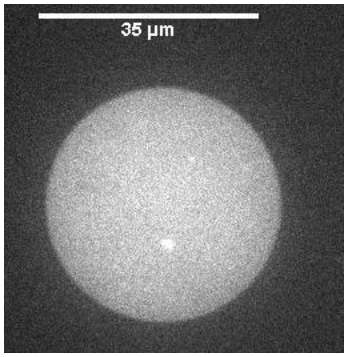


**Figure 31.** 9h49.

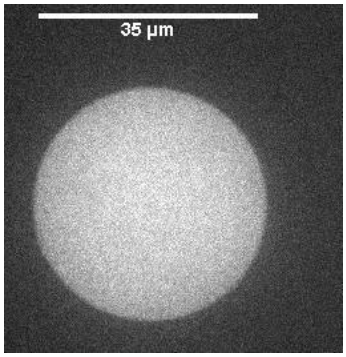


**Figure 32.** 10h04.

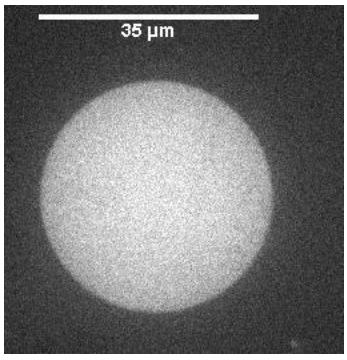


**Figure 33.** 10h19.

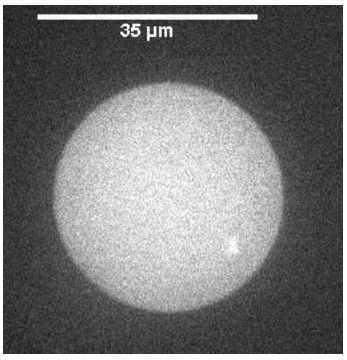


**Figure 34.** 10h34.

By analyzing the mean intensity of the global lumen, this intensity seemed to increase for this system, for the first time compared to cell mimics observed before this timepoint (see Table 25 and Figures 35 and 36).

**Table 25.** Fluorescence intensity with time of Figures 35-39

| Time | Area | Mean Fluorescence Intensity | Minimum Intensity | Maximum Intensity |
|---|---|---|---|---|
| 9h34 | 1099.87 | 2025.553 | 1547 | 2516 |
| 9h49 | 1099.87 | 2117 | 1486 | 2860 |
| 10h04 | 1099.87 | 2138.819 | 1481 | 2589 |
| 10h19 | 1099.87 | 2158.947 | 1437 | 2719 |
| 10h34 | 1099.87 | 2172.293 | 1391 | 2811 |

However, to estimate the errors bars of these mean intensities, we took three consecutive frames of this vesicle at some point to visualize the mean Intensities fluctuations (Table 26). Standard deviation is 62.6 and standard error, used to draw the error bars is 36.1 (standard deviation divided by the square root of number of measurements, here 3).

**Table 26.** Fluorescence intensity fluctuations for Figures 35&36.

| Area | Mean Fluorescence Intensity | Minimum Intensity | Maximum Intensity |
|---|---|---|---|
| 24601 | 2024.867 | 1501 | 2460 |
| 24601 | 2080.714 | 1473 | 2655 |
| 24601 | 2149.761 | 1534 | 2698 |

While the error bars are important, a slight increase between various timepoints is indubitably there. Finally, we do not only have a fluorescence in our polymersomes in polymersomes, evidencing the concept, but also a slight increase through time; the enzymatic cascade reaction producing a dye is indeed occurring in the cell mimics. It is also exciting to sometimes observe bright spots (Figures 31 and 34); they tentatively can be explained by the nanosize PS-*b*-PIAT loaded with ADH, in which the resorufin is generated before diffusing out in the lumen of PB-*b*-PEO. Of course, this was a preliminary experiment that needs to be investigated further.

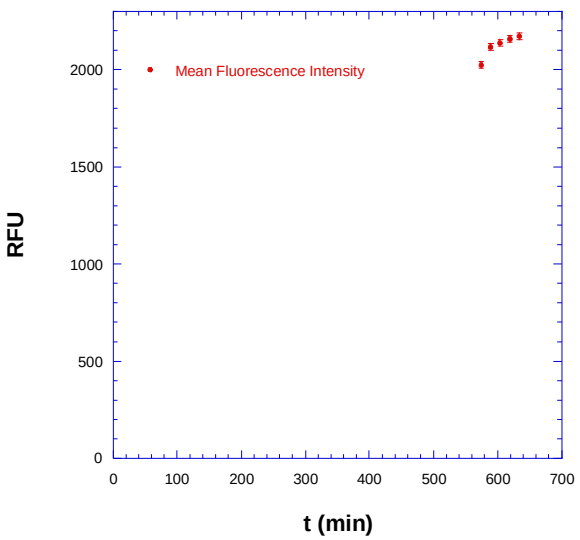


**Figure 35.** Intensity with time of Figures 35-39.

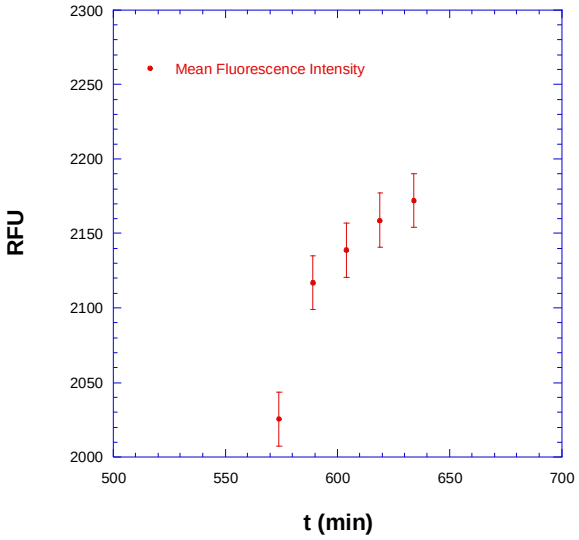


**Figure 36.** Zoom of Intensity with time of Figures 30-34.

Finally, we still need to test photoinitiation, which would be a very elegant way to start the reaction on demand, after shelf-storage for example, important for future long-term applications. Regarding that aspect, a real hurdle lies in the slowness of the cascade, which is also not ideal for the stopwatch method. Indeed in the few examples of enzymatic reactions inside multicompartmentalized materials so far, that have been detailed in the introduction, detection is instantaneous and overall reaction, fast. Furthermore, we have actually no knowledge or experience about decaging this molecule (see Figure 37) with a 405 nm laser under a microscope.

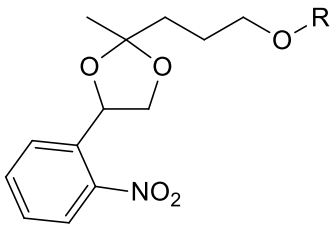


**Figure 37.** Photocaged substrate.

Scientists that bleach on purpose or decage in such a way, usually have a response immediately, so they know right away their decaging settings were right. We already know this will not be possible for our system and we will have to wait before detection of fluorescence. This makes the decaging even more difficult and time-consuming as we know for now that we will have to wait at least 3 hours (Figure 25), to detect anything, photocaged or non caged substrate; i.e. it takes at least 3 hours to assess if the decaging settings were accurate, worked or not. Illuminating a long amount of time to be sure everything is decaged

is not an option because even if 405 nm is very far from the excitation spectrum of resorufin (maximum at 561 nm), there is a risk of bleaching the fluorescent group of the substrate.
In principle, it is possible as Ruud Peters assessed the ability to decage the substrate, by illuminating a solution in a quartz cuvette with a powerful UV lamp (300 W), and checking absorbance (see Figure 38) until it resembles absorbance of the non-caged substrate (after 2 minutes, this is nearly reached, at about 80%).

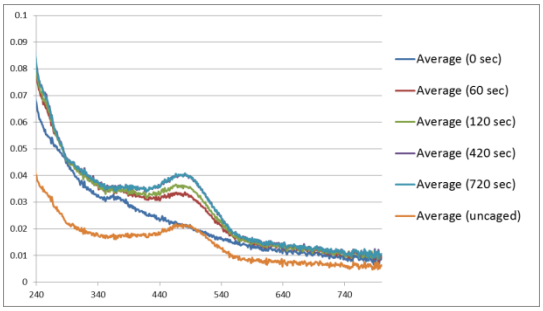


**Figure 38.** Absorbance of photocaged substrate with increasing UV illumination time.

## 5. Conclusion

In this chapter, we wanted to make a three enzymes cascade to proceed in PS-*b*-PIAT nanoreactors in PB-*b*-PEO polymersomes, in collaboration with Jan van Hest's group. The cascade alone is already very original, and rather complex as it involves natural cofactors; a BVMO enzyme, CRE2-PAMO, using NADPH, is the first enzyme, followed by CalB, and finally ADH, using the $NADP^+$ cofactor. This complexity explains the amount of time we needed to optimize this mixture well enough for the final objective. This part is rather detailed in this chapter.
After conditions were found that led to a sufficient intensity (which was achieved by letting the least efficient enzyme, CRE2-PAMO, free instead of loaded), we could proceed to the final objective, loading this nanoreactor cascade mixture via the emulsion-centrifugation (as detailed in chapters 2 and 3). The objective was to observe the cascade reaction confined into the PB-*b*-PEO vesicles by confocal microscopy. Results so far generated look very promising because a clear and confined fluorescence can be observed, proving the reaction in the PiPs. Furthermore, we even observed at least one time a relevant increase in fluorescence intensity, really evidencing the generation of resorufin inside the cell mimics.

However, these are first experiments that need to be investigated further and thoroughly, in order to assess or not reproducibility, repeatability and so on. Indeed, not many and certainly not enough, experiments have been performed and monitored so far; we have been limited by time as the preparation in itself is already very time-consuming (3 full days) and we cannot keep the nanoreactors for too long (especially if we want to compare samples from one day to samples from another one). Ideally, we would like to get the initial slope of the reaction (for that enough time points are requested to generate a relevant slope), and compare them.

In any case, with a much faster cascade, the experiments would be a lot easier and also take less time to acquire valuable proofs. A faster reaction would furthermore be necessary in any case for decaging the photocaged substrate with the 405 nm laser, and monitor the fluorescence. The faster the kinetics, the sooner it should be possible to detect fluorescence intensity by microscopy. It that step takes 3 hours, it seems a little tricky to optimize decaging conditions, as one will not know if the decaging step worked, the reaction just being too slow, or if one has to keep decaging. In the same time, too much 405 nm laser power, presents a risk of bleaching too much the Resorufin group (thus inducing errors).

## References


1. Marguet, M.; Sandre, O.; Lecommandoux, S., *Langmuir* **2012,** *28* (4), 2035–2043.
2. Marguet, M.; Edembe, L.; Lecommandoux, S., *Angewandte Chemie International Edition* **2012,** *51* (5), 1173-1176.
3. Peters, R. J. R. W.; Louzao, I.; van Hest, J. C. M., *Chemical Science* **2012,** *3* (2), 335-342.
4. Tanner, P.; Baumann, P.; Enea, R.; Onaca, O.; Palivan, C.; Meier, W., *Accounts of Chemical Research* **2011,** *44* (10), 1039-1049.
5. Tanner, P.; Egli, S.; Balasubramanian, V.; Onaca, O.; Palivan, C. G.; Meier, W., *FEBS Letters* **2011,** *585* (11), 1699-1706.
6. Palivan, C. G.; Fischer-Onaca, O.; Delcea, M.; Itel, F.; Meier, W., *Chemical Society Reviews* **2012,** *41* (7), 2800-2823.
7. Bolinger, P. Y.; Stamou, D.; Vogel, H., *Angewandte Chemie - International Edition* **2008,** *47* (30), 5544-5549.
8. Stadler, B.; Chandrawati, R.; Price, A. D.; Chong, S. F.; Breheney, K.; Postma, A.; Connal, L. A.; Zelikin, A. N.; Caruso, F., *Angewandte Chemie - International Edition* **2009,** *48* (24), 4359-4362.
9. Chandrawati, R.; Hosta-Rigau, L.; Vanderstraaten, D.; Lokuliyana, S. A.; Stadler, B.; Albericio, F.; Caruso, F., *ACS Nano* **2010,** *4* (3), 1351-1361.
10. Kreft, O.; Prevot, M.; Möhwald, H.; Sukhorukov, G. B., *Angewandte Chemie - International Edition* **2007,** *46* (29), 5605-5608.
11. Kreft, O.; Skirtach, A. G.; Sukhorukov, G. B.; Möhwald, H., *Advanced Materials* **2007,** *19* (20), 3142-3145.
12. Bäumler, H.; Georgieva, R., *Biomacromolecules* **2010,** *11* (6), 1480-1487.
13. Chandrawati, R.; Odermatt, P. D.; Chong, S.-F.; Price, A. D.; Städler, B.; Caruso, F., *Nano Letters* **2011,** *11* (11), 4958-4963.
14. Bolinger, P. Y.; Stamou, D.; Vogel, H., *Journal of the American Chemical Society* **2004,** *126* (28), 8594-8595.
15. Nardin, C.; Thoeni, S.; Widmer, J.; Winterhalter, M.; Meier, W., *Chemical Communications* **2000,** (15), 1433-1434.
16. Nardin, C.; Widmer, J.; Winterhalter, M.; Meier, W., *European Physical Journal E* **2001,** *4* (4), 403-410.
17. Ranquin, A.; Versées, W.; Meier, W.; Steyaert, J.; Van Gelder, P., *Nano Letters* **2005,** *5* (11), 2220-2224.
18. Broz, P.; Driamov, S.; Ziegler, J.; Ben-Haim, N.; Marsch, S.; Meier, W.; Hunziker, P., *Nano Letters* **2006,** *6* (10), 2349-2353.
19. Ben-Haim, N.; Broz, P.; Marsch, S.; Meier, W.; Hunziker, P., *Nano Letters* **2008,** *8* (5), 1368-1373.
20. Onaca, O.; Hughes, D. W.; Balasubramanian, V.; Grzelakowski, M.; Meier, W.; Palivan, C. G., *Macromolecular Bioscience* **2010,** *10* (5), 531-538.
21. Vriezema, D. M.; Hoogboom, J.; Velonia, K.; Takazawa, K.; Christianen, P. C. M.; Maan, J. C.; Rowan, A. E.; Nolte, R. J. M., *Angewandte Chemie - International Edition* **2003,** *42* (7), 772-776.
22. Nallani, M.; de Hoog, H. P. M.; Cornelissen, J. J. L. M.; Palmans, A. R. A.; van Hest, J. C. M.; Nolte, R. J. M., *Biomacromolecules* **2007,** *8* (12), 3723-3728.

23. Vriezema, D. M.; Garcia, P. M. L.; Sancho Oltra, N.; Hatzakis, N. S.; Kuiper, S. M.; Nolte, R. J. M.; Rowan, A. E.; Van Hest, J. C. M., *Angewandte Chemie - International Edition* **2007,** *46* (39), 7378-7382.
24. Kuiper, S. M.; Nallani, M.; Vriezema, D. M.; Cornelissen, J. J. L. M.; Van Hest, J. C. M.; Nolte, R. J. M.; Rowan, A. E., *Organic and Biomolecular Chemistry* **2008,** *6* (23), 4315-4318.
25. Van Dongen, S. F. M.; Nallani, M.; Cornelissen, J. J. L. M.; Nolte, R. J. M.; Van Hest, J. C. M., *Chemistry - A European Journal* **2009,** *15* (5), 1107-1114.
26. Van Dongen, S. F. M.; Verdurmen, W. P. R.; Peters, R. J. R. W.; Nolte, R. J. M.; Brock, R.; Van Hest, J. C. M., *Angewandte Chemie - International Edition* **2010,** *49* (40), 7213-7216.
27. Fraaije, M. W.; Wu, J.; Heuts, D. P. H. M.; van Hellemond, E. W.; Spelberg, J. H. L.; Janssen, D. B., *Applied Microbiology and Biotechnology* **2005,** *66* (4), 393-400.
28. Torres Pazmiño, D. E.; Snajdrova, R.; Baas, B.-J.; Ghobrial, M.; Mihovilovic, M. D.; Fraaije, M. W., *Angewandte Chemie International Edition* **2008,** *47* (12), 2275-2278.
29. Torres Pazmiño, D. E.; Riebel, A.; de Lange, J.; Rudroff, F.; Mihovilovic, M. D.; Fraaije, M. W., *ChemBioChem* **2009,** *10* (16), 2595-2598.
30. Meeuwissen, S. A.; Rioz-Martínez, A.; De Gonzalo, G.; Fraaije, M. W.; Gotor, V.; Van Hest, J. C. M., *Journal of Materials Chemistry* **2011,** *21* (47), 18923-18926.
31. Gutierrez, M. C.; Sleegers, A.; Simpson, H. D.; Alphand, V.; Furstoss, R., *Organic & Biomolecular Chemistry* **2003,** *1* (20), 3500-3506.

# General Conclusion and Perspectives

The challenge of this PhD project lied in the controlled formation of structural eukaryotic cells mimics with polymersomes and polymer-based materials in general, as "building blocks". First and foremost, an appropriate preparation method, had to be chosen and developed. Then, it could be used for the formation of the desired objects and establishment of corresponding proofs of concepts thanks to relevant characterization tools. Finally, the work could be extended to not only structural, but also functional cell mimics with the incorporation of enzymatic cascade reactions *in situ*.

The strategy is based on a two-step batch process (**Chapter 2**); first, biodegradable nanosize polymersomes of poly(trimethylene carbonate)-*b*-poly(L-glutamic acid) (PTMC-*b*-PGA) are formed *via* nanoprecipitation as developed in the laboratory. [1] Then, they are loaded inside micrometric polymersomes of poly(butadiene)-*b*-poly(ethylene oxide) (PB-*b*-PEO) during the formation of the latter with the emulsion-centrifugation method. This method is based on an inverted emulsion (where the aqueous suspension of inner nanosize PTMC-*b*-PGA polymersomes constitutes the water droplets of the emulsion), which suggests a 100% encapsulation efficiency, as has been proved in the Weitz group. [2] The PB-*b*-PEO diblock copolymer is dissolved in the oil phase and stabilizes the emulsion droplets (thus forming the inner leaflet of the final polymer bilayer) at their interface. A small fraction of an inverted emulsion is then poured over an interface of oil phase and pure water phase. In a final step, centrifugal force causes these droplets to cross the interface and to be enveloped by a second leaflet of amphiphilic PB-*b*-PEO block copolymer, resulting in the final giant polymersomes. The control provided by this process enabled to assess the structure of the multicompartmentalized polymersomes or "polymersomes in polymersomes" (PiPs) with specific fluorophore labeling and spinning disk confocal microscopy as both size ranges were chosen to be visible. We also presented a movie where red fluorescent inner nanosize polymersomes can clearly been observed moving in the lumen of a green fluorescent outer micrometric polymersome[8]. The 2D motion of these structural organelle mimics was tracked down in this movie and their motion was confirmed to still be Brownian (as motion stayed isotropic, and data respected a Gaussian, or random, distribution) inside the volume of an approximately 20 µm giant polymersome. Furthermore we found the same size and diffusion coefficient of inner nanosize vesicles after their encapsulation by this particle tracking analysis than by dynamic light scattering on the solution before loading. These results

[8] Movie s1, http://onlinelibrary.wiley.com/doi/10.1002/anie.201106410/suppinfo

assessed the validity of our particle tracking analysis and confirmed that the nanosize vesicles were not disturbed during the encapsulation process. Regarding cell biomimicry, cytoplasm confinement plays an important role in cellular activity and regulation. Of course, there are again many interesting properties arising when mimicking a viscoelastic cytoplasm, the first certainly being a better protection and thus stability and shape integrity by absorption of mechanical stress. The highly complex cytoskeleton is far from easy to mimic, as it is composed of the actin protein filaments, microtubules and intermediate filaments, formed by nucleation-elongation processes. The growth of the protein filaments of this cytoskeleton is driven by non covalent interactions, with constant association/dissociation processes, making them very dynamic.[3] In addition to the obvious mechanical properties given by the cytoskeleton, the high macromolecular concentrations found intracellularly are responsible for the so-called macromolecular crowding effect.[4-6] In 2001, R. John Ellis and co-workers[6] launched a call to biochemists to stop neglecting this "macromolecular crowding" in their studies, which is known in polymer science as the "excluded volume effect". All together, macromolecules in the cytoplasm, cytoskeleton, and internal compartments occupy 20−30 vol.% of a cell, generating a strong steric repulsion between them. The consequences on the cell machinery had been rarely considered. For instance, most biochemical reactions are studied in dilute (ideal) solutions, while in real cells one should consider the activity coefficients for both thermodynamic and kinetic studies. In order to consider these parameters,[7] a suspension of nanosize inner polymersomes of PTMC-*b*-PGA was this time encapsulated in giant polymersomes of PB-*b*-PEO together with highly concentrated, hence viscous, alginate or dextran solutions, thanks to the emulsion-centrifugation process (see Figure 1).

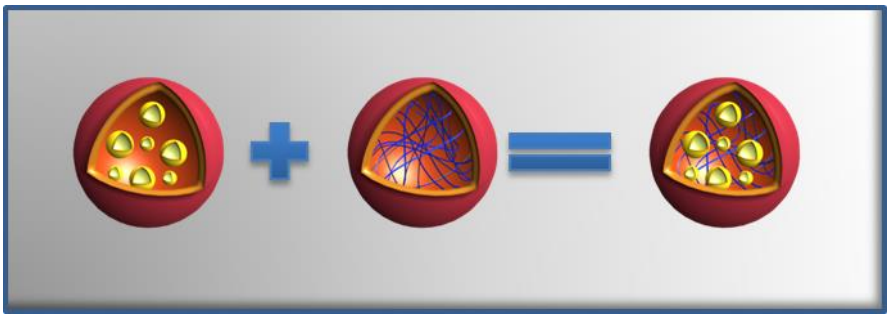

**Figure 1.** Scheme summarizing goals of Chapter 2.

A movie of these structures was acquired and the motion of the PTMC-*b*-PGA tracked down again. This time, their motion was proven to be efficiently hindered as confirmed by a 6.6 times smaller diffusion coefficient (Figure 2). Furthermore, the

concentration of 300 mg/mL of polysaccharide dextran increased viscosity above 0.01 Pa.s, in the range of red blood cell cytoplasm viscosity,[8] a volume fraction near 30%, and an osmotic pressure above 1 MPa resembling the intracellular conditions caused by cellular proteins. By reproducing the intracellular "macromolecular crowding effect", which plays a crucial role in the cell machinery, we believe that this synthetic and simplified approach constitutes an appropriate cytoplasm mimic. There have been reports of liposomes in liposomes, cytoplasm mimics in liposomes or polymersomes, capsules or liposomes in capsules (as detailed in chapter 1), and even capsules in a capsule with a cytoplasm mimic. However, to the best of our knowledge, the combination of these two mimics had never been reported so far in polymersomes.

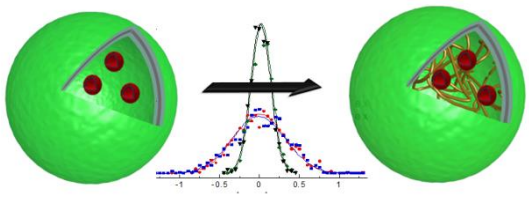

**Figure 2.** Addition of a cytosol mimics brings a decrease in rate of displacement and Brownian motion of organelle mimics.

In **Chapter 3**, we investigate benefits resulting from a multicompartmentalized structure for drug delivery and the biomedical field in general. Such a structure should be of particular interest for the delivery of multiple active components.[9] To address this point, a solution of two different PTMC-*b*-PGA suspensions, labeled respectively with red and green fluorophores was encapsulated instead of a single nanosize vesicle suspension (Figure 3). The two nanosize polymersomes are clearly localized in the same giant polymersome[9].

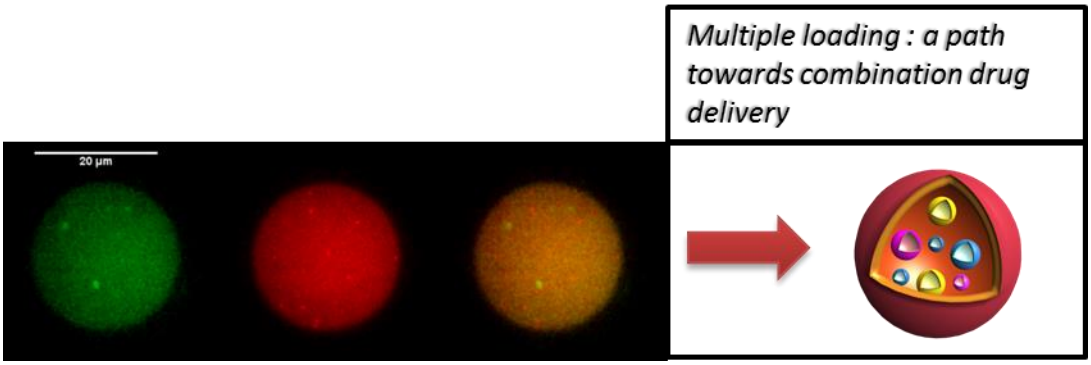


**Figure 3.** Multiple organelle loading, green population left, red in the middle, overlay right.

[9] Movie s3, http://onlinelibrary.wiley.com/doi/10.1002/anie.201106410/suppinfo

As long as the inner polymersome suspensions that are mixed are concentrated enough, this encapsulation can be extended to far more than two different populations.

Finally, we were able to further increase the complexity of this system by co-encapsulating a large polymer, FITC-dextran, with a red nanosize vesicle suspension (Figure 4). As the FITC-dextran was already green fluorescent, the membrane was this time labeled in blue, allowing separate imaging of the giant vesicles (blue), the inner nanosize vesicles (red) and the loaded dextran (green) in the giant lumen. Such a three-compartment encapsulation in vesicles was, to the best of our knowledge, the first reported to date. This multiple encapsulation strategies open avenues for future applications in multiple drug delivery. Such an approach is especially interesting in oncology amongst others, with the new possibility of loading (thus potentially delivering) various, even incompatible, components (like an anticancer drug cocktail) in one larger vector, hence in a high enough drug payload to get a large and synergetic therapeutic response.

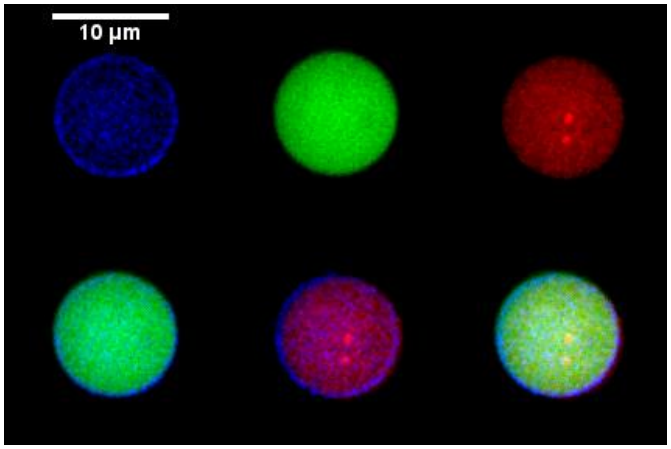


**Figure 4.** Multiple compartment loading.

In a sustained and controlled drug delivery approach, we were then able to study the *in vitro* release kinetics of anticancer drug doxorubicin loaded in the nanosize vesicles. As expected, the release kinetics were significantly decreased when the nanosize vesicles were protected by an additional polymer membrane of PB-*b*-PEO, i.e. additional diffusion barrier. In the latter scenario, permeation of doxorubicin through the polymeric membranes, induced by the chemical gradient in the release setup, could only last longer. By representing the release data differently, with a law established by Peppas and Ritger[10] and extracting the kinetic constants k for each system, it could be quantitatively determined that the release rate was indeed about twice (≈2.3) slower with an additional diffusion barrier. With this additional membrane, we could thus demonstrate the following properties arising: a better control of

release kinetics with a resulting controlled permeability tuning, and a better protection of loaded actives in theory. Moreover, thanks to their polymeric nature, these two successive membranes could now be designed to allow a specific stability and orthogonal disruption in different environments. Such designs would be crucial for challenging means of administration than the intravenous one, like transcutaneous,[11] and oral administration,[12] the future challenges in drug delivery and cancer therapy. Our strategy thus presents a straightforward approach and new opportunities for the application of these polymersomes in polymersomes in biomedical or cosmetic applications, where the encapsulation of multiple, distinct and fragile ingredients are required, together with specific release conditions.

The last and most complex property to master, which arises from such structures, is the ability to use the inner compartments as reactors. Such a structure can for example impact the way we design a chemical reaction or induce a reaction only when different components (confined in various inner compartments) are mixed. In the last chapter (**Chapter 4)**, we therefore strove to replace in our cell mimics, our internal structural "organelles" by functional ones, in which enzymatic reactions take place (Figure 5).

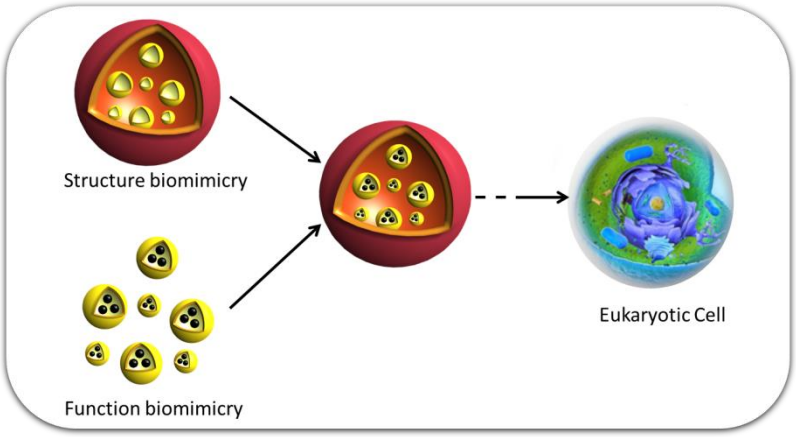


**Figure 4.** Scheme summarizing chapter 4.

The choice of complex enzymatic reactions, instead of any classic chemical reaction, was of course relevant in a perspective of Cell Biomimicry and also in a "green chemistry" perspective pursued by the laboratory. Indeed, in the confined, crowded environments of the cell, reactions are not occurring in ideal (dilute) solutions. This is what we wished to address and model, going from a structural to a functional Cell Biomimicry.

A biomimetic cascade reaction based upon three enzymes destined to function in three different PS-*b*-PIAT polymersome populations was designed in collaboration with Professor J. van Hest's group. The idea was to load the cascade mixture (including substrate and cofactor(s)) in PB-*b*-PEO polymersomes, ideally initiate the reaction via decaging of a

photocaged substrate, under a confocal microscope, and follow the increase of the final product's red fluorescence intensity. This chapter focuses mainly on the optimization of the nanoreactor cascade, as these functional artificial organelles, based on PS-*b*-PIAT nanosize polymersomes loaded with enzymes, need to communicate together in the right concentration ratios for an optimal reaction. This step indeed revealed to be a little problematic given the final objective. In the end, we were however able to provide a relevant proof of concept: when observing the functional cell mimics by confocal microscopy, with a reaction based upon the non-caged substrate, red fluorescence was actually detectable after a few hours. This ambitious project requires however some further investigations. There is definitely a challenge in mastering reactions on attoliter volumes, as well as a potential long-term industrial interest arising (if reactives are fragile, very expensive or polluting for instance). Such investigations open avenues in the Biotechnological field, and in the construction of complex therapeutics and therapeutic artificial cells,[13, 14] in addition to the use of these systems simply as relevant models for a better comprehension of Nature's cell.

Regarding perspectives, this original project is paving the way for numerous possibilities.

1) **Cell models** for biology, biochemistry and biophysics studies. Sometimes, using actual cells (to develop a technique, a method for example), which are expensive, may not be necessary; robust and accurate models would be sufficient. Furthermore, a biological cell is so complex, that studies would perhaps sometimes benefit from the use of models, in order to investigate only a limited number of phenomena at the same time and understand them correctly; complexity can not always be understood at once, but may be established step by step. However, existing models or modellings may be described sometimes as too limited. Enzymatic reactions are for example mostly studied in test tubes, in dilute (ideal) solutions, when they are actually happening in confined and crowded compartments of the cell, as emphasized throughout this thesis. That is why, accurate and relevant cellular models are required and we believe our structural, and furthermore our functional, cell mimics to constitute one possible response to such challenges.

2) **Loading of magnetic nanoparticles** for hyperthermia (release of actives triggered by application of alternating magnetic field inducing local heating thus increase of permeability) is in growing expansion. The concept of "theranostics" implies co-loading actives (therapy) and magnetic nanoparticles for diagnosis. The challenge lies however in the actual co-encapsulation of these species in a high enough concentration. A

multicompartmentalized structure as ours, offers a wide range of possible compartments: multiple inner compartments (not necessarily made of the same material), giant polymersome's lumen and membrane. Moreover, it is especially interesting to use the emulsion-centrifugation method to load quantitatively an aqueous suspension of magnetic nanoparticles in the lumen of giant PB-*b*-PEO polymersomes; usually their loading is problematic because of the low encapsulation efficiencies of classic methods. This way, a significant number of particles could get loaded, enough to generate responsive (to magnetic field) giant polymersomes. This was assessed by loading a suspension at 0.1 v.% (pH 7.7, poly(acrylic acid) coating, $\rho_{apparent}$=1.004 g/mL, $R_H$=0.55 nm with a PDI of 0.17) maghemite nanoparticles and observing their responsiveness to a magnet moving near the microscopy chamber (see Figures 5 and 6).

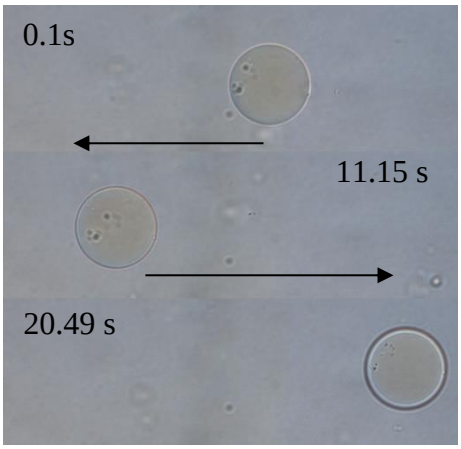


**Fig. 5.** Giant PB-*b*-PEO polymersomes loaded with magnetic nanoparticles (giving this yellowish-brownish cavity). From top to bottom: timepoint 0.1s with magnet moving to the left so that vesicle has moved left on time point 11.15 s. Then magnet moves right and vesicle follows until timepoint.20.49 s.

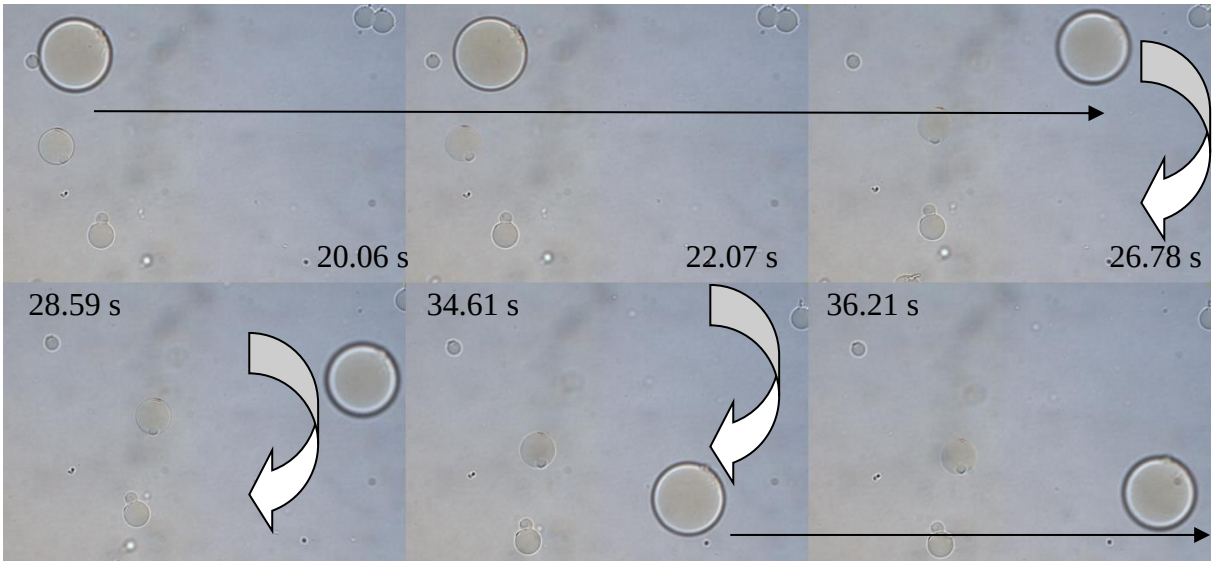


**Fig. 6**. Other polymersomes evidencing the dependence of size (thus number of inner particles) on the response to magnetic field. From top left to bottom right: timepoint 20.6 to 22.07 then 26.78 s with magnet moving to the right. Then from the timepoint 26.78 to 28.59 to 34.61 s, the magnet is describing a cercle. Finally, from 34.61 to

36.21 s, the vesicle is moving to the right again. The largest vesicle is moving visibly faster than the other ones, that are smaller.

The experiment revealed to be successful: the vesicles were yellowish-brownish and reactive to magnets (the larger, hence the most particle-containing in number, the more reactive).

Going further, a potential limiting parameter with the emulsion-centrifugation method, lies the presence of concentrated sucrose (130 mg/mL), especially when working with biological material (actual cells cannot survive such a high concentration for example). If concentrated enough, the loading of inert colloids like magnetic dense nanoparticles could enable the same goals but avoid the presence of sucrose. Indeed, while water has a density of 1 g/mL, maghemite particles are at about 5 g/mL. Sucrose and glucose are used in the process because their difference in density helps the sedimentation of the vesicles in the current centrifugation conditions. Suppressing sucrose completely in the inner droplets hence implies also suppressing completely glucose in the lower solution of the interface. To calculate the density of the maghemite nanoparticle suspension needed to give the same conditions as our sucrose, we need to calculate first the difference of density between sucrose and glucose, both at our working concentration of 380 mM:

$$\Delta\rho_{sucrose-glucose} = (342-180)\frac{g}{mol}\cdot 0.380\frac{mol}{L} \approx 0.065 g/mL = \Delta\rho_{maghemite\ fluid-water}$$

So, an aqueous suspension of maghemite nanoparticles to use instead would thus need to be at $\rho_{water} + \Delta\rho_{sucrose\text{-}glucose} = \rho_{maghmeite\ fluid}$ =1.065 g/mL

Given the apparent density of a maghemite nanoparticle suspension $\rho_{apparent\ maghemite} = \rho_{apparent\ maghemite} \cdot \Phi_{maghemite} + \rho_{water}(1-\Phi_{maghemite})$, this suspension should be at a volume fraction of: $\Phi_{maghemite} = 1.6\ vol.\%$

The application of such parameter is currently under investigation.

To finish, we see a last interesting possibility generated by loading magnetic particles: the ability to manipulate them via magnetic field application. This can either bring to deformation of the vesicles (with constant field), hence more or less important increase in permeability that can be tuned of demand. Such work is fundamentally interesting (how much can it be deformed while staying intact for example) but is also exciting in a potential long-term application of drug delivery, a fine and precise tuning of permeability is important to control sustained or burst release kinetics on demand. This deformation on vesicles has been for example published with liposomes before,[15] raising another question, will it be possible to deform polymersomes the same way than liposomes? And if yes, it would be interesting to study their differences in behavior: this can also be a way to have access to the membrane

properties. Because of otherwise too limited encapsulation efficiencies, the authors were forced to microinject in every single liposome the magnetic content, a classic method. This is tedious and as it has to be performed under a microscope, the sample already in a microscopy chamber cannot be retrieved out of it and used for biomedical purposes. In another perspective, the ability to have a vesicle responsive to a magnetic field gradient, i.e. a vesicle following the motion of a magnet for example, raises exciting potential long-term applications where the vector could be commanded *in vivo* perhaps, but more simply and feasibly *ex vivo*, *in vitro*, for cell cultures for example, *etc*.

3) **The development of fully biocompatible and/or biodegradable multicompartmentalized polymersomes** for future applications. The group in which this project was conducted, usually works with at least biocompatible (preferably biodegradable or better bioresorbable) polymers, whether the projects involve concrete in *vitro* or in *vivo* studies right away or not (like this one). Originally for this project, PTMC-*b*-PEO was supposed be used instead of model copolymer PB-*b*-PEO. PTMC was synthesized from TMC via ring-opening polymerization from diethyle zinc. It was then later clicked to PEG via Huisgen 1,3 Dipolar cycloaddition and copper catalyst. The range of copolymers synthesized was $PMTC_x$-*b*-$PEO_{45}$ with x=37, 32, 23 and respective approximate molar hydrophilic ratios of 33, 36 and 44 %. To stabilize an inverted emulsion of water in oil, the amphiphile has to more lipophilic than hydrophilic, meaning a low HLB (between 3 and 6, maximum 8). So theoretically, the lower this hydrophilic ratio, the better it should stabilize the emulsion. However, these three copolymers revealed themselves unable to stabilize the toluene/water interfaces of the process, droplets would coalesce immediately. Possibly, PTMC-*b*-PEO was just not amphiphilic enough and with a low enough HLB to stabilize that interface in the given conditions. Increasing the concentration from 3 to 6 mg/mL did not improve anything.
We checked other biocompatible or biodegradable polymers available at the laboratory were not more suitable: but Dow Corning 5329® did not stabilize the droplets, PEG-*b*-PLA (1000-*b*-750 g/mol reference 24378 from Polysciences, Inc.) was not even soluble in toluene and PEG-*b*-PCL (2000-*b*-5000 g/mol, I=1.3 reference P5042-EOCl from Polymer Source) seemed to stabilize the emulsion but no vesicles could be retrieved at the end of this process. While this was not problematic for the proofs of concept we wanted to establish (which is why we pursued the work with process model copolymer PB-*b*-PEO), that did not involve *in vitro* or *in vivo* studies, it would be interesting to find a suitable biodegradable polymer for the future, especially for biomedical applications but also to allow a controlled biodegradation.

The difficulty lies in the fact that the process requires an organic, oil phase, able to dissolve the copolymer. Furthermore, this phase needs to be less dense than water and immiscible with water. The last two requirements alone, suppress a lot of possibilities. The best strategy would perhaps lie in, first the choice of the best, least toxic suitable organic phase (for liposomes, oils can be used). Then, a copolymer would have to be carefully designed to, on one hand be soluble in this organic phase, but on the other hand, not too well soluble, as it has to be amphiphilic enough to stabilize the various interfaces. It would be in any case and perhaps more importantly, interesting to find another suitable solvent than the toxic, reprotoxic even, toluene; possible traces of toluene in the final aqueous PiPs suspension were indeed not problematic for the present work, but could be for future studies.

The solvents that we judged to meet the process requirements and tested in order to make use of PTMC-*b*-PEO were: silicon oil, squalene, mineral oil, dodecane, and cyclohexane. Unfortunately, the copolymer was soluble in none of them.

To finish, we were however able to get successful with a blend of PB-*b*-PEO/ $PMTC_{37}$-*b*-$PEO_{45}$ 50/50 wt.% and 25/75% (75/25% was not stable) with the current conditions. This is interesting to know, as PMTC has been shown in earlier work in the laboratory to be biodegradable, in acidic or basic conditions, and prone to lipase degradation as well. In principle, a certain permeability, porosity could thus be tuned over time (with specific conditions where the PB in the membrane blend would remain intact), possibly leading to complete disruption at some point.

4) **Process improvement**. This process in itself was also sufficient for this project; the idea was to use a method able to generate the needed low quantities on a laboratory scale to establish proofs of concept. In industry, it is only once proofs of concepts have been established on the laboratory scale, that it becomes time and worthwile to pursue with larger scales (various pilot units, and finally production unit) by scaling-up the method or sometimes by changing it completely just to improve it or for the actual scale-up. Furthermore, the quantities were maybe already too low for this project as in the end, we retrieve about 50 µL of a very diluted suspension of cell mimics, which was problematic for the *in vitro* drug release and may be limiting for further studies. Hence, to push this work further, in terms of quantities generated, also if possible with a safer solvent as traces of toxic toluene may remain, maybe a completely new process has to be designed or the current process has to be scaled-up and/or improved; Abkarian *et al.* [16] for example, using phospholipids, improved it into a process that was still batch-mode, but one-pot, not sequential any more, and not too greedy in terms of most inner aqueous solution (which may contain biological material) to

load. For the biomedical and biotechnological field, where expensive and rare drugs, proteins, enzymes, *etc*, may need to be loaded, small batch modes seem optimal.

With a better, improved process, various applications for the biomedical field could then be investigated.

5) **Multicompartment systems as the ultimate multifunctional vectors**. Thanks to the exquisite state of current polymer science, each kind of membrane of the multicompartment system could now actually be carefully designed to bear different ligands, present a specific texture (rough or smooth, generating different responses of the immune system), and above all a specific chemical nature to control release kinetics; each kind of membrane could present a specific degradability or stimuli-sensitiveness (to pH, T, ionic force, redox) in an orthogonal fashion, so that destabilisation or degradation (thus release) can be triggered consecutively. Single polymersomes have been designed and investigated as smart and functionalized vectors for a decade now, and this knowledge can be made of use for multicompartmentalized polymersomes. By using our method, the most important challenge perhaps would lie in choice of suitable copolymer for the outer membrane, i.e. a copolymer soluble in a process relevant organic phase.

6) **Challenge of global size and different administration pathways.** Actually designing, generating and studying *in vitro* and *in vivo* such multicompartmentalized systems, makes another important challenge arise, namely the choice of delivery pathway. Nanovectors are injected intravenously; the technological challenge for classic single compartment vesicles already lies in achieving a suitable final size, below 200 nm. Above that size their elimination out of the body is indeed too fast to observe any benefits. For a multicompartmentalized structure, a process enabling an outer membrane size below 200 nm is even more challenging. With our method, the emulsion droplets are templating the outer polymersomes, so in order to get nanometric sizes, one would need to drastically decrease the droplets size, for example *via* sonication (although it is not really recommended on supramolecular self-assembled amphiphilic structures, and inner structures would already be suspended in the droplets). Or if the polymer has a low enough Tg, one could extrude the final multicompartmentalized structures as was performed on multicompartmentalized liposomes (or vesosomes) in Zasadzinski's group. Going further, we believe another important challenge for the use of vectors in the biomedical field lies in other methods of delivery, like transcutaneous and more importantly, oral administration. By taking the example of cancer therapy, oral administration would hugely improve patient's compliance, day to day treatment and life, and also health

costs. In that perspective, it would be interesting to design a multicompartmentalized system, able to remain intact until its arrival in the intestine. Nowadays, many oral classic formulations, such as tablets and capsules, present coatings of so-called gastro resistant polymers; polysaccharides (chitosan or dextran), acrylic copolymers (Eudragit®), or cellulosic derivatives (cellulose acetate phthalate CAT, cellulose acetate trimellitate CAP and hydroxypropyl methylcellulose phthalate HPMCP), *etc*.[17] Using such polymers for the outer membrane (or for an additional coating) should thus also confer the system the ability to resist very acidic gastric pH (< 5) but to be degraded or disrupted later, in the intestine at physiological pH of 7.4. This would provoke the release of the inner robust compartments; these could be classic nanovectors possibly functionalized for effective targeting and below 100-200 nm. Then we can imagine several potential possibilities. Either, these nanovectors would then need to find a way into blood circulation through intestine tissue while remaining intact.[18] Either, and this would be the only acceptable theory for opponents to this intact crossing hypothesis, the nanoparticles could be internalized by various intestinal cells and the active would only then be released to the bloodstream; it would not be a nanovector drug delivery scenario anymore. There is also research about particles able to adhere to the intestinal mucus, either via electrostatic interactions (as one of its main components, the mucin protein is negatively charged) or *via* disulfure bridges, enabling a localized high aggregation, thus concentration, and a potential delivery to the bloodstream (also probably with destruction of nanoparticles). The approach would then be more pragmatic for pharmaceutical needs for efficient oral administration of particular actives with a high enough bioavailability. More simply, we can imagine their aggregation into “gastric patches”, against ulcers, or other similar issues.

7) **Multi-therapeutic vectors.** Sometimes, a therapy involves not only one active, but two or more that may interact differently together than alone, synergistically. Current treatment for HIV is based on tritherapy for example. Cancer treatment also involves combination therapies, for example the liposomal doxorubicin Myocet™ used in combination with cyclophosphamide against metastatic breast cancer. We have addressed the challenge of multiple encapsulation in this work. Each inner compartment can be individually loaded with a different component, which can be incompatible, degrade one another, *etc*, some of them can act synergistically once at the target site, *etc*. It would now be interesting to proceed further, from multiple encapsulation to actual multiple delivery, prove this concept. Moreover, if such systems would be injected intravenously, it should logically increase the drug payload at the target, enough to get a therapeutic response while decreasing polymeric carrier mass.

All the various desired therapeutics would reach the right target at the same time. So, once the process is ready for such a challenge and/or submicrometer range is possible, it would be interesting to really investigate such scenarios *in vitro* and *in vivo*, and assess feasibilities.

8) Last but least, we believe the field of **multicompartmentalized reactors** full of promises, particularly for the biomedical field and as bioreactors, which still has to be fully and thoroughly explored.

- Microreactors for chemical and /or enzymatic catalysis in biotechnological industries are interesting as they should enable miniaturized reactions to take place, potentially limiting waste production, sample consumption, safety issues as the quantities of toxic, polluting reactives or intermediates are miniaturized as well. Moreover, confinement in compartments, or reactions of so small volumes may have influences on the way the reactions proceeds, maybe improve some parameters compared to the macroscopic scale, *etc*. There is currently some research about continuous flow chemistry that tries to address these challenges, revealing the potential of this approach. [19]
- This concept can also be transferred to the biomedical field, in the same way artificial organelles are being designed to function intracellularly. As Caruso's group has been pointing out for their capsosomes, multicompartmentalized structures can indeed serve as biomedical platforms. We can imagine reactions on prodrugs for example, where, while travelling in the body to the target size, a reaction would proceed (initiated *ex vivo* or *in vivo* on demand) to give a cytotoxic and/or unstable reaction product in the end, upon arrival on the target size. Moreover, in combination with multi-therapy, several different compartments could be loaded with several different prodrugs. As in one of Caruso's last report detailed in **chapters 1** and **4**, one can also imagine the reaction of a large prodrug macromolecule into a small drug, hence a molecule small enough to permeate rapidly outside, in a release triggering reaction mechanism. One can also think of systems where a reaction *in situ* will conduct to the degradation or disruption of one or more polymer membranes, to generate the desired release of species; in that case these species would need to remain unaffected by the reaction. More simply polymer membranes have been reported to get degraded by enzymes.[1] One can also design a system where any kind of disturbance generated by one kind of reaction, would lead to release of the inner contents in the outer lumen and thus initiation of a second (set) of reaction(s), thus controlling volume ratios and initiation time. This concept has been reported by Vogel and coworkers (**Chapters 1 and 4**), even though in their case a permeability tuning,

not a reaction was responsible for release, hence initiation. Such a concept is also highly useful for microreactors.

Technologically, multicompartmentalized reactors represent the most difficult hurdle to overcome, but who knows how fast and successfully this research will expand.

---

1. Sanson, C.; Schatz, C.; Le Meins, J. F.; Brûlet, A.; Soum, A.; Lecommandoux, S., *Langmuir* **2010,** *26* (4), 2751-2760.
2. Pautot, S.; Frisken, B. J.; Weitz, D. A., *Langmuir* **2003,** *19* (7), 2870-2879.
3. Brizard, A. M.; Van Esch, J. H., *Soft Matter* **2009,** *5* (7), 1320-1327.
4. Jesorka, A.; Markström, M.; Karlsson, M.; Orwar, O., *Journal of Physical Chemistry B* **2005,** *109* (31), 14759-14763.
5. Long, M. S.; Jones, C. D.; Helfrich, M. R.; Mangeney-Slavin, L. K.; Keating, C. D., *Proceedings of the National Academy of Sciences* **2005,** *102* (17), 5920-5925.
6. R.John, E., *Trends in Biochemical Sciences* **2001,** *26* (10), 597-604.
7. Marguet, M.; Sandre, O.; Lecommandoux, S., *Langmuir* **2011**.
8. Campillo, C.; Pépin-Donat, B.; Viallat, A., *Soft Matter* **2007,** *3* (11), 1421-1427.
9. Al-Jamal, W. T.; Kostarelos, K., *International Journal of Pharmaceutics* **2007,** *331* (2), 182-185.
10. Ritger, P. L.; Peppas, N. A., *J. Controlled Release* **1987,** *5* (1), 23-36.
11. Mishra, V.; Mahor, S.; Rawat, A.; Dubey, P.; Gupta, P. N.; Singh, P.; Vyas, S. P., *Vaccine* **2006,** *24* (27-28), 5559-5570.
12. Ebato, Y.; Kato, Y.; Onishi, H.; Nagai, T.; Machida, Y., *Drug Development Research* **2003,** *58* (3), 253-257.
13. Orive, G.; Hernandez, R. M.; Gascon, A. R.; Calafiore, R.; Chang, T. M. S.; Vos, P. D.; Hortelano, G.; Hunkeler, D.; Lacik, I.; Shapiro, A. M. J.; Pedraz, J. L., *Nat Med* **2003,** *9* (1), 104-107.
14. LeDuc, P. R.; Wong, M. S.; Ferreira, P. M.; Groff, R. E.; Haslinger, K.; Koonce, M. P.; Lee, W. Y.; Love, J. C.; McCammon, J. A.; Monteiro-Riviere, N. A.; Rotello, V. M.; Rubloff, G. W.; Westervelt, R.; Yoda, M., *Nat Nano* **2007,** *2* (1), 3-7.
15. Sandre, O.; Ménager, C.; Prost, J.; Cabuil, V.; Bacri, J. C.; Cebers, A., *Physical Review E - Statistical Physics, Plasmas, Fluids, and Related Interdisciplinary Topics* **2000,** *62* (3 B), 3865-3870.
16. Abkarian, M.; Loiseau, E.; Massiera, G., *Soft Matter* **2011,** *7* (10), 4610-4614.
17. Mazzaferro, S.; Bouchemal, K.; Ponchel, G., *Drug Discovery Today* (0).
18. Roger, E.; Lagarce, F.; Garcion, E.; Benoit, J. P., *Journal of Controlled Release* **2009,** *140* (2), 174-181.
19. van den Broek, S. A. M. W.; Leliveld, J. R.; Becker, R.; Delville, M. M. E.; Nieuwland, P. J.; Koch, K.; Rutjes, F. P. J. T., *Organic Process Research & Development* **2012,** *16* (5), 934-938.